# Dynamics of calcite cementation in response to oil charge and reservoir evolution: Thamama, Group, U.A.E


**Amena Dhawi Juma Mayoof Al Harthi**

Thesis submitted for the degree of Doctor of Philosophy

University of Edinburgh

2018

# DECLARATION

I declare that this thesis is entirely my own work, except where stated otherwise. This work has been submitted or accepted for any degree at The University of Edinburgh or at any other university worldwide.

Amena Dhawi Alharthi

March 2018

# DEDICATION

This thesis is dedicated to my parents, sisters and brothers for their endless support, encouragement and love.

# ACKNOWLEDGEMENTS

First of all, I am grateful to my principle supervisor Rachel Wood for her great assistance, encouragement and support during the last four years. Her support is priceless. I would also like to thank my second supervisor Mark Wilkinson and my advisor Linda Kirstein, Ian Bulter and Stuart Haszeldine for their help and advice to complete this project. Many thanks go to John Craven, Chris Hayward, Mike Hall, and Nicola Cayzer for their technical assistance.

I am grateful also to Abu Dhabi National Company (ADNOC) for sponsoring this project and The Abu Dhabi Company for Oil Operation (ADCO) for providing the necessary data. I would also like to thank Hesham Shebl and Sadoon Morad for their useful discussions and for providing relevant publications.

My sincere thanks to my mother, father, sisters (Alya, Ayesha, Fatima, Mariam, Khadija and Khulood) and brothers (Yousif, Abdullah, Salem, Juma and Mohammed) for their endless encouragement to get this degree. They were patient to have me away from them for the first time for four years. They gave me the full support as the first young female to stay abroad and get the PhD. I would like to extend my gratitude to uncle Juma, Badar Al Kaabi and all my friends in Abu Dhabi and Edinburgh. My cousin, brother and friend Khamis deserves tremendous thanks for his continuous support. Special thanks go to my closest fiend Maryam Al Blooshi for being friend, sister and mother in Edinburgh while I am away from my family. I should also thank my closest friends in Abu Dhabi Mariam Alattar and Miaad Alhammadi for keeping in contact with me and helping me remotely.

Finally, I would like to say that without my supervisor, family, friends and all nice people surrounding me I will not be where I am today. Thank you All.

# ABSTRACT

Carbonate rocks consider as significant reservoirs for hydrocarbon. More than 60% of the world's hydrocarbon is placed in carbonate reservoirs. Carbonate rocks are heterogeneous and contain complex pore system. This complexity causes the hydrocarbon recovery from these reservoirs difficult; having less than 35% of hydrocarbon is being recovered. The heterogeneity and the variation in pore system are a result of various depositional settings and successive diagenetic overprints. Diagenetic overprints account for most of the pore system complexity in subsurface. This project undertakes one of the important diagenetic processes, calcite cementation, which though to have major impact on reservoir quality. The project aims to better understand the controls on calcite cementation in five Lower Cretaceous Reservoirs, in particular the role of calcite cementation with relation to oil charge in reservoir quality. Other diagenetic processes were also asses including dolomitization, dissolution, micritization and chemical compaction.

The five reservoirs (A, B, C, F & G) are from Field A which is located in Abu Dhabi, UAE. The reservoirs comprise of interbedded porous "Reservoir" and low porosity-permeability "Dense" limestones deposited in broad range of settings, ranging from restricted to open marine platform. Reservoir intervals are part of HSTs, deposited during higher sea level time. The dense intervals were deposited during TST and thought to be cemented early resulting in early compartmentalization in all reservoirs.

The mMg/Ca and in-situ (SIMS) $\delta^{18}O_{VPDB}$ were measured through complete calcite cement stratigraphy obtained from equant, syntaxial and blocky calcite in all reservoirs. Both mMg/Ca and $\delta^{18}O_{VPDB}$ of oldest calcite cement zone are matching with published mMg/Ca and $\delta^{18}O_{VPDB}$ of Lower Cretaceous, suggesting precipitation from Lower Cretaceous seawater. The mMg/Ca and $\delta^{18}O_{VPDB}$ also vary from reservoir to another reflecting change in Cretaceous seawater. These data also coincide with trace element observations particularly Mn and Sr. All these parameters show fluctuations in Cretaceous seawater during 135-123Ma caused by global changes in climate and oceanic crust production rates. Lower reservoirs including F (133Ma) and

C (130Ma) were more probably affected by the Hauterivian global cooling which resulted in higher $\delta^{18}O_{VPDB}$ in the early precipitated cements. Precipitation in upper Reservoir B (126Ma) was most likely affected by the abrupt warm episode just before the OAE1. Reservoir A (123Ma) precipitation may be affected by the Early Aptian cooling episode and the OAE1. Reservoir G is the only one not recording $\delta^{18}O_{VPDB}$ similar of Cretaceous seawater. Cementation in Reservoir G was affected by depleted $\delta^{18}O_{VPDB}$ fluids from early stage, perhaps hot, basinal waters.

More interestingly, the mMg/Ca, $\delta^{18}O_{VPDB}$ Mn and Sr means of younger calcite cement zones which thought to be evolved during burial show similar trend to the oldest cement zones with various offsets. This suggests that calcite cement in each reservoir evolved in a relatively close system inferring by this that the reservoirs are compartmentalized. The compartmentalization is probably due to the sysedimentary or early cemented hardgrounds in the Dense Zones. The Dense Zones acted as seals for the reservoirs from early stage causing the later precipitated calcite cement which is diagenetically affected to behave in predictable and similar way. Moreover, calcite precipitation temperatures inferred from mMg/Ca and $\delta^{18}O_{VPDB}$ show progressive increase towards younger cement zones indicating fluid evolution with burial in also relatively close system.

In-situ $\delta^{18}O_{VPDB}$ and oil inclusions suggest earlier oil charge in the shallower reservoirs compared with deeper reservoirs and coeval water leg. Consequently, cementation in the shallower reservoirs continued with lower rate and hence preserved some primary and secondary pores. Conversely, in the water leg cementation continue to occlude most of the pore spaces. Furthermore, early oil emplacement in the shallower reservoirs increased the cementation temperature of calcite in the oil leg to reach maximum precipitation temperatures of ~144˚C. Whereas, in the water leg and deeper reservoirs, cementation continued to a temperature of ~110˚C.

Overall, reservoir quality in Thamama Group was affected by various diagenetic processes. Some have resulted in reservoir quality enhancement such as dolimitization which involves formation of microporosity as a result of replacive rhombic dolomite, dissolution particularly the late one which believed to be due organic acid, and micritization with yield microporosity particularly in Reservoir B. Open fractures

might have also enhanced reservoir quality to some extent. Diagenetic events that have deteriorated reservoir quality include calcite and saddle dolomite cementation as well as stylolitization. Greater calcite cementation can be found in water leg compared with oil leg because oil thought to decrease cementation rate.

# LAY SUMMARY

Porosity and permeability are two important properties in rocks need to be considered for better hydrocarbon productivity. These two properties can be affected considerably by processes called diagenesis. Diagenesis refer to all processes which affect and alter the rock after deposition and can start at shallower depth and continue to deeper burial. Such processes often alter the original depositional porosity and permeability making them difficult to correlate and predict in subsurface particularly in carbonate rocks. Porosity and permeability can be enhanced by diagenesis such as dissolution or destroyed by cementation. Moreover, these two properties can be preserved if oil charge have occurred at earlier time because oil thought to retard of stope cementation. In carbonate rocks, calcite and dolomite are the most dominant types of cement. This study looks at the dynamics and the impact of calcite cementation with relation to oil charge in reservoir quality. The study examines carbonate rocks of five reservoirs from Lower Cretaceous Thamama Group, UAE. Main methods used to complete this study include petrographic examination (conventional and cathodoluminescence), Electron Probe Microanalysis (EPM), oil inclusions examination and Ion Microprobe (In-situ $\delta^{18}O_{VPDB}$ Evaluation). Comprising all data obtained from all these different methods helped to understand the evolution of calcite cementation through time and relative to oil charge. We see that early oil charge in some reservoirs have preserved some porosity and hence resulted in better reservoir quality. Whereas, in other reservoirs where oil charge came later calcite cementation went further and hence decreased the porosity.

# CONTENTS

# LIST OF FIGURES

# LIST OF TABLES

# Chapter 1: Introduction

## 1. Introduction

More than 60% of global hydrocarbons are conserved in carbonate reservoirs, but <35% of hydrocarbon is being recovered (Burchette, 2012; Xie et al., 2005). This is mainly due to the complexity and heterogeneity caused particularly by various pore systems. Pore size can range from micro to macro scale with diverse pore shapes. The variation in pore size and shape is attributed to the wide range of depositional settings of carbonates as well as diagenesis. Diagenesis can extensively modify original pore systems making porosity and permeability correlation difficult to understand and predict in subsurface (Ehrenberg and Nadeau, 2005; Ehrenberg et al., 2008; Lucia, 2007). One of the main diagenetic events that can effectively reduce pore space is cementation. Dissolution can increase pore space resulting higher porosity and permeability.

The Lower Cretaceous (Berriasian to Aptian) Thamama Group hosts important oil reservoirs and is one of the main producing carbonates in the United Arab Emirates (UAE) (Alsharhan et al., 2000). Several studies have been conducted to characterize the giant anticlinal structure oil fields of onshore and offshore Abu Dhabi (Figure 1.1), and it has been reported that porosity varies dramatically across the anticlinal structures, where the crest rocks hold higher porosity compared to those in the flank (Figure 1.2; Alsharhan and Sadd, 2000; Melville et al., 2004) . This porosity variation has been related to the greater extent of calcite cementation in the flank (water leg) than in the crest (oil leg) because oil charge is thought to retard or stop diagenesis completely (Neilson et al., 1998; Oswald et al., 1995; Paganoni et al., 2016; Strohmenger et al., 2006). Therefore,

understanding, the dynamics of the calcite cementation in response to oil charge is vital to predict the evolution of reservoir quality.

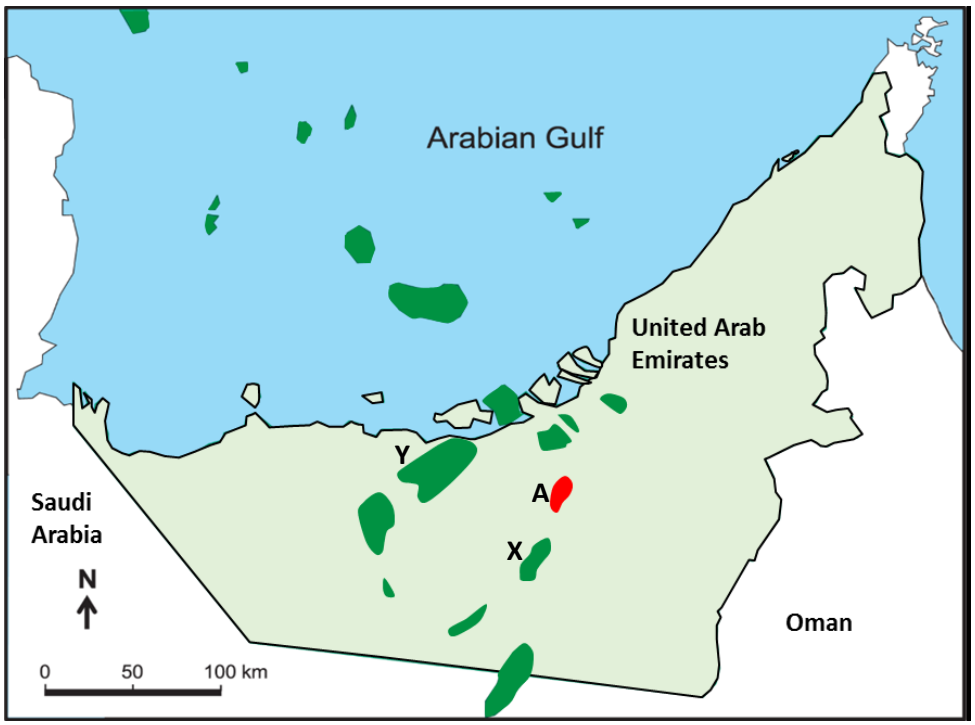


Figure 1.1: Location map of onshore and offshore oil Files in Abu Dhabi, UAE. Modified after Ehrenberg et al. (2016). Field of study is shown in red (A). X and Y are two nearby Fields producing from Lower Cretaceous Thamama Group.

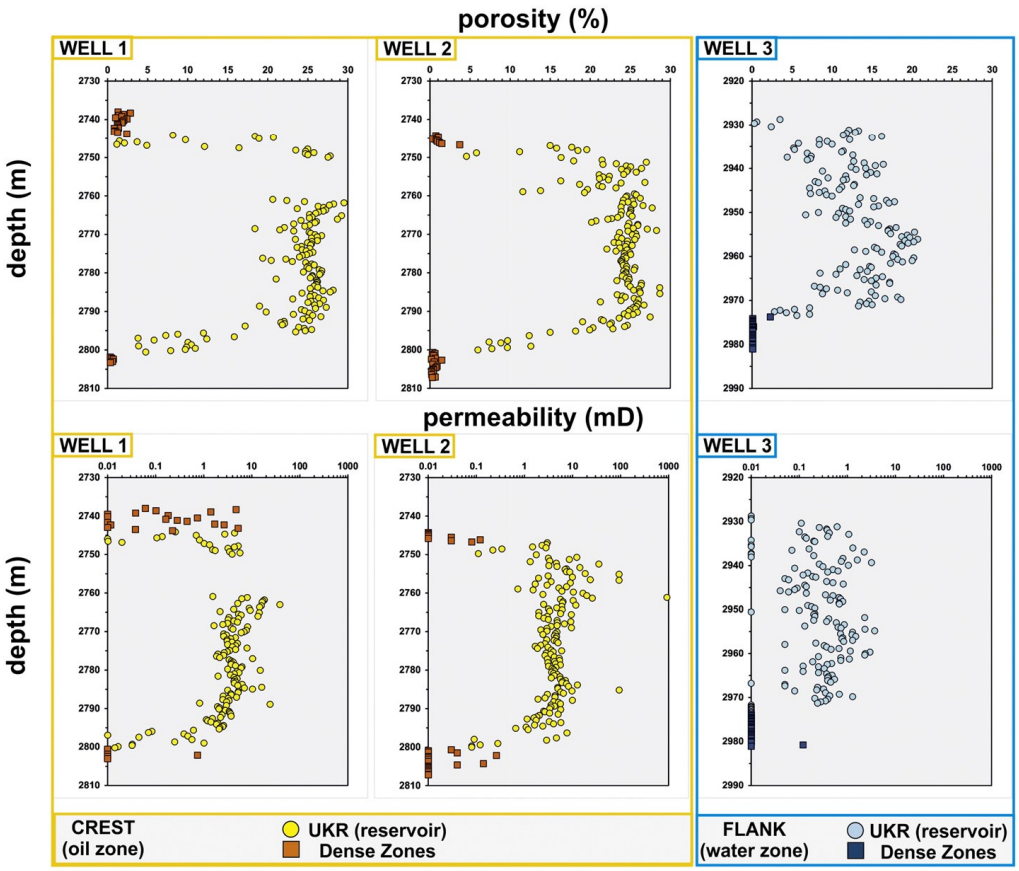


Figure 1.2: Porosity and permeability data vs depth of 3 wells; two from crest and one from flank containing upper Kharaib porous reservoir and low poroperm Dense Zone (Paganoni et al., 2016). The upper Kharaib reservoir shows higher poroperm in the crest compared with the flank.

The Thamama Group consists of thick sequence (800-1000 m) that was deposited in shallow-marine, shelf environment. It is characterized by interbedded porous and low porosity-permeability limestones. The low porosity-permeability intervals are known as Dense Zones which represent the shaded intervals in Figure 1.3. The Group is divided into four main Formations, including the Shuaiba, Kharaib, Lekhwair, and Habshan from youngest to oldest respectively (Alsharhan, 1990). It is further subdivided into smaller subunits with different subdivisions for onshore and offshore fields (Figure 1.3).

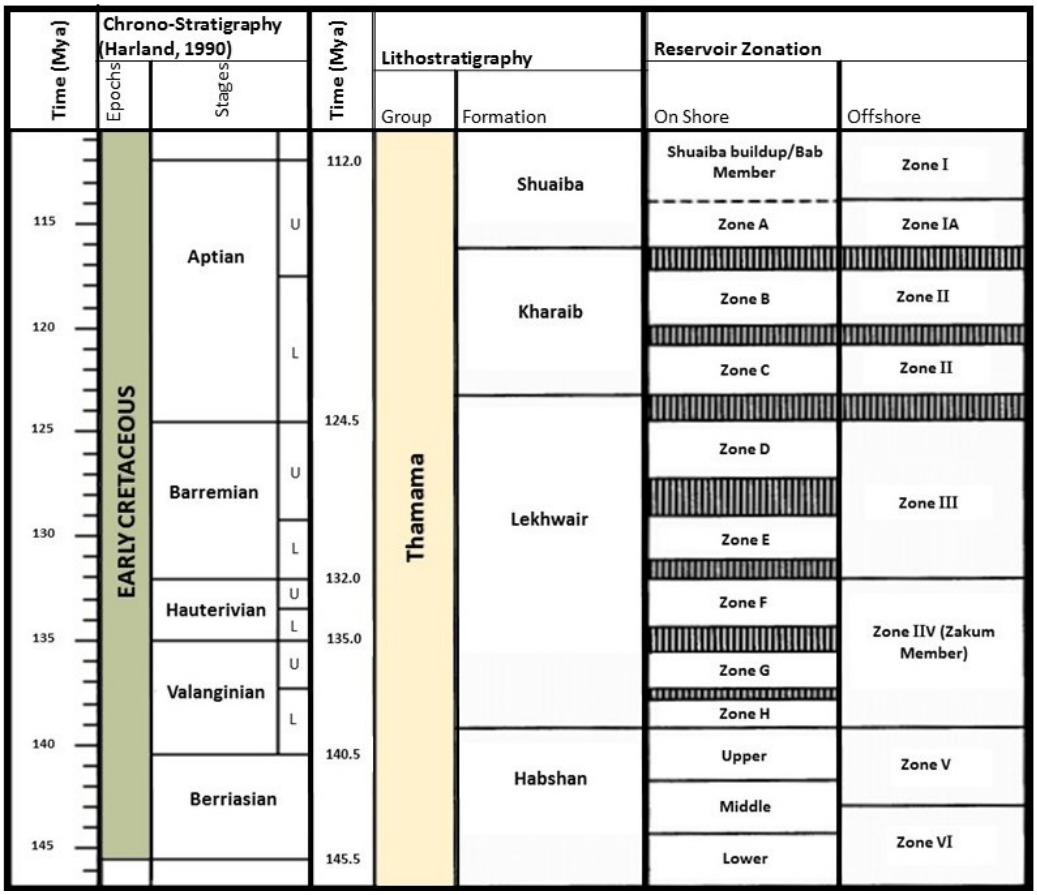


Figure 1.3: Chronostratigraphy and subdivision of Early Cretaceous Thamama Group into main Formations and subzones, onshore and offshore Abu Dhabi. Modified from Vahrenkamp (1996) and Alsharhan and Sadd (2000).

This project undertakes a study of the Group including five reservoirs in an onshore Field (Field A) in U.A.E (Figure 1.1) to better understand relationship between oil charge and calcite cementation by quantifying the dynamics of the calcite cementation and constraining the conditions and controls under which cements in the oil and water leg were precipitated. In another words, how much has cement been precipitated, and where and when?

To complete this work, several methods have been undertaken. Conventional petrography was completed to obtain comprehensive record on overall diagenesis processes, timing of each diagenetic process relative to the other and the impact of these processes on reservoir quality. Ion Microprobe along with cathodoluminescence (CL), electron probe microanalysis (EPMA) and fluid inclusions analysis is a complementary way to understand the dynamics of calcite cementation in response to oil charge (Cox et al., 2010; Heydari and Moore, 1993; Lyon et al., 2000; Thorpe, 2014). CL was used at the beginning to distinguish and identify several calcite zones within cement and therefore construct cement stratigraphy. CL was used also to see how the pore space is occluded and to quantify total precipitated cement in oil versus water leg. Using the cement stratigraphy, trace elements and $\delta^{18}O_{VPDB}$ were obtained to understand origin, temperature and pore fluid chemistry evolution from oldest to youngest cement zone. This also was used to understand the controls on cementation at several precipitation time. The presence of oil fluid inclusions (FI) was utilized to understand the timing relationship between calcite growth and oil charge (Cox et al., 2010; Neilson et al., 1998; Thorpe, 2014).

## 1.2 Research Hypotheses

This study considers five carbonate Reservoirs (A, B, C, F & G) from Field A which is situated in the Rub Al Khali Basin in United Arab Emirates (Figures 1.1 & 1.3). This is an onshore giant oil field characterized by faulted and fractured anticline with a length of approximately 25 km and a width of 7.5 km. The five reservoirs were deposited during the second second-order supersequence of Thamama Group (Valanginian-Aptian) and dominated by packstone and grainstone facies. The main oil production come from Reservoir B which is the thickest reservoir.

In order to better understand controls and dynamic of calcite cementation and its relation to reservoir quality, the following hypotheses have been tested:

***Oil charge retards diagenesis and retains better reservoir quality***

- A full diagenetic assessment was conducted to 1) understand and compare diagenesis in oil versus water leg and their impact on reservoir quality, 2) construct paragenetic sequences to understand timing of each diagenetic event relative to other diagenesis and to oil emplacement. 3) assess cement abundance in both oil and water legs to understand the impact of diagenesis on reservoir quality in two different zones.
- A cement stratigraphy of the main pore occluding cements was constructed based on CL zonation to 1) distinguish several cementation growth based on ferroan and non-ferroan criteria, 2) to quantify total precipitated calcite cement in oil versus water leg.

***Calcite cementation is dynamic and sensitive to change in fluid composition, temperature and oil charge***

- A geochemical study of different calcite cements was undertaken in order to 1) unravel the chemical composition and origin of pore fluids corresponding to precipitation of different calcite cements in oil and water legs using Sr variation and the redox sensitive elements Fe and Mn, 2) investigate the palaeotemperature of the fluids of the precipitated cements using $^{m}Mg/^{m}Ca$ molar ratio both in oil and water leg. This is to understand dynamic of calcite cementation in oil versus water leg.

- The chemical composition of dolomite cement in the Thamama Reservoirs was also investigated to unravel the origin of pore fluids which involved in its formation and its relation to the latest phase of calcite cementation (the second generation of blocky calcite).

- A study of high resolution Secondary Ion Mass Spectrometer (SIMS) in-situ $\delta^{18}O_{VPDB}$ study was conducted for different calcite types to 1) investigate the temperature evolution of pore fluids of calcite cements, 2) reconstruct the timing and chemical conditions of individual calcite cements relative to each other and to the timing of oil emplacement.

- A final comparison and correlation was made between mMg/Ca ratio and in-situ $\delta^{18}O$ data to elucidate the temperature evolution of pore fluid stratigraphically and across individual reservoirs and thus understand dynamic of calcite cementation using more than one proxy. Trace elements including Mn and Sr were also correlated with the two independent proxies to investigate precipitation conditions.

## 1.3 The Early Cretaceous Climate

The Early Cretaceous is known to be a time of greenhouse climate characterized by higher sea-level (100 ± 50 m) compared with present day sea-level (Föllmi, 2012; Miller et al., 2005). The greenhouse period is mostly attributed to the major increase in *p*CO2 (50-70%) caused by oceanic crust spreading and related volcanic activities (Balthasar and Cusack, 2015; Bots et al., 2011; Hardie, 1996; Larson, 1991; Larson and Erba, 1999; Morse et al., 1997; Steuber and Veizer, 2002; Timofeeff et al., 2006). Indeed, these activates have also caused variation in seawater chemistry (e.g. mMg/Ca).

However, within Early Cretaceous there were periods of major cooling related to the possible development of ice caps at higher latitudes. These cooling events probably caused the Early Cretaceous climate to fluctuate between arid and humid conditions (Föllmi, 2012; Steuber et al., 2005). One of the major cooling event was found at Berriasian-Valanginian boundary identified from glendonites, tillites and

dropstones and $\delta^{18}O_{VPDB}$ of belemnites found at higher latitudes (Föllmi, 2012; Price and Mutterlose, 2004; Price, 1999; Price and Nunn, 2010). Two more cooling events were recognised from $\delta^{18}O_{VPDB}$ of rudists during Late Valanginian, and Early Aptian (Pucéat et al., 2003; Steuber et al., 2005).

The mineralogy and chemistry of carbonate sediments is thought to be controlled by seawater chemistry. Early Cretaceous is classified as a Calcite Sea having low-Mg calcite precipitates (Figure 1.4; Dickson, 2004; Hardie, 1996). Low-Mg calcite precipitation is commonly favoured by a molar (m) Mg/Ca below 2 (Folk, 1974). Above an mMg/Ca of 2, high-Mg calcite and aragonite cements are dominant (Hardie, 1996; Sandberg, 1983; 1985; Spencer and Hardie, 1990). The mMg/Ca of Early Cretaceous low-Mg calcite cement was 1:1 lower compared with today's (5:1) aragonite cement (Dickson, 2004; Dickson et al., 2008; Hardie, 1996).

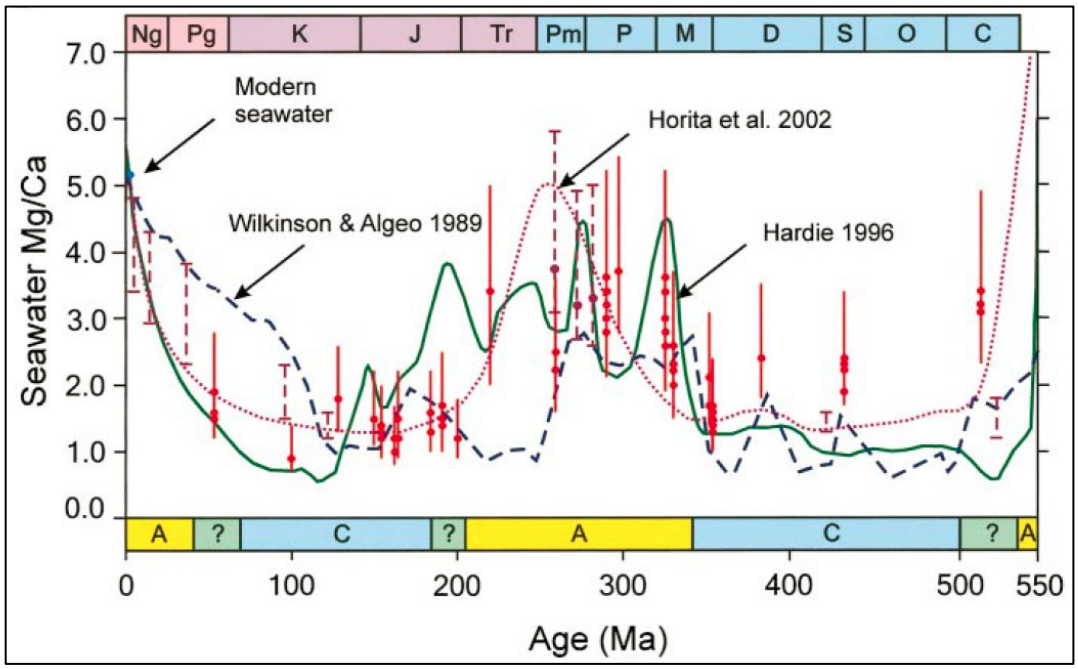


Figure 1.4: Variation in seawater chemistry (Mg/Ca molar ratio) during Pherozoic. C: Calcite Sea, A: Aragonite Sea. Early Cretaceous Mg/Ca ranges from ~0.7 to 2 (red dots; Dickson, 2004).

## 1.4 The Thamama 'Group'

### 1.4.1 General Tectonic and Stratigraphic Setting of the Region

The main tectonic events that have affected the UAE region are summarized below followed by focused tectonic and stratigraphic setting of Thamama Group.

- Late Precambrian Najd shear-zone-related rifting which resulted in formation of rift salt basins (Alsharhan, 2014).
- Late Carboniferous uplift and erosion event caused by Hercynian Orogeny (Pinnington, 1981).
- Mid Permian rifting event which separated parts of Iran (central and northwest) and Turkey from Gondwana margin which resulted in Neo-Tethys 1 opening (Ali and Watts, 2009; Ziegler, 2001).
- Late Triassic-Early Jurassic rifting and sea-floor spreading which is following the previous Mid Precambrian rifting caused the spreading of Neo-Tethys 1 in Oman and Zagros and formation of Neo-Tethys 2 in East Iran (Alsahrhan and Kendall, 1991).
- Late Cretaceous compressional deformation event which comprised the ophiolite obduction onto SW Tethyan rifted margin (Ali and Watts, 2009; Glennie, 2000).
- Paleogen-Quaternary compressional event which included the Arabian and Eurasian plates collision that resulted in formation of Zagros orogenesis build-up (Ali and Watts, 2009; Glennie, 2000).

The Thamama Group was deposited on the rifted margin of the Tethyan Ocean started at around 145 Ma with the Habshan Formation (Ali and Watts, 2009; Glennie, 2000). The structural development of most UAE fields including Thamama Formations

was established in Late Cretaceous (Late Cenomanian-end of the Early Masstrichtian) as a result of the compressional deformation which resulted in emplacement of number of NE Oman orogenic belts including Semail Ophiolite onto SW Tethyan rifted margin deposits (Ali and Watts, 2009; Glennie, 2000; Oswald et al., 1995). The orogenic belts in the nearby Oman Mountains and the ophiolites obduction resulted in doming of Precambrian salts and formation of number of anticlines and faults in the region as well as the development of a westward foreland basin in the UAE. An early oil-water contact (OWC) was established in each affected field (Oswald et al., 1995). The formation of salt domes is interpreted to be as a result of diapirism of the Precambrian Hormuz salt during Jurassic (Alsharhan et al., 2001; Alsharhan and Salah, 1997; Murris, 1980). The Hormuz salt covers mostly the offshore area. However, the diapirism of this salt is thought to have caused formation of traps in some onshore fields (Alsharhan and Salah, 1997).

The region remained stable until Late Eocene-Miocene second compressional event after deposition of Upper Cretaceous and Lower Tertiary successions (Figure 1.5). The second compressional event comprised of the collision of Arabian and Eurasian Plates which resulted in the Zagros orogenesis build-up, re-activation of preexisting faults and folds, formation of large scale folds, and uplift in the western flank of the northern Oman Mountains (Ali and Watts, 2009; Glennie, 2000). The structures continued to evolve as a result of continuous deformations in Oman and Zagros Mountains. The same deformations caused tilting to a number of existing fields into the water leg and therefore establishment of new OWC; e.g. “A” Field (Oswald et al., 1995). The tilting of the Field A structure into water leg caused stylolitization and calcite cementation, and hence a deterioration of reservoir quality. Abundant stylolites with significant amplitudes were recorded in the flanks in the regional fields (Ehrenberg, 2016; Paganoni, 2016).The well-developed stylolites can partly explain the thinning in the strata observed toward the flanks of the structure (Alsharhan and Sadd, 2000; Oswald et al., 1995).

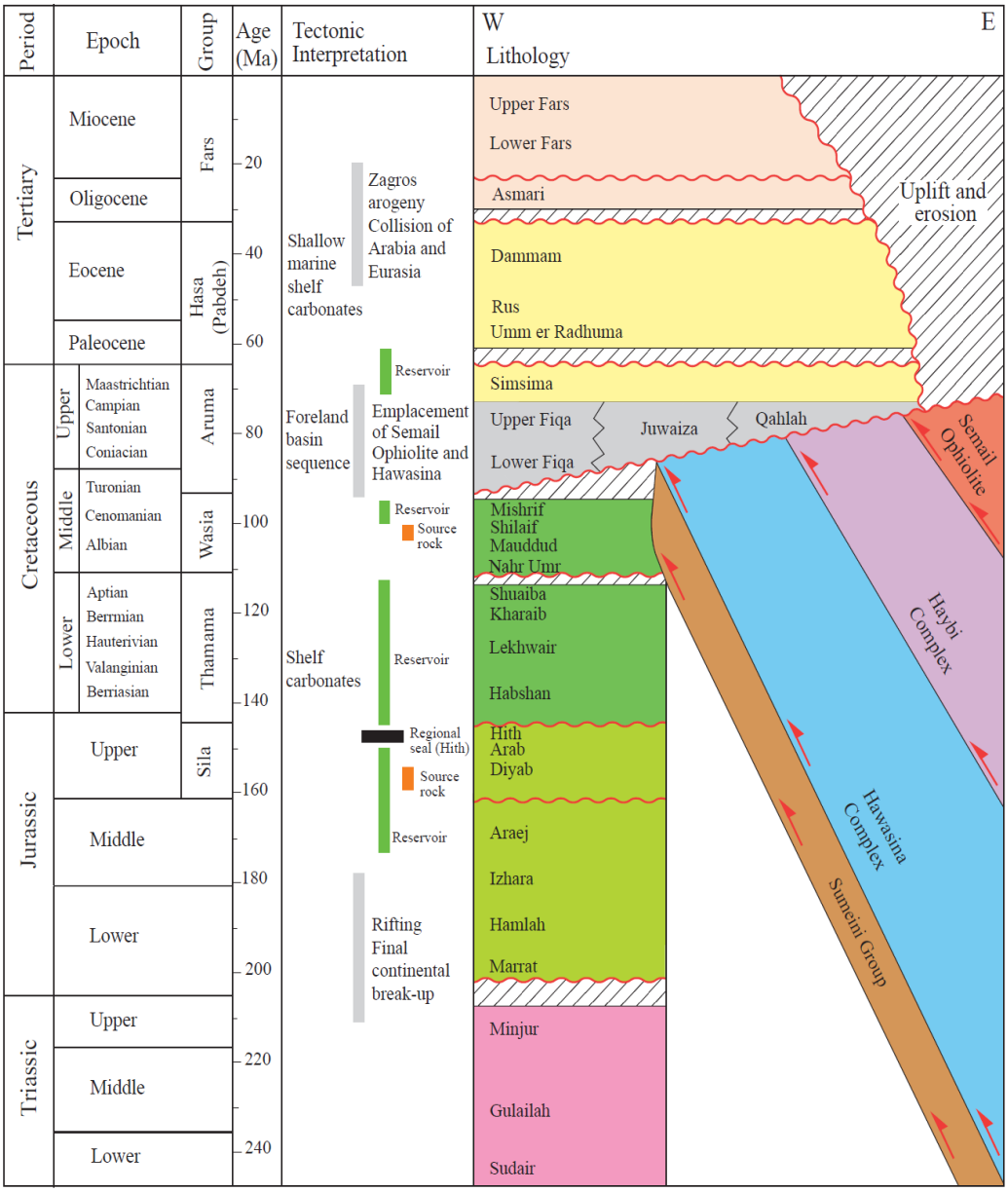


Figure 1.5: Tectonic and stratigraphic column of UAE rift margin and foreland basin sequence, West–East UAE region (Ali and Watts, 2009).

The Field of study comprises lots of parallel faults oriented NW-SE. These faults are arranged in conjugate sets oriented as N75°W & N45°W (Morad et al., 2010). Most of the major faults in this area are believed to be developed during Eocene-Miocene compressional event (Zagros orogenesis). There are two main fracture sets in the area one

is oriented E-W and other one N-S (Sirat et al., 2007a, b). These fracture sets were most likely developed as a result of continuous deformation in the region from Late Cretaceous to Late Eocene compressional stresses as well as the red sea rifting.

### 1.4.2 Sequence Stratigraphic Framework and Depositional Environment of Thamama Group

The Thamama Group comprises of two second-order supersequences (Figure 1.6) which contain transgressive and highstand sequence sets (Sharland et al., 2013; Strohmenger et al., 2006). The older supersequence includes Habshan Formation and it is Berriasian and early Valanginian in age. The younger supersequence, Valanginian to Aptian in age, includes top Habshan, Lekhwair, Kharaib and Shuaiba Formations including Hawar (upper Dense Zone). This study comprises rocks only from Lekhwair, Kharaib and few from Shuaiba however, brief description about Habshan Formation will be given.

Thamama Group was deposited in a wide range of depositional environments ranging from restricted to open platform margin (Figures 1.7 & 1.8). Reservoir facies were deposited in open platform, shoal and mainly ramp setting (Figure 1.7). Dense Zones were mostly deposited in restricted platform, subtidal to inner shoal (Figure 1.8). These Zones are highly cemented, low porosity and permeability rocks and known to be effective barriers for reservoirs (Alsharhan and Sadd, 2000; Strohmenger et al., 2006).

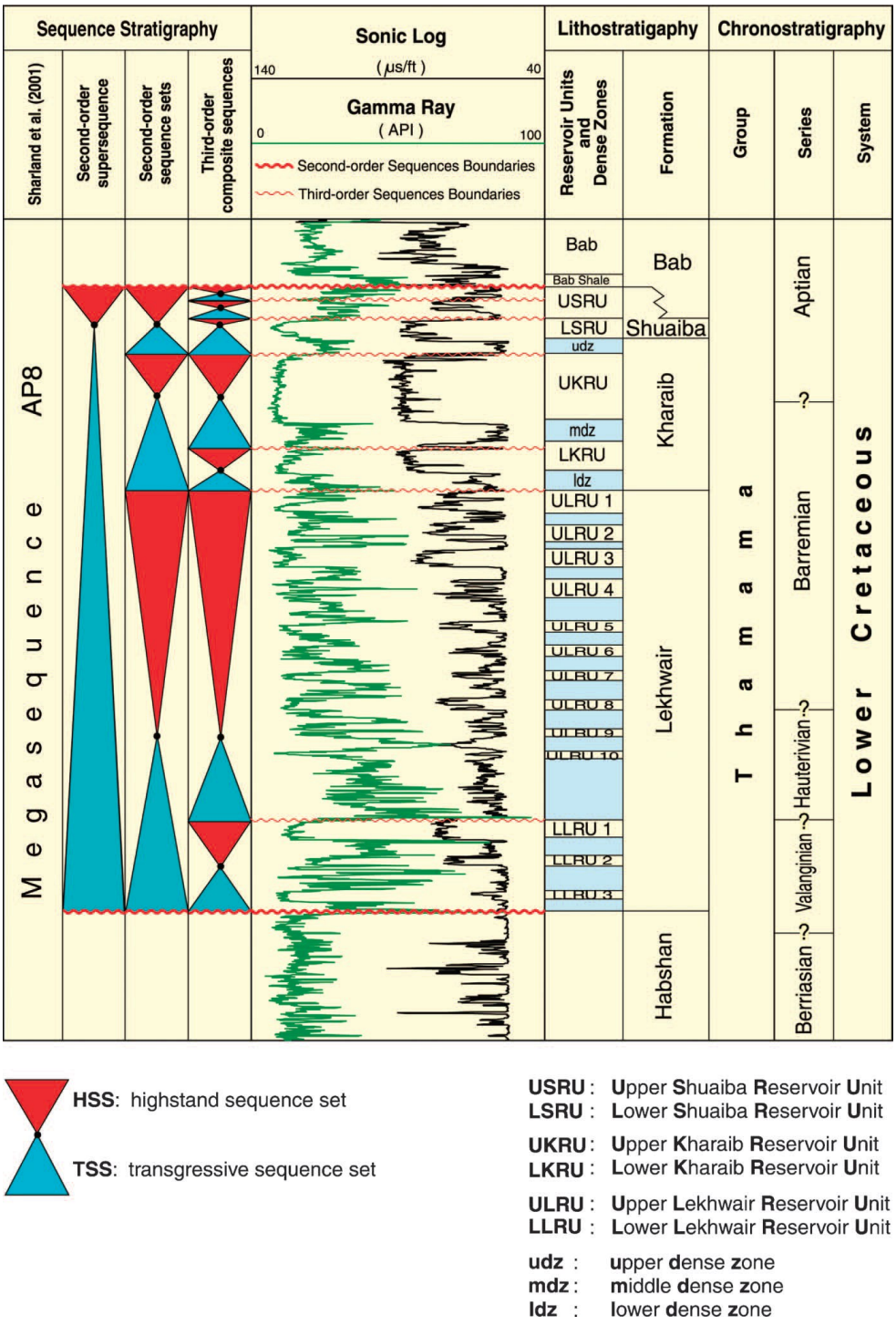


Figure 1.6: Sequence stratigraphic framework of Lower Cretaceous Thamama Group showing second-order supersequences, second-order sequence sets and third-order composite sequences (Strohmenger et al., 2006).

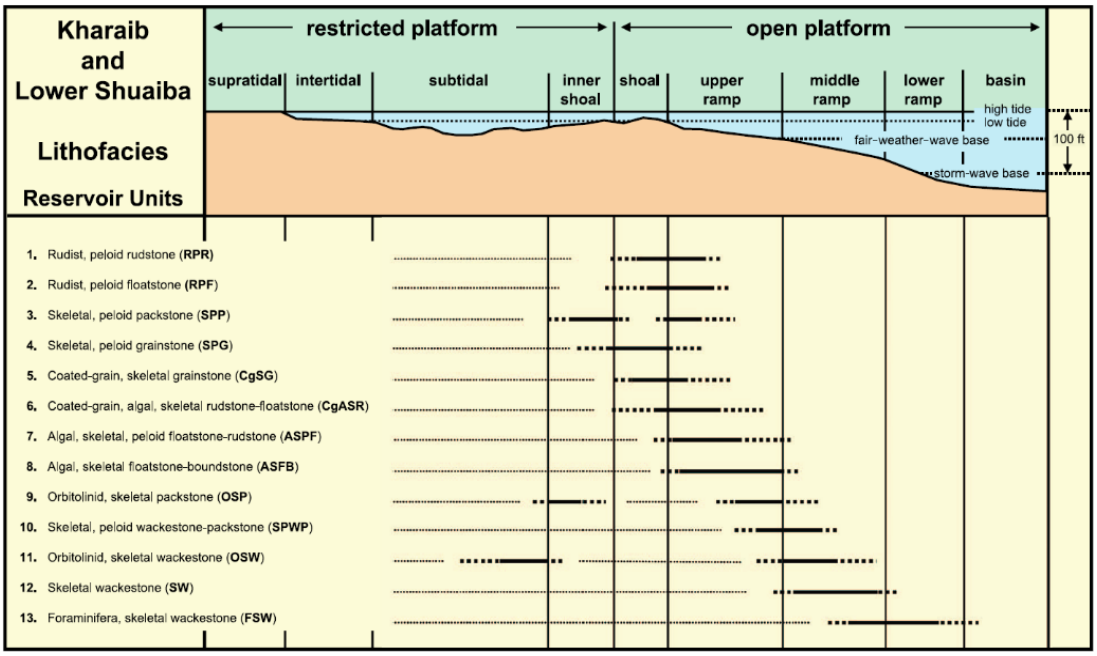


Figure 1.7: Depositional environment of Kharaib and Lower Shuaiba lithofacies of reservoir intervals, can be apply also for Habshan and Lekhwair (Strohmenger et al., 2006).

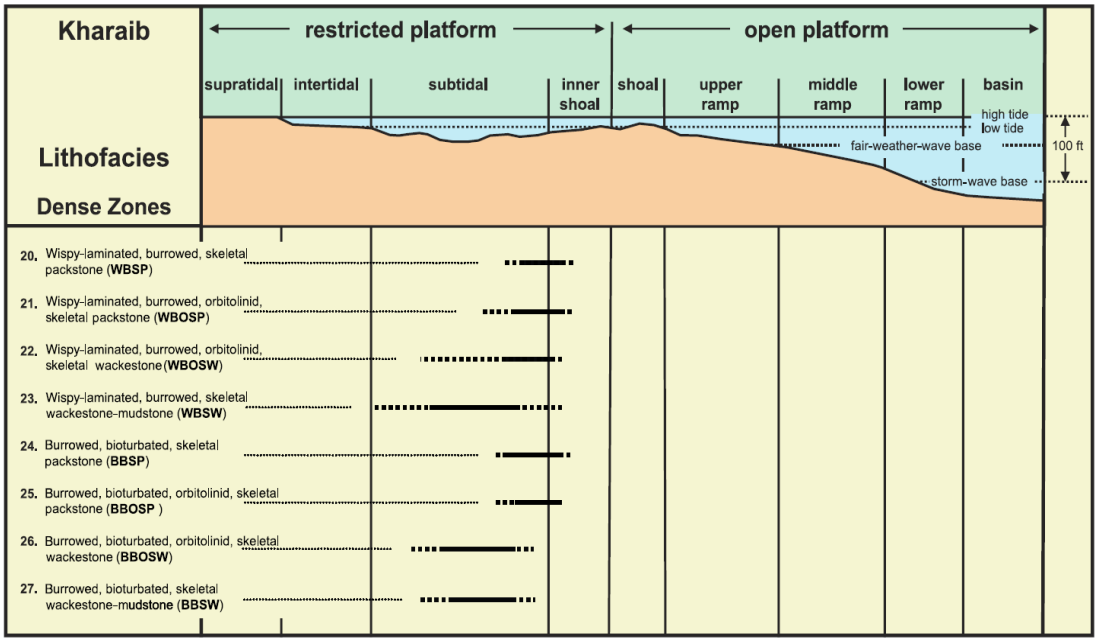


Figure 1.8: Depositional environment Dense Zone lithofacies (Strohmenger et al., 2006).

The Habshan Formation represents the early transgressive sequence (ETST) set of the old supersequence showing generally progradational patterns towards East Abu Dhabi (Al-Zaabi et al., 2005; Harris et al., 1984). The Habshan Formation of Abu Dhabi is dominated by lagoonal lime mudstones and wackestones to the west and high energy self-margin oolitic packstone/grainstone to the east (Al-Zaabi et al., 2005; Alsharhan, 1993). The oolitic packstone/grainstone are considered as the main reservoir facies of Habshan Formation. The ETST of Habshan Formation composes of two second-order composite sequences; lower second-order composite sequence which consists of two third-order composite sequences (transgressive and highstand sequence sets), and upper second-order composite sequence that made up by three third-order composite sequences (Lowstand (LSS), Transgressive (TSS) and Highstand (HSS) Sequence Sets).

The Lekhwair Formation belongs to the late trangressive sequence (Figure 1.6) set of the younger Thamama supersequence which also covers sequences from top Habshan to top Kharaib Formation and part of Lower Shuaiba Formation (Al-Hosani, 2006; Strohmenger et al., 2006). Lekhwair Formation represents the first third-order composite sequence of the younger supersequence and it is composed of three fourth-order High Frequency Cycles (HFCs) including; three reservoir intervals and three non-reservoir intervals (Dense Zones). The Lekhwair Formation of Abu Dhabi represents cycles of normal marine deposites; alternating pattern of high porosity-permeability reservoir facies and low porosity-permeability Dense Zones recording sea-level fluctuation (Azer and Toland, 1993; Al-Hosani, 2006; Alsharhan, 1993; Harris et al., 1984). The reservoir intervals (LLRU & ULRU; Figure 1.6) are characterized by *Bacinella/Lithocodium* packstone-floatstone, floatstone-rudstone, and boundstone deposited in open platform, upper to middle ramp to restricted platform subtidal to intertidal environment (Alsharhan, 1989; Alsharhan and Kendall, 1991). The Dense Zones are marked by bioturbated aragonitic and non-aragonitic (siliciclastic) wackestone and packstone deposited in an inner platform environment (Al-Hosani, 2006; Granier et al., 2003). The transition from Lekhwair to Kharaib is marked by third-order Sequence Boundary (SB, K50) that can be extended for hundreds of kilometres on the platform (Hillgärtner et al., 2003; van Buchem

et al., 2002; Strohmenger et al., 2006). This SB is suggested to be a subaerial exposure surface in which the leaching of aragonitic bioclasts occurred (Granier et al., 2003). Enhanced depositional porosity also suggested to be occurred during time of relative sea-level falls as a result of freshwater leaching (Alsharhan and Kendall, 1991).

The second and third third-order HFCs of the younger Thamama supersequence are within the Kharaib Formation (Alsharhan and Kendall, 1991; Strohmenger et al., 2006). The two third order composite sequences show aggradational and progradational stacking patterns of fourteen fourth-order parasequence sets and several fifth-order parasequences (Figure 1.9) (Alsharhan and Kendall, 1991; Strohmenger et al., 2006; Vahrenkamp, 2010; Van Buchem et al., 2010). However, Granier et al. (2003) subdivided Kharaib into four third order cycles. The Kharaib Formation in Abu Dhabi shows a similar cyclic pattern to that recorded in Lekhwair Formation. It is dominated by mud-supported facies (firmgrounds and interbedded organic and siliciclastic-rich limestone) in the lower part and grading up to show diverse marine fauna and flora dominated by *Orbitolina*, peloid, bioturbated and burrowed skeletal fragments packstones, grainstones and rudstone. The mud-supported facies (middle dense facies) represent the TSTs of Kharaib Formation and can be correlated for tens to hundreds of kilometers across the platform (Strohmenger et al., 2006). The grain dominated facies represent the HSTs of Kharaib Formation which deposited during highest sea-level episodes (Hillgärtner et al., 2003). The depositional environment of the dense and reservoir facies is ranging from low energy restricted to moderate-high energy open marine platform respectively (Figures 1.7 & 1.8). According to the sequence stratigraphic framework established by Stronhmenger et al. (2006), four third-order composite sequence boundaries (SB), three composite maximum flooding surfaces (MFS), and thirteen third-or higher order marine flooding surfaces of Kharaib and Lower Shuaiba Formations can be identified (Figure 1.9). The two SBs of Kharaib are interpreted to be subaerial exposure surfaces (Strohmenger et al., 2006), while no evidence of such surfaces found by Granier et al. (2003). The K60 is placed between LKRU and UKRU (Figures 1.6 & 1.9) (Strohmenger et al., 2006; Van Buchem et al.,

2010) or within LKRU as the case of Wadi Mu' Ayin (Van Buchem et al., 2002a). The K70 is typically located at top of UKRU and the base of Dense Zone (equivalent Hawar).

The final Shuaiba Formation was deposited during third-order depositional sequences made up of two transgressive sequences and a highstand sequence of the upper second-order supersequence (Figures 1.6 & 1.9; Alsharhan et al., 2000; Haq et al., 1988; Strohmenger et al., 2006). The Shuaiba Formation is divided into two main units; Lower Shuaiba Member and Upper Shuaiba Member. The Lower Shuaiba Member (Reservoir Unit (LSRU)) consists of shallow to deep water limestone (algal boundstone, skeletal, peloid wackestone-packstone and foraminifera, skeletal wackestone) in the lower section (Hawar TST) and deep to shallow marine limestone (foraminifera, skeletal mudstone-wackestone shallowing-upward to skeletal, peloid wackestone-packstone) in the upper section (HST) (Alsharhan, 1993; Alsharhan et al., 2000; Strohmenger et al., 2006). The top of LSRU is marked by third order subaerial exposure SB (K80; Figure 1.9) which contradict with Granier et al. (2003) where no evidence of subaerial exposure found. The Upper Shuaiba Member (Reservoir Unit (USRU)) is characterized by shallowing upward rudist and algal platform sediments which form progradational stacking pattern known as "Shuaiba clinoforms" (Alsharhan, 1993; Granier et al., 2003). The Bab Member is equivalent to Upper Shuaiba Member which developed in the central Abu Dhabi intrashelf basin (mid-ramp) (Alsharhan and Nairn, 1986; Azer and Toland, 1993; Alsharhan et al., 2000). It is made up of deep-water argillaceous mudstone, peloidal argillaceous packstone-wackstone and skeletal foraminiferal argillaceous wackstone-packstone. The USRU which represents the last deposition of Thamama Formation is well marked by second order exposed SB (K90) (Alsharhan and Kendall, 1991; Strohmenger et al., 2006).

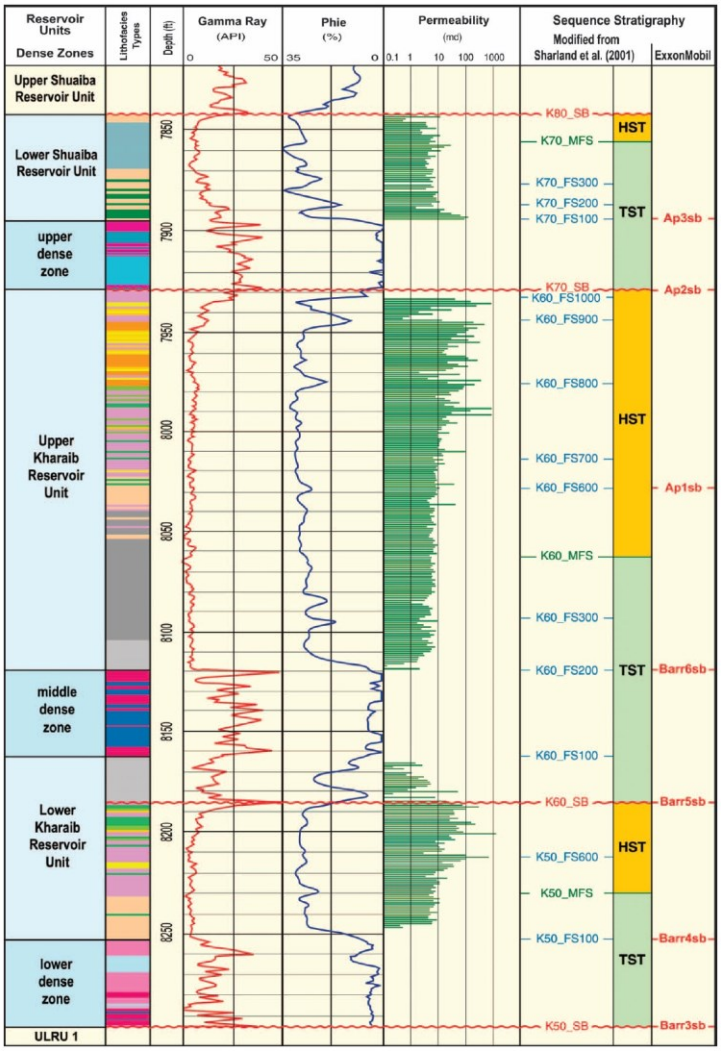


Figure 1.9: High resolution sequence stratigraphic framework of the Kharaib and Lower Shuaiba Formations (Strohmenger et al., 2006).

### 1.4.3 Diagenesis and Reservoir Quality in Thamama Group

Reservoir quality in Thamama Formations is controlled by depositional facies and diagenetic overprints affecting these depositional facies (Alsharhan, 1990; Oswald et al., 1995). The various depositional facies in Thamama Formations introduce variation in porosity and permeability. The preserved depositional primary pores including intergranular and macroporosity (vuggy and moldic) thought to have significant impact on pore system in grainstone and packstone facies (Neilson et al., 1996; 1998). However, the most significant control on reservoir quality in Thamama Reservoirs is attributed to diagenetic alterations which can occur early (shallow) and/or late (burial).

The early diagenesis in Thamama Formations can be mainly summarized by formation of early circumgranular calcite precipitated in shallow marine water, secondary porosity (including moldic intragranular and vuggy) formed during meteoric vadose leaching during relative sea-level fall and lowstand below SBs or during carbonate stabilization in marine phreatic zone, and local dolomitization (Azer and Toland, 1993; Melville et al., 2004; Thorpe, 2014). By mechanical compaction higher porosity can be lost in mud-supported texture than in grain-supported texture where the calcite circumgranular prevent further grain compaction (Morad et al., 2012; Oswald et al., 1995).

Late diagenesis (burial) is believed to have significant effect on the reservoir quality of Thamama Formations (Paganoni et al., 2016). Cementation and stylolitization are considered as important burial diagenesis that affect reservoir quality variation across most of the Thamama Formations. The late calcite cements occlude the large primary and secondary pore spaces in the reservoir, resulting in porosity and permeability reduction mostly in water leg. Total porosity in the water leg is mostly from micropores, whereas macro and micro pores count for total porosity in oil leg. Micro-porosity can be produced by partial dissolution and/or recrystallization of micrite in meteoric or during burial diagenesis (Al-Aasm and Azmy, 1996; Budd, 1989; Moshier, 1989). Porosity is better

preserved in the oil (in the crest) than the water (the flank) in the Thamama Reservoirs particularly in the reservoirs where oil have been charged earlier (Neilson et al., 1998).) Petroleum charging to Thamama Group started Late Cretaceous prior-relative to stylolitization and burial cementation, and therefore preserve macroporosity in the productive Thamama Reservoirs (Alsharhan, 1989).

Stylolites are developed more in the water leg than in the oil leg because oil though to retard or stop diagenesis in carbonate reservoirs (Feazel, 1985; Koepnick, 1987; Paganoni et al., 2016). Abundant and well-developed stylolites were recorded in water leg that coincide with calcite cementation and porosity-permeability reduction (Alsharhan, 1990; Oswald et al., 1995; Alsharhan and Saad, 2000). Chemical compaction including stylolitization is suggested to derive calcium carbonate that can be used for calcite cementation. Moreover, during stylolite development microfractures can be developed which may contribute to the final permeability if they remain opened (Alsharhan and Sadd, 2000; Paganoni et al., 2016). In addition, fractures and faults developed during different tectonic events could be good conduits for hydrocarbon migration. These fractures and faults could be also conduits for hydrothermal fluids flow which can promote further cementation (Callot et al., 2010).

The studies conducted by Neilson et al. (1998) and Alsharhan et al. (2000) on oxygen stable isotopes of calcite cements reveal precipitation at high burial temperatures. Cox et al. (2010) and Thorpe (2014) also conducted more detailed ion microprobe studies of syntaxial calcite burial cement (with further cement types in Thorpe (2014) study including fringing, equant and blocky calcite cements) to understand the dynamics of cementation in response to oil charge. These studies measured the mean in-situ ion microprobe $\delta^{18}O_{VPDB}$ of different classified cathodolominancens zones (from oldest to youngest towards the crystal terminations) within each crystal of cement in both oil and water legs. Together with ion microprobe oxygen isotope data, the fluid inclusion (FI) technique has also been used to determine the presence of oil inclusions within the cement (Cox et al., 2010; Thorpe, 2014).

The results of these studies has shown that the youngest cement zones in the oil leg have lower $\delta^{18}O_{VPDB}$ compared to water leg. Likewise, depleted $\delta^{18}O_{VPDB}$ indicates a higher burial precipitation temperature of the cement. Oil inclusions were reported in some of the youngest cement zones in oil leg suggesting further precipitation of the cement simultaneously with oil charge. Carbonates in the oil leg still preserved most depositional pore spaces unlike water leg where youngest cement zones occluded most of pore spaces indicating further progress of the diagenesis in the water leg.

## 1.5 Materials and Methods

### 1.5.1 Data Set and Sample Preparation

#### 1.5.1.1 Data Set

Hand samples were collected from core reservoir and dense intervals from water versus oil leg to allow textural and petrophysical comparison between these two intervals. Reservoir intervals include Thamama Reservoirs A, B, C, F and G from Shuaiba, Kharaib and Lekhwair Formations (Figure 1.3; Table 1 in Appendix A). Ninety seven core slabs were collected from 8 wells, 5 from crest (oil leg) and 3 from flank (water leg), from ADCO core store, Abu Dhabi, UAE (Figure 1.10; Table 1.1; for more details see Table 1 in Appendix A). Each sample has been labeled with well number and depth.

Table 1.1: Well names, depth intervals and number of samples collected from oil and water legs.

| Leg | Well Name | Reservoir/Dense | No. Samples |
|---|---|---|---|
| Oil | well 1 | Dense F | 5 |
| | | Dense G | 3 |
| | | Reservoir F | 2 |
| | | Reservoir G | 11 |
| | well 2 | Dense B | 1 |
| | | Dense C | 1 |
| | | Reservoir C | 10 |
| | well 3 | Reservoir B | 9 |
| | well 4 | Dense A | 1 |
| | | Reservoir A/Bab Member | 6/2 |
| | well 5 | Dense A | 8 |
| | | Dense B | 2 |
| | | Reservoir B | 12 |
| Water | well 6 | Reservoir B | 13 |
| | well 7 | Reservoir C | 3 |
| | well 8 | Dense E | 1 |
| | | Dense F | 2 |
| | | Reservoir F | 5 |

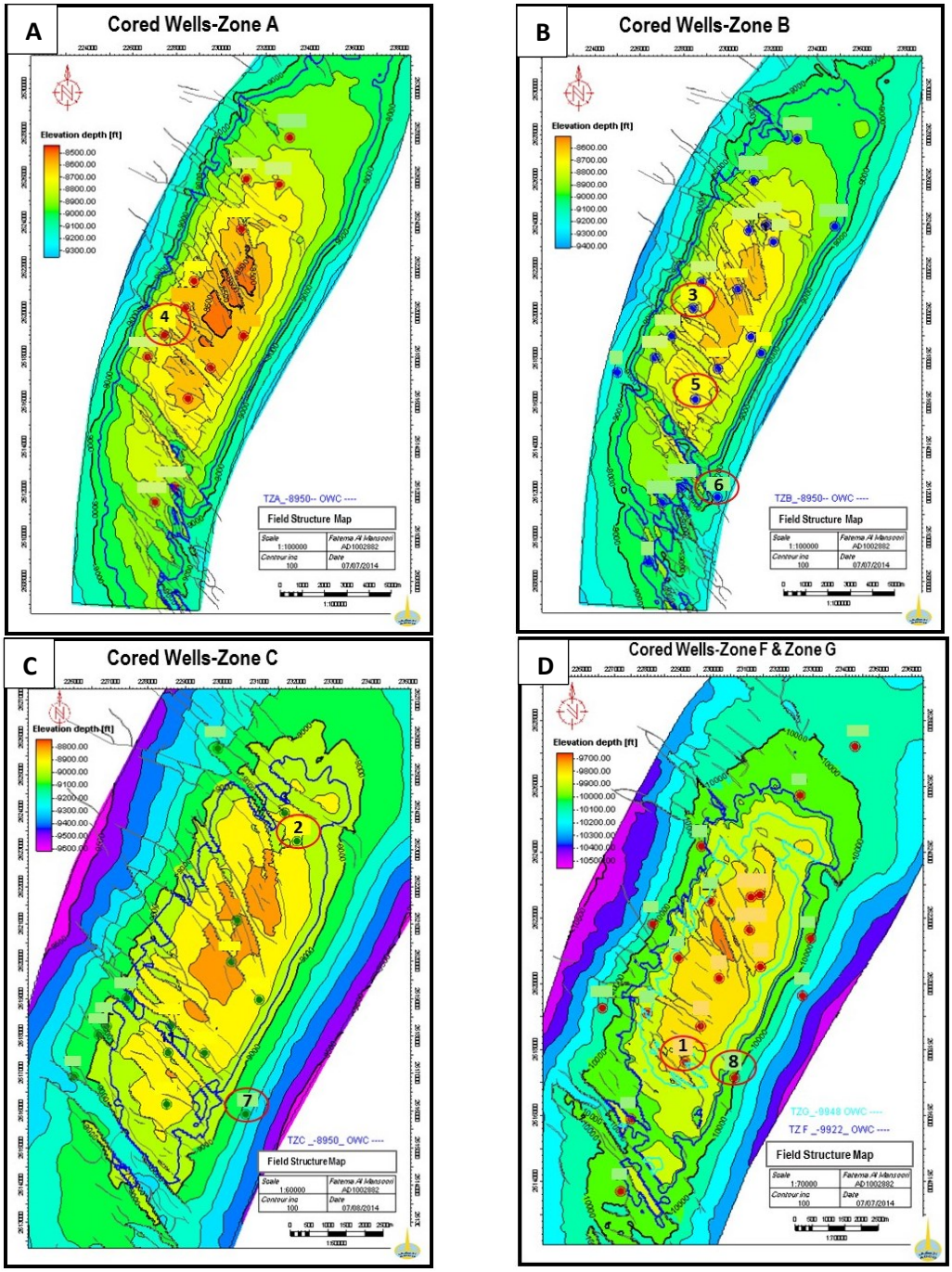


Figure 1.10: Structural map of the Field with locations of cored wells. Sampling was made from well circled by red. OWC shown in blue separates wells in the crest from wells in the flank. A) Reservoir A, well 4 from oil leg. B) Reservoir B, wells 3 and 5 from oil leg and well 6 from water leg. C) Reservoir C, well 2 from oil leg and well 7 from water leg. D) Reservoirs F and G, well 1 from oil leg (both F & G) and well 8 from water leg (only F). From ADCO.

Core logs have been photographed and stored for the record. In addition, detailed photographs of the interesting features on the visual scale have been documented. Data set also includes data that have be supplied by ADNOC and ADCO which are listed below.

- Four structural maps (Figures 1.10) of the Field with locations of cored wells, main faults and (Oil Water Contact) OWC. Some crestal wells such as wells 2, 3 and 4 are at the margin of the oil leg. These wells are probably in the transition zone where we should expect higher cementation compared with wells in oil zone (wells 1 & 5) at the top of the crest. Cementation should be lower at the top of the crest and increase downward the structure as we pass transition zone and become even higher down the OWC where the water zone located (wells 6, 7 & 8).
- Sheet of cored wells with depth intervals and reservoir name of each reservoir interval.
- Four reports on diagenesis for Field A and two nearby Fields (X and Y, Figure 1.1).

#### 1.5.1.2 Sample Preparation

The slabs were further sawed at the University of Edinburgh (UoE) for thin section preparation. Final oil leg samples were separated from water leg ones for cleaning before thin section preparation. Oil stripping was conducted in-house using soxhlet extraction. Six to eight samples were placed in a whatman cellulose filter in the soxhlet connected to a flask containing about 500 ml of Methanol which was placed in an electrothermal mantle sited up to stage 6 (Figure 1.11). A condenser was used to condense the evaporated Methanol which goes directly to the soxhlet. The condenser was connected to a water supply to allow steady water flow and cool. The extraction was carried out until the condensate runs clear. Then, the procedure was repeated with the same setup using Toluene to clean up the remaining oil. Same solvents can be used for more than one run; until large quantity of residual is precipitated. Waste solvents should be collected after cooling in glass bottles and dispose via the School of Chemistry's waste disposal system.

Normal uncovered and highly polished thin sections were prepared in-house and were stained with blue resin to identify porosity. Thin sections have not been stained with alizarin red S to discriminate between ferroan and non-ferroan calcite and dolomite (Dickson, 1965). Alternatively, ferroan and non-ferroan calcite and dolomite have been identified using elemental data obtained from EPMA. The thin sections were used for petrographic examinations (conventional, cathodoluminescence, fluorescence) as well as other analyses including EPMA, SEM and SIMS.

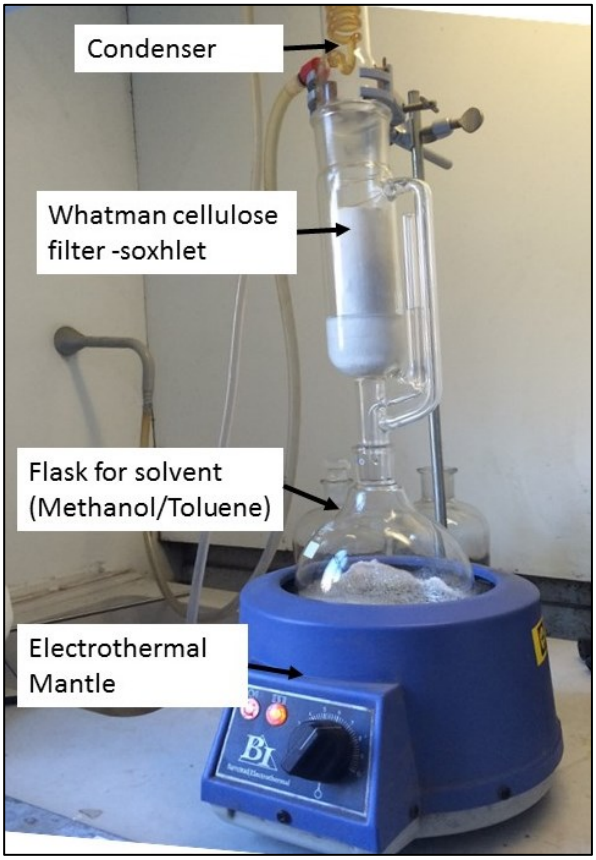


Figure 1.11: Soxhlet extraction using Methanol and Toluene at UoE.

### 1.5.2 Methods

#### 1.5.2.1 Cathodoluminescence (CL)

Cathodoluminescence (CL) assessment provides qualitative evaluation on fluid composition of particular cement. The luminescence and non- luminescence criteria are controlled by $Fe^{2+}$ and $Mn^{2+}$ concentrations which reflects the chemistry of pore water during precipitation ( Barnaby and Rimstidt, 1989; Boggs and Krinsley, 2006). The $Mn^{2+}$ is thought to be the main activator in calcite and dolomite whereas $Fe^{2+}$ is considered as a main quenching agent (Machel, 1985). Basically, calcite or dolomite cements with higher $Fe^{2+}$ relative to $Mn^{2+}$ will show dull luminescence, whereas cements with lower $Fe^{2+}$ and relatively higher $Mn^{2+}$ will display bright luminescence. This criteria was used to track different stages "zones" of cement growth occluding pores and construct micro-cement stratigraphy. The cement stratigraphy was then used to measure in-situ $^{18}O_{VPDB}$ and trace elements of each cement zone. A cathodoluminescence cold cathode CITL 8200 MK3A was used at UoE to examine thin sections and identify different cement zones.

#### 1.5.2.2 Oil Inclusions

Fluid-inclusion (FI) petrography and microthermometry are generally performed to reconstruct the conditions at which each cement was formed, including formation temperature, fluid compositions and relative timing of cement growth. Fluid inclusions can be of primary or secondary origin (Goldstein and Reynolds, 1994). Primary fluid inclusions are typically formed during crystal growth whereas secondary inclusions are formed after crystal growth and fractured. Pseudosecondary fluid inclusions might be trapped during crystal growth if fracturing occurs during crystal growth. Secondary FI cannot be used to reveal the conditions and timing of crystal growth therefore they will be disregarded in this study. Aqueous and petroleum FI can be examined under UV light to

distinguish between these two end members (Burruss, 1991). Most petroleum fluid inclusions fluoresce under UV light, whereas aqueous inclusions do not fluoresce. Oil inclusions will be related to CL cement zones to indicate possible timing of oil charge.

For this study, a Leitz Metallux Leica 3 microscope with a 100w Hg HBO 103W/2 bulb and a blue filter creating UV light at UoE, was used to identify oil inclusions in polished thin sections. Unfortunately, the resolution and quality of microscope were not sufficiently good to carry out details examination of oil inclusions. Oil inclusions documentation was also gathered and correlated from other studies (Cox. et al., 2010; Thorpe, 2014).

### 1.5.2.3 Electron Probe Microanalysis (EPMA)

Electron probe microanalysis is widely used to determine chemical composition of 1 μm diameter solid rock (Hutchins, 1979). This technique is based on criteria that each element in a solid rock emits distinct x-ray spectrum when bombard with electron beam. The characteristic of each emitted x-ray spectrum line reveal the presence and concentration of particular element.

The EPMA was conducted for this carbonate study to obtain elemental concentration of calcite cement which further used to indicate origin of pore water at time of cementation (Boles, 1998; Boles et al., 2004; Heydari and Moore, 1993; Morad, 2009). Magnesium to calcite ratio (mMg/Ca) is thought to be good temperature proxy for carbonates (Carpenter, 1980; Heydari and Moore, 1993; Volery et al., 2009). The mMg/Ca ratio can be compared with in-situ $\delta^{18}O_{VPDB}$ data to constrain the precipitation temperature of calcite cement (Thorpe, 2014).

EPMA was conducted in the University of Edinburgh using a Cameca SX100. It was applied for 18 polished (0.5-1mm thick) thin sections (from all reservoirs) to obtain

concentrations of Mg, Ca, Mn, Fe, and Sr for calcite cement including syntaxial, equant and blocky. Thin sections were cleaned to remove abrasive particles and lubricants and then coated with a thin layer of carbon before the analysis. EPMA can take two samples each round and each sample take around 7-8 hours depending on numbers of areas to be analyzed. Thus, some measurements were set to be taken automatically overnight. Samples were bombarded with an incident electron beam with a diameter size of 5µm and 15 KV. Calcite-Silicarb_Ca standard was placed in a separate holder and was calibrated twice; before and after the analyses in each round. The obtained concentrations were reported in Weight % and Parts Per Million (ppm).

#### 1.5.2.4 Scanning Electron Microscope (SEM)

Five thin sections were mapped under the SEM in order to make the navigation under the ion microprobe easier. SEM was used also after acquiring measurement from ion microprobe to check anomalies in certain measurements; check if these anomalies have passed through fractures or holes in the cement. The thin sections were cleaned and coated by thin layer of carbon before SEM imaging. Samples were placed under high vacuum evaporation and bombarded by an electron beam with voltage of 10kV to acquire high resolution images. The instrument resolution ranges from 1.9 nm at 1 kV to 1 nm at 15 kV.

#### 1.5.2.5 Ion Microprobe (SIMS)

Five polished thin sections were used to obtain in-situ $\delta^{18}O_{VPDB}$ for different types of calcite including syntaxial, equant and blocky of each reservoir. These thin sections were used before for EPMA and CL studies. The point of using the same thin sections is to understand cementation condition (temperature, fluid composition and relative timing) using different independent variables. Unlike separate component analysis, ion

microprobe provides more accurate micrometer scale measurements of isotopic ratio using focusing primary ion beam (Cs) (Valley and Kita, 2009).

Samples should be 24 - 24.5mm in diameter and less than 12 mm thick. Analysis can cover the area within ~9 mm of the center but for high precision the coverage was reduced to +/- 5 mm from the center. The calcite standard can be mounted in a single block and placed in a separate holder or can be mounted within the sample which is ideal for higher precision. For all performed analysis the standard was mounted within the samples. Two methods were used to prepare the samples. In the first method, an ultrasonic drill was used to drill a hole (~ 2.5 mm) in the center of the 24 - 24.5 mm diameter sample and the standard was embedded in the hole. Standard was placed by covering the unpolished surface of the thin section with a tape and then in the other side (polished side) the standard was placed in the drilled hole to be stacked into the tape. The hole was then filled with Epo-thin epoxy resin. After drying the tape was removed followed by careful grind and re-polish to the thin section to have the sample and the standard flat in a polished surface. In the second method, multiple specimens were mounted into an Indium block together with the standard. Areas of interest were marked in the thin sections using ink marker and then were cored using the ultrasonic drill. Each core is ~ 2.0 mm in diameter. Cores were washed with de-ionised water to remove the abrasive powder and allowed to dry. The cored samples were then pressed into an Indium mount together with the calcite standard.

All prepared samples were then cleaned with Acetone and then Ethanol followed by gold coating before being placed within Cameca 1270 in-house ion microprobe (SIMS). The instrument can take up to two samples at a time and each sample needs four to five hours to be analyzed. The internal precision of each spot can be ranged between 0.009 and 0.015 (% standard Error). The external precision is estimated according to the consecutive analysis of a UWC (University of Wisconsin Calcite) standard (~0.3‰-0.4‰) and is assessed to be homogenous.

Before final cleaning and gold coating, samples were mapped for easier navigation during the analysis. Navigating for areas of interest in the ion microprobe is difficult. Thus, samples should be mapped and areas of interests should be known very well before performing the analysis. For mapping, first SEM was used and the optioned images were far away from what can be seen under the ion microprobe thus difficult to track the areas of interest. Second, images of the samples were taken under reflected light microscope. The Reflected light photo-micrograph provided much closer view to the ion microprobe and hence were used to navigate to the desirable areas under ion probe.

### 1.5.3 Research Workflow

Main procedures of this study are outlined in Figures 1.12. First, determination of the origin (primary vs secondary) and type of pores were made via conventional petrography. Diagenetic overprint (volume of cement occlusion) is then quantified and evaluated in terms of reservoir quality using normal and CL petrography. CL was also used to create a micro-cement stratigraphy, which then used for EPMA and in-situ sampling of $\delta^{18}O_{VPDB}$, to infer the relative timing of cementation, temperature and evolution of pore-fluid chemistry at different stratigraphic (Reservoir A vs G) and structural (oil crest vs flank). Cement evolution constructed by mMg/Ca ratio and SIMS $\delta^{18}O_{VPDB}$ then was used to assess pore space evolution through time and to understand dynamic of calcite cementation in oil vs water leg. Documentation of oil inclusions was used to infer to the possible time of oil charge and its effect on calcite cementation.

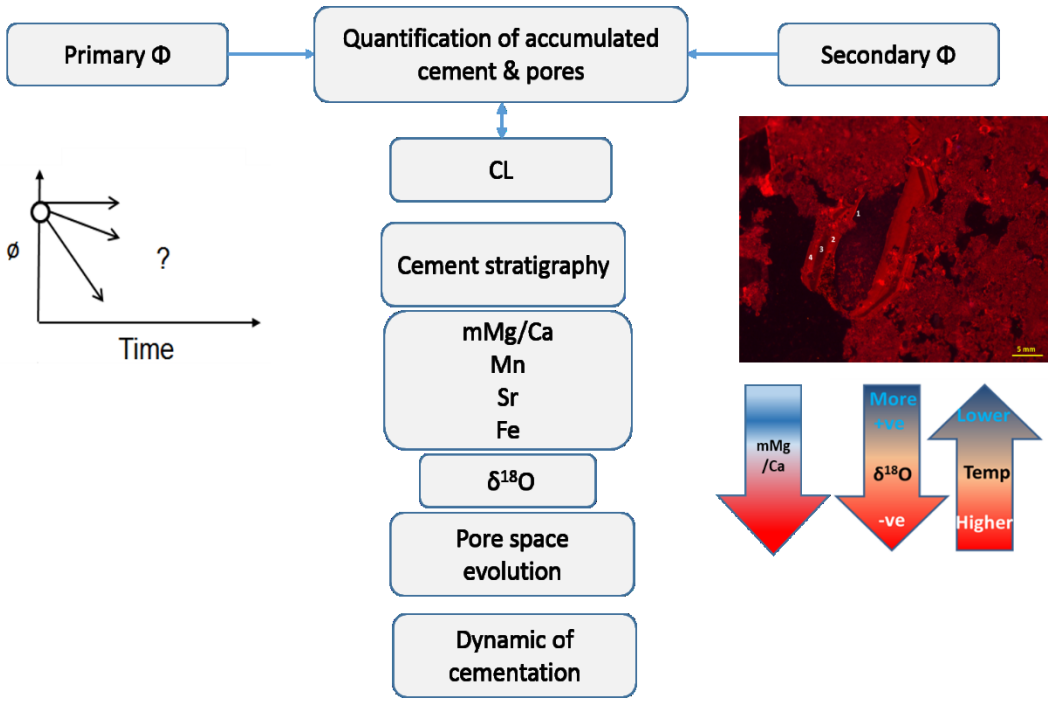


Figure 1.12: Methodology for quantifying the dynamics of calcite cementation.

## 1.6 Thesis Outline

***Chapter 2*** provides information about the depositional rock fabric and diagenetic overprint affecting the Thamama carbonates. The primary "depositional" and secondary "diagenetic" pores were identified and assessed in terms of their preservation and occlusion by further cementation in both oil and water legs. This was undertaken to compare and understand the effect of diagenesis on same rock in two different settings (oil vs water). The relative timing of diagenetic events was constrained using cross cutting relationship observed from petrography. This is to constrain relative timing of each diagenetic event, particularly calcite cementation events, to others and relate this to oil emplacement into the reservoir. Then, the impact of major diagenetic events on the overall

reservoir quality was assessed. The late dissolution event found in reservoirs was interpreted to be one of the significant diagenetic events that enhanced reservoir quality.

***Chapter 3*** uses CL zonation principle as a basis to construct cement stratigraphy and cement volumetric models for calcite in each reservoir. The cement stratigraphy was constructed to track fluid composition changes through time. The volumetric models were built to understand cementation history through time in terms of cementation rate at a certain times and fluid properties (ferroan vs non-ferroan). These models were also used to understand reservoir quality evolution during different cementation steps in oil versus water leg.

***Chapter 4*** aims to improve our understanding on origin and evolution of fluid composition through time. This was done by interpreting the variation in Sr, redox sensitive elements Fe and Mn, and mMg/Ca ratio obtained from EPMA for individual cement zones of the main pore occluding calcite cement types (syntaxial, equant and blocky). The previously established cement stratigraphy was used for targeting individual cement zones. This assessment also gave important clues on the palaeotemperature of the fluids from which calcite cements were precipitated both in oil and water legs by using mMg/Ca molar ratio. These analyses helped to understand dynamic of calcite cementation in oil versus water leg.

***Chapter 5*** represents another geochemical study of dolomite cement. Dolomite, particularly saddle dolomite, is often distributed throughout Thamama Reservoirs so it was important to assess this cement type. The assessment was conducted to investigate the chemical composition of the different dolomite types (rhombic, coarse and saddle) in the Thamama using EMPA in order to unravel the origin of pore fluids which involved in the formation of dolomite. The evolution of dolomitization fluid was tracked using Sr and redox elements sensitivity (Fe and Mn). Parallel to this, the mMg:Ca ratios and Sr were used to understand potential origin of pore fluid and its evolution through dolomitization.

Finally, different dolomitization models were proposed that can better explain formation mechanism of different types of dolomite.

***Chapter 6*** assesses the dynamics of calcite cementation through time and relative to oil charge. This was done first by investigating the temperature evolution of pore fluids from which equant, syntaxial and blocky calcite cements were precipitated using SIMS $\delta^{18}O$ data. The high resolution in-situ $\delta^{18}O$ of cement zones in each calcite type was obtained based on the cement stratigraphy. Then, in-situ $\delta^{18}O$ data was compared with another proxy which is mMg/Ca ratio to elucidate the temperature evolution of pore fluid stratigraphically and across individual reservoirs using these two independent proxies. $\delta^{18}O$ and mMg/Ca ratio were also used to reconstruct the timing and chemical conditions of individual calcite cements relative to each other. The timing of oil charge was assessed using the presence of primary oil inclusions in individual cement zone. This then provided better understanding on the effect of oil charge on calcite cementation including precipitation temperature and conditions. This chapter also highlights the origin of the early calcite cement zones and how there are correlated with global Cretaceous seawater chemistry. More interestingly, the diagenetically affected calcite cements (younger cement zones) follow general seawater signature, highlighting the importance of reservoir compartmentalization in all reservoirs, thought to be established early by early cementation of hardgrounds which acts as seals for individual reservoir. This early sealing caused pore fluids to evolve through burial in relatively close system reflected by progressive depletion of $\delta^{18}O$ moving towards younger cement zones.

***Chapter 7*** gathers and correlates all significant findings from this thesis. In particular this highlights how we have gained a better understanding of 1) calcite cement evolution with relation to oil charge and reservoir quality in Thamama Reservoirs, and 2) reservoir compartmentalization and correlation of local Cretaceous marine signature with global seawater signatures. The chapter also highlights further works that could be undertaken.

# Chapter 2: Diagenesis and Reservoir Quality in Thamama Reservoirs

## 2.1 Introduction

Depositional rock fabrics in carbonates can be altered partially or completely by several diagenetic processes to form dramatically different fabrics. These may enhance and/or destroy the reservoir quality. Diagenetic processes can start very early, immediately after sediment deposition and continue into burial environments. Diagenetic processes include mechanical and chemical compaction, micritization, dissolution, recystalization, calcite cementation, dolomitization, and the cementation of other minerals. Reservoir quality in Thamama formation is affected significantly by diagenesis (Alsharhan, 1990; Neilson et al., 1998; Oswald et al., 1995). Thus, understanding diagenesis and its impacts on rock properties is crucial to better understand and enhance reservoir quality for better productivity.

The lateral and vertical reservoir quality in Thamama Formations is a function of depositional facies and diagenetic alterations of the original facies (Alsharhan, 1990; Oswald et al., 1995). Thamama Formations exhibit a wide range of depositional facies which result in porosity and permeability variation. Primary intergranular macroporosity which formed during deposition is thought to have a significant impact on the pore system in grainstone and packstone facies unless they are preserved from early time from extensive cementation by for example oil emplacement (Neilson et al., 1998). However, the most significant effect on reservoir quality is attributed to diagenetic alteration. Thamama Reservoir rock properties (porosity and permeability) has been suggested to be mostly controlled by early subaerial and burial diagenesis (Alsharhan, 1990). Subaerial diagenesis in Thamama rocks is probably induced by percolation of meteoric waters. Such process can result in cementation of early

circumgranular calcite rims around grains and dissolution which creates “secondary” porosity (including moldic, intragranular, and vuggy) and local dolomitization ( Alsharhan and Kendall, 1991; Azer and Toland, 1993; Melville et al., 2004). However, subaerial exposure in Thamama has been contradicted by other authors since no evidence of subaerial exposure was found (Dickson et al., 2008; Granier et al., 2003). Alternatively, Lower Cretaceous is a well-known time for Calcite Sea in which dissolution of high-Mg calcite and aragonite is possible in marine phreatic zone which can result in the formation of moldic and vuggy pores (Dickson et al., 2008; Hardie, 1996; Thorpe, 2014). Circumgranular calcite can be also precipitated in marine phreatic zone from pore fluid of marine water (Thorpe, 2014). The cementation of early circumgranular calcite can preserve some of the depositional “primary” intergranular porosity by supporting the grain framework from existing compaction (Oswald et al., 1995; Morad et al., 2012). Thus, mechanical compaction can result in higher porosity reduction in mud-supported textures than in grain-supported textures. Survived porosity from mechanical compaction due to early circumgranular calcite is thought to enhance reservoir quality unless it remains opened and connected.

Stylolitization and cementation are two of the significant mid-late burial diagenesis that resulted in variation in the reservoir quality across most of the Thamama fields. The equant and early blocky calcite cements which occlude partially to completely primary and secondary pores resulted in porosity and permeability reduction. Likewise, saddle dolomite and late blocky calcite associated with stylolilitization and fracturing in Thamama Reservoirs have occluded fractures and some pores nearby. Dolomitization which includes micrite replacement by microcrystalline rhombic dolomite can enhance the porosity by introducing new microporosity to the rock fabrics. Microporosity can be created as a result of partial dissolution and/or recrystallization of micrite by meteoric flux or by increase temperature and pressure during deeper burial diagenesis (Al-Aasm and Azmy, 1996; Budd, 1989; Moshier, 1989).

Microporosity forms important part of carbonate rocks of Middle East's oil reservoirs (Morad et al., 2016; Lambert et al., 2006; Budd, 1989). Microporosity can be depositional or diagenetic in origin, induced during shallow to deeper burial environment (Al-Asam and Azmy, 1996; de Periere, et al., 2011). It can also be formed during subaerial exposure as a result of meteoric water flux and/or during shallow to intermediate burial from evolved marine water (Al-Asam and Azmy, 1996; de Periere, et al., 2011; Volery et al., 2010). The formation of microporosity has been attributed to several mechanisms including neomorphism which involves the transformation of metastable minerals (e.g. aragonite and HMC) into a more stable phase (e.g. LMC). Moreover, microporosity interpreted to be formed by early lithification, extensive recrystallization and chemical equilibrium in the Upper Cretaceous chalks (Holail and Lohmann, 1994). Volery et al. (2010) highlighted two important factors that can influence microporosity formation including (1) the stable LMC crystals that retain the original minerology and (2) the preservation of a microcrystalline framework from shallow burial due to the rock rigidity that resulted from early diagenesis cementation (calcite overgrowth). Microporosity in LMC can also be generated at moderately high temperature by recrystallization derived by organic acids which produced by kerogen maturation (Heydari and Wade, 2002; Morad et al., 2016). Heydari and Wade (2002) found that this process occurs in lime mudstone that is rich in organic matter other than organic-poor lime mudstone.

The late cementation resulting in porosity and permeability reduction mostly in water leg. Presence of oil in the crest could possibly result in porosity preservation as evidenced by Neilson et al. (1998), which showed frequent association of petroleum fluid inclusions with more porous samples than low porous cemented samples. Alsharhan (1989), Oswald et al. (1995) and Nielson et al. (1998) agreed that petroleum charging to Thamama Group started prior-relative to stylolitization and burial cementation, during the Late Cretaceous and which preserve macroporosity in the productive reservoirs.

Stylolites are developed more in the water leg than in the oil leg because oil though to retard or stop diagenesis in carbonate reservoirs (Feazel, 1985; Koepnick, 1987). According to Alsharhan (1990), Oswald et al. (1995) and Alsharhan and Saad (2000), chemical compaction process, i.e. stylolitization, is believed to be an important process that derived calcium carbonate for calcite cementation in Thamama Reservoirs. Indeed, the authors relate the greater extent of calcite cementation and porosity-permeability reduction in the water leg to stylolite development where they noted abundant, well-developed stylolites. Microfractures associated with stylolite development may contribute to the final permeability if they remain unfilled (Alsharhan and Sadd, 2000). In addition, fractures and faults developed during different tectonic events could be considered as good conduits for hydrothermal fluids flow and hence promote calcite cementation and dolomitization (Callot et al., 2010).

## 2.2 Aims

This chapter aims to understand main diagenetic overprints affecting the five Reservoirs (A, B, C, F & G) of Thamama Group and their impact on reservoir quality, by:

- Understanding and comparing diagenesis in oil versus water leg to see effect of diagenesis on the same rock but in two different settings,
- Constructing paragenetic sequences for each reservoir to reconstruct the relative timing of diagenesis.
- Understanding the impact of diagenesis on reservoir quality. This also focuses on timing and the role of dissolution on reservoir quality. Reservoir quality in this chapter is discussed in terms of diagenesis and not real porosity and permeability data. Real porosity and permeability data have not been provided.

## 2.3 Methods and Sampling Procedure

Samples were collected from different reservoirs of water and oil leg to allow comparison between rock properties in water versus oil leg. Reservoirs include Thamama Reservoirs A, B, C, F and G. Ninety seven core slabs were collected from 8 wells, 5 from crest (oil leg) and 3 from flank (water leg), from ADCO core store (Table 1.1; for more details see Table 1 in Appendix A). The slabs were further sawed at the University of Edinburgh for thin section preparation. Final oil leg samples were separated from water leg ones for cleaning before thin section preparation. For more details see Section 1.5.1.

Normal uncovered and highly polished thin sections were prepared in-house and filled with stained with blue resin to identify porosity, as well as with alizarin red S to discriminate between ferroan and non-ferroan calcite and dolomite (Dickson, 1965). The thin sections were used for petrographic examinations (conventional, cathodoluminescence, fluorescence) as well as other analyses to evaluate pore types, cement types, different calcite cement morphologies and its evolution through time, as well as cross cutting relationship to construct paragenetic sequence for each reservoir.

## 2.4 Results

In this section, I will first describe the main depositional facies, then the main diagenetic features (cements, chemical compaction and porosity-forming features). Then, paragenetic sequences for each reservoir followed by summary of reservoir quality in Thamama Reservoirs will be described in the next section.

### 2.4.1 Main Depositional Facies

According to the petrographic descriptions of thin sections and core observation, the Thamama Reservoirs A, B C, F and G are classified as limestones (Figure 1.3). The limestone textures include mostly peloidal grainstones, packstones and wackestones. Reservoir G starts with HST packestone and deepen upwards into muddier packestone and mudstone of the TST (Figure 2.1). Reservoir F starts with muddier facies shallowing upwards into more grainy HST facies (Figure 2.2).

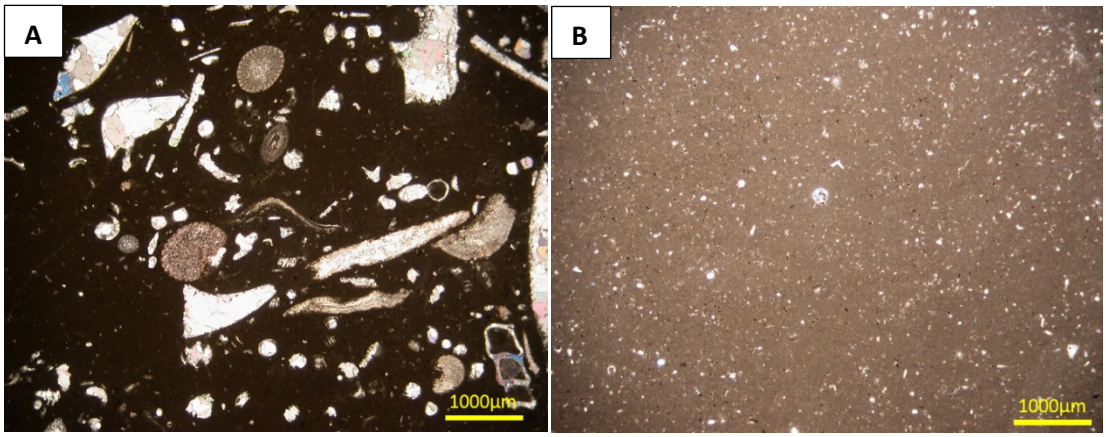


Figure 2.1: Main facies in Reservoir G. A) Coarse grain packstone with echinoderm, gastropod and shell fragments (HST). B) Muddy pack-mudstone with mostly peloids (TST).

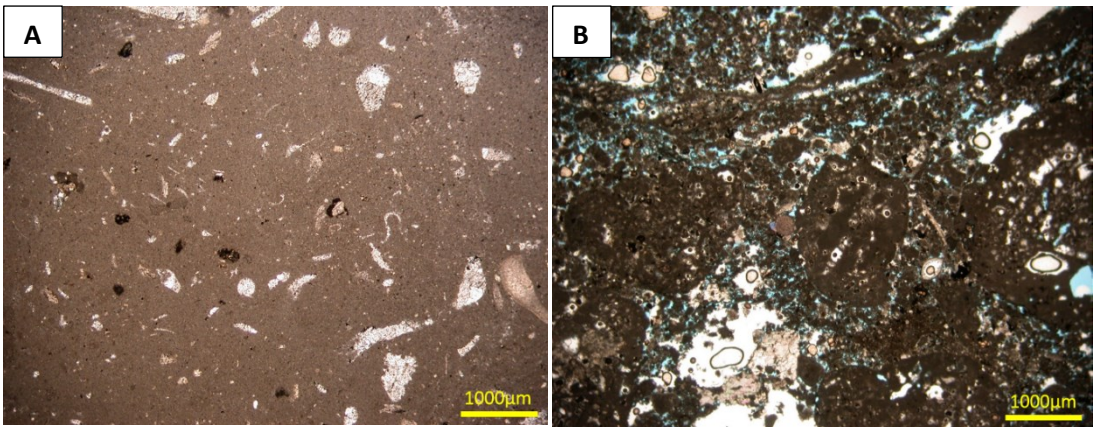


Figure 2.2: Main facies in Reservoir F. A) Muddy pack-mudstone with peloids, echinoderm and shell fragments (TST). B) *Bacinella-Lithocodium* packstone-floatstone, with peloids (HST).

Reservoir C is dominated by peloidal and *Orbitolina* packstone at the bottom of the reservoir which is shallowed up into grainstone-packstone with mixture of ooids, peloids, gastropods, forams, echinoders, *Orbitolina,* rudist and bacinella lithocodium (Figure 2.3).

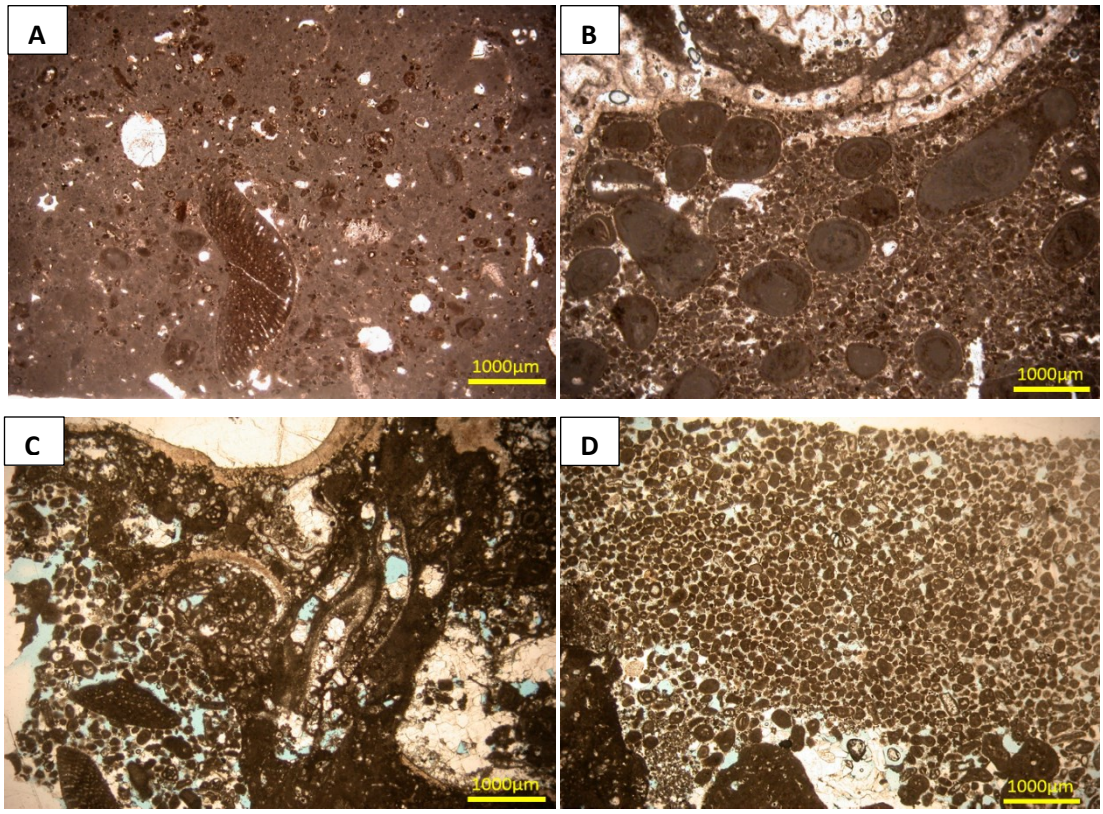


Figure 2.3: Main facies in Reservoir C. A) Muddy pack-mudstone with peloids and *Orbitolina* (TST). B) Grainstone-packstone with ooids, peloids, aggregate and *Bacinella-Lithocodium* (HST). C) Packstone-floatstone with *Bacinella-Lithocodium, Orbitolina,* miliolid forams and peloids. D) Grainstone with peloids, miliolid and benthic forams, echinoderm and *Bacinella-Lithocodium*.

In Reservoir B, grains become more abundant particularly the *Orbitolina*, other forams, peloids, rudists and to some extent gastropod. *Orbitolina* is abundant in the middle section of the reservoir (Figure 2.4B & C) and becomes less abundant moving towards the top of the reservoir (Figure 2.4D, E & F). The facies are muddier at the bottom of the reservoir representing TST deposits (Figure 2.4A, B & C) and grainy at the top of the reservoirs representing HST deposits (Figure 2.4D, E & F).

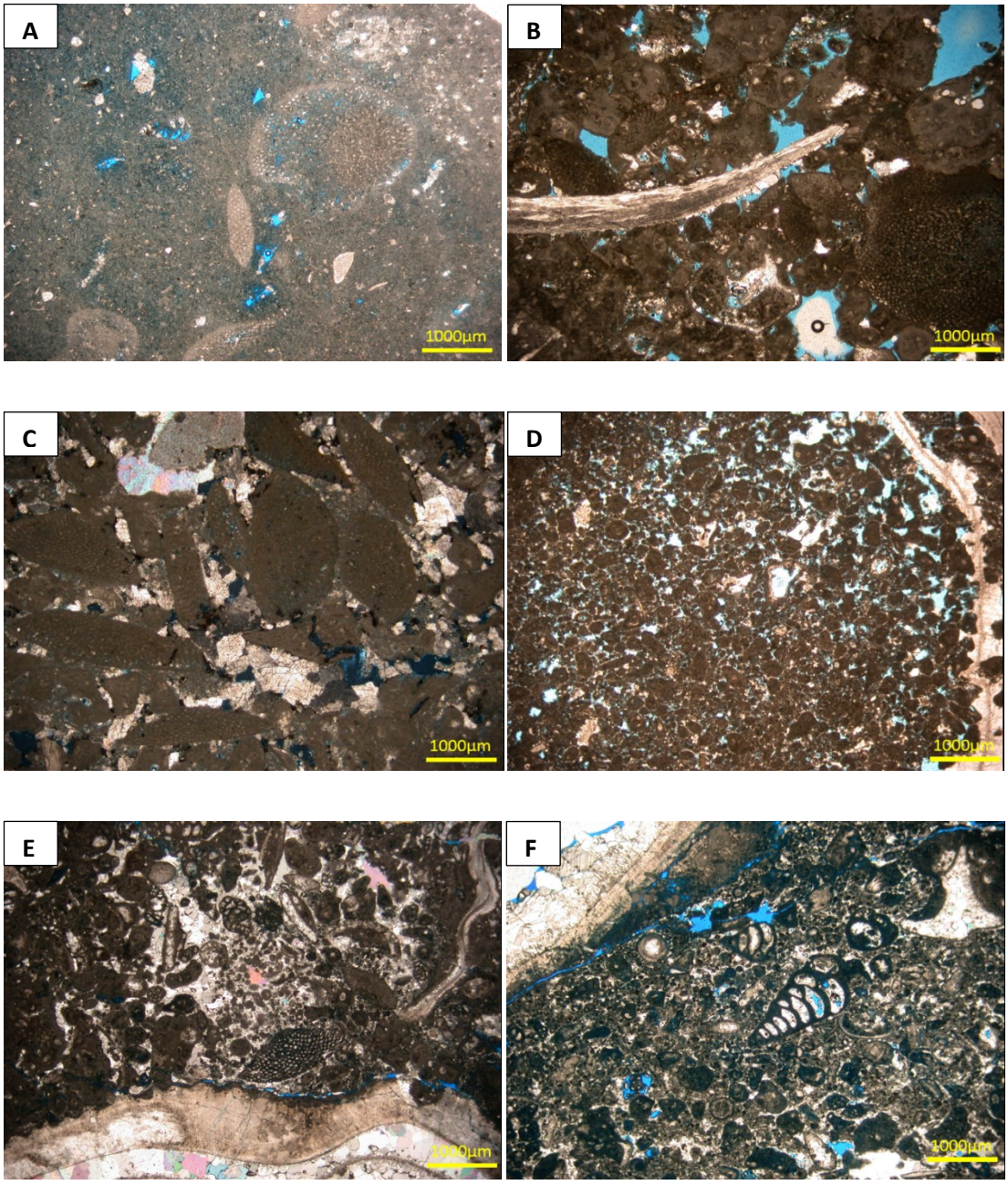


Figure 2.4: Main facies in Reservoir B. A) Muddy packstone-floatstone with peloids and *Orbitolina*, at the base of the reservoir (TST). B) Peloidal and *Orbitolina* grainstone-packstone with aggregates. C) *Orbitolina* packstone-grainstone. D) Peloidal grainstone-packstone with forams and echinoderms. E & F) Packstone-floatstone with rudists, *Orbitolina*, benthic forams, echinoderms and peloidal at the top of the reservoir (HST).

Most of the collected samples from Reservoir A are classified as packstones. The calcareous green algae including *Hensonella* and Dasycladacea as well as echinoderm and benthic forams become abundant in this reservoir (Figure 2.5).

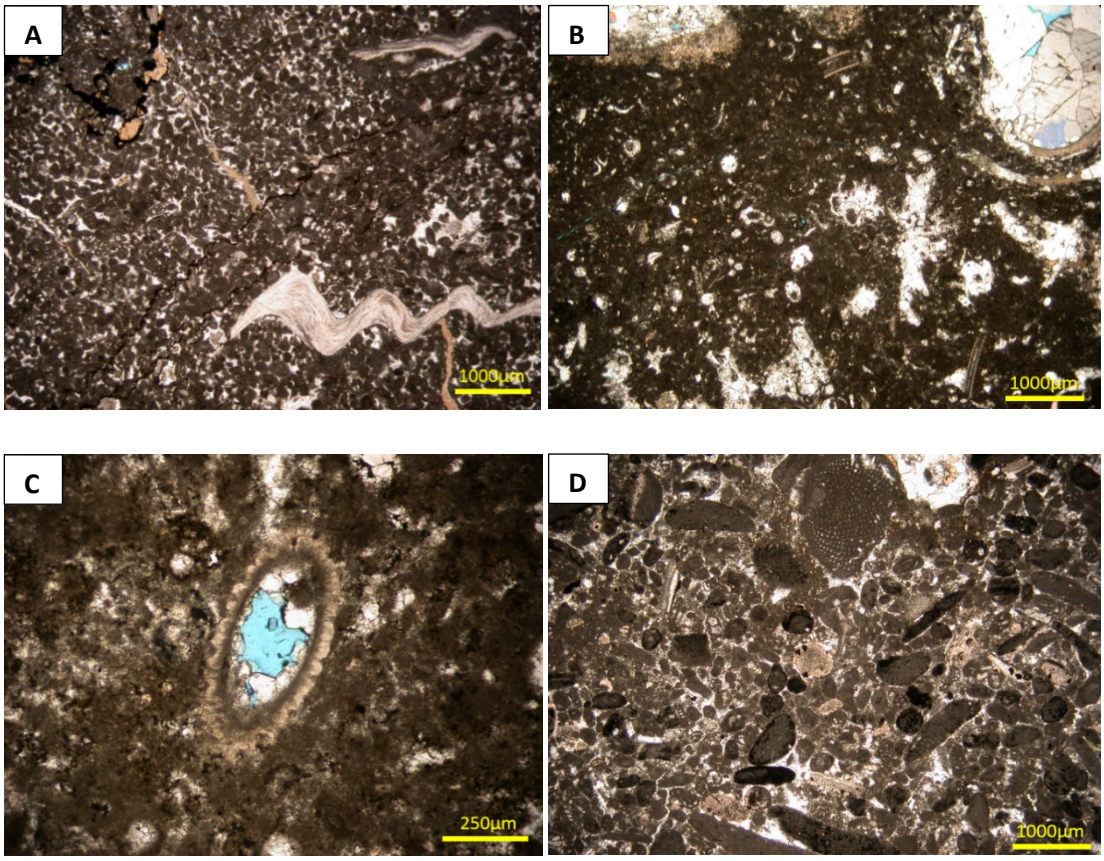


Figure 2.5: Main facies in Reservoir A. A) Packstone with peloids, echinoderms, benthic forams and rudist fragments. B) Packstone with rudist, peloid, *Hensonella dinarica* (Dasycladacean). C) *Hensonella* in the packstone. D) Grainstone-packstone with peloids, benthic forams, echinoderm and *Orbitolina*.

### 2.4.2 Main Diagenetic Features

Main diagenetic alterations in these limestones include: dissolution, cementation by carbonates and other minor minerals, dolomitization, micritization, and chemical compaction.

### 2.4.2.1 Dissolution Features and Porosity

Thamama reservoirs exhibit wide range of dissolution features ranging from early shallower environment (mostly) to late deeper environment. The dissolution features together with the primary depositional pores make up the total porosity in the Thamama Reservoirs. The primary depositional porosity is dominated by intergranular macroporosity in grainstones and packstones (Figures 2.6). The intergranular pores can be found partially and/or completely cemented mostly by calcite and commonly-rarely by dolomite (Figure 2.6). This type of pores is rare in Reservoir G and common in Reservoirs A, B, C and F. In Reservoir A, most of the intergranular pores are cemented in Dense Zone (Figure 2.6A).

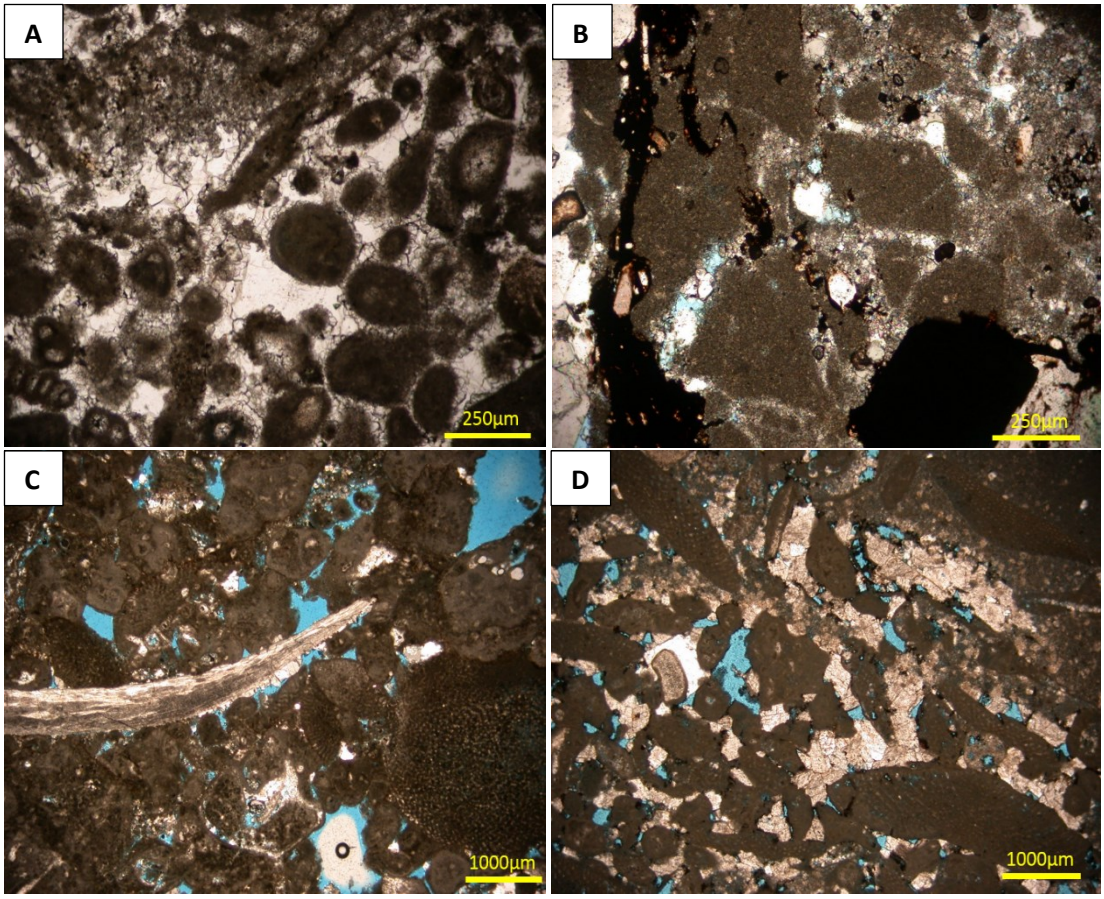

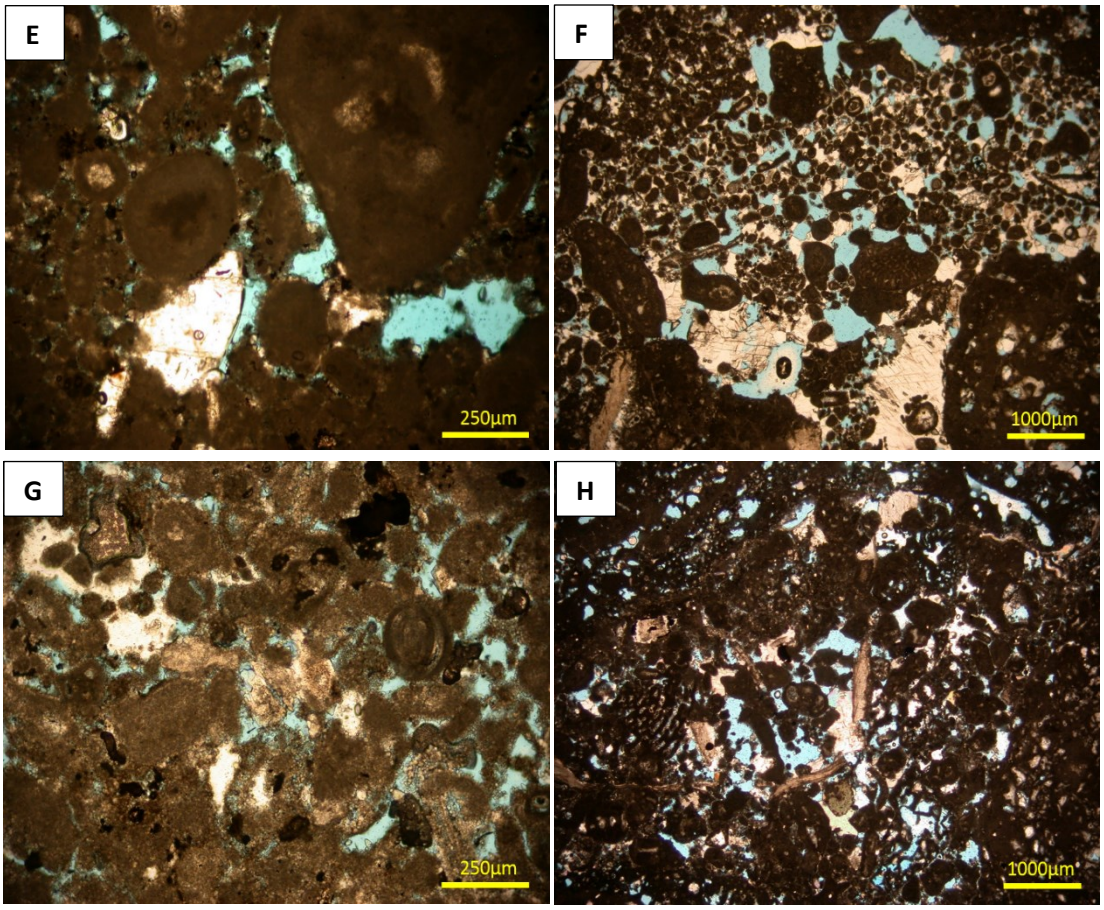


Figure 2.6: Primary intergranular porosity in all reservoirs. A) Reservoir A "oil". It is completely cemented by calcite (Dense Zone). B) Reservoir G "oil". Partial to complete calcite cementation. C) Reservoir B "oil". Occluded partially by calcite cement. D) Reservoir B "water". Dolomite cement occludes the intergranular pores. E) Reservoir C "oil". Partially cemented by blocky calcite cement. F) Reservoir C "water". Calcite and saddle dolomite cements partially fill the pores. G) Reservoir F "oil". H) Reservoir F "water". Pores are partially cemented by saddle dolomite and syntaxial calcite cements.

The secondary porosity includes diagenetically-induced dissolution features created by dissolution due to differences in fluid saturation in the system. In Thamama Reservoirs, secondary pores can be classified as type I which formed earlier, and type II which formed later during burial. Type I includes dissolution features formed during

aragonite leaching such as moldic, vuggy and intragranular pores (Figure 2.7). These pores can be found open, partially cemented or completely cemented by calcite (Figures 2.7A, B, E, F & G), dolomite (Figure 2.7C & D) and/or miner mineral such as anhydrite, in both oil and water legs. Cementation in the moldic pores in the water leg is higher than oil leg. They can be found open to partially cemented mostly in Reservoir B (Figure 2.9A & D) and commonly to rarely in Reservoirs A, C, F and G (Figures 2.7 & 2.9B & C). The fully cemented secondary pores can be found in dense intervals as well as intervals nearby and close to fractures and stylolites (Figures 2.7E & G, 2.8). Type II includes vuggy pores, micropores (Figure 2.9) and dissolved patches along and within vicinity of dissolution seams, stylolites and fractures (Figure 2.8). These type of pores are also associated with kaolinite more frequently in Reservoir A (Figure 2.8I & J) and bitumen/organic matter almost in all reservoirs along stylolites (Figure 2.8B-H). In Reservoir F, the vuggy pores cross cut a cemented fracture and partially dissolve the pre-existing cement precipitated in the fracture (Figure 2.8A).

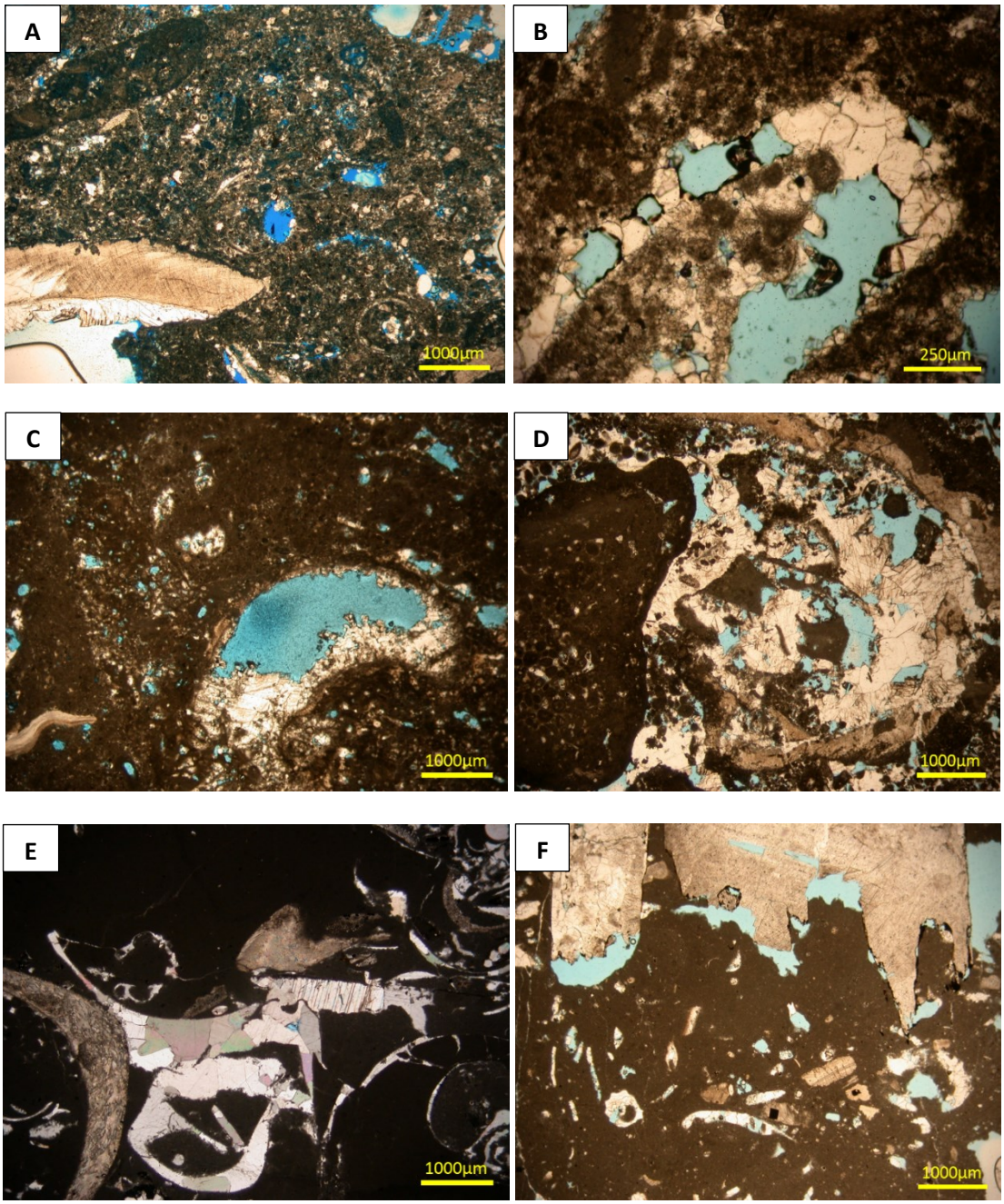
A
1000µm
B
250µm
C
1000µm
D
1000µm
E
1000µm
F
1000µm

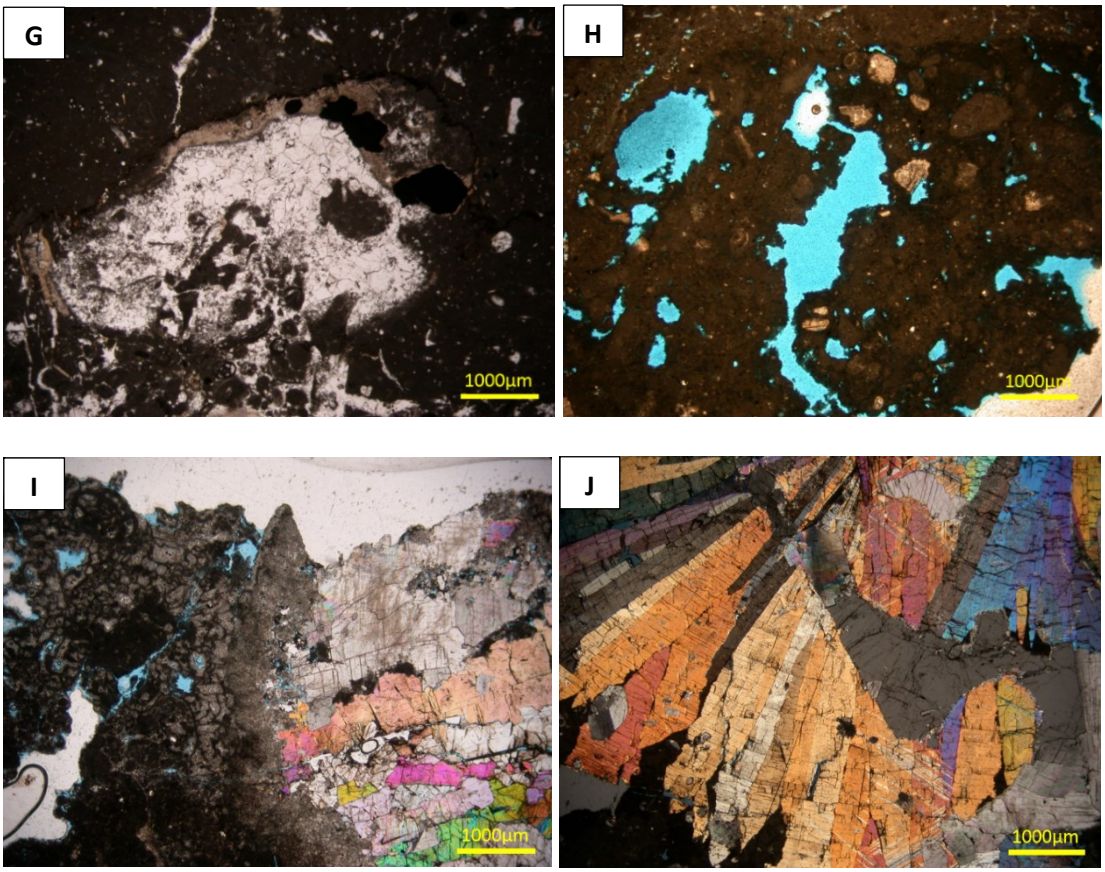


Figure 2.7: Secondary porosity type I in all reservoirs. A) Reservoir B "oil" showing vuggy and moldic pores. B) Reservoir B "water" showing moldic pore. Partial calcite cementation in the pore. C) Reservoir C "oil" showing moldic and intragranular pores occluded partially by calcite and saddle dolomite cements. D) Reservoir C "water" showing moldic and intragranular pores which are partially cemented by calcite and saddle dolomite cements. E) Reservoir F "water". Moldic pore filled completely by blocky calcite cement in Dense Zone. F) Reservoir G "oil". Partially cemented vuggy and moldic pores by calcite cement. G) Reservoir A "oil". Moldic pore filled completely by granular calcite cement in Dense Zone. H) Reservoir C "oil" showing open vuggy pores. I) Reservoir F "water". Moldic pore filled with saddle dolomite and anhydrite cements (under XPL). J) Reservoir B "water" showing moldic pore cemented with saddle dolomite and anhydrite cements (under XPL).

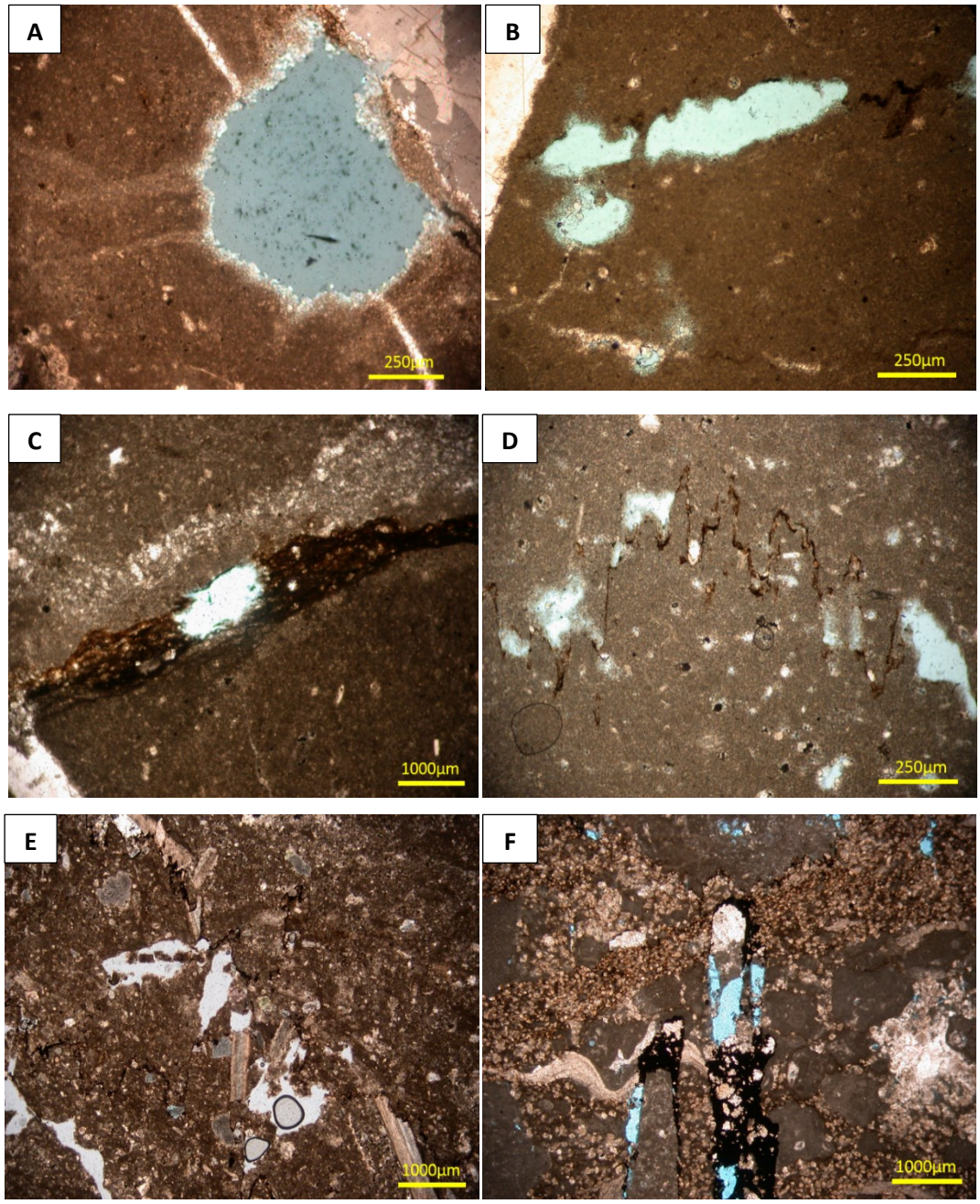
A
250µm
B
250µm
C
1000µm
D
250µm
E
1000µm
F
1000µm

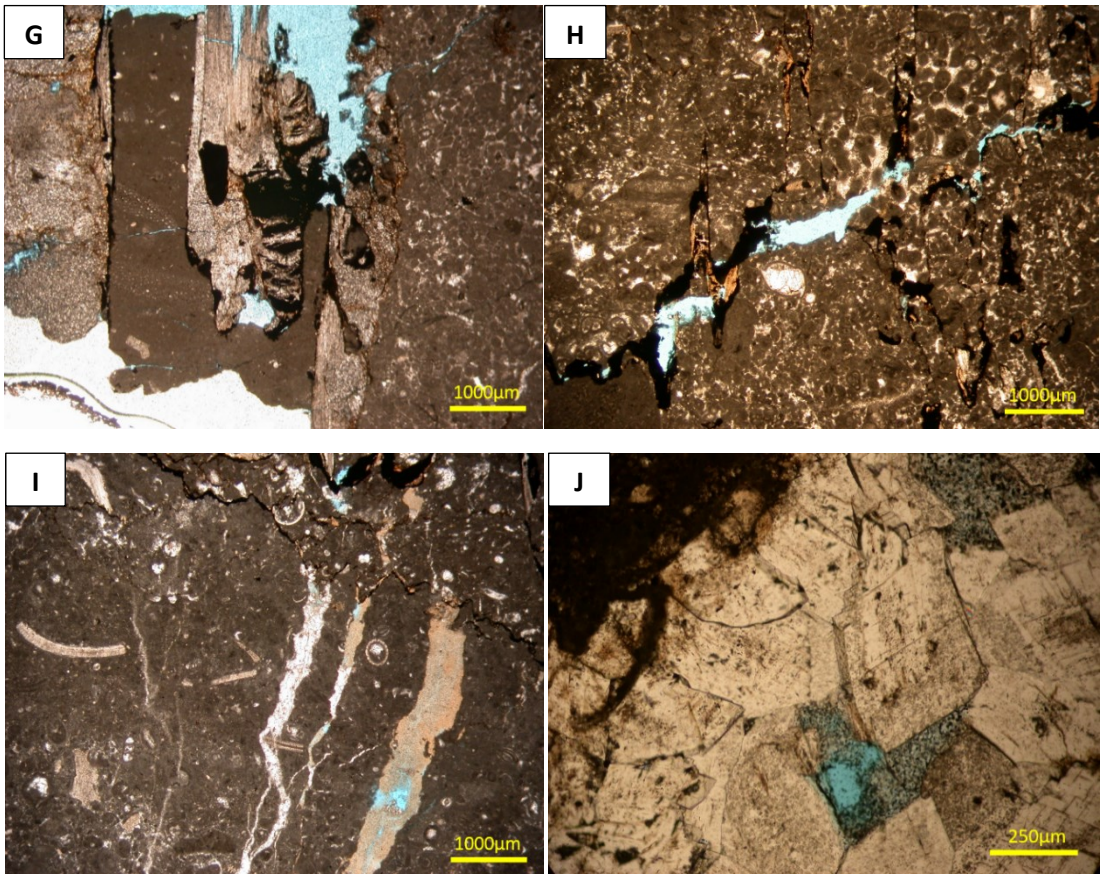


Figure 2.8: Secondary porosity type II in all reservoirs. A) Reservoir F "oil" showing vug crossing thin cemented fracture. B) Reservoir G "oil". The vuggy pores are close to fracture and along stylolite. C) Reservoir F "oil". Note dissolution along dissolution seams. D) Reservoir G "oil" showing dissolution patches along stylolite. E) Reservoir B "oil". Dissolution features are close to and along stylolite. F) Reservoir B "water" showing dissolution of bitumen and rhombic dolomite along stylolite. G) Reservoir C "oil" showing dissolution along stylolite. H) Reservoir A "oil" showing dissolution of bitumen along stylolite. I) Reservoir A "oil". Dissolution of kaolinite precipitated in fractures and along stylolite. J) Reservoir C "oil" showing dissolution of kaolinite which replaces saddle dolomite.

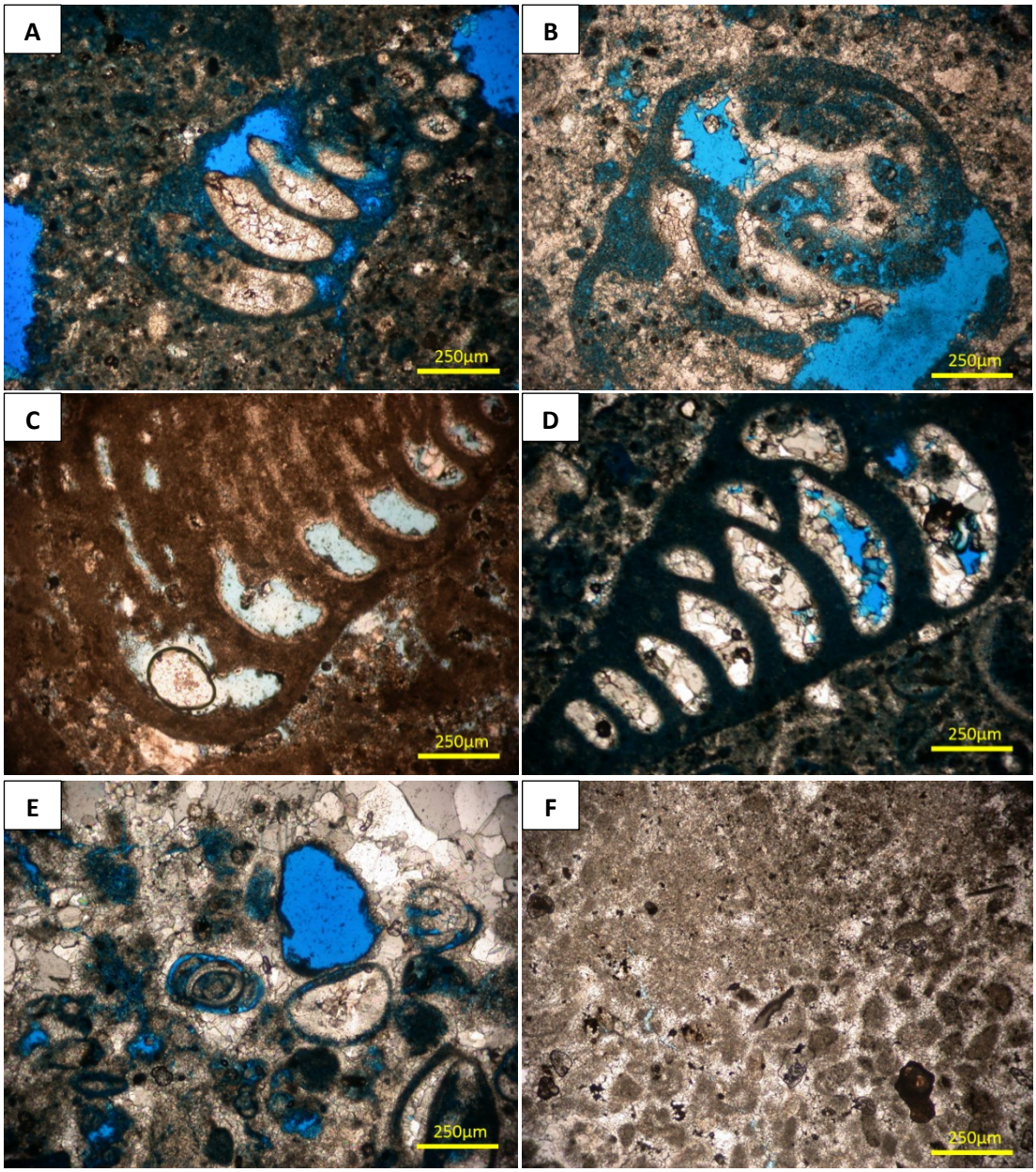


Figure 2.9: Microporosity in micritized grains. A) Micrite envelope around foram in muddy facies in Reservoir B "oil". Note how the dissolution extends to partially dissolve the cement inside the mold. B) Another dissolved micrite envelope in cemented facie also in Reservoir A "oil". The dissolution extends to partially dissolve the cement inside the mold. C) Micritized foram with intragranular porosity in muddy facies showing no clear dissolution, Reservoir F "water". D) Micritized foram with dissolved micrite envelope, Reservoir B "oil". Note how the cement inside the grain shows no dissolution as shown in figures A & B. Note also the dissolved foram and peloids around the grain. E) Reservoir B "oil" with dissolved micrite in cemented rock. F) Reservoir F "oil" showing micritized grains with no dissolution in cemented rock. Note the difference in the dissolution between this image and image E even though they have same facies.

Another source of porosity apart from dissolution features that can be found in Thamama Reservoirs is fractures. Fractures were recorded in all studied reservoirs ranging in size from micro to macro scale (Figure 2.10). They can be found open, partially cemented and completely cemented by calcite, dolomite and other mineral such as kaolinite. Fractures are not restricted to a particular facies; they can be found in different facies including grainstones, packstones, mudstones and wackstones.

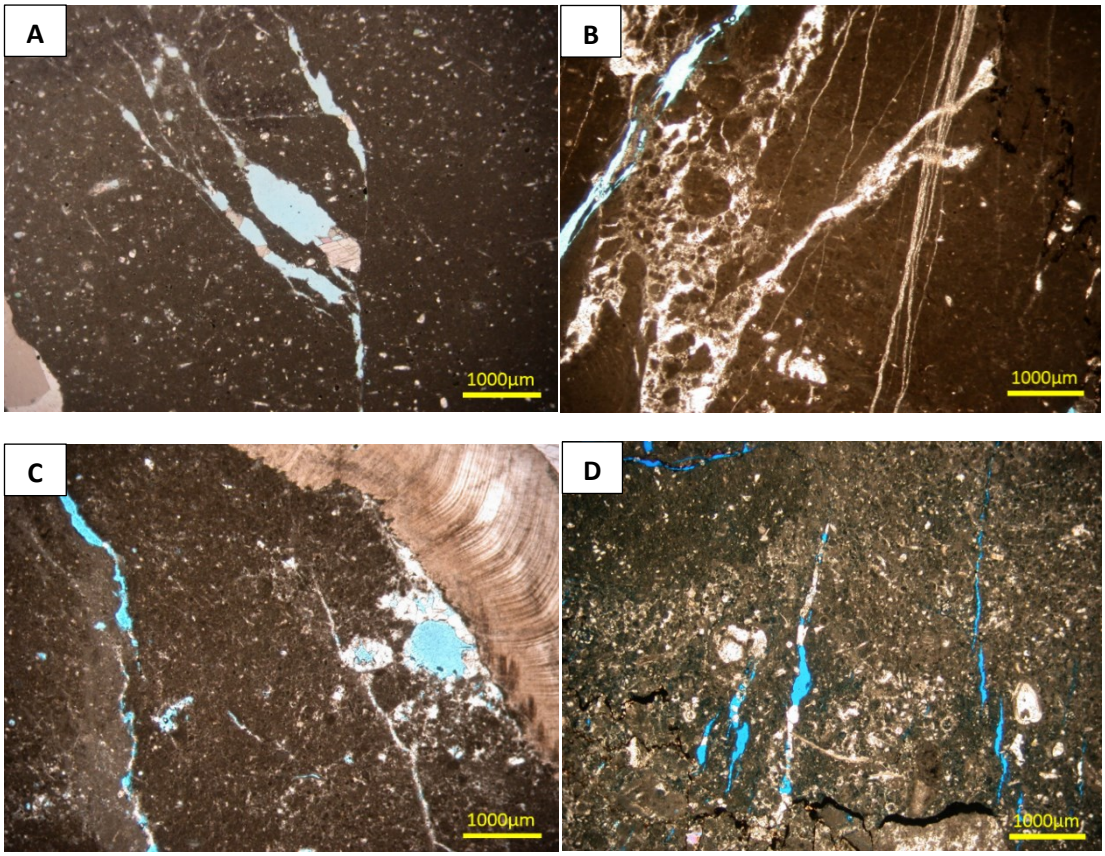

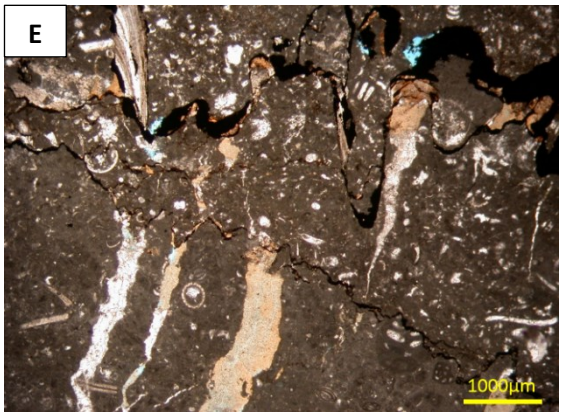


Figure 2.10: Secondary porosity type II in. A) Reservoir F "oil" showing vug crossing thin cemented fracture. B) Reservoir G "oil". Note the vuggy pores close to fracture and along stylolite. C) Reservoir F "oil" with dissolution seams. D) Reservoir G "oil" showing dissolution patches along stylolite. E) Reservoir B "oil". Note dissolution features close to and along stylolite. F) Reservoir B "water" showing dissolution of bitumen and rhombic dolomite along stylolite. G) Reservoir C "oil" showing dissolution along stylolite. H) Reservoir A "oil" showing dissolution of bitumen along stylolite.

### 2.4.2.2 Micritization

Micritization in Thamama Reservoirs has affected the outer parts of the allochems resulted in the formation of micrite envelops (Figures 2.9A-E & 2.11A-H). Moreover, it has altered the whole original fabric of some allochams causing them difficult to be distinguished (Figures 2.9F & 2.11C, E, F, G & H). Micritization features are abundant in packstone and grainstone facies commonly in Reservoir B (Figure 2.11C & D) and rarely in Reservoir G (Figure 2.11B). Most of the micrite envelopes in Reservoir B were gone through dissolution creating microporosity particularly in oil leg (Figure 2.11C).

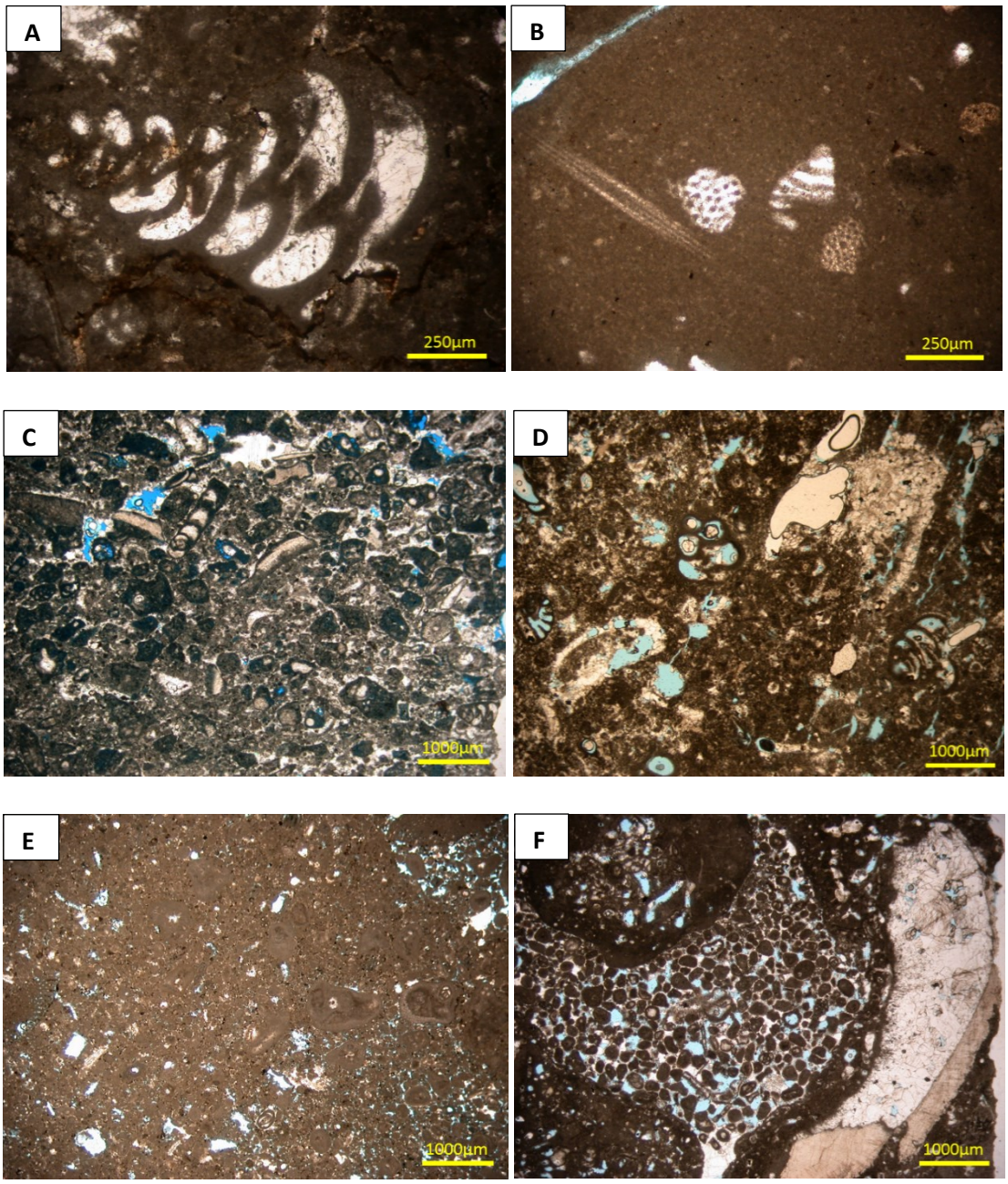
A
250µm
B
250µm
C
1000µm
D
1000µm
E
1000µm
F
1000µm

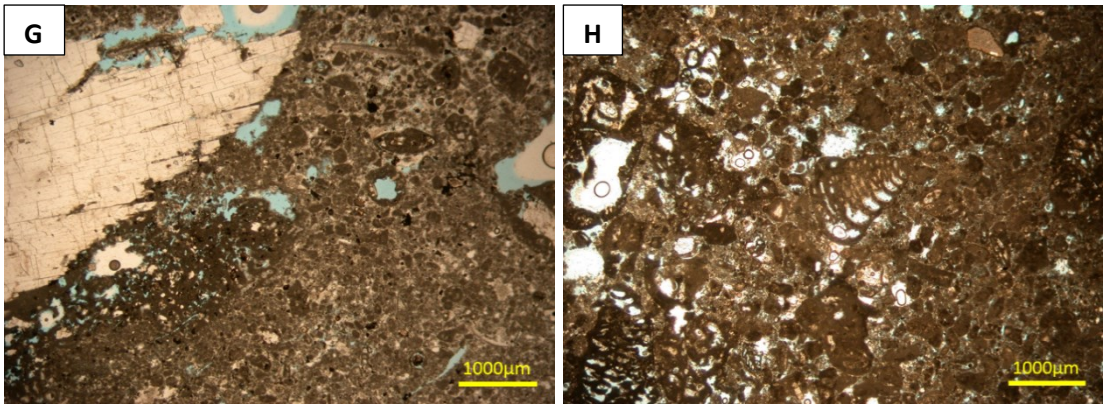


Figure 2.11: Micritization. A) Reservoir A "oil". Outer part of forams altered and the inner part is cemented. B) Reservoir G "oil". Micrite envelops around different grains in mudstone. C) Reservoir B "oil". Some grains been completely micritized. D) Reservoir B "water". Micrite envelopes around forams. E) Reservoir C "oil" with completely micritized grains and micrite envelopes. F) Reservoir C "water". Extensive micritization in packstone. G) Reservoir F "oil". H) Reservoir F "water". Micrite envelops around forams and the complete micritzed grains in both water and oil of Reservoir F.

### 2.4.2.3 Calcite Cementation

#### General Calcite Morphologies in Thamama Rocks

Calcite cementation is one of the significant diagenetic processes in the Thamama Reservoirs. Different calcite morphologies were recorded in the water and oil legs. Circumgranular calcite occurs in grainy facies precipitating around grains (Figure 2.12A-D). This type of calcite is the first to precipitate in the calcite and even entire cementation history of Thamama Reservoirs. Equant calcite with various crystal sizes (few µm to ~150 µm) is the third most abundant calcite cement after blocky and syntaxial calcite. Equant calcite can be seen filling intergranular, intragranular, vuggy and moldic pores as well as few fractures (Figure 2.12A, B, D, E & F). Equant calcite can exhibit coarsening towards the pore centre, and hence can be called a drusy calcite (Figure 2.12G).

Syntaxial overgrowth cement is typically associated with echinoderm grains (Figure 2.12D, E, H & I). This type of cement the second abundant calcite type. The overgrowth cement has exteneded to partly filled the adjacent intergranular pores. The size of the syntaxial calcite ranges between 150 and 600 μm. Relative timing of equant and syntaxial calcite vary a little bit across the reservoirs but both follow circumgranular calcite. The relative timing of both calcite types will be given for each reservoir in the paragenetic sequence Section 2.5.1 and cement stratigraphy Section 3.3.1. The most abundant calcite that can be noted in these reservoirs is the blocky calcite (> 200 μm). Blocky calcite occurs in all pore types. There are two blocky calcite generations in Reservoirs A, B and C. The first blocky calcite generation (BI) occurs in some moldic, intergranular and intragranular pores (Figures 2.12A, I, & J & 2.13A). This generation is predating stylolitization and fractures. The second blocky calcite generation (BII) is postdating stylolitization and precipitated along stylolite, in fracture and some in the adjacent pores (Figure 2.13). Commonly, both blocky calcite generations postdates the circumgranular calcite and the first cement zones of equant and syntaxial calcite. Granular calcite is rarely found in the reservoirs (Figure 2.12K).

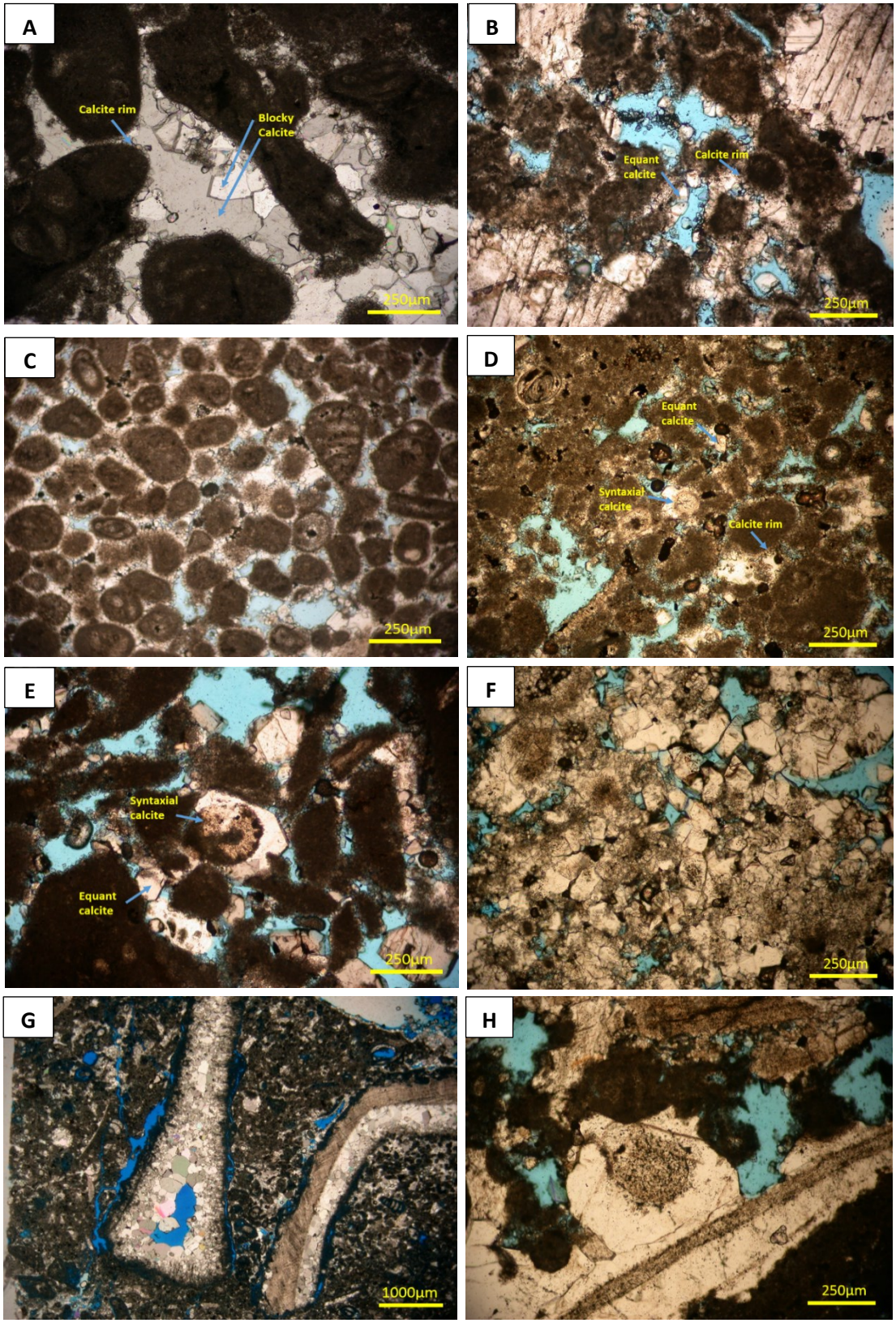
A
Calcite rim
Blocky Calcite
250µm
B
Equant calcite
Calcite rim
250µm
C
250µm
D
Equant calcite
Syntaxial calcite
Calcite rim
250µm
E
Syntaxial calcite
Equant calcite
250µm
F
250µm
G
1000µm
H
250µm

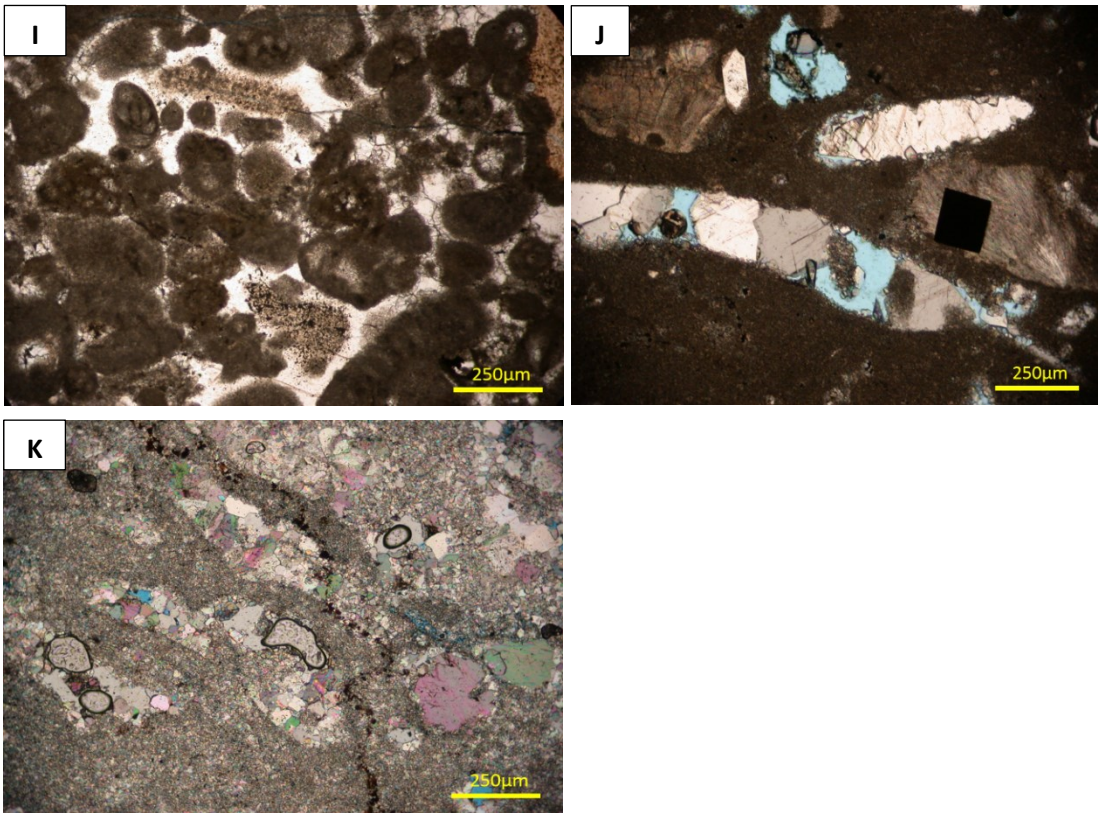


Figure 2.12: Different calcite cement morphologies. A) Reservoir A "oil" with calcite rim around grain and blocky calcite (BI) filling intergranular pore. B) Reservoir B "water" showing calcite rim around grain and equant calcite filling intergranular pore. C) Reservoir C "water" showing calcite rim around grains. D) Reservoir F "oil" with calcite rim around grains, equant and syntaxial calcite in intergranular pore. E) Reservoir G "oil" showing equant and syntaxial calcite in intergranular pore. F) Reservoir C "oil" showing equant calcite. G) Reservoir B "oil" with drusy calcite in moldic pore. H) Reservoir B "water" showing syntaxial calcite. I) Reservoir A "oil" with syntaxial calcite in intergranular pore. J) Reservoir G "oil". Blocky calcite (BI) partially filling molds. K) Reservoir B "oil" showing granular calcite filling intragranular pores.

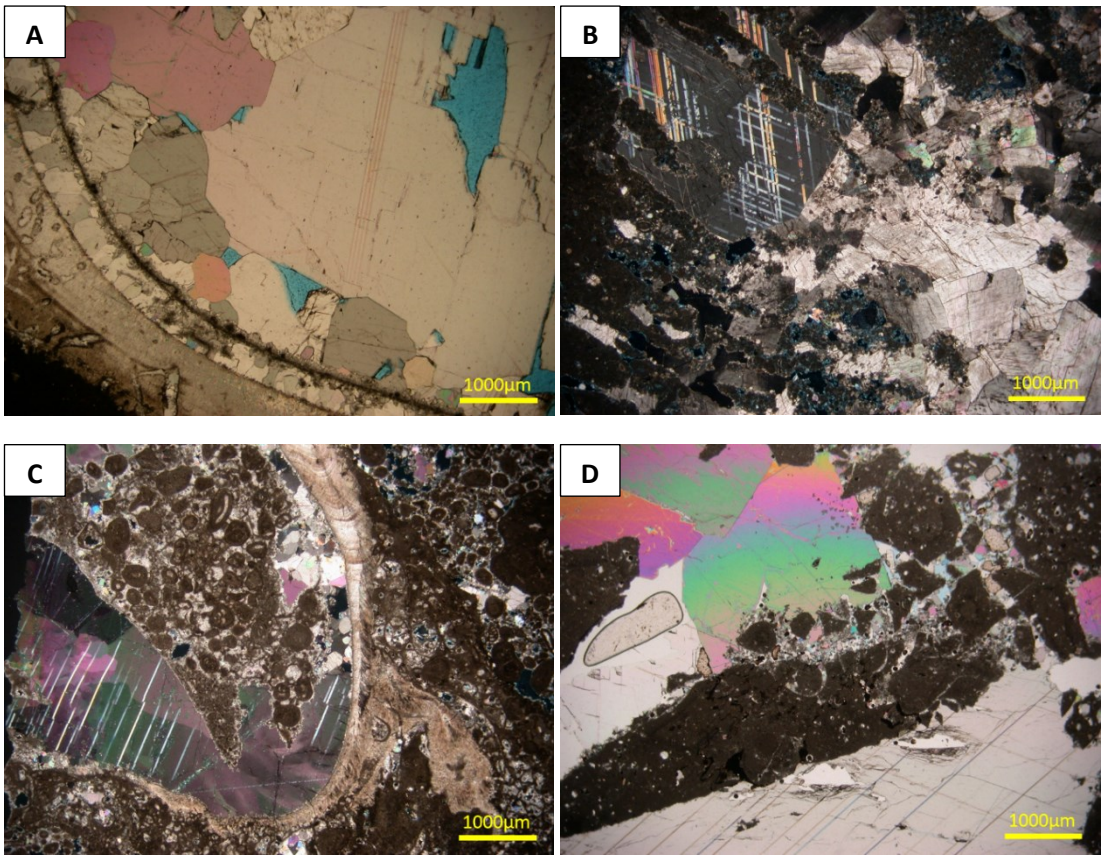


Figure 2.13: Second generation of blocky calcite (BII) in. A) Reservoir A "oil" with very coarse blocky calcite in a mold. B) Reservoir B "water" showing blocky calcite with twinning in a mold and extends to adjacent intergranular pore. C) Reservoir C "water" with twinned blocky calcite in a mold. D) Reservoir G "oil" showing twinned blocky calcite precipitated in breccia and fracture.

### 2.4.2.4 Dolomitization

Dolomite in Thamama Reservoirs can be classified into three types; (Type 1) micro-rhombic dolomite, (Type 2) coarser dolomite and (Type 3) saddle dolomite. The micro-rhombic dolomite is commonly found in wackestones and, less commonly, in packstones and grainstones (Figure 2.14). The coarse (Figure 2.15) and saddle dolomites (Figure 2.16) are mostly found in packstones and grainstones.

Rhombic dolomite is the first dolomite to precipitate in the Thamama. It is a micro-crystalline dolomite (=< 10 μm across) with planar; subhedral-euhedral crystals (Figure 2.14). This type of dolomite is a replacive form; replacing micrite partially or completely in mud rich facies (Figure 2.14A, B, D & E). This type of dolomite has zoned crystals under the CL in certain reservoirs reflecting ferroan and non-ferroan zones. The maximum number of CL cement zones found in this dolomite is five (Figure 2.14H). In the oil leg, Type 1 can be only found in Reservoirs A, B and C. More volumetrically in Reservoirs B and C concentrated along dissolution seams and scattered in mud rich facies or replacing the entire mud facies (Figure 2.14D, E & G). Rhombic dolomite can be also found precipitated and further developed along stylolites (Figure 2.14I). Similarly, in the water leg, rhombic dolomite is found along dissolution seams and scattered in mud rich facies in Reservoirs B and F. It could not be traced in other reservoirs from the water leg as no samples were collected from A and G and few samples from C are available. The progressive replacement of micrite by rhombic dolomite has created micropores (Figure 2. 14A-D). Oil sample has higher micropore compared with water sample.

The coarse dolomite is the second to precipitate. It consists of subhedral-anhedral coarse crystals (>50 μm) with sweeping extinction (Figure 2.15). This dolomite can be seen filling vugs together with micrite in completely dolomitized rock (dolostone) (Figure 2.15B). The micrite and partly coarse dolomite have been dissolved (Figure 2.15B). Most of the crystals show cement zonation (2-3 zones) under the CL (Figure 2.15B). This dolomite occurs only in Reservoirs B, C and F of oil leg;

along stylolites, and in molds and vugs. In the water leg this type of cement can be only found in Reservoir B based on the available samples.

Saddle dolomite is the last to precipitate. This dolomite is characterized by non-planar (anhedral), very coarse crystals (>250 µm) distinguished by undulose extinction (Figure 2.16). Saddle dolomite in all reservoirs has at least three distinguished CL zones as in Reservoir F and C in oil leg and Reservoir B in water leg (Figure 2.16F). Reservoirs F and C "water" contain up to four CL zones (Figure 2.16E). The two common CL zones across all reservoirs are the very dark thick older cement zone and the very bright luminance thick younger cement zone (Figure 2.16E & F). This dolomite was reported in all reservoirs in oil leg except Reservoir A. In water leg, only three reservoirs were studied including F, C and B. Saddle dolomite can be found in different pore types, and in fractures and along stylolites.

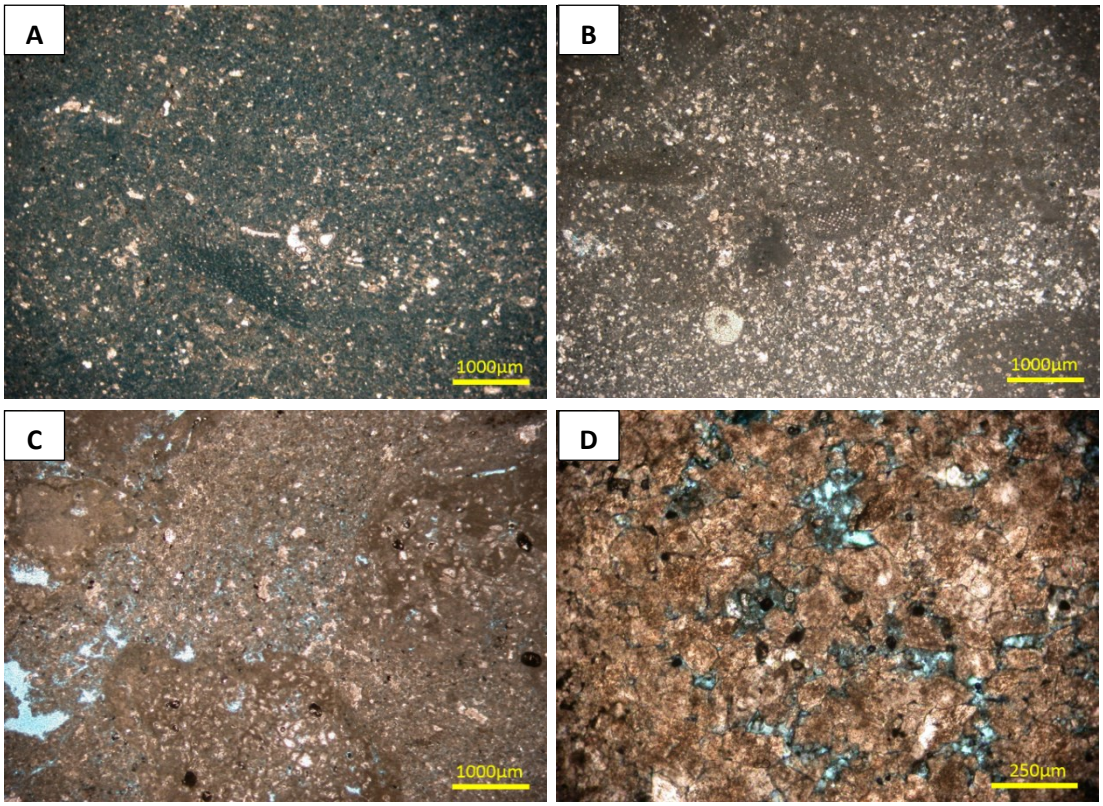

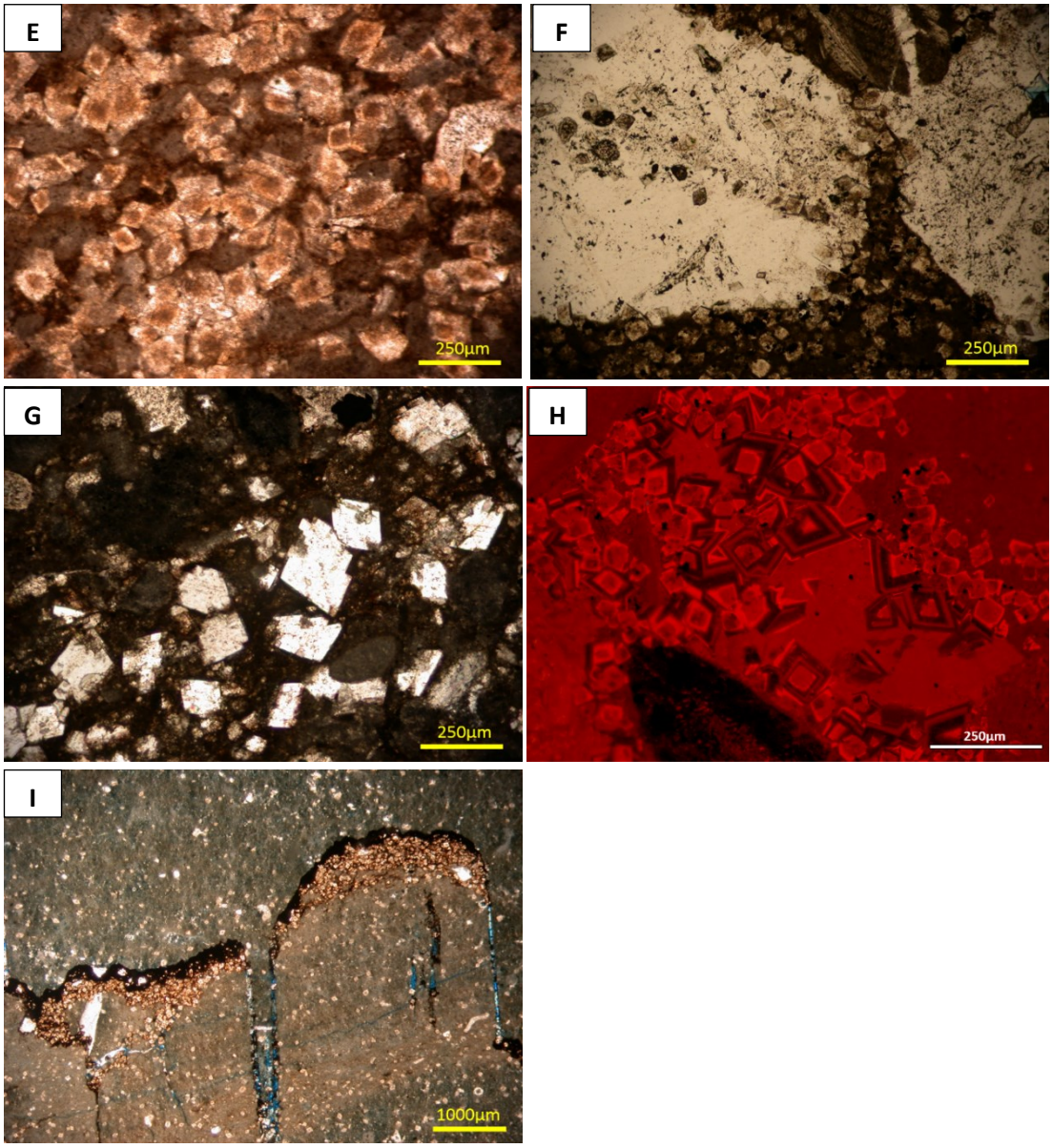


Figure 2.14: Replacive micro-rhombic dolomite. A) Reservoir B "oil", scattered in much-rich facies. B) Reservoir B "water", scattered in much-rich facies. Note the difference in microporosity between the dolomitized mudstone-packstone in the oil versus water. C) Reservoir F "water". Rhombic dolomite replacing micrite in packstone. D) Reservoir B "oil". Note the microporosity created by dolomitization. E) Reservoir C "oil" showing replacive dolomite with no clear development of microporosity. F) Reservoir B "oil". Note how rhombic dolomite is growing after the blocky calcite. G) Reservoir A "oil". Rhombic dolomite along dissolution seams. H) Reservoir B "oil". Typical zonation of rhombic dolomite found in most rhombic dolomite. Rhombic dolomite is replacing blocky calcite. I) Reservoir B "oil". Rhombic dolomite concentrated and further developed along a stylolite. Note the rhombic dolomite scattered in matrix and along clay laminae which is cut by stylolite.

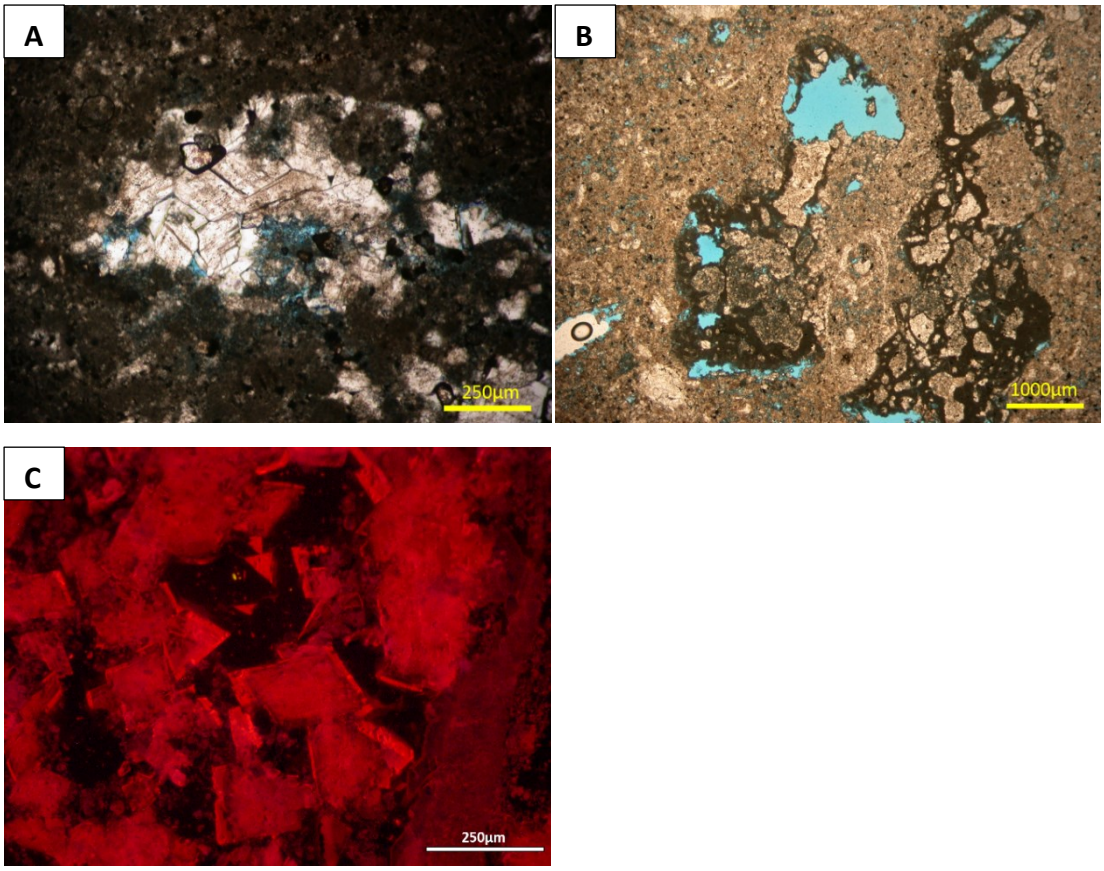


Figure 2.15: Coarse dolomite in Reservoir B "oil". A) Filling vuggy pore in muddy facies. B) Coarse dolomite cemented in vuggy pore with micrite. Note the dissolution of micrite and coarse dolomite. Note also rhombic dolomite in matrix owing to coarse dolomite. C) Typical zonation of coarse dolomite under CL.

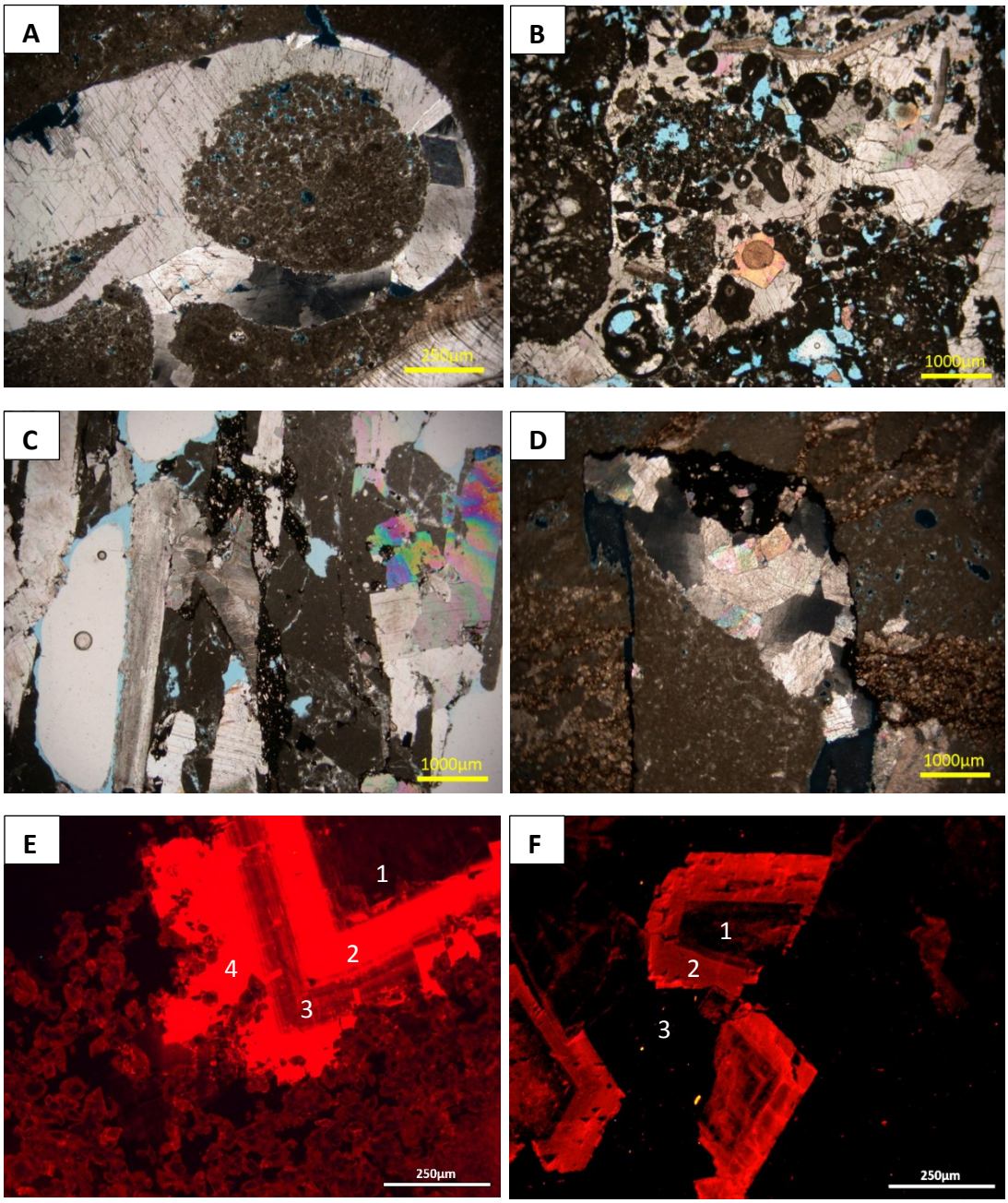


Figure 2.16: Saddle dolomite. A) Reservoir C "oil", filling a mold. B) Reservoir F "water", occluding an intergranular pore. C) Reservoir G "oil", accumulated along stylolite. D) Reservoir B "water", precipitated along a stylolite. E) Reservoir F "water", showing typical zonation of saddle dolomite in water leg. F) Reservoir B "oil", showing typical zonation of saddle dolomite in oil leg.

### 2.4.2.5 Chemical Compaction and associated cements

Chemical compaction features in the Thamama Reservoirs include stylolites and dissolution seams. Dissolution seams are abundant in oil leg than water leg (Figure 2.17). They are commonly concentrated in dense intervals both in oil and water legs. Well-developed stylolites are more common in the water leg than oil leg and in the deeper Reservoirs F and G. Most of the stylolites in the water leg are rectangular, high amplitude (up to 12 cm) and associated with coarse-crystalline calcite and dolomite cements (Figure 2.17C). Stylolites in the oil leg are extensive and abundant in Reservoirs G and F, and rare-common in Reservoirs A, B and C. In the oil leg, stylolites are rectangular-triangular with an amplitude up to 9 cm (Figure 2.17D-H). Stylolites with high amplitudes (Figure 2.17E & D) were observed in few samples of muddy facies (mud/wackstone) from the oil leg. Generally, stylolites occur in all reservoir facies including grain supported texture facies in both water and oil legs (Figure 2.17G & H). The orientation of stylolites and dissolution seams is horizontal.

Bitumen and laminae of clay minerals are noted along stylolites and dissolution seams. Clay minerals/organic matter can be found mostly along seams of variable thickness and abundance (Figure 2.17A & B) whereas along stylolites the bitumen is abundant (Figure 2.17C-H). Sometimes stylolites appear as a barrier separating dissolved matrix rich in high microporosity from less microporous matrix (Figure 2.17G). The dissolution may progress to higher amounts of dissolution in the matrix trapped within stylolite (Figure 2.17H).

Cements including blocky calcite, saddle dolomite, and sometimes kaolinite and pyrite occur with variable amounts along most of the stylolites (Figure 2.17A, C & D & 2.18A & H). Small fractures (around 1- 5 mm long and 100-360 μm wide), which are oriented perpendicular to the stylolites, are commonly filled with calcite, dolomite and/or kaolin (Figure 2.18A & B). Kaolin [$Al_2Si_2O_5(OH)_4$] was found mainly filling small fractures (arranged perpendicular to stylolites) and moldic pores as well as in the vicinity and along stylolite (Figure 2.18A).

Pyrite occurs as framboidal scattered, replacive coarse-crystalline and as euhedral coarse pyrite. The framboidal pyrite is found replacing calcite and scattered in shells and matrix (Figure 2.18C & D). Coarse-crystalline pyrite is replacing some shells and calcite (Figure 2.18E & F). Euhedral coarse pyrite was documented only in Reservoir G, floating around stylolites and fractures (Figure 2.18G & H).

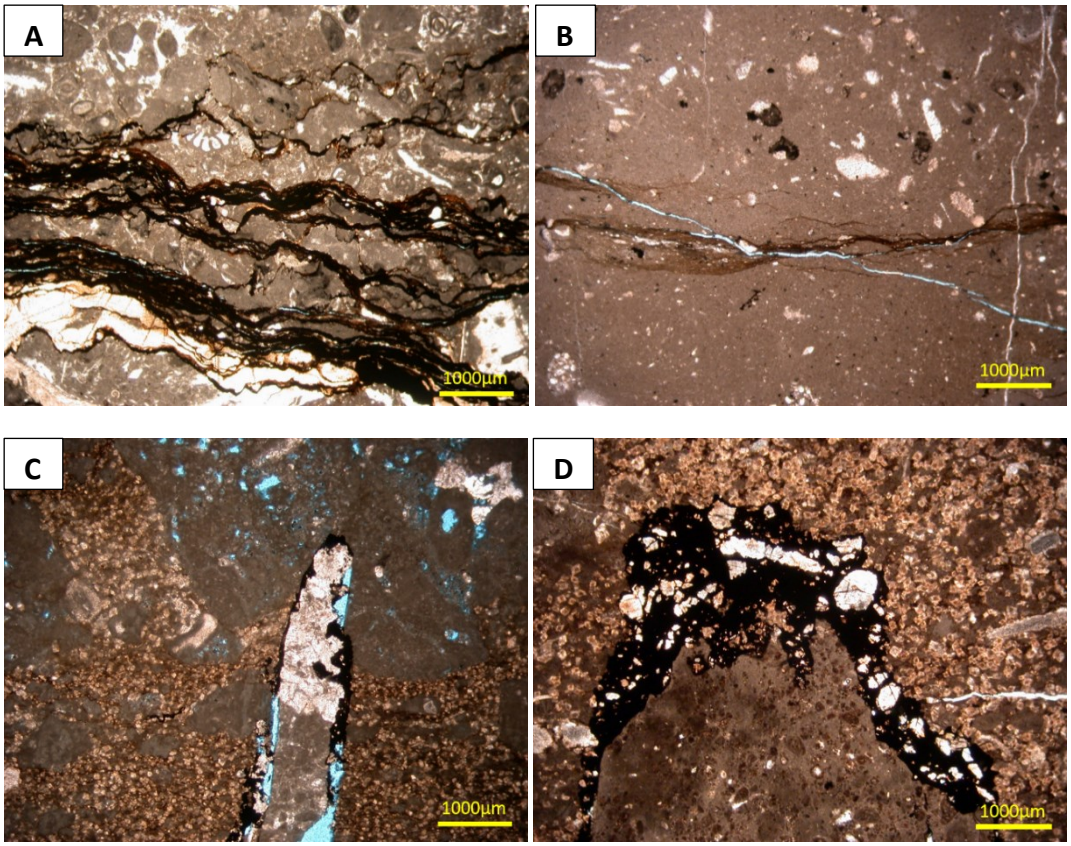

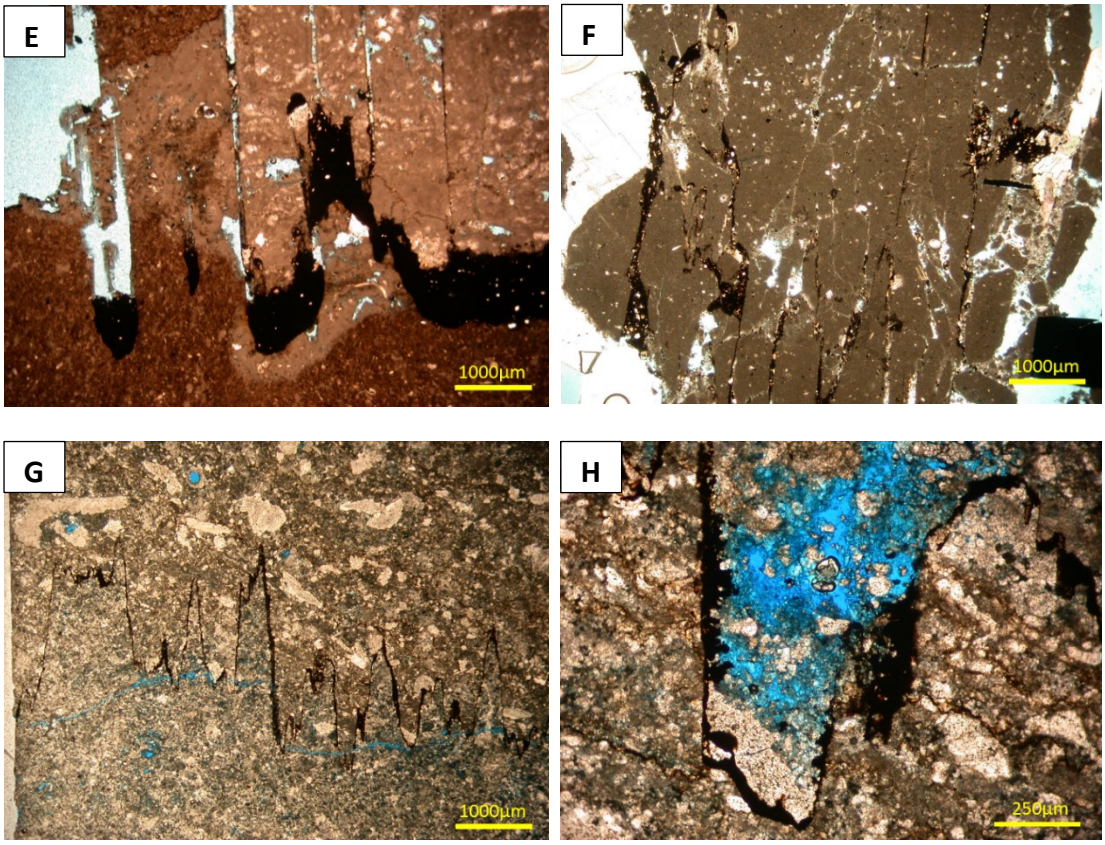


Figure 2.17: Chemical compaction features in. A) Reservoir A "oil" showing dissolution seam with thick clay/organic matter. B) Reservoir F "oil" with dissolution seam with clay laminae. C) Reservoir B "water". Note how some grains been completely micritized. D) Reservoir B "water" showing rectangular stylolite with a high amplitude. Note the saddle dolomite along stylolite and also how the stylolite cross cuts the dissolution seam and rhombic dolomite. E) Reservoir F "oil" showing rectangular high amplitude stylolite in a mud-rich facies. F) Reservoir G "oil". Note the extensive stylolitization with triangular amplitude. G) Reservoir B "oil" with triangular stylolite acting as a barrier for fluid flow separating microporous rock from non-microporous rock. H) Reservoir B "oil". Note the dissolved matrix trapped within stylolite.

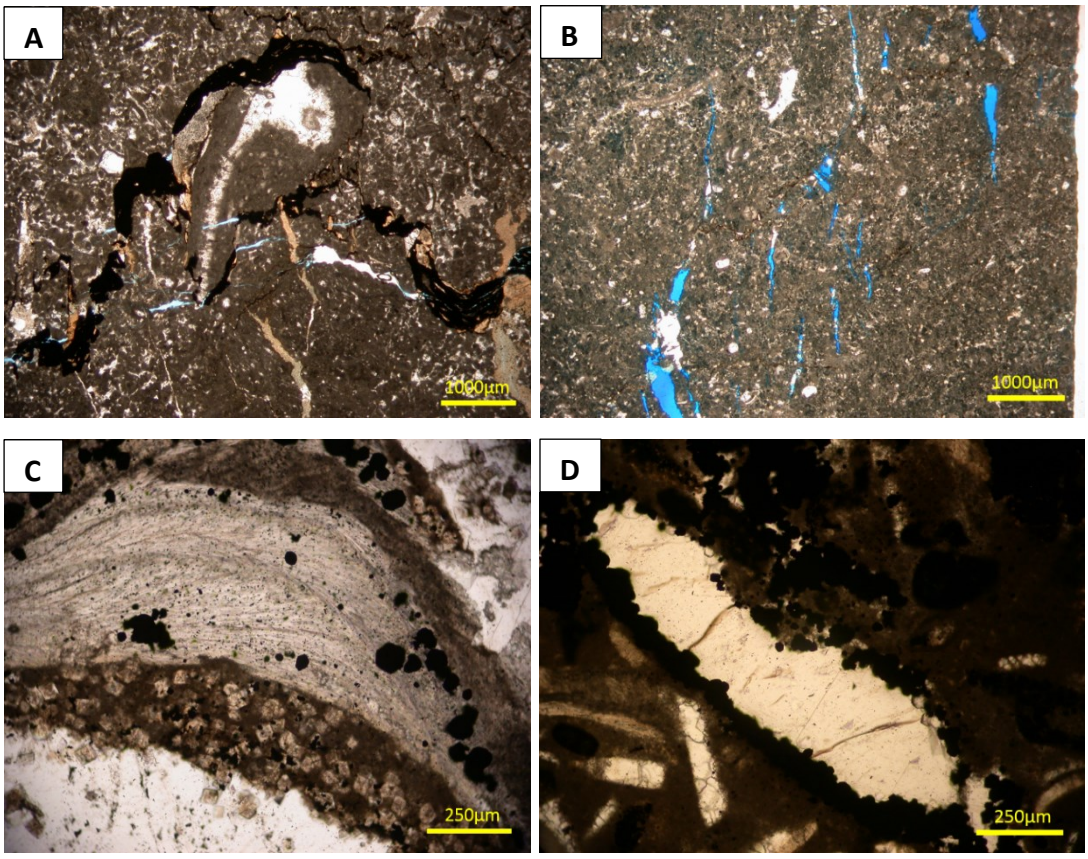
A
1000µm
B
1000µm
C
250µm
D
250µm

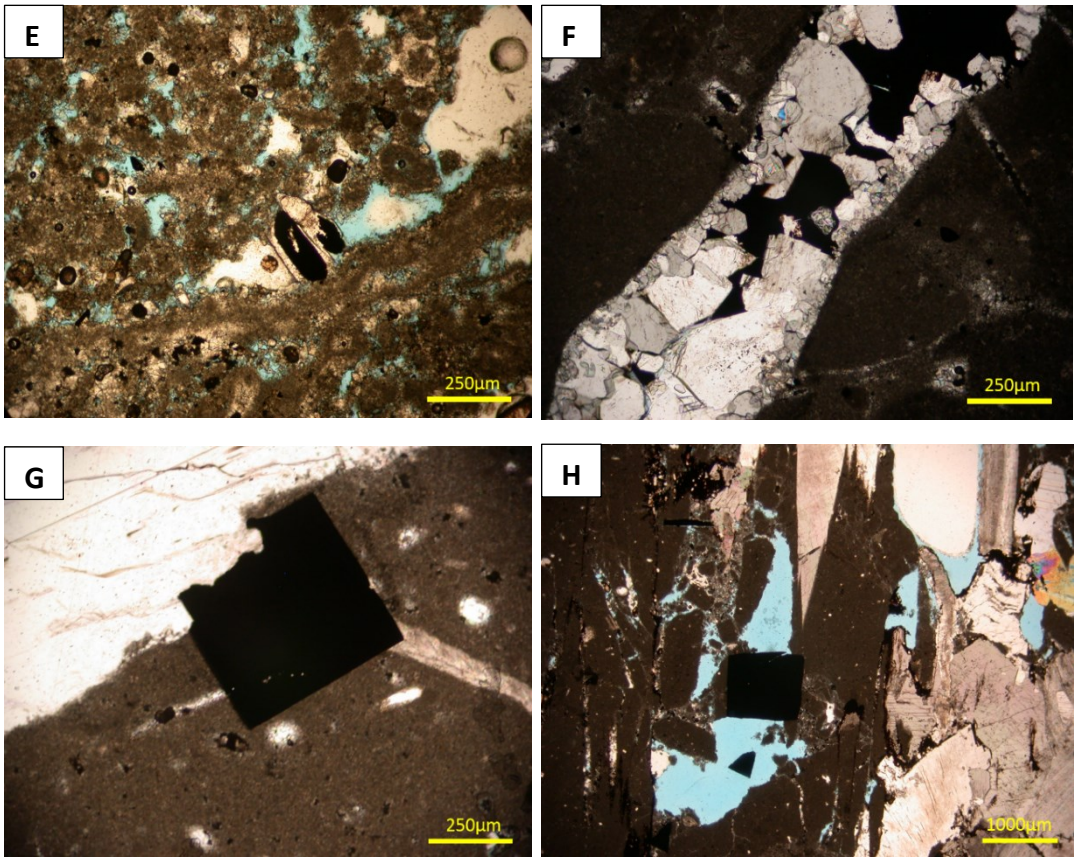


Figure 2.18: Fractures and cements along stylolites. A) Reservoir A "oil". Fractures formed perpendicular to stylolites and are filled with calcite and kaolinite. Also bitumen associated with kaolinite is along stylolite. B) Reservoir B "oil". Fractures are perpendicular to stylolite and partially filled with blocky calcite. C) Reservoir A "oil". Framboidal-coarser pyrite replacing calcite. D) Reservoir B "oil". Framboidal pyrite scattered in matrix and shell. E) Reservoir F "oil". Coarse-crystalline pyrite replacing calcite. F) Reservoir G "oil". Coarse-crystalline pyrite replacing calcite. G) Reservoir G "oil". Coarse euhedral pyrite floating and partially replacing calcite around fracture. H) Reservoir G "oil". Coarse euhedral pyrite along stylolite.

## 2.5 Summary of Diagenetic Events

Diagenetic events in Thamama Reservoirs can be summarized as micritization, early and late dissolution, calcite cementation, dolomitization and dolomite cement, chemical compaction and cementation of other types of cement. These diagenetic events are unequally distributed through Thamama Reservoirs (Table 2.1). The most diagenetically affected reservoir is B, while A is least affected. Tectonic events which correspond to fracture formation can also be placed within the paragenetic sequence context. The relative timing of the diagenetic events varies slightly across Thamama Reservoirs. This section should provide details on common diagenesis found in Thamama Reservoirs.

Table 2.1: Main Diagenesis in Thamama Reservoirs and their relative abundance. A: Abundant, C: Common, R: Rare, N: Not Found.

| Diagenetic Features | Reservoir A | Reservoir B | Reservoir C | Reservoir F | Reservoir G |
|---|---|---|---|---|---|
| Micritization | C | A | C | C | C |
| Circumgranular calcite | C | C | C | C | R |
| Framboidal pyrite | C | R | R | C | R |
| Syntaxial overgrowth | C | C | C | R-C | R |
| Aragonite dissolution | C | C | C | C | R-C |
| Equant calcite | R | C-A | C | A | R-C |
| Dissolution seams | A | C | R | C | C |
| Rhombic dolomite | R | C | R | R | NF |
| Blocky calcite | A | A | C | A | A |
| Stylolitization | R-C | R-C | R-C | C | C |
| Coarse-euhedral pyrite | NF | NF | NF | R | C |
| Saddle dolomite | NF | C | C | C | C |
| Anhydrite | NF | R | R | R | R |
| Microporosity | C | A | C | C | C |
| Late/burial dissolution | C | C | C | C | C |

### 2.5.1 Paragenetic Sequence in Thamama Reservoirs A, B, C, F and G

The paragenetic sequence history of each reservoir is described below. Fracture formation is also placed within the paragenetic sequence context. Information about fractures was gathered from materials of other PhD student working on Thamama fractures.

#### 2.5.1.1 Paragenetic Sequence History of Reservoir A

Figure 2.19 illustrates the diagenetic events and their relative timing in Reservoir A. The hardground was probably formed as synsedimentary or early cementation at seafloor in all reservoirs. Micritization occurred first followed by circumgranular cement and then equant. The syntaxial calcite precipitated parallel or slightly later than circumgranular calcite and predating the precipitation of blocky calcite. Aragonite dissolution might have provided the solutes for the formation of circumgranular calcite. Aragonite dissolution can be interpreted to occur before and during circumgranular calcite precipitation. The precipitation of BI cements in the matrix (intergranular, intragranular and moldic pores) had completed before stylolitization. Following this, dissolution seams developed, which triggered the formation of rhombic dolomite and then framboidal pyrite formed. Stylolitization cross cut the dissolution seams. During stylolitization, the first fracture generation (width: ~0.3-0.5 mm) was formed perpendicular to the stylolites. The later formed blocky cements precipitated in the newly formed fractures (and some along stylolites and in nearby moldic pores). Precipitation of bitumen and kaolinite seems to be occurred at the same time. Kaolinite replaced the blocky calcite in the fractures and accumulated along stylolites and dissolution seams as well as in intragranular pores (between rhombic dolomite crystals). The second fracture generation (width: ~0.1 mm) formed parallel to the stylolites and perpendicular to the first fracture generation. This generation contains open fractures. The last event in the reservoir seems to be the dissolution event that washed away some bitumen and partially dissolved kaolinite.

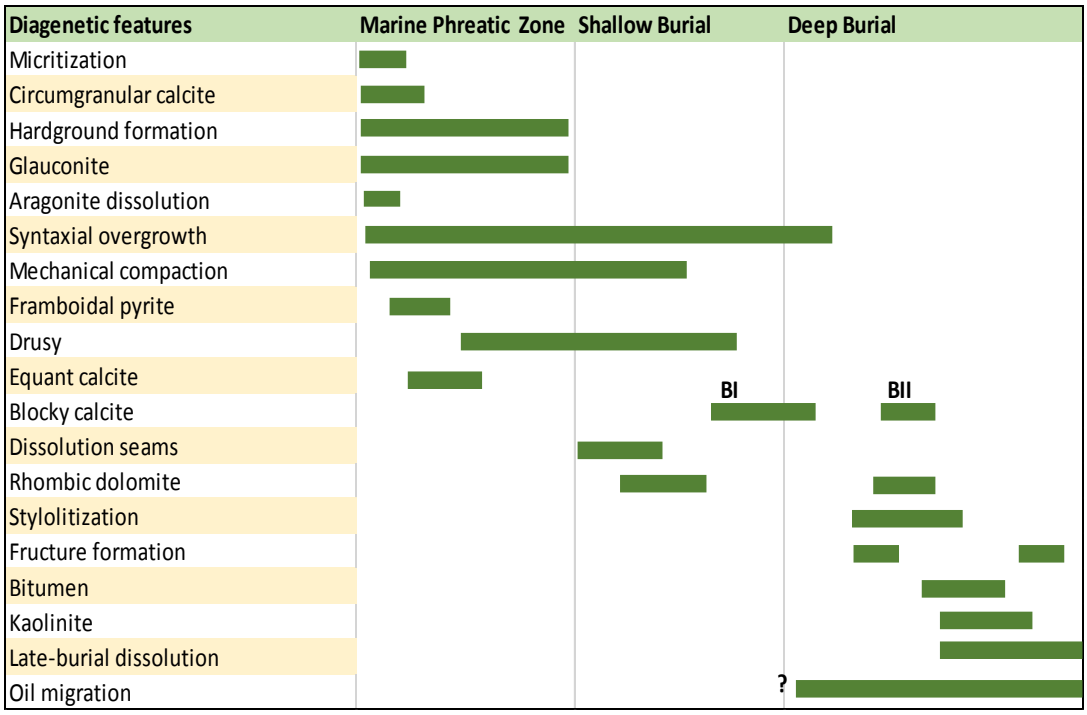


Figure 2.19: Paragenetic sequence of Reservoir A.

### 2.5.1.2 Paragenetic Sequence History of Reservoir B

Reservoir B contains a notably different diagenetic overprint compared with Reservoir A. Diagenesis in B started with the typical micritization process resulting in the first introduction of microporosity into the reservoir (Figure 2.20). Then, circumgranular calcite cement precipitated which supported the rock texture and prevented further mechanical compaction that preserved intergranular pores. Aragonite dissolution was established before and during circumgranular cementation which provided dissolved carbonate for early calcite cementation. After that, the syntaxial cement started to precipitate followed granular, drusy, blocky calcite (BI) and then equant. The early blocky cements (BI) in matrix (intergranular, intragranular and moldic pores) were precipitated before stylolitization. Following this, dissolution seams were developed providing good conditions for rhombic dolomite formation. The framboidal pyrite came next to precipitate after rhombic dolomite and blocky calcite. Then, stylolitization developed with fractures (width: ~0.1 mm) forming perpendicular to the stylolites. Stylolites cross cut the dissolution seams and rhombic dolomite.

Rhombic dolomite and framboidal pyrite continued to develop further after stylolitization to form coarser euhedral dolomite and pyrite. The later formed fractures have been filled partially with blocky calcite (BII). The BII, saddle dolomite and rare anhydrite precipitated along stylolites and few pores in matrix (intergranular, intragranular and moldic pores). Bitumen and kaolinite were precipitated next at the same time. The second fracture generation (width: ~0.1 mm) formed parallel to the stylolites and perpendicular to the first fracture generation. Fractures of this generation are open. Late dissolution is believed to be the last event to occur in the reservoir. During this event some bitumen were washed away, some cements (calcite, dolomite) were partially dissolved, microporosity progressed further by dissolving more micrite.

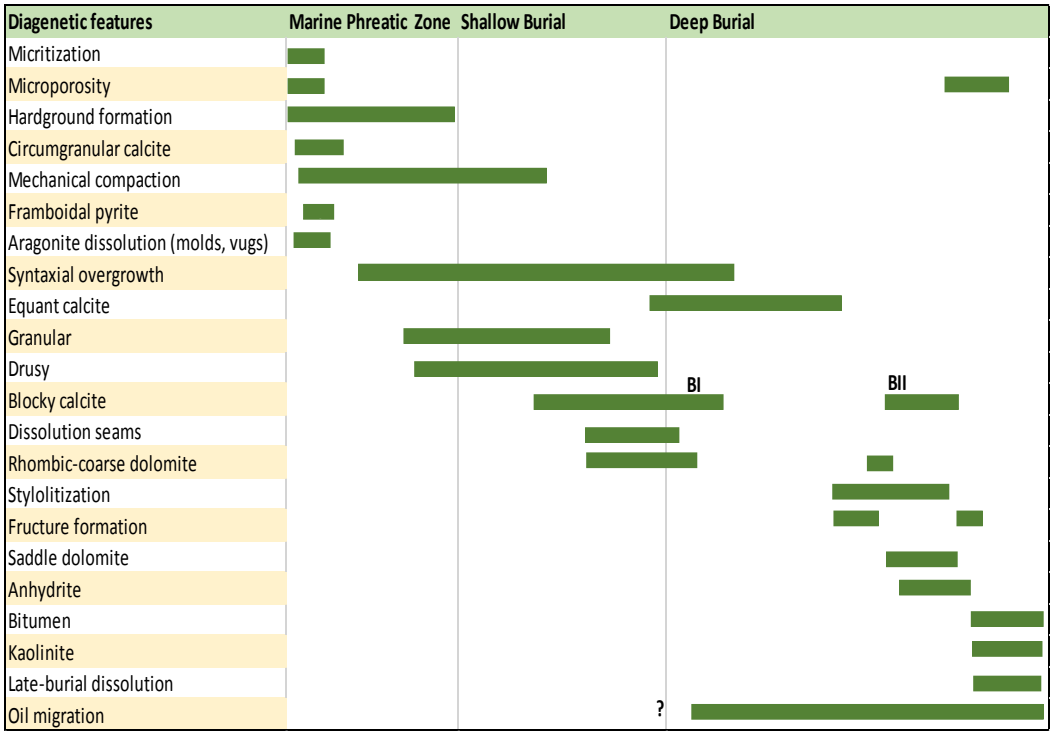


Figure 2.20: Paragenetic sequence of Reservoir B.

### 2.5.1.3 Paragenetic Sequence History of Reservoir C

The paragenetic story in Reservoir C is quite similar to B. The differences in diagenesis between these two reservoirs are in the relative timing of precipitation of different calcite morphologies, and the abundance of microporosity (Figure 2.21). Calcite morphology in Reservoir B is more varied compared to Reservoir C. The relative timing of syntaxial and equant calcite differs in Reservoir C compared with Reservoir B: equant calcite in Reservoir C started to precipitate simultaneously with syntaxial calcite, whereas in Reservoir B equant calcite started later relative to syntaxial calcite. Moreover, Reservoir B contains much more microporosity compared with Reservoir C. Two fracture generations are also documented in this reservoir, but the timing of the first generation relative to stylolitization was difficult to constrain. The orientation of the first fracture generation was compared with the reservoir above (A and B) and it was found that they all follow the same orientation. In addition, this generation contains partially to completely cemented fractures with equant and blocky calcite just like Reservoir B. Thus, the relative timing of this fracture generation is interpreted to be similar to the above reservoirs; equivalent to stylolite formation. The second fracture generation (width: ~0.1 mm) is open, parallel to stylolite and perpendicular to the first fracture generations (similar to Reservoirs A and B). Late dissolution, as evidenced by dissolution of kaolinite and saddle dolomite, was also documented in this reservoir.

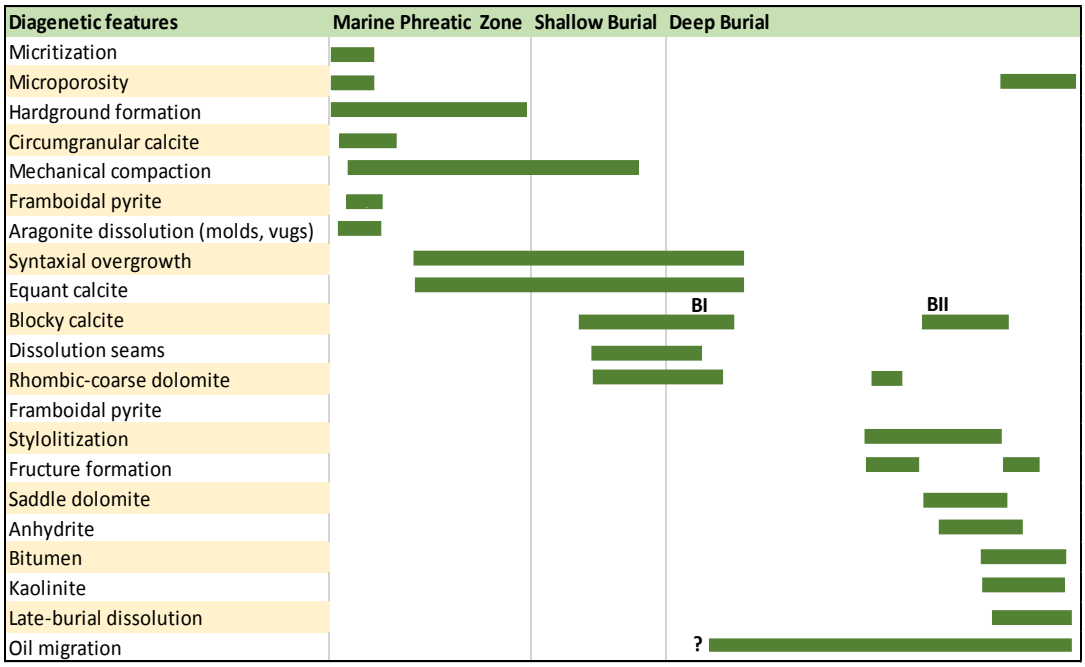


Figure 2.21: Paragenetic sequence of Reservoir C.

### 2.5.1.4 Paragenetic Sequence History of Reservoir F

As all other reservoirs early diagenesis in Reservoir F started with micritization and then precipitation of circumgranular calcite cement simultaneously with aragonite dissolution (Figure 2.22). Then, cementation history of calcite cements continues with the precipitation of equant, syntaxial and blocky cements. The interesting phenomenon in Reservoir F is that precipitation intervals of syntaxial, equant and blocky calcite are similar, particularly in the water leg. These three calcite morphologies contain similar correlative CL cement zones (Section 3.3.1). Thus, they presumably were precipitated broadly at the same time. After that, fracture formation started with first fracture generation. The first fracturing resulted in breccia that was then partially cemented. Following this, dissolution seams/stylolites (first generation) developed with fractures, which formed perpendicular to the stylolites. Fractures formed with first stylolite generation are thin (width: ~0.1 mm) and cross cut the breccia. Then, fluids move through stylolite to fill the breccia and newly formed fractures. After that, the second stylolite generation developed to cross cut the thin fractures. Following this, a third

fracture generation developed forming very big fractures (width: ~8.7 mm) with minor associated small fractures. The later formed blocky calcite and saddle dolomite cements precipitated in the newly formed fractures along stylolites, with limited formation in the matrix. Precipitation of bitumen and kaolinite came after, which occurred broadly concurrently. A fourth open fracture generation (width: ~0.5 mm) followed the precipitation of late cements. The last event in the reservoir seems to be a dissolution event that washed away some bitumen, partially dissolved calcite, enhanced microporosity formation, and created vugs that cross cut the small fractures of the third fracture generation. The dissolution occurred along stylolites and dissolution seams as well as in the matrix.

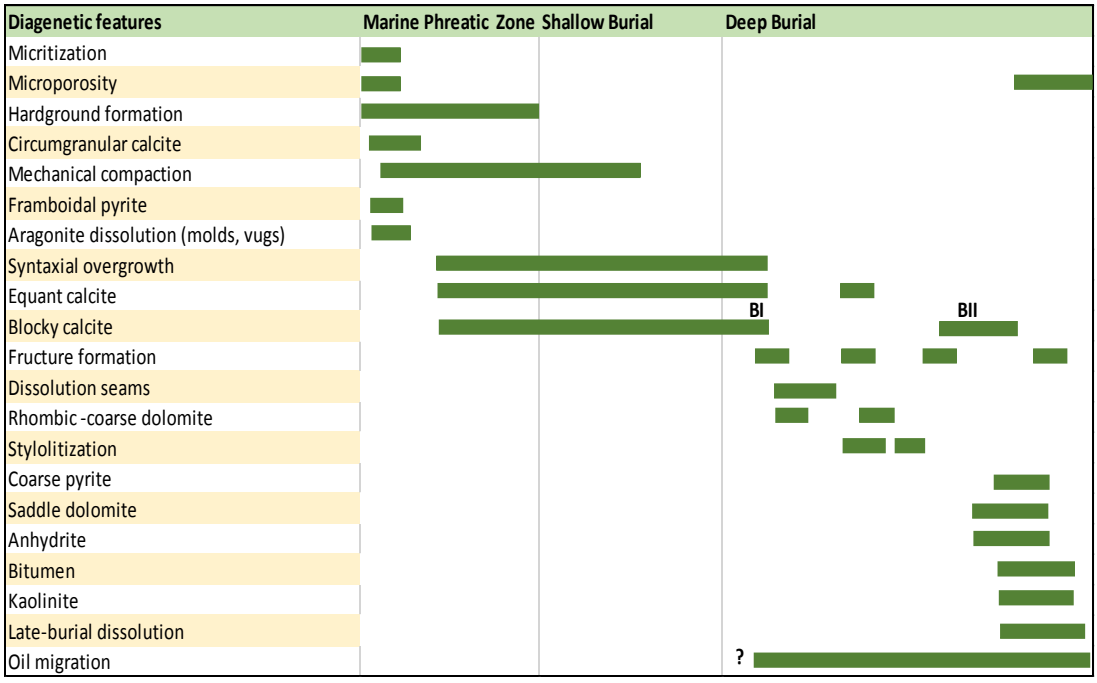


Figure 2.22: Paragenetic sequence of Reservoir F.

### 2.5.1.5 Paragenetic Sequence History of Reservoir G

The common micritization process happened near the seafloor occurred first in the diagenetic history of Reservoir G (Figure 2.23). Circumgranular calcite cement came next. After that, syntaxial and equant calcite started to precipitate. It is still

uncertain whether the blocky calcite started simultaneously with equant and syntaxial or slightly later. Mostly, cements in the matrix (intergranular, intragranular and moldic pores) precipitated with small volumes of cement before stylolitization and fracturing. Then, the first fracture generation developed containing larger (width: ~6 mm) and thinner (width: ~1.2 mm) fractures cemented later with granular calcite. After that, calcite cementation progressed to a limited extent in the matrix. Following this, the second fracture generation formed big (width: ~3 mm) fractures with breccia and flower structure fractures. After this, dissolution seams/stylolitization developed. The third fracture generation cross cut the stylolites and flower structure fractures of the second fracture generation. Then, fluids transported through fractures and stylolites created the cements that filled both the old and the newly formed fractures and some pores nearby. Cementation includes blocky calcite, saddle dolomite and rare anhydrite. After that, the second stylolite generation developed to cross cut the first fracture generation. The same event that formed the late stylolites activated the first stylolite to develop further along the border of the third fracture generation and to cross few of them. The later formed stylolite provided fluid to precipitate blocky calcite and saddle dolomite cement along stylolites. Blocky calcite continue to precipitate in moldic and vuggy pores near stylolite zones. Precipitation of bitumen, kaolinite and coarse euhedral pyrite came after and they seem to have precipitated broadly concurrently. Finally, a dissolution event washed away some bitumen, partially dissolved calcite, and created vugs in the matrix and along stylolites.

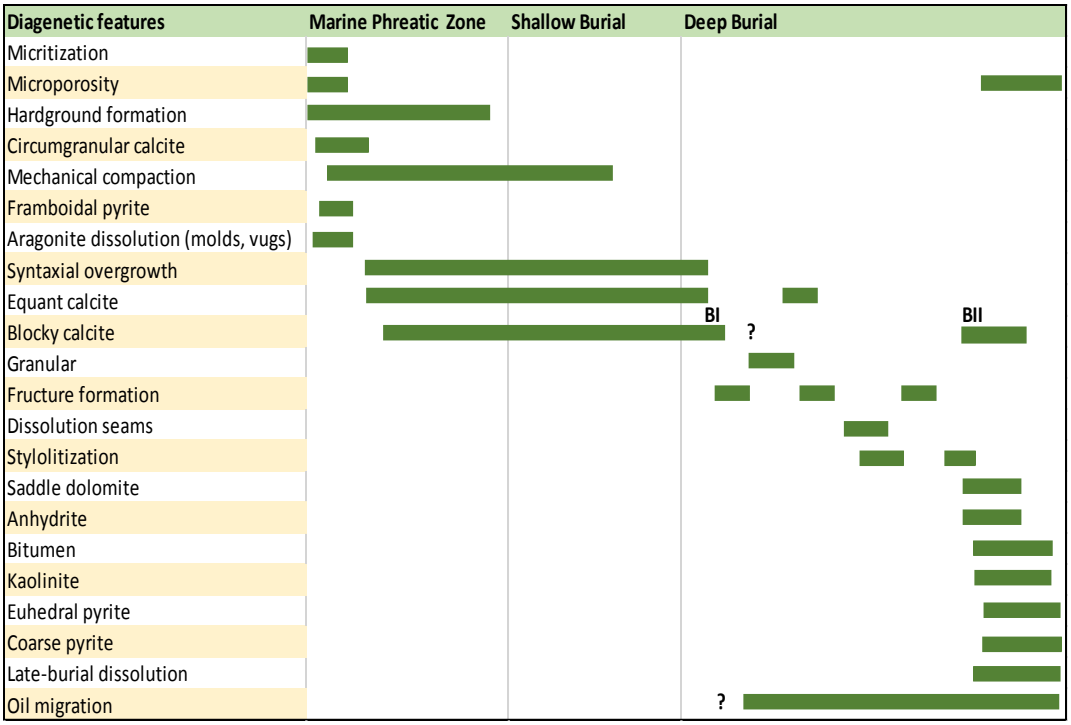


Figure 2.23: Paragenetic sequence of Reservoir G.

### 2.5.2 Micritization, Micro and Macro Pores in Thamama Reservoirs

#### 2.5.2.1 Micritization

Micritization is reported as a shallow-water marine, syngenetic to early diagenetic process (Bathurst, 1966, 1975; Tucker, 2009). The micritization process of an allochem starts with the outer part of the allochem and may continue to the centre to completely convert the whole allochem into micrite. The mechanism of micritization is not well constrained in the literature. However, several authors agreed that micritization can be formed by endolithic algae, bacteria and fungi boring in quiet-water environments which subsequently filled by micrite (Bathurst, 1966, 1975; Morad et al., 2016; Tucker, 2009).

Micrite can also be precipitated in-situ by chemical and microbiological processes (Monty, 1995). Reid and Macintyre (2000) suggested three mechanisms in which micritization can be formed, including: (1) traditional microbial boring process (Bathurst, 1975), (2) concurrent infilling, (3) recrystallization (Reid and Macintyre, 1998). Concurrent infilling engages simultaneous process of microboring and rapid carbonate precipitation. Micritization by recrystallization involves transformation of original skeletal fabric on the sea floor into equant micritic fabrics. This process is initiated by living organisms and continue further on shallow-sea floor by recrystallization to progressive micritization (Reid and Macintyre, 1998). This process still requires further understanding of the nature of carbonate crystal structure, mechanisms of crystal growth, and causes of crystal alteration associated with carbonate recrystallization in shallow marine (Reid and Macintyre, 1998).

A study conducted by Morad et al. (2016) on Reservoir B of the same field, SEM images of micrite particles in packstones and grainstone facies from both oil and water legs show different micrite morphologies in the oil versus water leg. The Oil leg comprises mainly of spheroidal micrite with smooth surface and mixed spheroidal and subhedral micrite. The water leg is dominated by micro-rhombic, subhedral micrite and some mixed spheroidal and subhedral micrite. Micrite with spheroidal shapes and smooth surfaces have been interpreted as a product of microbial precipitation and such shape cannot be produced diagenetically by dissolution and reprecipitation phenomenon. These authors suggest that microbial micritization may continue to alter the allochems into peloids which could introduce microporosity into the rock.

Morad et al. (2016) also proposed another mechanism in which micritization and microporosity can develop, which highlights the concept of micro-overgrowth similar to the well-known model of syntaxial overgrowth of calcite cement. The micro-overgrowth model suggests that the spheroidal/subhedral micrite acted as a nuclei to precipitate extremely thin layer of calcite as overgrowth to form subhedral to euhedral crystals of micrite and microspar. The authors provided many evidences supporting this model including the association of spheroidal micrite with subhedral and euhedral

micrite, the rounded holes found in micro-rhombic micrite which could be as a result of spheroidal/subhedral micrite detachment, and other supporting evidence.

#### 2.5.2.2 Porosity in the Thamama Reservoirs

Microporosity can be also formed as a result of transformation of metastable minerals into more stable phase which encounter dissolution and reprecipitation (Al-Asam and Azmy, 1996; de Periere, et al., 2011; Volery et al., 2010). This process can occur in subaerial exposure areas as a result of meteoric water flux, and/or during shallow to intermediate burial from evolved marine water and/or organic acids (Asam and Azmy, 1996; Heydari and Wade, 2002; Volery et al., 2010).

There is still uncertainty as to where and when the microporosity created by dissolution of micrite occurred in the studied rocks. From petrography it is clear that the dissolution of micrite envelops is postdating the cement in the intragranular pores in certain samples (Figure 2.9A & B) but in other samples with similar facies (packstones and grainstones) this relation cannot be observed. In some cases the intragranular pores are opened or partially cemented and no clear dissolution of micrite can be observed (Figure 2.9C). This is a little bit confusing because if the micrite envelop dissolution happened first during early diagenesis why we do see dissolution just in the micrite envelop but not effectively in the cement precipitated inside the intragranular pores (Figure 2.9 D) and why we don't see dissolution of micrite envelops around the dissolved molds in the other cases.

One possible interpretation could be that there are two stages of micro and macro porosity formation. One is early diagenesis and associated with meteoric flux or carbonate stabilisation and the other one with burial fluids such as organic acid and unsaturated fluids with respect to pore fluids. The first one is a well-known phenomenon where rocks interact with meteoric fluids either with subaerial exposure or passing through freshwater zone which resulted in dissolution of metastable minerals and reprecipitation of more stable minerals. The formation of moldic and

vuggy pores is interpreted to be a product of such leaching. In the studied samples, moldic and vuggy pores are present but no clear evidences of subaerial exposure were found in the reservoirs. Thus, the moldic and vuggy pores found in Reservoir B are interpreted to be formed as a result of aragonite and high-Mg calcite at marine phreatic zone (Thorpe, 2014).

The second generation of macro pores and possibly micro pores is suggested to be due to dissolution by organic acid and/or unsaturated fluids during burial. The organic acid generated by hydrocarbon maturation/migration might has partially dissolved the bitumen and the kaolinite found along dissolution seams and stylolites, replacing blocky calcite and rarely saddle dolomite (Figure 2.8J). The precipitation of kaolinite is complicated because of the $Al^{3+}$source and the low solubility of $Al^{3+}$ in natural water (see Section 2.5.6 for more explanation). The organic acid has the tendency to transport aluminium for longer distance by forming complex compounds (De Bona et al. 2008; Maliva et al., 1999). Thus, the presence and the effect of organic acid is more likely to be the reason behind the creation of macro porosity and microporosity (Heydari and Wade, 2002). Moreover, macro and micro pores which are believed to be created at relatively deeper burial are in fact found to postdate several features such as cemented fractures in Reservoir F (Figure 2.8A), bitumen along stylolites and dissolution seams (Figure 2.8C, F, G & H), and saddle dolomite (Figure 2.8J).

Thus, it can be concluded that microporosity as well as macro porosity in Thamama Reservoirs is a function of depositional and diagenetic overprints. Porosity preserved from deposition are as micropores and intergranular macropores, while the diagenetically induced one can be seen as moldic, vuggy and intragranular pores as well as further micropores.

### 2.5.3 Calcite Cementation

The first calcite cement to be formed in Thamama Reservoir rocks is a circumgranular calcite around allochems. This type of calcite is known to be formed during early diagenesis. It has been documented in the literature that this type of calcite cement typically precipitates from meteoric or marine waters in a phreatic environment (Alsharhan, 1990; Moore and Wade, 1989; Pucéat et al., 2003; Wygrala, 1989). Furthermore, it has been suggested that such cement could be sourced by the dissolution of metastable aragonite and high-Mg calcite (Kaufmann and Wendt, 2000; Stentoft et al., 2003; Vieira et al., 2007; Vieira and De Ros, 2006). Petrography shows that this type of cement predates both equant and blocky calcite (Figure 2.12A-D). In addition, the engulfment of the latest zones of syntaxial calcite to the circumgranular calcite suggest that these latest cement zones were precipitated at a later time relative to the circumgranular calcite (Figure 2.12D & I). Indeed, the first dull black CL cement zone in both syntaxial and circumgranular calcite seems to be correlated which could infer similar timing of precipitation. The origin of pore water of this cement was not constrained in this study due to small crystal size and the low cement volume; this cement has not significantly affected reservoir porosity. However, the origin of pore water from which same type of cement has been precipitated was constrained using in-situ ion microprobe oxygen isotopes on Thamama Reservoir rocks by a PhD student (Thorpe, 2014). Data show that circumgranular calcite can be inferred to have precipitated at a temperature similar to Cretaceous seawater thus revealing early precipitation from pore water which hosts a Cretaceous marine signature.

The origin of pore-fluids and the conditions of cementation by syntaxial overgrowths is not well constrained in the literature. Some studies suggest that this type of cement can precipitate early from meteoric water (Chafetz and Reid, 2000; Tucker, 2009). It can also be formed early in a shallow seawater environment and continue into deeper burial providing a full cementation record of the reservoir (Cox et al., 2010). Equant calcite found growing nearby syntaxial growth show that they either grown simultaneously, or syntaxial calcite was initiated first. CL analysis show that there is some similarity in few CL cement zones of equant and syntaxial calcite

(Section 3.3.1). This may reveal that at certain time during syntaxial precipitation, equant calcite started to grow in parallel to syntaxial more probably during younger CL cement zones. Other equant calcite thought to be after syntaxial calcite precipitation like the case in Reservoir B (Table 3.2). Electron probe microanalysis (EPMA) and stable isotopes of syntaxial and equant will provide more details on fluid compositions and precipitation temperature and thus will better constrain relative timing of the formation of these two cements. No EPMA or stable isotopes were collected for drusy or granular cements. These two calcite cements have interpreted to be developed in near-surface meteoric and burial environment (Flügel, 2004).

Blocky calcite was precipitated in two stages. The first stage includes the precipitation of first blocky calcite generation (BI). This generation contains crystals with size ranging between 200-1000μm. BI engulfs circumgranular calcite, equant & syntaxial cements of calcite in intergranular pores suggesting that precipitation of BI postdates these types of calcite. BI could be precipitated concurrently with syntaxial calcite at some points, as indicated by CL which shows some correlative cement zones between these two types of calcite (Table 3.2; Figures 3.1-3.5). The second stage includes cementation of second blocky calcite generation (BII). Crystals of this generation are >1000μm in size and can show twinning (Figure 2.13). BII is found engulfing syntaxial cement and hence postdates syntaxial calcite formation. Some of this cement is found filling intergranular and intragranular porosity but is mostly found filling large fractures and along stylolites. Blocky calcite can be precipitated from meteoric water at shallow burial depth (Al-Aasm et al., 2009; Flügel, 2004). It can be also formed at burial environment from modified seawater and basinal brine (Haeri-Ardakani et al., 2012; Egeberg and Aagaard, 1989). Most of the BI cement in Thamama Reservoirs is interpreted to be precipitated from marine seawater and modified seawater during early burial diagenesis, while the BII from basinal brine during late burial diagenesis. The origin of blocky calcite cement in Thamama Reservoirs is further discussed in Chapters 4 and 6.

### 2.5.4 Dolomitization

The replacive rhombic dolomite is the first dolomite type formed in the Thamama Reservoir rocks. The formation of rhombic dolomite is suggested to start in the host limestone more or less parallel to the dissolution seams and prior to stylolitization. This can be shown by the cross cutting relationships which shows that stylolites clearly cross cut rhombic dolomite and dissolution seam (Figures 2.14I & 2.17C & D). Furthermore, rhombic dolomite can be found in various mud-supported facies that have no record of stylolitization. The origin of this dolomite has been constrained by Paganoni et al., (2016) which found consistent carbon isotopic values (+2.8‰ to +4.2‰) of rhombic dolomite similar to Cretaceous seawater. This suggests that the dissolved carbon related to rhombic dolomite formation has been most probably sourced from the host limestone. The presence of rhombic dolomite along dissolution seams and stylolites could indicate that rhombic dolomite formation progressed further during and after chemical dissolution process (Figure 2.14I). As a consequence of further burial and stylolite development, rhombic dolomite continued to replace limestone forming coarser crystals of dolomite (Figures 2.14D & 2.15). Progressive dolomitization can result in the formation of latter dolomite as coarser, sub- to anhedral crystals (Merino and Canals, 2011; Wierzbicki et al., 2006). Haeri-Ardakani et al. (2013), suggested that matrix replacive dolomite can be initiated during early diagenesis from seawater and further recrystallized during burial or late hydrothermal flux.

The concentration of saddle dolomite concentrated mainly along stylolite and more volumetrically filling large fractures suggests that fluids were transported via stylolites and fractures. It has been widely documented that saddle dolomite is more likely precipitated from deep basinal hydrothermal fluids (Breesch et al., 2010; Lavoie and Morin, 2004; Luczaj et al., 2006; Machel, 2005; Merino and Canals, 2011; Sirat et al, 2016). More closely, a number of studies linked hydrothermal dolomitization to the tectonic faulting and fracturing (Haeri-Ardakani et al., 2013; Davies and Smith, 2006; Lonnee and Machel, 2006). A significant number of large fractures were

documented in Reservoirs G and F and all are filled with saddle dolomite and twining blocky calcite as well as rare anhydrite. Shallower reservoirs (A, B, and C) have less fractures and volumetrically less saddle dolomite compared with deeper reservoirs (G and F). Thus, it can be suggested that saddle dolomite formation in Thamama Reservoirs is a late burial diagenesis process and is closely linked to fractures and to some extent stylolites. Saddle dolomite postdates most of the cements including circumgranular calcite, equant calcite, and first generation of blocky calcite. In some cases it is uncertain whether the saddle dolomite precipitated before, simultaneously or after BII (Figure 2.13B.). Thus, the relative timing of second blocky calcite generation and saddle dolomite remains open. More details on the origin of the three types of dolomite is given in a separate Chapter (Chapter 5).

### 2.5.5 Chemical Compaction Features

Existence of dissolution seams and stylolites in rocks of both crest (oil leg) and flank (water leg) implies that the whole structure was subjected to chemical compaction. The occurrence of these features in different reservoir facies suggests that these features are not facies controlled. Pressure dissolution features have been recorded in various carbonate facies including muddy and grainy facies (Alsharhan and Sadd, 2000; Ehrenberg et al., 2016; Lambert et al., 2006; Paganoni et al., 2016). The horizontal orientation of stylolites and dissolution seams suggests formation from vertical stress which is most likely the overburden pressure.

The common association of dissolution seams and clay laminae found intensively in Dense Zones may propose that clay either has a role in enhancing pressure dissolution or just accumulated as insoluble residue (Alsharhan and Sadd, 2000; Ehrenberg et al., 2016; Moore, 1997; Prokopovich, 1952). The more abundant distribution of high amplitude stylolites in the water leg than oil leg and in deeper reservoirs could be due to the higher stress concentrated in the deeper part of the structure (Leythaeuser et al., 1995). Water could also have a role in enhancing stylolite development in the flank (Melville et al., 2004; Neilson et al., 1998; Oswald et al.,

1995). It has been suggested that the thinning of the strata towards the structure's flanks can be partly explained by the abundant stylolites distributed in the flanks (Alsharhan and Sadd, 2000; Oswald et al., 1995).

Cements found along stylolites implies that these cements have been either precipitated in-situ as a products of stylolitization or have been supplied by an external source. Carbonates dissolved during pressure dissolution are more likely re-precipitated nearby however, such process cannot generate massive mass of cement like the one found in this study. In addition, existence of various cement types such as saddle dolomite, large blocky calcite, kaolinite, rare anhydrite and coarse pyrite along and in the vicinity of stylolites indicates source of exotic fluids. Thus, stylolites have acted as conduits for fluid transfer out of the system. The thick concentrated bitumen found along stylolites infers that bitumen was accumulated later or parallel to stylolite development.

### 2.5.6 Origin of Kaolinite and Pyrite

The precipitation of kaolinite is complicated because (1) it needs source of $Al^{3+}$ and (2) the solubility of $Al^{3+}$ in natural water known to be very low. Thus, $Al^{3+}$ cannot be transported for a long distance by natural water (Maliva et al., 1999; De Bona et al. 2008). However, the organic acids can increase the mobility of aluminium since the acid has the tendency to complex aluminium into organo-aluminium complexes (Maliva et al., 1999). The aluminium can then be released after destabilization of organo- aluminium complexes and precipitate as clay mineral nearby.

The presence of kaolin along dissolution seams and stylolites proposes that organo-aluminium could be migrated along stylolites and precipitated as kaolin along and close to stylolites in matrix pore spaces and fractures. Furthermore, the occurrence of kaolin cement in the fractures perpendicular to the stylolite reveals that kaolin precipitation occurred after stylolite formation. Kaolin cement can be found also associated with bitumen (Figure 2.8A). Bitumen found coating kaolin cement gathered

from different areas including Abu Dhabi (Cretaceous samples), has inclusions (oil + aqueous) with temperature above 90˚C suggesting formation at a late burial time (Neilson and Oxtoby, 2018). Kaolin may suggest that the hydrocarbon source rocks are rich in siliciclastic and Fe minerals. The possible source rock for the Kharaib is Bab member source rocks, probably Lower Shuaiba shale or Upper Jurassic Diyab formation (Alsharhan and Scott, 2000; Al-Suwaidi et al., 2000; Gumati, 1993; Loutfi and El Beshlawy, 1986; Murris, 1980; Oswald et al., 1995;).

The fromboidal pyrite is commonly found in Dense Zones and early calcite cement of these intervals. This pyrite is thought to be formed by bacterial sulfate reduction (BSR) under reducing conditions (Taylor and Macquaker, 2000). BSR requires dissolved sulfate to produce $H_2S$ which reacts then with $Fe^{+2}$ to form framboidal pyrite (Al-Asam et al., 1996; Morad, 1998). Sulfur can be obtained from seawater.

Another type of pyrite which is coarse euhedral pyrite is found in Reservoir G. This type of pyrite can be formed by thermochemical sulfate reduction (TSR) at deeper environment (Machel, 1998; Worden et al., 1996). The TSR mass is possibly derived from other sources since this is not common in the lower Thamama Reservoirs. Possible sources for TSR mass are Arab or Khuff formations which are two well know formations for sulfate products (Warren, 2000; Worden et al., 1996). The frequent presence of abundant coarse euhedral pyrite along stylolites supports the flux of fluids from deeper parts of the basin, which were affected by TSR. Coarse-crystalline pyrite was also found in Reservoir G and few in F replacing some blocky calcite cements. This pyrite was more likely formed during same TSR event.

## 2.6 Summary: Reservoir Quality in Thamama Reservoirs

The main rock textures in the Thamama Reservoirs are grainstones, packstones, mudstones and wackestones. These rocks include micropores, intergranular, vugs and moldic pores. The intergranular porosity is depositional in origin. The vuggy and moldic pores are secondary in origin which can be created as a result of meteoric, early or later burial diagenetic dissolution. Micropores can be depositional or diagenetic in origin (early-late).

Moldic and vuggy pores which formed due to freshwater leaching during subaerial exposure or aragonite stabilization at marine phreatic zone are more concentrated at the top of each reservoir and below the above dense zone. As going down into each reservoir, these types of porosity become less abundant. Furthermore, these macropores are abundant in the shallower reservoirs particularly B and can be rarely found in deeper reservoir G. The abundance of these pores at the top of reservoir B can be due to the K70 SB when access of freshwater leaching was allowed at that time. This is also could be due to carbonate stabilisation which encounter dissolution of high-Mg calcite and aragonite to more stable low-Mg calcite. Similarly, higher macro pores at the top of each reservoir can be attributed to the fall in relative sea-level at that time or/and carbonate stabilisation. Cores of this study do not reach the top second order exposed SB that marks the end of deposition of Shuaiba and Thamama Formation, so no evidence of such event is suspected to be found here. Cores in Filed A cover only Lower Shuaiba (55 ft). The effect of this SB can be seen on the top porous part of the progradational stacking pattern (Shuaiba clinoforms) which is located 90 Km Northwest from Field A (Strohmenger et al., 2010; Alsharhan, 1993; Granier et al., 2003).

**Depositional Features**

According to the petrographic work, reservoir quality distribution in Thamama reservoirs can be attributed to both depositional and diagenetic overprints. The preserved intergranular macroporosity is believed to have significant impact on pore

system in grainstone and packstone facies. However, in the cases where intergranular pores are filled with cements the reservoir quality is degraded. Moreover, micropores preserved from early micrite resulted in higher porosity particularly in the oil leg where the oil is being introduced earlier into the reservoir and retarded the further modification of the micrite. Rocks with macro and micropores can retain higher permeability (10's – 100's mD, Neilson et al., 1996). However, micropores of rocks with extensive cementation retain low permeability (<10mD). Thus, even though microporosity is high in cemented samples, it does not contribute to reservoir quality enhancement considerably.

## Diagenetic Features

### Marine Phreatic

Reservoir quality in Thamama Reservoirs is mostly controlled by the diagenetic overprint. Dissolution of aragonite and high-Mg calcite has also impact on reservoir properties. This process has improved reservoir quality by creating moldic and vuggy pores in addition to precipitation of circumgranular calcite around the grains in grainstones and packstones. The presence of circumgranular calcite around the grains has helped to some extent in preserving some of the depositional intergranular porosity. Formation of early phases of syntaxial and equant calcite cements early at marine phreatic zone had minor deterioration on reservoir quality. Moreover, micritization has significant impact on reservoir properties particularly in Reservoir B (oil leg) in rocks rich with partially cemented to open macropores (Figure 2.9). The spherical micrite particles possibly induced from microbial activity increased the reservoir properties. These tiny micrite particles have increased the microporosity in certain micritized facies and indeed microporosity is thought to be the one of the major porosity in most of the Thamama Reservoirs (Morad et al., 2016; Lambert et al., 2006; Budd, 1989).

### Early Burial

Precipitation of blocky calcite and later phases of syntaxial and equant calcite had reduced reservoir quality at shallow burial diagenesis. Dissolution seams were developed probably during this stage of diagenesis and though to have provided good conditions for rhombic dolomite formation. This have been interpreted based on the frequent association of dissolution seams and rhombic dolomite. Dissolution seams might have provided solute with Mg that has been used for dolomitization nearby and along dissolution. Dolomitization has altered and replaced micrite by microcrystalline rhombic dolomite which generated new microporosity in the rock fabrics. This new microporosity has increased the porosity and thus enhanced reservoir quality.

### Late Burial

Water is considered as a good medium for chemical reactions whereas oil as a poor medium. The presence of water in the flank resulted in extensive diagenesis including cementation and chemical compaction which therefore destroy to some extent the reservoir quality. Late burial diagenesis for example stylolitization is abundant in the flank (water leg) of the structure and in the deeper reservoirs as seen from petrography. In some cases, stylolitization has likely supplied dissolved carbon and calcium needed for calcite and dolomite cementation, which deteriorated the reservoir quality mostly in the vicinity of stylolitic zones. In other cases, porosity development can be seen around stylolties suggesting that stylolitization aided somehow to reservoir quality enhancement. Porosity enhancement could be attributed to flux of corrosive fluids, including $CO_2$, $H_2S$ and organic acids along stylolites. These corrosive fluids are typically generated from thermal maturation of organic matter. The flux of corrosive fluid might be the cause for late stage dissolution event which resulted in some microporosity creation, vugs and molds development along and around stylolites, and kaolinite dissolution, which therefore increased the reservoir quality.

Fracturing resulted in reservoir quality enhancement at the beginning when fractures were opened. However, later on, the fractures as well as stylolites have acted

as conduits for the flux of fluids allowing further cementation of blocky calcite and saddle dolomite mostly in fractures and along stylolites which extended partially into the matrix. In the matrix, the blocky calcite and saddle dolomite was precipitated in large molds and few in intergranular pores. The high amount of precipitated saddle dolomite has affected reservoir quality considerably since most of the large molds might be connected with the whole pore system via microporosity. Furthermore, the precipitated cement in the fractures has retard reservoir quality effectively. The created fractures would be good conduits for oil migration if they have not been cemented.

# Chapter 3: Cement Stratigraphy and Dynamics of Calcite Cementation

## 3.1 Introduction

Calcite can be precipitated from environments ranging from the sea floor to deeper burial environments (Flugel, 2004). Precipitation at shallower temperature environments can be from either marine or meteoric water as well as water-rock interactions. At deeper, higher temperature environments calcite precipitation is due to water-rock interaction and/or the introduction of exotic fluids. Pore fluids evolve as a result of rock-water interaction through burial affecting calcite cementation (Uwe and Veizer, 1980; Heydari and Moore, 1993; Al-Aasm and Azmy, 1996; Sharpe, 2017). Walderhoug (1994) suggested that the rate of cement precipitation increases with increasing temperature. The process of water-rock interaction can continue even in the presence of wettability changes due to hydrocarbons (Worden and Heasley, 2000; Cox et al. 2010). This is because some pores in rocks in oil reservoirs can remain water-wet due to irreducible water saturation (Heasley et al., 2000; Marzouk et al., 1995).

In order to have cementation, pore fluids should be supersaturated with respect to the mineral (Tucker and Bathurst, 1990; Flugel, 2004). Thus, one should suspect that a higher rate of supersaturated fluid could yield higher precipitation rates and thus a higher volume of precipitated cement. Higher volumes of precipitated cement could also suggest longer precipitation time similar to the sequence stratigraphy concept.

This chapter aims to understand relative dynamics of calcite cementation through time in the different reservoirs both in oil and water legs by, 1) constructing cement stratigraphy for different calcite types, 2) evaluating the cementation rate

qualitatively through time inferred from apparent widths of precipitated cement zones, 3) provide estimates of total precipitated cement (thickness) through time in the oil and water legs and thus infer to the total volume of cement.

## 3.2 Methodology

Cathodoluminescence (CL) imaging was used to elucidate cement generations in order to create a cement stratigraphy for each calcite morphology (equant, syntaxial and blocky). Under CL, cement zones with different luminescence can be easily distinguished due to the difference in quenching ($Fe^{2+}$) and activating ($Mn^{2+}$) agents. This also infers the relative timing of cementation, rate of solute, cement thickness in two dimensions, and the evolution of pore-fluid chemistry in different stratigraphic reservoirs (A to G) and structural (oil crest vs flank) units.

Calcite cement zone stratigraphy is based on information gathered from several types of calcite cement in each reservoir, which vary in abundance (Table 3.1).

Table 3.1: Relative abundance of equant, syntaxial and blocky calcite in matrix of each reservoir in oil and water legs. R: Rare, C: Common, A: Abundant.

| Reservoir | Cement Type | Oil Leg | Water Leg |
|---|---|---|---|
| **A** | Equant | R | No samples |
| | Syntaxial | C | |
| | Blocky | A | |
| **B** | Equant | A | C |
| | Syntaxial | C | A |
| | Blocky | A | R |
| **C** | Equant | C | R |
| | Syntaxial | A | C |
| | Blocky | C | C |
| **F** | Equant | C | R |
| | Syntaxial | R | C |
| | Blocky | R | R |
| **G** | Equant | R | No samples |
| | Syntaxial | R | |
| | Blocky | A | |

CL images have been used to obtain the apparent width for each identified CL zone. This has been simply accomplished by measuring and estimating the maximum apparent width using an image scale as a measuring tool. This approach does not of course give a volume of cement, but offers a qualitative sense on how much calcite cement has been precipitated in different stratigraphic units and at different times. The number of measurements of apparent maximum width obtained from each reservoir are shown in Table 3.2. These measurements have been taken from cements in intergranular (syntaxial, equant and blocky) and moldic (equant and blocky) pores.

Final width (thickness) of each cement zone is an average of a number of measurements.

Table 3.2: Measurements of the maximum apparent width gathered from different types of calcite cement in different reservoirs.

| Reservoir | Number of Measurements | Type of Calcite Cement |
|---|---|---|
| A | Oil: 20 | Syntaxial & blocky |
| B | Oil: 38 | Syntaxial, equant & blocky |
| | Water: 31 | Syntaxial & equant |
| C | Oil: 32 | Syntaxial, equant & blocky |
| | Water: 57 | Syntaxial & blocky |
| F | Oil: 81 | Syntaxial, equant & blocky |
| | Water: 73 | Syntaxial, equant & blocky |
| G | Oil: 100 | Syntaxial, equant & blocky |

## 3.3 Results

### 3.3.1 CL Cement Stratigraphy of Calcite

The final cement stratigraphy scheme for each calcite type is shown in Figures 3.1-3.5. The cement zone number in Figures 3.1-3.5 start from the centre of the crystal with number 1 as the oldest moving towards the edge of the crystal to the youngest cement.

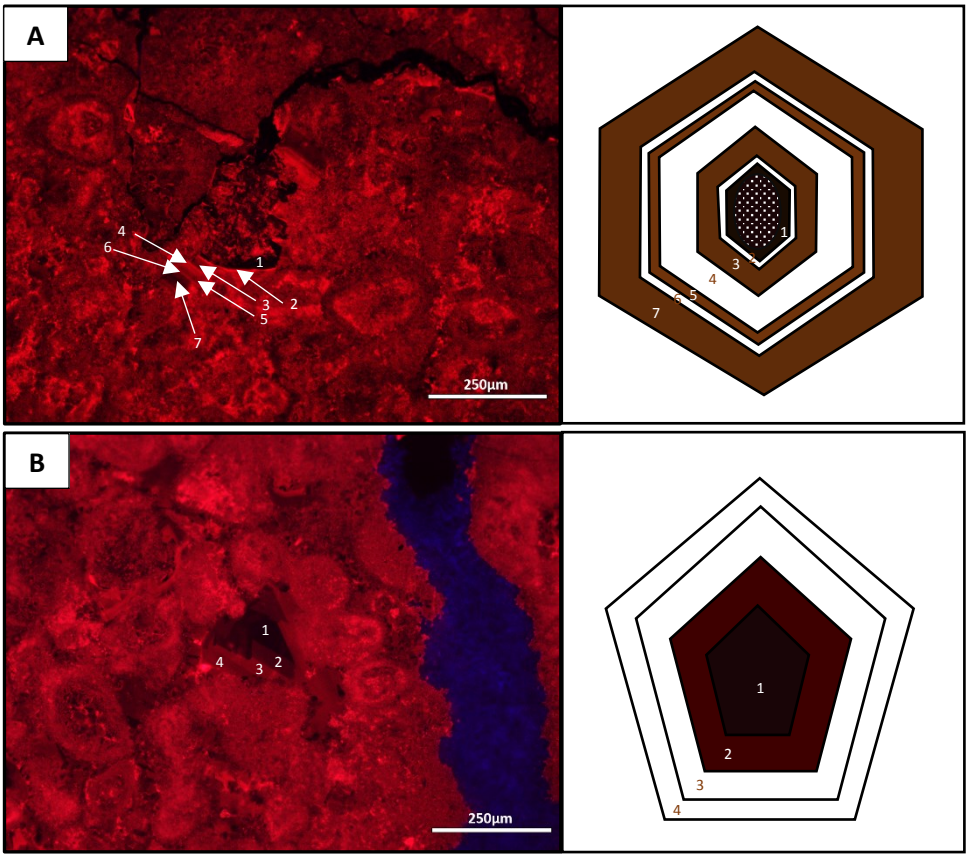


Figure 3.1: CL cement zonation of calcite in Reservoir A "oil" with general scheme in the right illustrating the number of the zone and the approximate thickness of each cement zone. A) Syntaxial calcite with 7 CL zones. B) Blocky calcite with 4 CL zones.

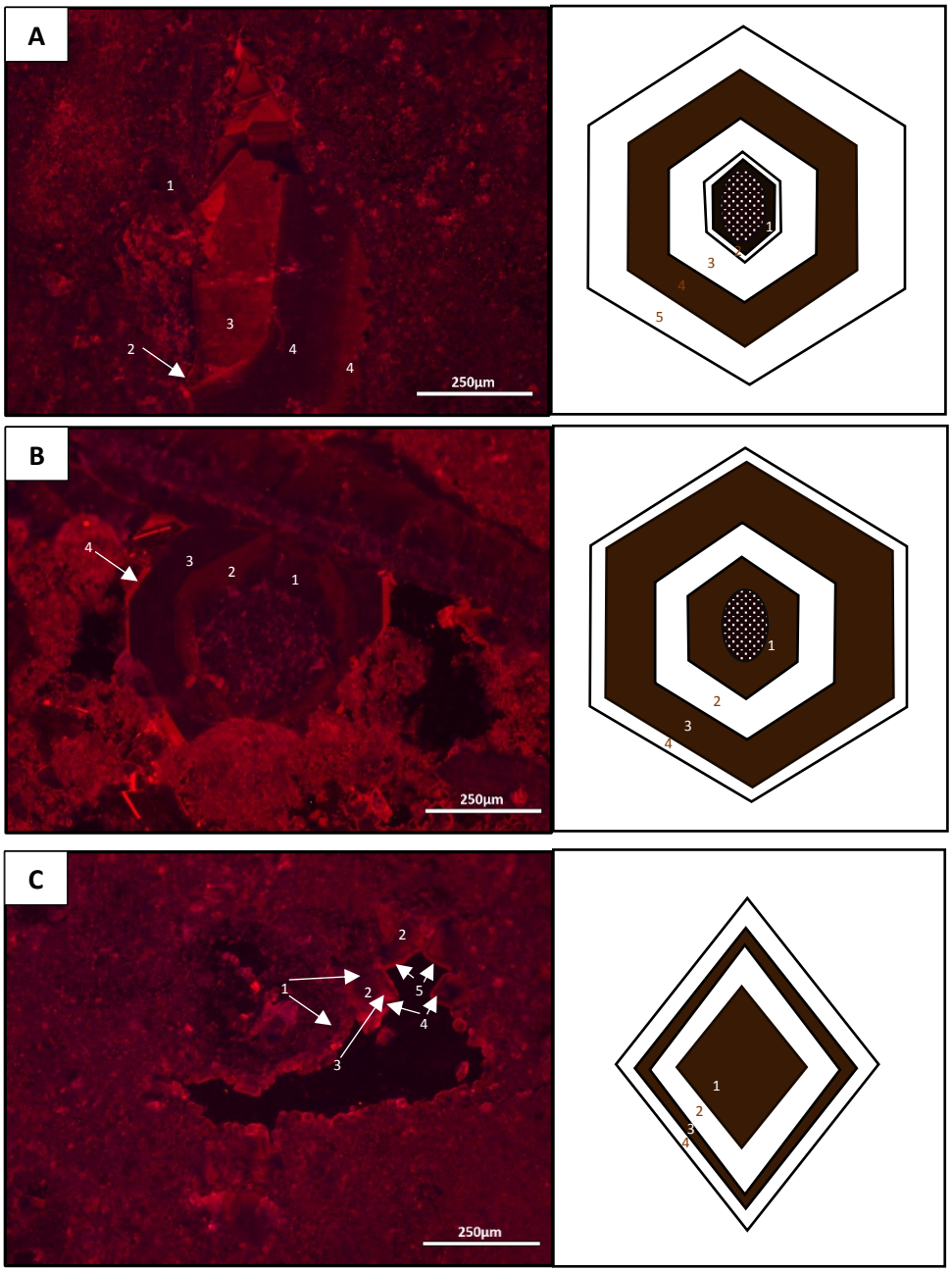
A
1
2
3
4
4
250µm
1
2
3
4
5
B
4
3
2
1
250µm
1
2
3
4
C
2
1
2
5
4
3
250µm
1
2
3
4

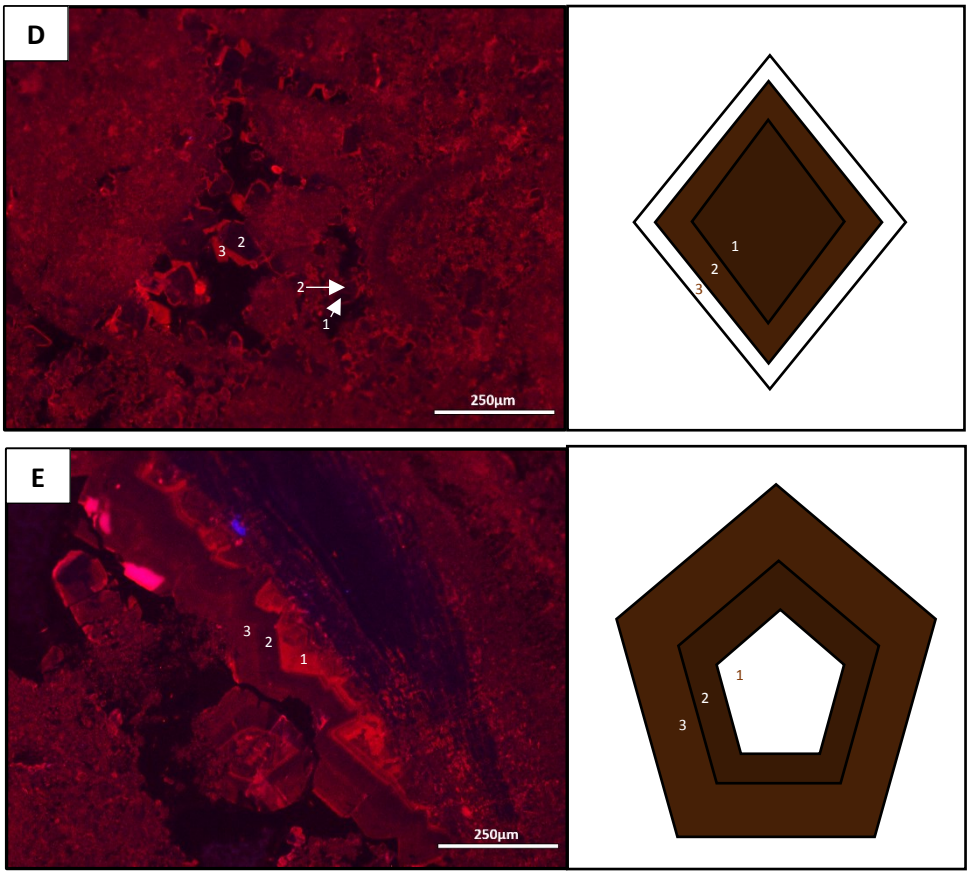


Figure 3.2: CL cement zonation of calcite in Reservoir B with general scheme in the right illustrating the number of the zone and the approximate thickness of each cement zone. A) Syntaxial calcite with 5 CL zones in oil leg. B) Syntaxial calcite with 4 CL zones in water leg. C) Equant calcite with 4 CL zones in oil leg. D) Equant calcite with 3 CL zones in water leg. E) Blocky calcite with 3 CL zones in oil leg.

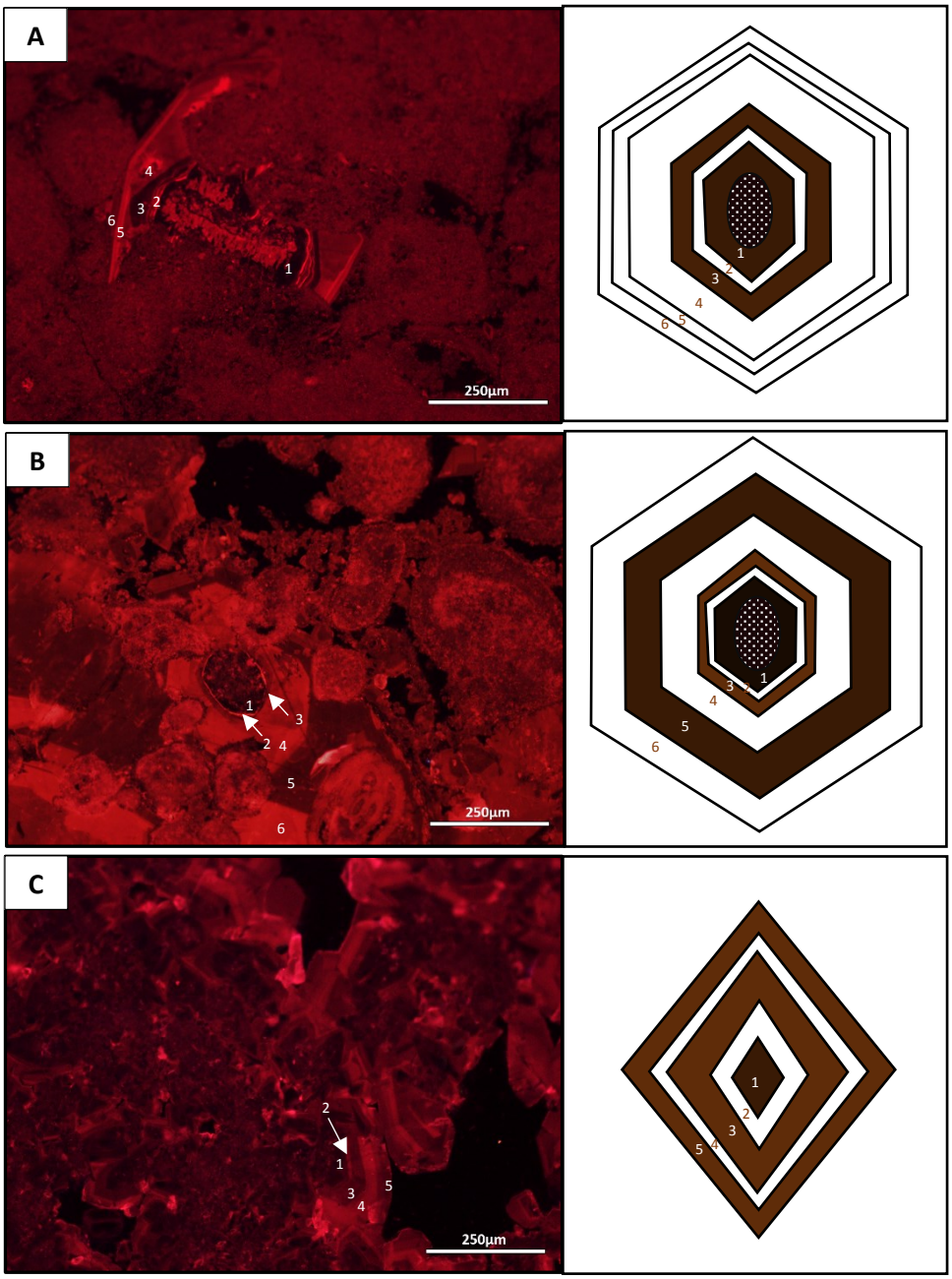
A
4
3
2
6
5
1
250µm
1
2
3
4
6
5
B
1
3
2
4
5
6
250µm
1
3
2
4
5
6
C
2
1
3
4
5
250µm
1
2
3
5
4

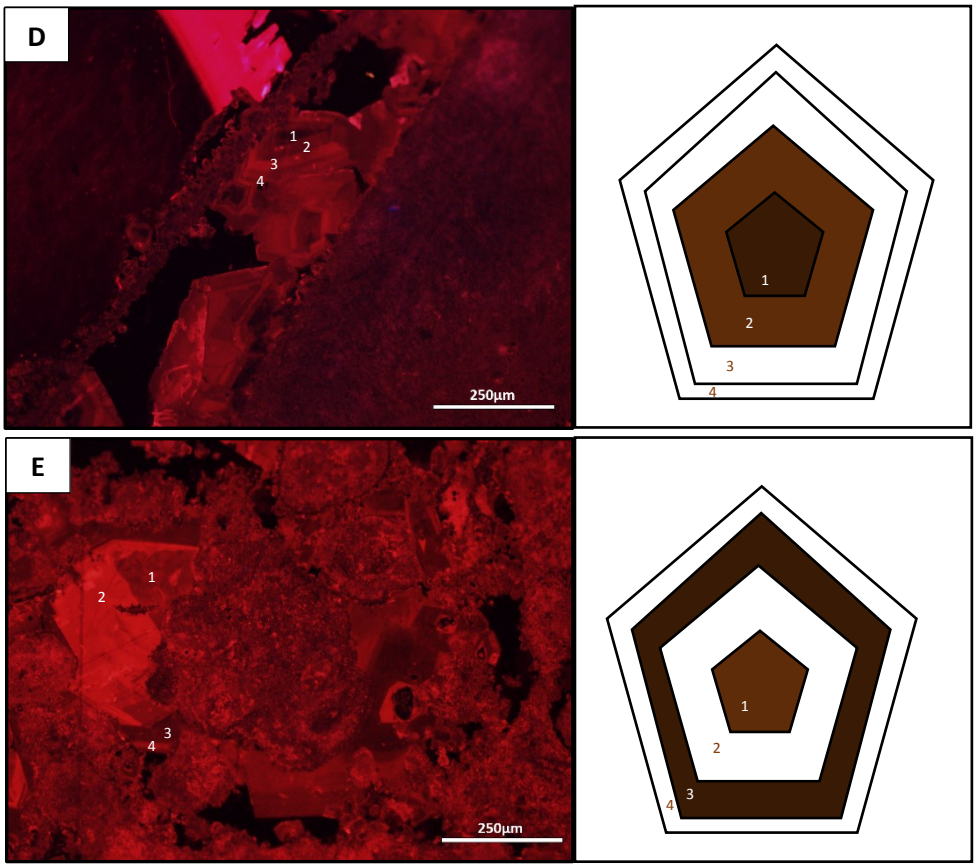


Figure 3.3: CL cement zonation of calcite in Reservoir C with general scheme in the right illustrating the number of the zone and the approximate thickness of each cement zone. A) Syntaxial calcite with 6 CL zones in oil leg. B) Syntaxial calcite with 6 CL zones in water leg. C) Equant calcite with 5 CL zones in oil leg. D) Blocky calcite with 4 CL zones in oil leg. E) Blocky calcite with 4 CL zones in water leg.

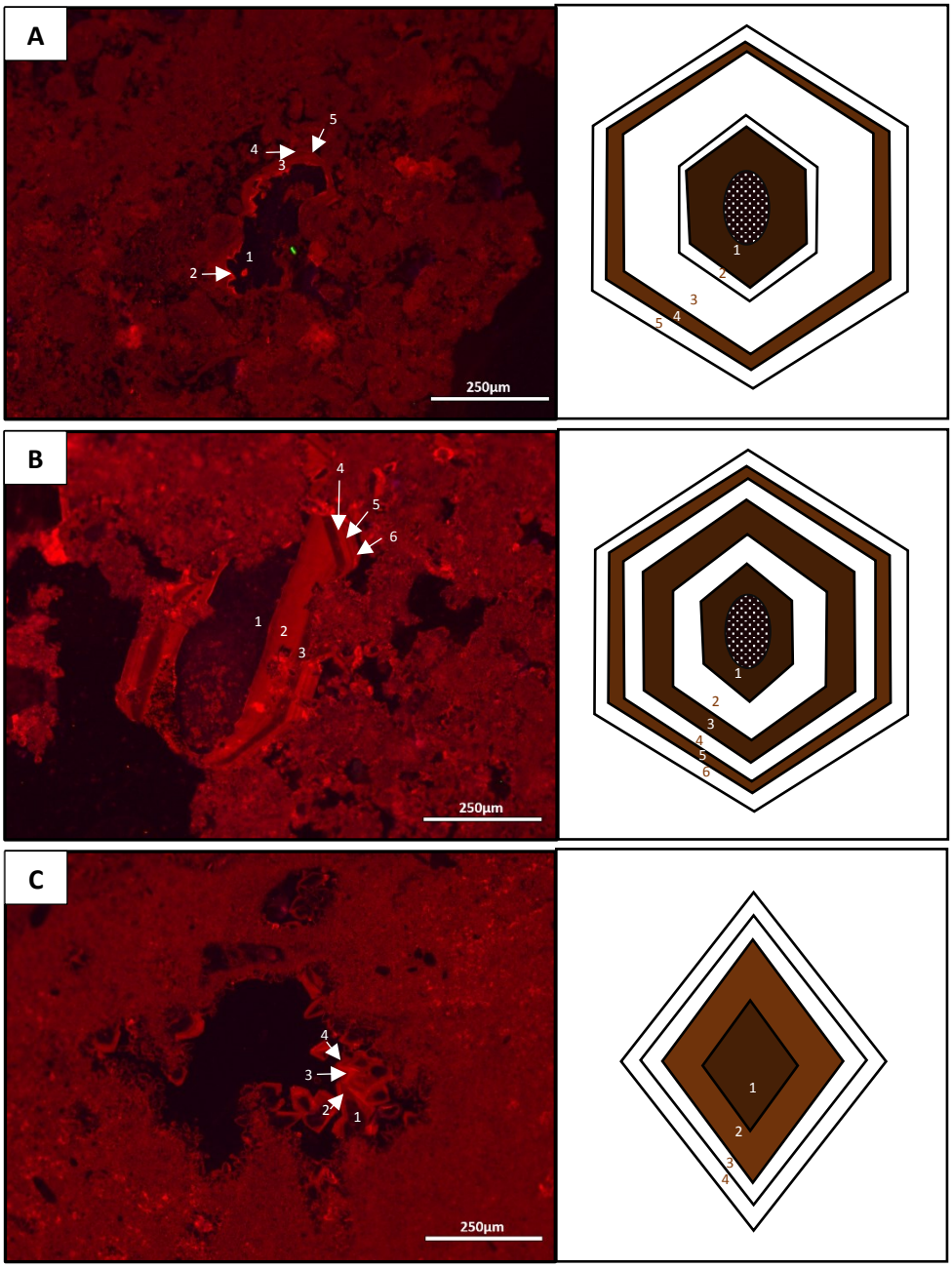
A
5
4
3
2
1
250µm
1
2
3
4
5
B
4
5
6
1
2
3
250µm
1
2
3
4
5
6
C
4
3
2
1
250µm
1
2
3
4

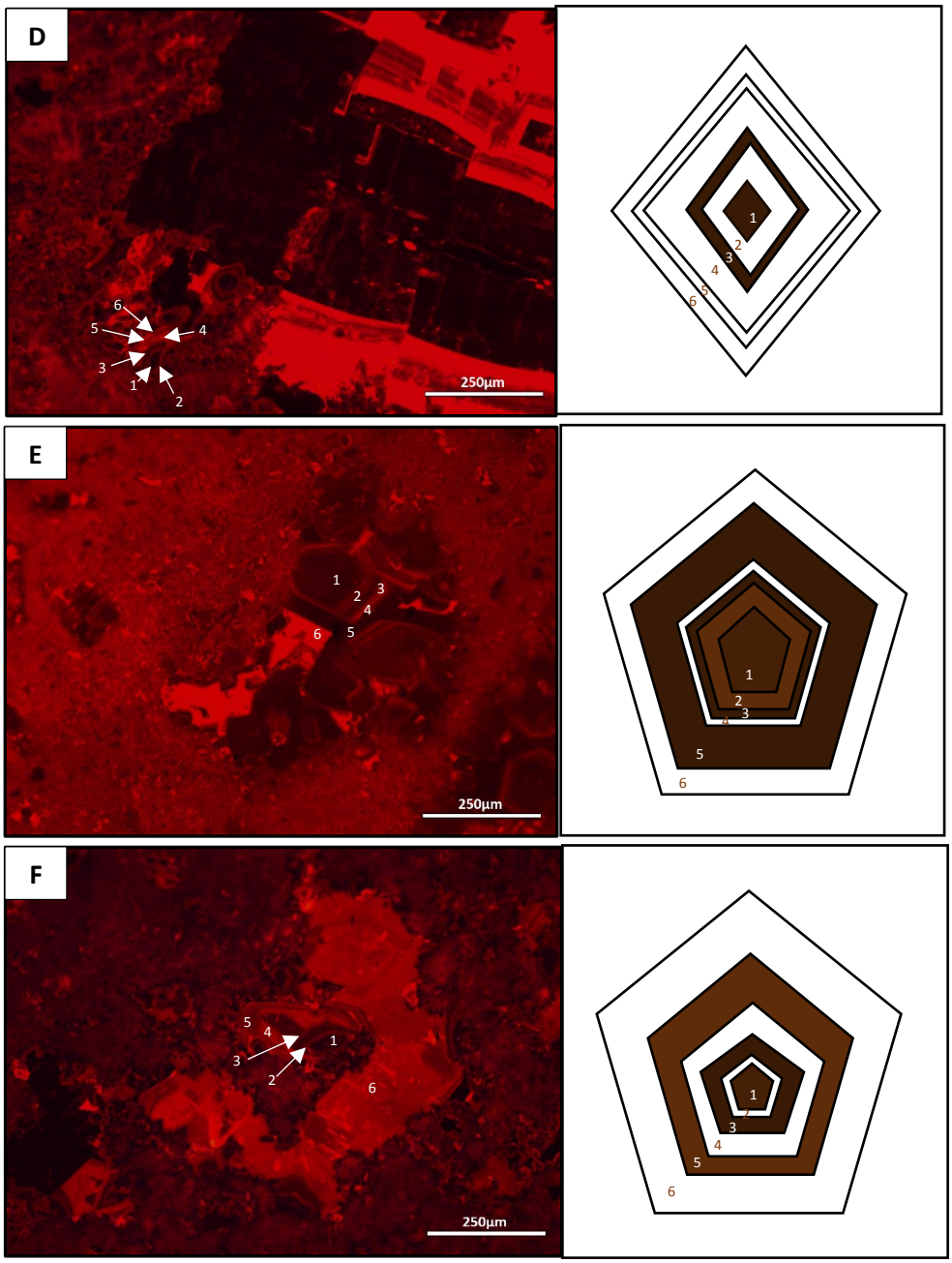


Figure 3.4: CL cement zonation of calcite in Reservoir F with general scheme in the right illustrating the number of the zone and the approximate thickness of each cement zone. A) Syntaxial calcite with 5 CL zones in oil leg. B) Syntaxial calcite with 6 CL zones in water leg. C) Equant calcite with 4 CL zones in oil leg. D) Equant calcite with 6 CL zones in water leg. E) Blocky calcite with 6 CL zones in oil leg. F) Blocky calcite with 6 CL zones in water leg.

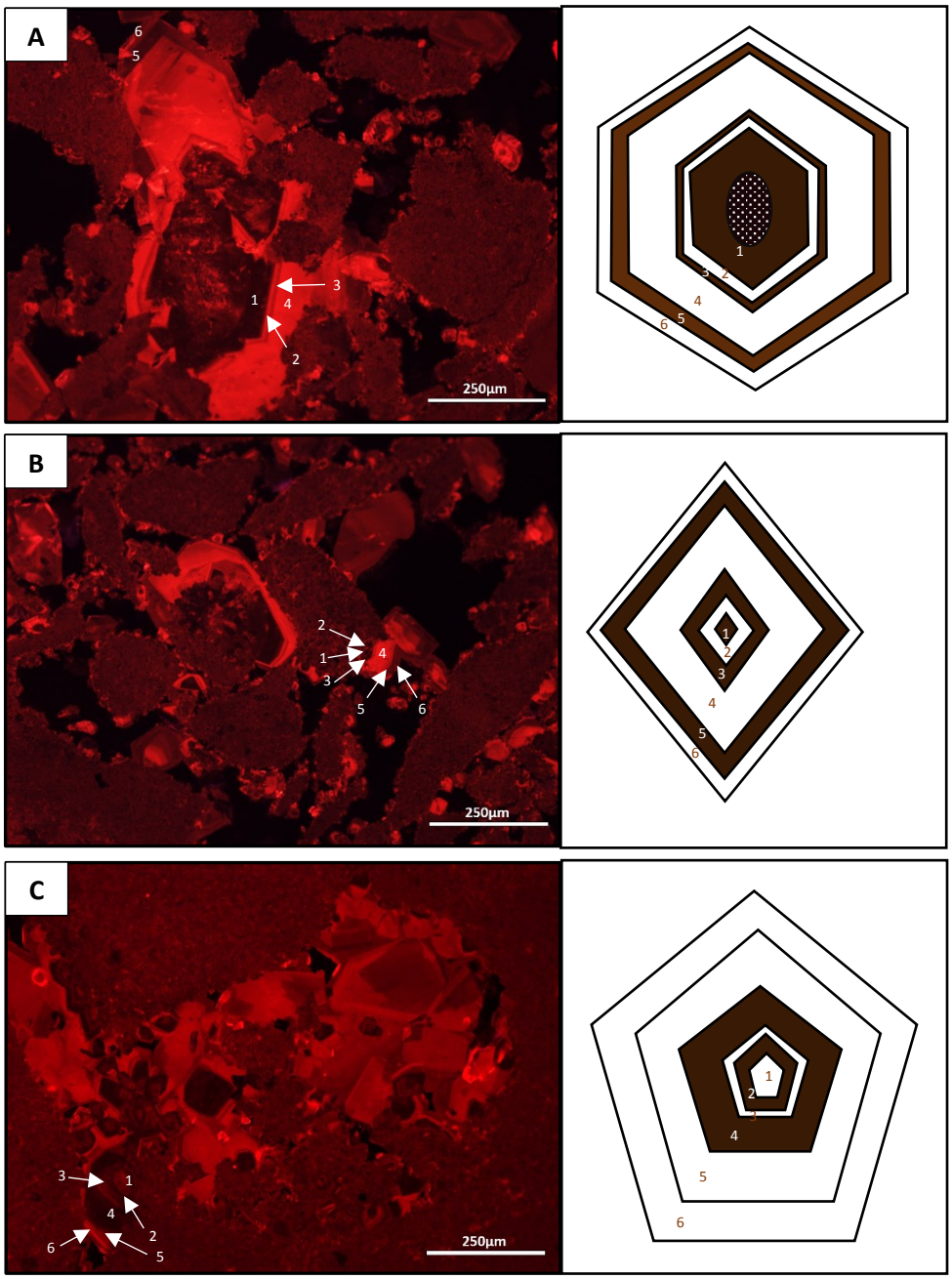


Figure 3.5: CL cement zonation of calcite in Reservoir G "oil" with general scheme in the right illustrating the number of the zone and the approximate thickness of each cement zone. A) Syntaxial calcite with 6 CL zones. Note first dull dark zone in calcite rim similar to first dull zone in syntaxial calcite. B) Equant calcite with 6 CL zones. Note first dull dark zone in calcite rim similar to first dull zone in syntaxial calcite. C) Blocky calcite with 6 CL zones.

The abundance of equant calcite varies stratigraphically (Table 3.1). It was very hard to find and establish CL cement stratigraphy for equant calcite of Reservoir A "oil" and Reservoir C "water". The CL cement stratigraphy of equant calcite for the rest of reservoirs with apparent maximum width is illustrated in Figures 3.2C & D, 3.3C, 3.4C & D, 3.5B. Equant calcite exhibits various cement zonation across the reservoirs. The maximum number of CL zones was found in deeper Reservoirs G and F, total of 6 zones. In contrast, the minimum number of CL zones was found in shallower Reservoir B "water" (3 zones). Equant calcite in all reservoirs shows cycles of extremely non-luminance (some are ferroan and some non-ferroan) and luminance calcite.

The abundance of syntaxial calcite also varies stratigraphically (Table 3.1). Cement stratigraphy for this calcite has been constructed for all reservoirs (Figures 3.1A, 3.2A & B, 3.3A & B, 3.4A & B, & 3.5A). Like equant calcite, syntaxial calcite shows a different number of zones in different reservoirs. The number of zones in all reservoirs is between 4 and 7. Syntaxial calcite with 7 zones can be found in Reservoir A "oil", whereas the minimum number of 4 zones can be found in Reservoir B "water". The zones alternate between ferroan and non-ferroan calcite with various thicknesses. However, most syntaxial calcite in all reservoirs share two common distinguished zones, the first thick dull black zone and the second very thin bright red zone.

Cement stratigraphy of blocky calcite for all reservoirs except B "water" is illustrated in Figures 3.1B, 3.2E, 3.3D & E, 3.4E & F, & 3.5C). Blocky calcite in Reservoir B "water" is not abundant in the matrix. Similar to the equant calcite, the maximum number of zones was reported in deeper Reservoirs G and F, while the minimum number is found in shallower Reservoir B. The number of zones ranges from 3-6.

The general cement zone stratigraphy for equant, syntaxial and blocky calcite and their possible correlation in each reservoir is shown in Table 3.3. Some CL zones of equant, syntaxial and blocky calcite can be correlated within each reservoir (Table 3.3). Generally, moving down to deeper reservoirs, CL cement zones are correlative

from earlier stage across syntaxial, equant and blocky calcite. Each reservoir has been treated separately.

Table 3.3: Correlation of CL zones in equant, syntaxial and blocky calcite in each reservoir, oil versus water. D: Dull, M: Moderate luminescence, B: Bright luminescence. The ferroan zones are marked by "*".

| Calcite Cement | CL Zones of Reservoir A "oil" | | | | | | | | |
|---|---|---|---|---|---|---|---|---|---|
| Syntaxial | 1 D black | 2 B red | 3 D red | 4 M red | 5 D red | 6 M red | 7 D red-dark red | | |
| Equant | No record | | | | | | | | |
| Blocky | | | | | | | 1 D black? -2 D dark red | 3 M red | 4 B red |
| | CL Zones of Reservoir B "oil" | | | | | | | | |
| Syntaxial | 1 D black | 2 B red | 3 M red | 4 D dark red | 5 M red | | | | |
| Equant | | | | 1 D dark red? | 2 M-B red? | 3 D dark red | 4 M red | 5 B red | |
| Blocky | | | 1 M red | 2 D dark red-black | 3 D-M red | | | | |
| | CL Zones of Reservoir B "water" | | | | | | | | |
| Syntaxial | 1 D black | 2 D-M red | 3 D dark red-black | 4 B red | | | | | |
| Equant | | 2 D-M red | 1 D black | 3 B red | | | | | |
| Blocky | No record | | | | | | | | |
| | CL Zones of Reservoir C "oil" | | | | | | | | |
| Syntaxial | 1 D black | 2 B red | 3 D black | 4 D-M red | 5 B red | 6 D-M red* | | | |
| Equant | 1 D black | 2 B red? | | 3 M red* | 4 B red | 5 M red* | | | |
| Blocky | | | 1 D dark red* | 2 M red* | 3 B red | 4 M red | | | |
| | CL Zones of Reservoir C "water" | | | | | | | | |
| Syntaxial | 1 D black | 2 B red | 3 D-M red | 4 B red | 5 D dark red* | 6 M red | | | |
| Equant | No record | | | | | | | | |
| Blocky | | | 1 D-M red | 2 B red | 3 D dark red* | 4 M red | | | |
| | CL Zones of Reservoir F "oil" | | | | | | | | |
| Syntaxial | 1 D black* | 2 B red | 3 M red* | 4 D red | 5 M-B red | | | | |
| Equant | 1 D black* | | 2 M red | | 3 M-B red* | 4 M red? | | | |
| Blocky | 1 D dark red?* | | 2 M red* | 3 D red | 4 M-B red | 5 D dark red* | 6 B red | | |
| | CL Zones of Reservoir F "water" | | | | | | | | |
| Syntaxial | 1 D black* | 2 B-M red | 3 D red* | 4 M-B red* | 5 D red* | 6 M-B red* | | | |
| Equant | 1 D black | 2 M red | 3 D red* | 4 M-B red* | 5 D red* | 6 M-B red | | | |
| Blocky | 1 D black | 2 M red* | 3 D red* | 4 M-B red* | 5 D red* | 6 M-B red | | | |
| | CL Zones of Reservoir G "oil" | | | | | | | | |
| Syntaxial | | 1 D black* | 2 B red | 3 D-M red | 4 B red | 5 D red | 6 M red | | |
| Equant | | 1 D black* | 2 M-B red? | 3 D black/dark red | 4 B red | 5 D red | 6 M red | | |
| Blocky | 1 M red?* | 2 D dark red?* | 3 M red | 4 D dark red | 5 D-M red | 6 B red | 7 M red | | |

Note: Thin sections were not stained with alizarin red S to discriminate between ferroan and non-ferroan calcite. Alternatively, ferroan and non-ferroan calcite have been identified using elemental data obtained from EPMA (Chapter 4).

### 3.3.2 Calcite Cementation in Oil versus Water Leg

The means of the measured apparent zone widths were plotted versus the CL cement zone to provide a qualitative proxy for the rate of delivery of solute in each cement zone, and the relative time over which each cement zone precipitated. This can give a simple cementation history curve which can infer to cement evolution through time. Figures 3.6 & 3.7 illustrate the calcite cementation history for all reservoirs in oil leg and Reservoirs B, C and F in water leg respectively. These Figures also show

the total thickness of precipitated cement at each cement zone obtained from different calcite types and used as a qualitative proxy for the total volume of precipitated cement.

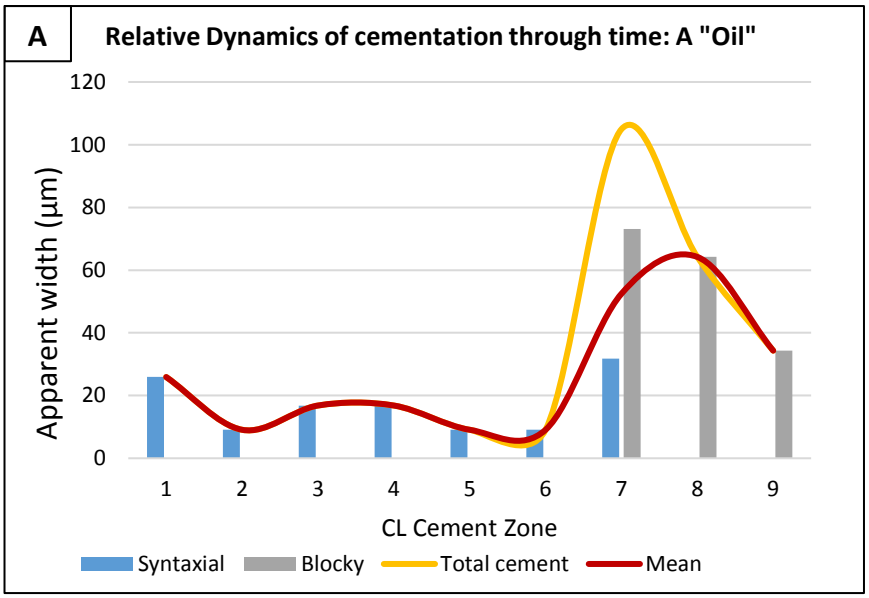


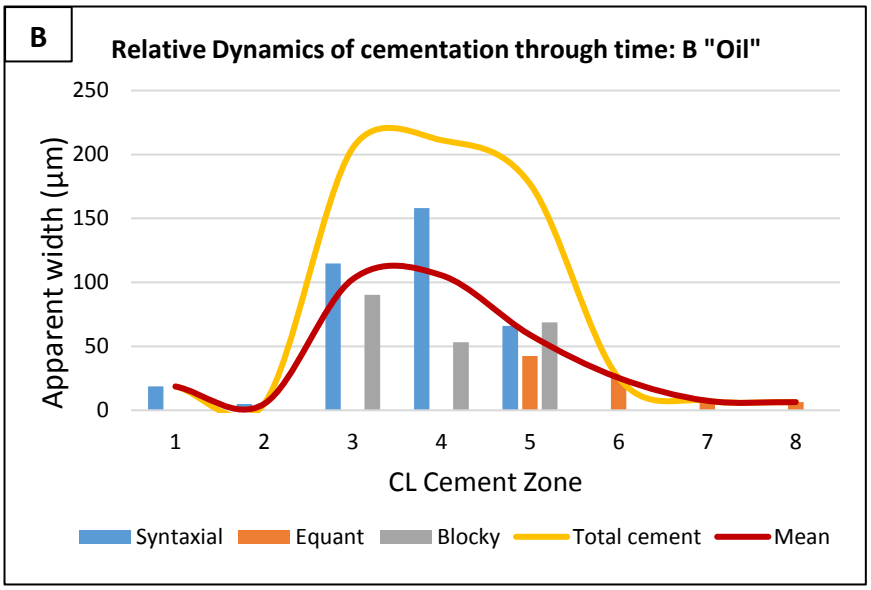

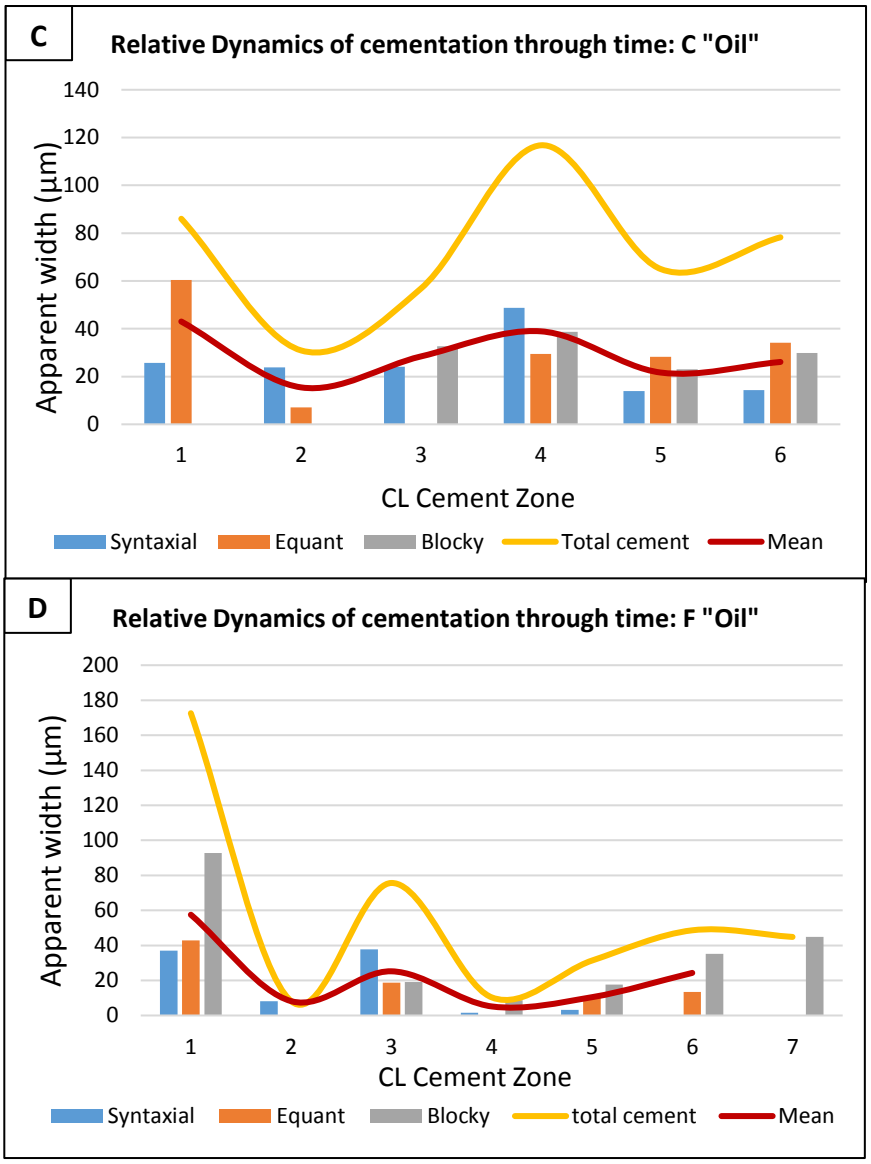
C
Relative Dynamics of cementation through time: C "Oil"
Apparent width (µm)
140
120
100
80
60
40
20
0
1
2
3
4
5
6
CL Cement Zone
Syntaxial
Equant
Blocky
Total cement
Mean
D
Relative Dynamics of cementation through time: F "Oil"
Apparent width (µm)
200
180
160
140
120
100
80
60
40
20
0
1
2
3
4
5
6
7
CL Cement Zone
Syntaxial
Equant
Blocky
total cement
Mean

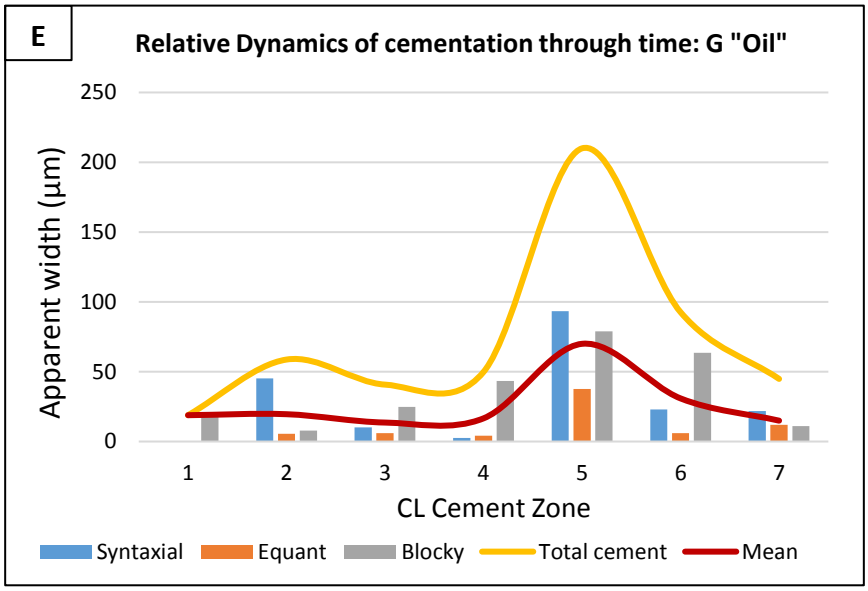


Figure 3.6: Relative dynamics of calcite cementation through time in the matrix of different stratigraphic units in oil leg. The columns represent the means of syntaxial, equant and blocky cements at each cement zone. The dark red curve represents the means of all types of calcite cement at certain cement zone. The yellow curve represents the total thickness at particular time. A) Calcite cementation in Reservoir A. B) Calcite cementation in Reservoir B. C) Calcite cementation in Reservoir C. D) Calcite cementation in Reservoir F. E) Calcite cementation in Reservoir G.

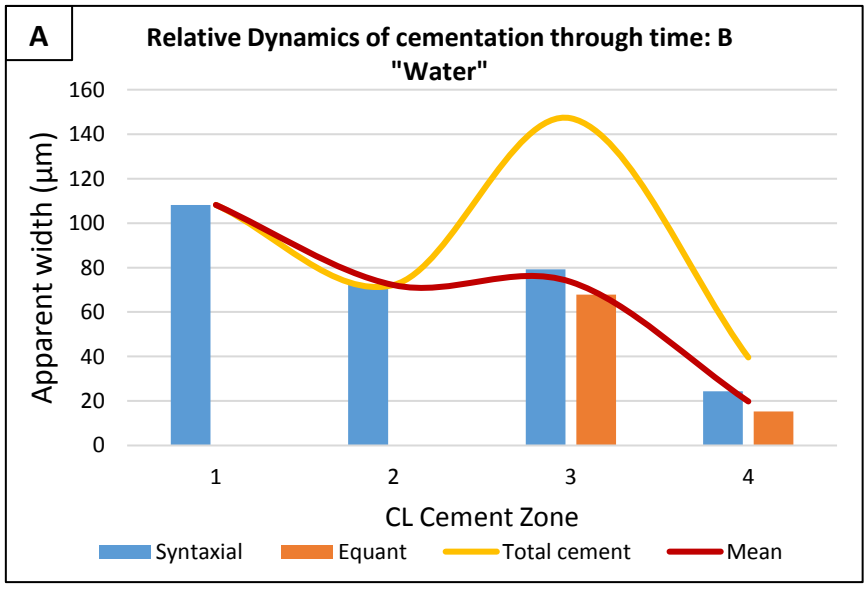

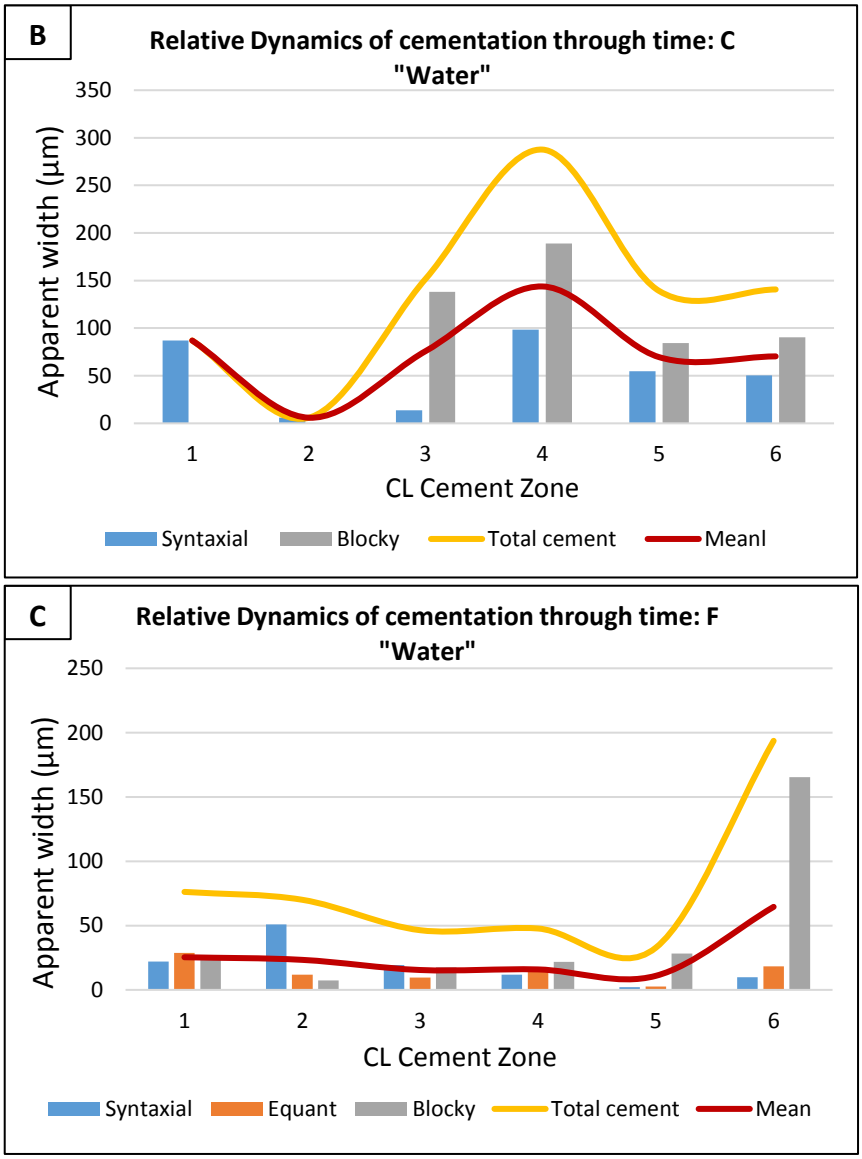


Figure 3.7: Relative dynamics of calcite cementation through time in the matrix of different stratigraphic units in water leg. The columns represent the means of syntaxial, equant and blocky cements at each cement zone. The dark red curve represents the means of all types of calcite cement at certain cement zone. The yellow curve represents the total thickness at particular time. A) Calcite cementation in Reservoir B. B) Calcite cementation in Reservoir C. C) Calcite cementation in Reservoir F.

Calcite cementation history varies across the reservoirs. In Reservoir A, the first cement was syntaxial calcite and the last was blocky calcite (Figure 3.6A). The

maximum volume of precipitated cement throughout calcite cementation history was at the time of cement Zone 7 precipitation (thickness = 105μm; mean = 64μm). At that time, calcite cementation was a function of both syntaxial and blocky calcite. This is also the time when the blocky calcite started to precipitate in the system. After that cementation decreased to Zone 9 (thickness = 30μm). Most calcite cement precipitation in this reservoir is from blocky calcite as it increased the total precipitation significantly during the later period of the cementation history.

For Reservoir B, the first cementation was syntaxial calcite until a mid-point when blocky calcite started to precipitate at cement Zone 3 (Figure 3.6B). The late time of cementation was mostly controlled by equant calcite. The maximum volume of precipitated calcite was during the mid-time (Zones 3 & 4) from both syntaxial and blocky calcite (thickness = 211μm; mean = 104μm). Equant calcite began to contribute to cementation at Zone 5 and continued to precipitate until final Zone 8 with a decreasing precipitation rate (mean = 59μm). In general, equant calcite has minor effect on the total precipitated calcite. The most significant cement contributor to the total volume in the matrix of this reservoir is the syntaxial cement followed by the blocky calcite.

The calcite cementation history in the water leg is different from the oil leg (Figure 3.7A). In Reservoir B, the number of calcite cement zones in water leg is less than in the oil leg. Moreover, the total estimated volume of precipitated cement in the matrix of the water leg is less than the oil leg. This is mainly because measurements from water leg were taken only for syntaxial and equant but not blocky cements. Most of the blocky calcite is precipitated in the fractures in the water leg. The main contributor to the total cement in the matrix in both oil and water leg is the same, which is the syntaxial calcite. Also, equant calcite in both oil and water leg started later relative to the syntaxial cement indicating that the full cementation record of calcite can be possibly found in syntaxial cement. The maximum volume of precipitated calcite can be found at Zone 3 (thickness = 147μm; mean = 74μm).

In Reservoir C "oil", three high cementation episodes can be identified (Figure 3.6C). The first one, was at the beginning of cementation history and is comprised of the cementation of syntaxial and equant calcite having the equant as the main contributor (thickness = 86µm; mean = 43µm). The second episode was at a mid-time point (at Zone 4) where the three types of calcite synchronously precipitated for the first time through cementation history (thickness = 147µm; mean = 74µm). At that time blocky calcite started to precipitate with its highest rate throughout the history of cementation. The main contributor to this high cementation episode is the syntaxial, then the blocky, followed by the equant cement. The third cementation peak occurred at the end of the cementation history and is the smallest compared with the first two cementation peaks (Zone 6; thickness = 78µm; mean = 26µm). At that time, equant and blocky calcite were competing whereas the syntaxial seems to have retarded to be the minor contributor. There is no huge difference between the amount of precipitated equant and blocky calcite, however, equant calcite can still be classified as the main contributor of the last high cementation episode. Overall, the three calcite types have more or less the same impact on the total precipitation of this reservoir throughout the whole cementation history.

The cementation history of Reservoir C in the water leg is similar to the oil leg except for the total amount of cement and the type of cement precipitated (Figure 2.28B). The highest precipitated cement can be found at time of precipitation of cement Zone 4 which is equivalent to the second higher cementation event in the oil leg. The total precipitated calcite cement at that time in the water leg (thickness = 288µm) was much higher than the oil leg (147µm) Moreover, equant calcite has no significant effect on the cementation history in the water leg. The main two contributors in the cement evolution are syntaxial and blocky calcite; mostly blocky calcite.

According to the CL observation, the relative time of blocky calcite cementation is interpreted to be equivalent to the time of equant and syntaxial calcite cementation in Reservoir F. Calcite cement in this reservoir has a similar cementation history to Reservoir C. Like Reservoir C, three episodes of high rates of cementation can be

recognized, with the first having the highest precipitated cement (Figure 3.6D). The first event which is the highest (thickness = 173µm; mean = 58µm) occurred at the beginning with the contribution of all calcite types, but the blocky calcite ranked as the main contributor. The second high cementation event was also contributed to by all three calcite types but in this case the most significant impact is attributed to the syntaxial calcite (thickness = 76µm; mean = 25µm). This event occurred at a mid-point of the precipitation history, during of cement Zone 3. The third high cementation event happened at the end of the cementation history curve. The total precipitated calcite in this event is 45 µm only from blocky calcite. Generally, blocky calcite is the significant contributor for the total volume of calcite throughout the whole cementation history.

The cementation history of Reservoir F in water leg is shown in Figure 3.7C. Like the oil leg, the three types of calcite cement all contribute to total precipitation, with blocky as the major contributor and equant as the minor contributor. The total precipitated cement in the water leg is higher than the oil leg. Generally, the cementation was higher and relative constant at Zones 1 and 2 (thickness = 70µm; mean = 23µm), decreased at Zone 5 (thickness = 33µm; mean = 11µm) and then increased at cement Zone 6 (thickness = 194µm; mean = 65µm). The decrease at Zone 5 was as a result of shutting down of both equant and syntaxial cement whoever at the same time the blocky calcite cementation rate was increasing in the larger pores. The increase in cementation at the last cement Zone 6 is attributed to the blocky calcite. The precipitation of both syntaxial and equant calcite increased at Zone 6.

Calcite cementation history of Reservoir G is shown in Figure 3.6E. Two cementation peaks can be recognized in this reservoir. The first high cementation event occurred during the precipitation of cement Zone 2 (thickness = 59µm; mean = 20µm). This high cementation rate is attributed to all three calcite types, with syntaxial calcite as the main contributor. The second cementation peak was at cement Zone 5. This event records the highest cement precipitation (thickness = 210µm; mean = 70µm) throughout the entire cementation history controlled by syntaxial and blocky calcite. The major effect of all calcite types on the total precipitated cement can be seen in the

younger cement zones. All calcite types cease together at the last cement Zone 6. Overall, the two main contributors for total precipitation in this reservoir are syntaxial and blocky calcite.

Figure 3.8 gives a summary of all means in different reservoirs both in oil and water legs.

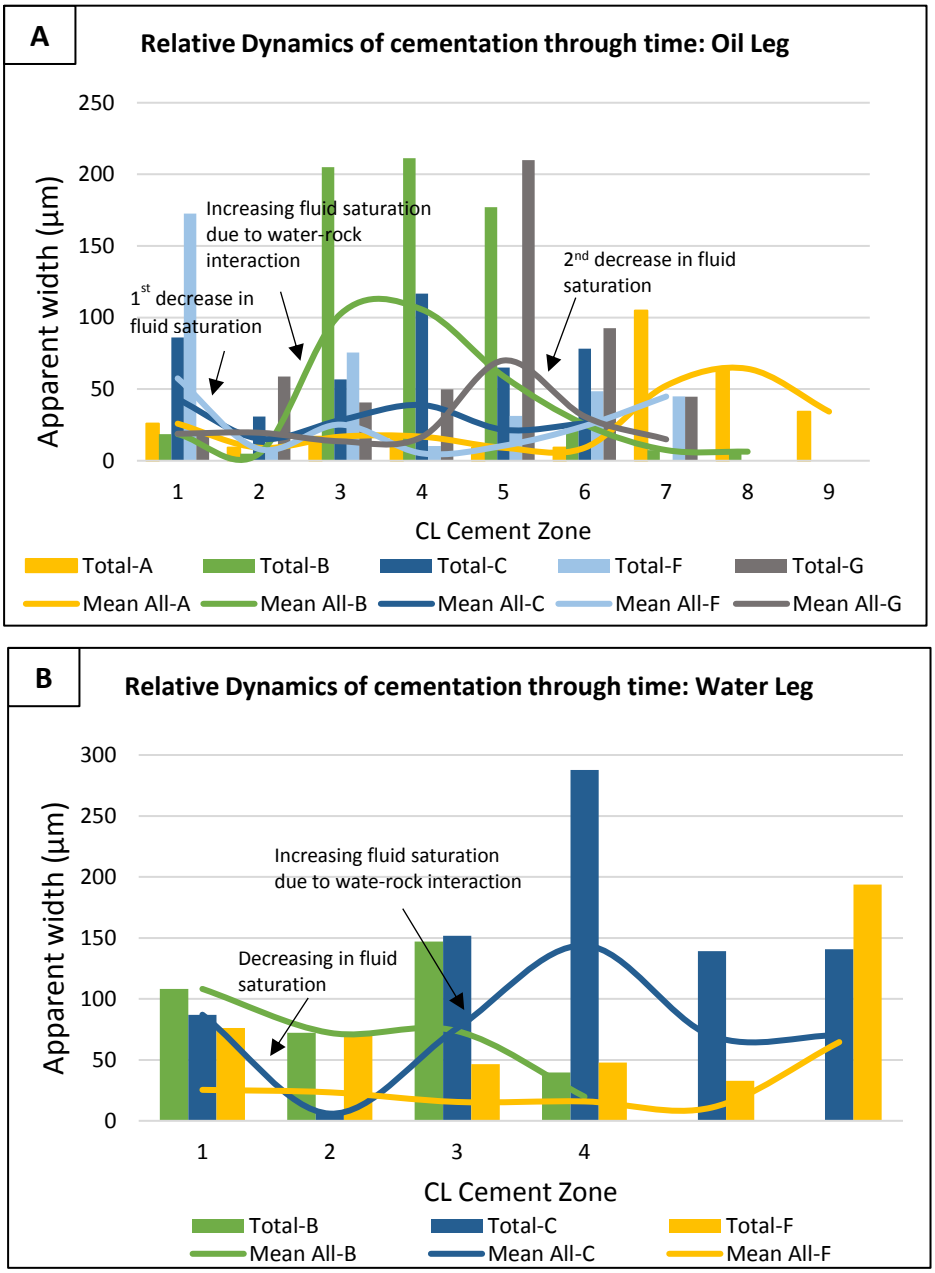

Figure 3.8: Summary Figure of relative dynamics of calcite cementation through time. The curve and column represent the means and total precipitated cements of all types of calcite cement at certain cement zone respectively. A) Oil leg. B) Water leg.

## 3.2 Discussion

### Relative Dynamics of Calcite cementation

The cementation history curve can provide some insight into the rate of fluid flux (delivery rate of solute) evolution through time. This can be inferred using the fact that the higher rate of supersaturated solute can result in higher cement precipitation and vice versa. Higher amounts of precipitated cement may also suggest longer time of precipitation. Cementation history curves for all reservoirs in the oil leg start with a higher cementation rate at the first cement zone which decreases towards the next cement zone (Figure 3.8A). This implies that at early cementation pore fluid was saturated (Zone 1, Figure 3.8A) which substantially decreases toward Zone 2 and became less saturated resulting in lower precipitation (1$^{st}$ decreasing phase). Following this decrease, a gradual increase in the cementation rate is also noted in all reservoirs (Zones 3 & 4, Figure 3.8A). The gradual increase infers that higher amounts of solute were being delivered at that time and possibly longer cementation times. This solute can be obtained as a result of increasing burial as more pore fluid interacts with rock (Heydari and Moore, 1993; Walderhoug, 1994). As cement precipitates, pore fluids become less saturated with dissolved ions and hence results in less precipitated amount of cement. Or the precipitation time was shorter for this particular zone. The decrease in fluid saturation can be seen in Figure 3.78A marked as a second decrease in cementation history (2$^{nd}$ decrease in fluid saturation). These cycles of cementation of higher and lower rate of solute can be repeated since water-rock interaction series can go on and on due to increasing burial with time; as rocks continue to bury over time, rate of water-rock interaction will increase as well provide solute for precipitation,

then, cement will precipitate and therefore solute will decrease until a second higher burial event come and rise again the in-situ solute.

However, the rate of cementation can vary according to the stratigraphic setting of the rock and influence of external factors such as hydrocarbon fluid charge and other exotic fluids. Looking at the different stratigraphic reservoirs, all reservoirs show repeating cycles of higher and lower cementation rates except Reservoir B (Figure 3.6). Reservoir B shows long-lived cycle which ends with very low cementation rate. This reduction in cementation rate could be due to oil charge. Primary oil inclusions were found in the cement zone precipitated in the equivalent time to cement Zone 5 in Reservoir B (equant and syntaxial, Figure 3.6B) (Thorpe, 2014; Nielson et al., 1998). Indeed, this is the time when the equant cement started to precipitate and the time where there is a notable reduction in syntaxial calcite precipitation (Reservoir B, Zone 5, syntaxial, Figure 3.6B). Thus, it can be suggested that oil charge caused a retardation in cementation rate, even though cementation continued with the available irreducible water (Heasley et al., 2000; Marzouk et al., 1995). In Reservoir A, primary oil inclusions were reported at time equivalent to Zones 5 and 6 (syntaxial, Figure 3.6A) (Thorpe, 2014; Cox. et al., 2010). At these two cement Zones, calcite cementation is lower which could be also due to oil charge. However, an increase in the cementation can be seen after this major decrease in Reservoir A (Zone 7, synaxial and blocky). This could be due to 1) miss interpreting the last cement zones of blocky calcite from CL observation; these zones could be placed earlier in the cement history, 2) a possibly higher rate of water-rock interaction with heat flux?, or 3) higher rate of fluid flux.

Oil charge into deeper Reservoirs (C, F & G) should be later compared with shallower Reservoirs (A & B) because oil filling starts from top of the crest downwards. The deeper Reservoirs C and F show similar cementation cycle (decrease-increase-decrease-increase, Figure 3.6C & D) inferring frequent episodes of higher and lower delivery rates of solute compared with shallower Reservoir B. This could be due to the late oil charge in the lower stratigraphic reservoirs which allowed for frequent and further cementation during burial. Reservoir G shows even more frequent episodes of higher and lower precipitation rate (Figure 3.6E). This could suggest that

this reservoir was subjected to several fluid fluxes at different times and cementation rate was not controlled only by water-rock interactions.

The limited measured CL zones in Reservoir B water leg make the interpretation difficult (Figure 3.7A). However, all of the higher and lower episodes of cementation in Reservoirs B, C and F can be interpreted similar to those in the oil leg; a higher rate of delivery of solute can result in higher cementation and vice versa (Figure 3.8B). In general, the total volume of precipitated cement in water leg is higher than oil leg indicating a higher availability of dissolved ions for calcite cementation.

## 3.5 Summary

Calcite cementation in matrix has affected reservoir quality by different magnitudes at different stages during burial. Overall, calcite cementation has a negative effect on reservoir properties. The amount of precipitated cement varies in the oil versus water leg, but overall the total precipitated cement in the water leg is higher than the oil leg. This indicates that calcite cementation has greater impact on reservoir quality in water leg than oil leg. The major effect of calcite cementation on reservoir quality varies, it can be found 1) between cement Zones 3 and 5 as in the case of Reservoirs B and C, 2) at younger cement Zones, as in the case of Reservoirs A and G, 3) very early as in the case of Reservoirs F and C. If we go back at the beginning of cementation history (Zone 2), reservoir quality would be the best if no further cementation occurred. The most important calcite cement type to contribute to reservoir quality destruction almost in all reservoirs, oil and water, is blocky calcite. This calcite has its greatest influence starting from the relative mid-time and towards the end of calcite precipitation history.

The higher apparent widths of each cement zone could also infer a higher precipitation rate, a higher fluid saturation, as well as longer precipitation time. Fluctuation between higher and lower fluid saturation episodes may suggest change in water-rock interaction caused by increasing burial through time.

Early oil charge in shallower Reservoir B probably lowered the cementation rate in this reservoir. By contrast, late oil charge in the deeper reservoirs allowed further cementation at higher rates compared with the shallower reservoirs and hence higher precipitated volume of cement.

# Chapter 4: Origin and Evolution of Calcite Cement in Thamama Reservoirs

## 4.1 Introduction

Seawater chemistry has varied substantially during the Phanerozoic, which resulted in significant shift in the carbonate mineralogy of skeletal and non-skeletal carbonates (Hardie, 1996; Mackenzie and Morse, 1992; Morse et al., 1997; Stanley and Hardie, 1998). Composition of carbonate cements can be also altered by introduction of exotic fluids into the system as well as diagenetic processes, such as dolomitization and dissolution. Trace element geochemistry of carbonates can be used as a tool for reconstructing the composition of fluids from which carbonate cements were precipitated (Uwe and Veizer, 1980; Vincent, et al, 2006). Examples of trace elements widely used in carbonate studies include Ca, Mg, Mn, Fe, and Sr, which were also selected for this study.

The main objectives of this geochemical study are to 1) unravel the chemical composition and origin of pore fluids corresponding to precipitation of different cements using Sr variation and the redox sensitive elements Fe and Mn, and 2) investigate the palaeotemperature evolution of the fluids of the precipitated cements using mMg/Ca molar ratio.

The concentrations of $Mn^{2+}$ and $Fe^{2+}$ have been widely used to determine the compositional variation in calcite cements (Barnaby and Rimstidt, 1989; Dromgoole and Walter, 1990; van Smeerdijk Hood and Wallace, 2015). This variation may introduce zonation in calcite cements when examined under CL microscopy which is used as a basis for cement stratigraphies. It is used to classify luminescent, non-luminescent, and dull luminescent calcite cements and relate them to diagenetic

environments (Braithwaite, 1993). Moreover, changes in $Mn^{2+}$ and $Fe^{2+}$ in pore fluid can be used to study the environment of cementation including the redox conditions of pore fluids. Cements with high $Mn^{2+}$ and $Fe^{2+}$ concentrations usually reflect redox-anoxic condition whereas cements with low concentrations represent an oxidizing-oxic environment (Barnaby and Rimstidt, 1989; Dromgoole and Walter, 1990; Mason, 1987). $Mn^{2+}$ and $Fe^{2+}$ can be derived from hydrothermal fluids from deep burial sources (Ali, 1995; Barnaby and Rimstidt, 1989; Vincent et al., 2006). In addition, erosion of exposed lands can serve as detrital input for $Mn^{2+}$ and $Fe^{2+}$. Higher concentrations of $Mn^{2+}$ and $Fe^{2+}$ can be also found in areas with high clay concentrations. Froelich et al. (1979) suggested another source for $Mn^{2+}$ which involves the oxidation of organic matter. This type of reaction provides high level of dissolved $Mn^{2+}$, which is maintained unless $Mn^{2+}$ is consumed in other reactions (Ali, 1995). $Mn^{2+}$ can be released into the system during pressure dissolution (Heydari and Moore, 1993; Paganoni et al., 2016). However, the amount of $Mn^{2+}$ released from this process might not be adequate to account for high $Mn^{2+}$ concentrations (Heydari and Moore, 1993).

The concentration of Sr can be affected by a number of factors including stratigraphic age, salinity, clay mineral content and depositional environment (Al-Hashimi, 1976). Sr content is higher in more distal open environments and can be depleted due to water-rock interactions which involve freshwater fluids with very low concentrations of Sr (Vincent et al., 2006). Vincent et al. (2006) suggested that Sr variations can be used as a tool for palaeosalinity indicator of seawater. In addition, processes such as the transformation of aragonite-calcite and diagenetic conditions (closed versus open systems) are thought to affect Sr content (Al-Hashimi, 1976). During dolomitization processes in relatively open system, significant amounts of Sr can be lost resulting in low Sr content in newly formed cement.

mMg/Ca molar ratio is sensitive to temperature changes and thus can be used as temperature proxy for pore fluids from which cements were precipitated (Carpenter, 1980; Heydari and Moore, 1993; Morse et al., 1997; Volery et al., 2009). It has been suggested that mMg/Ca of pore water decreases with increasing temperature (Heydari

and Moore, 1993). Typical mMg/Ca of pore fluids at 25˚C is close to 1 which decreases near linearly to 0.05 at 150˚C (Figure 4.1; Carpenter, 1980; Heydari and Moore, 1993). Low Mg cement can be precipitated from pore water of low mMg/Ca ratio, which is typical for subsurface water (Heydari and Moore, 1993). In addition, diagenetic alterations due to equilibrium of sea with meteoric water could result on a reduction in Mg content (Uwe and Veizer, 1980; Vincent et al., 2006). Elevated Mg can be derived from dolomitization/dedolimitization processes (Vincent et al., 2006). Moreover, several authors agreed that mMg/Ca ratio can be influenced by variation in seawater composition derived by changes in changes in continental weathering inputs, rates of global volcanic and mid ocean ridge (MOR) activity, and dissolved $SO_4$ (Balthasar and Cusack, 2015; Bots et al., 2011; Hardie, 1996; Larson, 1991; Larson and Erba, 1999; Morse et al., 1997; Steuber, 2002; Timofeeff et al., 2006).

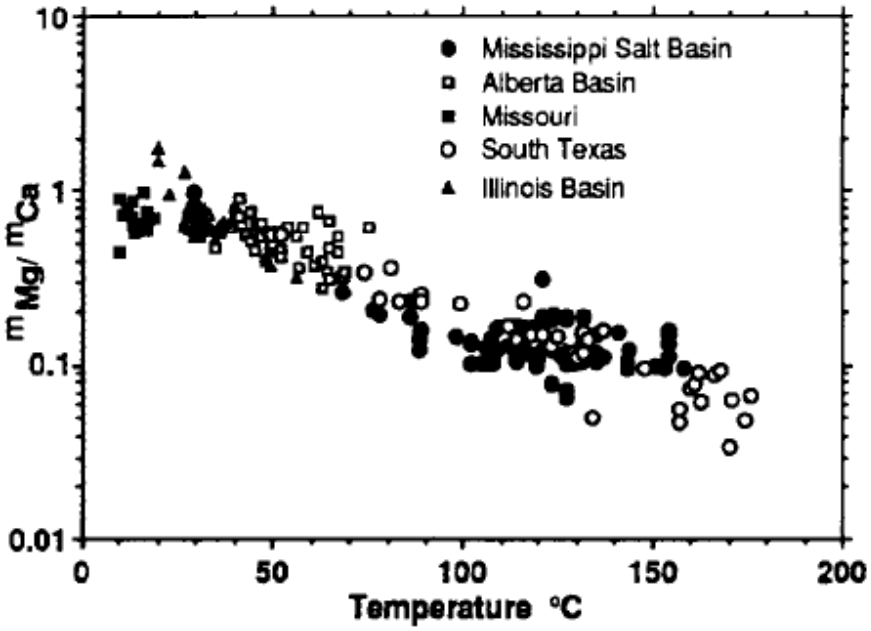


Figure 4.1: mMg/Ca molar ratio of pore water versus temperature of Mississippi Basin (Heydari & Moore, 1993). Note the near linear relationship of samples from several locations.

Hardie (1996) concluded that the variation in mMg/Ca ratio of seawater can be driven by changes in mid-oceanic ridge hydrothermal brine rates which subsequently resulted from changes in oceanic crust production rates. The prediction is based on a simple model that basically quantify ancient seawater chemistry from flux of MOR and river water (RW) ratio (MOR/RW) which are the two main contributors to ocean chemistry. Hardie (1996) added that as the rate of oceanic crust production increases, MOR/RW flux ratio increases. As a consequence seawater composition will have lower mMg/Ca ratio, depleted Mg and $SO_4$ and enriched Ca and K content.

The model of Hardie (1998) suggests that mMg/Ca ratio changed from~1.8 at 140 Ma to ~0.7 at 115 Ma. Wilkinson and Algeo (1989) model suggests mMg/Ca ratio varied from ~1.7 at 140 Ma to ~1.0 at 110 Ma. Another model by Berner (2004) suggests similar mMg/Ca ratio to Wilkinson and Algeo (1989) model; changing from ~1.7 at 140 Ma to 1.1 at 110 Ma. mMg/Ca ratios obtained from fluid inclusions in halite are higher than the Hardie (1998) model, ranging from 1 to 1.7 at ~120 Ma (Lowenstein et al., 2001), 1.1 to 1.3 from 121.0 to 112.2 Ma, and 1.2 to 1.7 from 112.2 to 93.5 Ma (Timofeeff et al., 2006). Both studies recorded the lowest Mg/Ca ratios during the Aptian, ~118 Ma. Two skeletal empirical proxies have also been used to quantify ancient seawater mMg/Ca ratios, again yielding slightly higher ratios than the Hardie (1998) model. First, well-preserved echinoderm stereom (originally High Mg calcite) from 130 Ma and 100 Ma yielded values of 1.7-1.8 and 0.9, respectively (Dickson, 2004), and secondly rudist shell calcite from 121.2 Ma and 106 Ma, which yielded ranges of 0.9-1.4 and 0.8-1.3, respectively (Steuber and Rauch, 2005).

S isotope values which are affected by riverine, volcanic and hydrothermal exchange rates follow mMg/Ca ratios of seawater during the Lower Cretaceous (Paytan et al., 2004), and the negative $^{87}Sr/^{86}Sr$ excursion of Aptian-Albian seawater coincides with the low mMg/Ca ratios and low S isotopes (Jones and Jenkyns, 2001).

The negative $^{87}Sr/^{86}Sr$ excursion was modeled based on decreasing river water (RW) flux of Sr which believed to be linked with higher ocean crust production at the

MORs. Other models of mMg/Ca (Wilkinson and Algeo, 1989; Hardie, 1996; Berner, 2004) which is based on MOR and RW flux shows lower mMg/Ca coincides with the time of higher MOR and RW flux. A higher rate of ocean crust production was reported during 125-80 Ma (Larson, 1991) and includes the biggest "volcanic pulse" around 126-112 Ma (Larson and Erba, 1999) or 120-100 Ma (Gaffin, 1987) for the past 160 m.y. (Hays and Pitman, 1973; Larson, 1991; Larson and Erba, 1999; Larson and Olson, 1991; Richards and Engebretson, 1992).

Here I present data study that provides important clues to the origin and geochemical evolution of fluids involved in calcite cementation of Thamama Reservoirs. Trace elements analyzed of syntaxial, equant and blocky cements in oil and water legs are presented and discussed below. All other relevant data are presented in Appendix B.

## 4.2 Sampling Procedure and Methodology

### 4.2.1 Sampling Procedure

The main objective in sample selection is to trace and capture trace element concentrations in each identified CL cement zone. This is to understand cement stratigraphy of each cement type including pore fluid evolution. The ideal way is to run a transect through each cement stratigraphy which is previously established from CL work.

The initial sample selection was based on 1) availability of cements in each reservoir, oil versus water leg, 2) cement stratigraphy; number of cement zones that can be identified in each type of cement. The first was decided by conventional petrography work. The second was based on CL work. The most abundant calcite cements in all reservoirs are equant, syntaxial and blocky. Reservoir A contains very low equant calcite which make the sampling difficult. However, syntaxial and blocky calcite are more abundant and hence adequate cement samples have been analysed (Table 4.1). Moreover, this reservoir has been only sampled from oil leg which allowed for no comparison between different fluid zones. Cements of Reservoir B have been sampled from both oil and water legs. All cement types are available in matrix of water and oil leg except the blocky calcite in water leg which occurs with higher volume in fractures. Cements in fractures were analysed by another PhD student. Similarly, cements in Reservoirs C and F were sampled from both legs water and oil except equant calcite in water leg of Reservoir C because it is less abundant and difficult to sample. Syntaxial cement in Reservoir F oil leg is less abundant than water leg. Blocky calcite in this reservoir can be found with higher volume in fractures. Yet, all cement types have been analysed in this reservoir including water and oil legs. Cements samples of Reservoir G were only taken from the oil leg. Equant, syntaxial and blocky calcite were analysed from this reservoir. Syntaxial calcite in Reservoir G is less common than other reservoirs particularly the upper reservoirs.

Table 4.1: Abundance of equant, syntaxial and blocky calcite in each reservoir in oil and water legs. R: Rare, C: Common, A: Abundant.

| Reservoir | Cement Type | Oil Leg | Water Leg |
|---|---|---|---|
| **A** | Equant | R | No samples |
| | Syntaxial | C | |
| | Blocky | A | |
| **B** | Equant | A | C |
| | Syntaxial | C | A |
| | Blocky | A | R |
| **C** | Equant | C | R |
| | Syntaxial | A | C |
| | Blocky | C | C |
| **F** | Equant | C | R |
| | Syntaxial | R | C |
| | Blocky | R | R |
| **G** | Equant | R | No samples |
| | Syntaxial | R | |
| | Blocky | A | |

The final sample selection was based on 1) apparent width of each crystal and number of CL zones in each crystal, 2) scaling difference between CL and EPMA results. The apparent length of each crystal and the number of CL zones of the same crystal were used to estimate the length of individual transect and the number of data points to be analysed through a single transect; spacing between data point in a single transect. The closest spacing that has been tested in order to capture the very thin CL zones is around 9.5 µm. The results show that data points are very close and there may be overlaps in some data points (Figure 4.2). Thus, it was difficult to capture the composition of very thin CL zones that are less than 9.5 µm through a single transect.

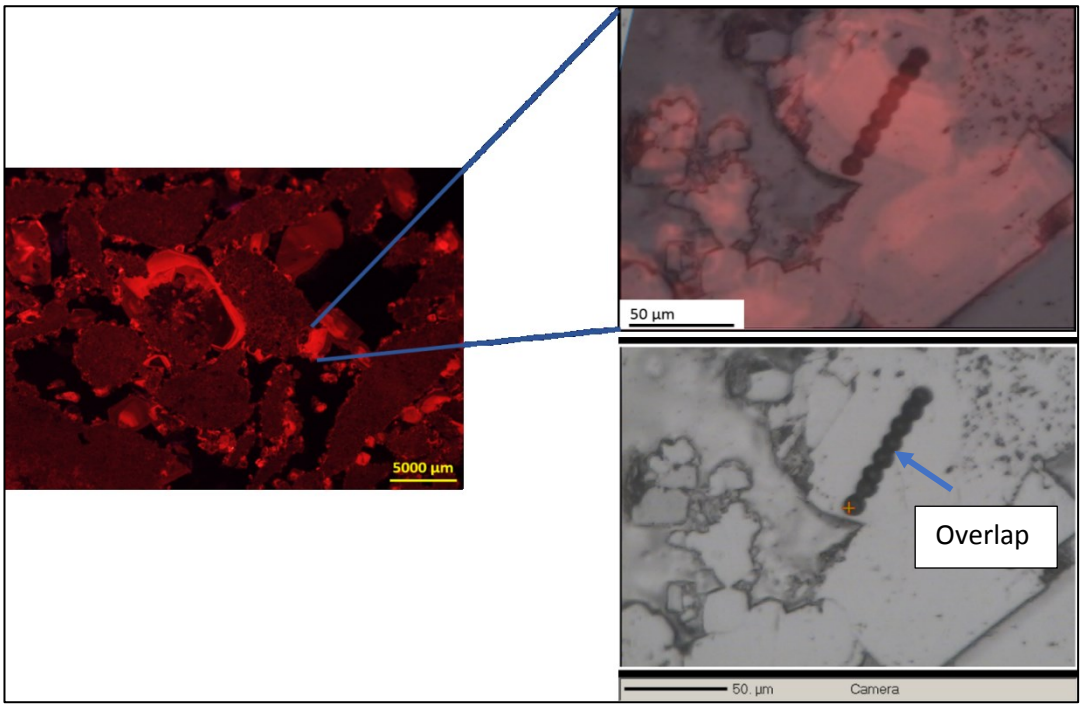


Figure 4.2: Combined images from CL and EPMA works, example from Reservoir G. Note how data points in the transect are close and overlap. Note also the difference in the scale.

Scaling was another criteria used for sample selection. The clearest CL image with good quality was taken under 10X lens which is equivalent to 5000 µm (Figure 4.2). Magnifications higher than 10X showed very poor images. Thus, the highest resolution from CL that can be taken is 5000 µm. However, EPMA images were taken down to 50 µm. This introduced a difficulty when fitting the two images into one scale in order to fit the transect with the CL zones. Therefore, some samples were eliminated due to scale issue. Table 4.2 shows the final number of useable transects and number of data points for each matrix cement type in water and oil legs.

Table 4.2: Number of transects and data points (n) analysed for each cement type across different reservoirs in oil and water legs. Note that you can compare the abundance of the cements with Table 4.1.

| Reservoir | Cement Type | Oil Leg | Water Leg |
|---|---|---|---|
| **A** | Equant | - | No samples |
| | Syntaxial | Transect: 4 n:19 | |
| | Blocky | Transect: 12 n:51 | |
| **B** | Equant | Transect: 10 n:32 | Transect: 5 n:17 |
| | Syntaxial | Transect: 4 n:23 | Transect: 12 n:59 |
| | Blocky | Transect: 7 n:31 | - |
| **C** | Equant | Transect: 4 n:17 | - |
| | Syntaxial | Transect: 9 n:46 | Transect: 4 n:24 |
| | Blocky | Transect: 5 n:24 | Transect: 4 n:17 |
| **F** | Equant | Transect: 4 n:13 | Transect: 3 n:14 |
| | Syntaxial | Transect: 2 n:8 | Transect: 4 n:21 |
| | Blocky | Transect: 3 n:25 | Transect: 3 n:23 |
| **G** | Equant | Transect: 3 n:16 | No samples |
| | Syntaxial | Transect: 2 n:14 | |
| | Blocky | Transect: 6 n:36 | |

### 4.2.3 Methodology

Electron probe microanalysis (EPMA) was conducted in the University of Edinburgh using a Cameca SX100. EPMA was applied for 18 polished (0.5-1mm thick) thin sections (from all reservoirs) to obtain concentrations of Mg, Ca, Mn, Fe, and Sr for calcite cement including syntaxial, equant and blocky. Thin sections were

cleaned to remove abrasive particles and lubricants and then coated with a thin layer of carbon before the analysis. EPMA can take two samples each round and each sample take around 7-8 hours depending on numbers of areas to be analysed. Thus, some measurements were set to be taken automatically overnight. Samples were bombarded with an incident electron beam with a diameter size of 5µm and 15 KV. Calcite-Silicarb_Ca standard was placed in a separate holder and was calibrated twice; before and after the analyses in each round. The obtained concentrations including the detection limits were reported in Parts Per Million (ppm).

Among the analysed elements, Fe is the least abundant element especially in the upper reservoirs. The detection limits of $Mn^{2+}$ and $Fe^{2+}$ in oil and water legs in all calcite cements are 100 ± 5 ppm and 130 ± 4 ppm respectively. Detection limit of Sr varies across reservoirs. In the lower Reservoirs F and G, Sr can be detected at 150 ± 3 ppm in both oil and water legs. In Reservoir C, Sr is detectable at 130 ± 1 ppm in oil and water legs. Similar to Reservoir C, Sr can be detected at 130 ± 1 ppm in Reservoir B in oil leg. Whereas in water leg Reservoir B, detection limit of Sr is 115 ± 5 ppm. Reservoir A with only oil samples has Sr that is detectable at 115 ± 3 ppm similar to Reservoir B water leg (Appendix B). Concentrations of all magnesium and calcium of calcite were converted to mMg/Ca ratio using $K_d$ of 0.021 (Rimstidt et al., 1998).

## 4.3 Results

The mMg/Ca ratio, Sr, Mn and Fe concentrations through different stratigraphic unit in oil versus water leg are described below. Results of each calcite type in each individual reservoir have been displayed using individual cement stratigraphic scheme generated using CL images (Table 3.3). Another integrated scheme was generated after interpreting and combining EPMA data of this chapter with CL images (Figure 4.28). The final integrated scheme should be used for Chapter 6 to compare mMg/Ca with $\delta^{18}O_{VPDB}$ data.

### 4.3.1 Oil Leg

#### 4.3.1.1 Syntaxial Calcite

Figure 4.3A illustrates Mn concentration through CL zones found in Reservoir G. Four CL zones (2, 3, 4 & 6) have just one data point. The Mn concentration generally decreases towards younger cement zones with highest drop at Zone 5 followed by an increase in Zone 6 to be again within same range of mean values. A unique Fe trend is found in this reservoir (Figure 4.3B). The trend shows significant Fe concentration (ferroan) in Zone 1 which drops dramatically to show no Fe content in the following younger zones. Same Zone 1 hosts the highest Sr content. Sr concentration decreases gradually towards Zones 2, 3, and 4 and then increases towards youngest Zones 5 & 6 (Figure 4.3C). Figure 4.3D displays mMg/Ca behaviour through CL zones of syntaxial cement in Reservoir G. mMg/Ca starts with mean value of 0.8 in Zone 1 which then increases to reach its highest mean value (1.0) in Zone 2. Afterword, it declines towards younger zones to reach a minimum mean value of 0.5 at Zone 5.

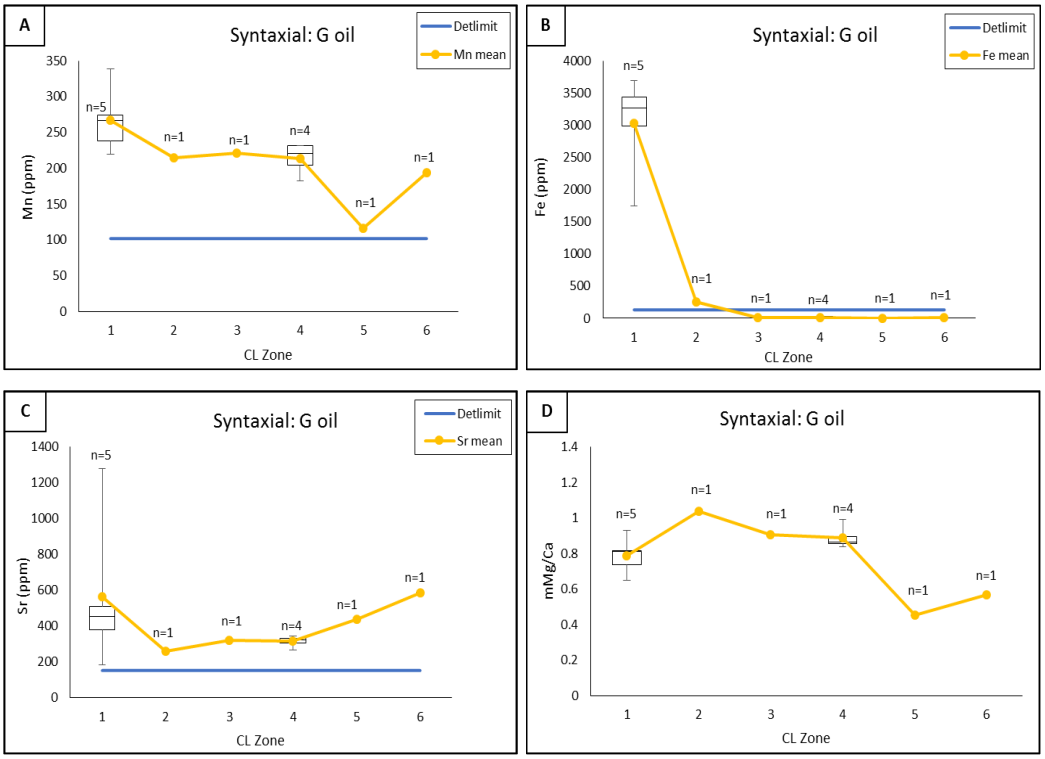


Figure 4.3: Element concentrations of syntaxial calcite cement in Reservoir G in oil leg: A) Mn content across CL zones with highest content in Zone 1 and lowest in Zone 5. B) Fe content across CL zones with highest content in Zone 1 (similar to Mn) and very low content in the rest of the zones. C) Sr content across CL zones. Note the highest Sr content in Zone 1 coincides with highest Mn and Fe contents. D) mMg/Ca ratio across CL zones with general decline towards younger cement zones. Note the low Mg/Ca ratio in Zone 1 reflecting lower Mg content.

Two CL zones were captured and analysed in Reservoir F. Based on these two zones Mn concertation shows slight increase from Zone 1 to Zone 3 (Figure 4.4A). Similar to Mn, Fe trend shows slight increase from Zone 1 to Zone 3 (Figure 4.4B). Unlike Mn and Fe, Sr and mMg/Ca contents decrease from Zone 1 to Zone 3 (Figure 4.4C & D).

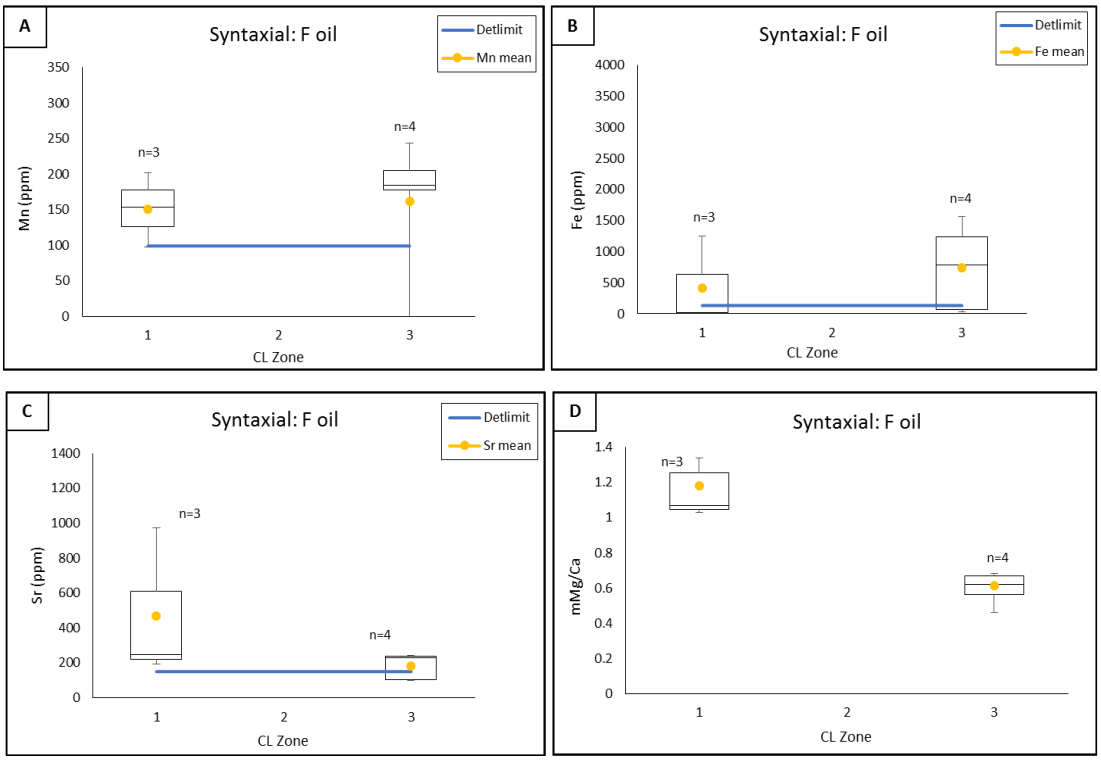


Figure 4.4: Element concentrations of syntaxial calcite cement in Reservoir F in oil leg: A) Mn content across two CL zones showing increase from Zone 1 to Zone 3. B) Fe content across two CL zones illustrating an increase in Fe content from Zone 1 to Zone 3 (similar to Mn). C) Sr content across CL zones. D) mMg/Ca ratio across CL zones. Note that both Sr content and mMg/Ca ratio decline from Zone 1 to Zone 3 contradicting Mn and Fe content.

The general Mn trend in Reservoir C is fluctuating through CL zones (Figure 4.5A). The trend starts with mean value below the detection limit in Zone 1 which gradually increase to reach mean value of 153 ppm at Zone 4, then significantly drops at Zone 5 below the detection limit (81 ppm). The trend finishes up with an increase in Mn concentration in Zone 6 (mean= 131 ppm). Looking at Fe content (Figure 4.5B), the trend starts with zero concentrations (below detection limit) at the first four Zones followed by a significant increase towards youngest zones (Zone 5=366 ppm & Zone 6 (ferroan) mean=702 ppm). Sr concentration declines moving towards younger zones to reach the lowest mean value at youngest Zone 6 (96 ppm) which is reversing Mn and Fe contents (Figure 4.5C). mMg/Ca molar ration starts with mean value around

1.0 at Zone 1 then decreases gradually towards younger cement zones to reach the minimum mean value of 0.3 at Zone 6 (Figure 4.5D).

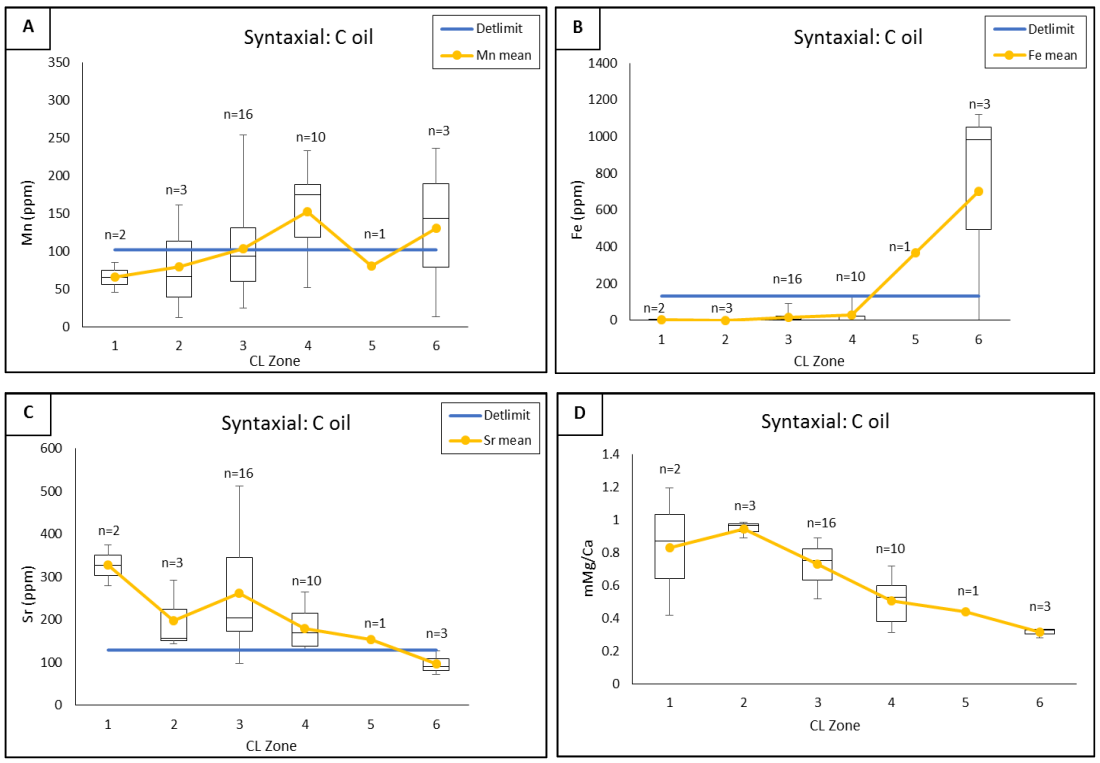


Figure 4.5: Element concentrations of syntaxial calcite cement in Reservoir C in oil leg: A) Mn content is fluctuating through CL cement zones. Major Mn content can be found in Zones 1, 4 and 6. B) Fe content across CL zones with detectable values only in youngest Zones 5 and 6. C) Sr content showing general decrease towards younger CL cement zones. Zones 1 and 3 have the highest Sr values. D) mMg/Ca ratio illustrating a general decline towards younger cement Zones. Note that both Sr content and mMg/Ca ratio have low values in Zone 6, whereas Mn and Fe values are high in the same zone.

In Reservoir B, Mn trend starts with zero to very low concentration which gradually increases to reach the highest concentration at Zone 5 (mean= 151 ppm; Figure 4.6A). Fe concentrations in all CL zones are below the detection limit (non-ferroan) (Figure 4.6B). Opposite to Mn concentration, Sr is highest in Zone 1 (307 ppm) and getting lower in the younger zones except for very slight increase at Zone 5

(mean= 161 ppm). Similarly, mMg/Ca trend in this reservoir shows a general decrease towards younger zones and reach a minimum mean value of 0.3 at Zone 5 (Figure 4.6D).

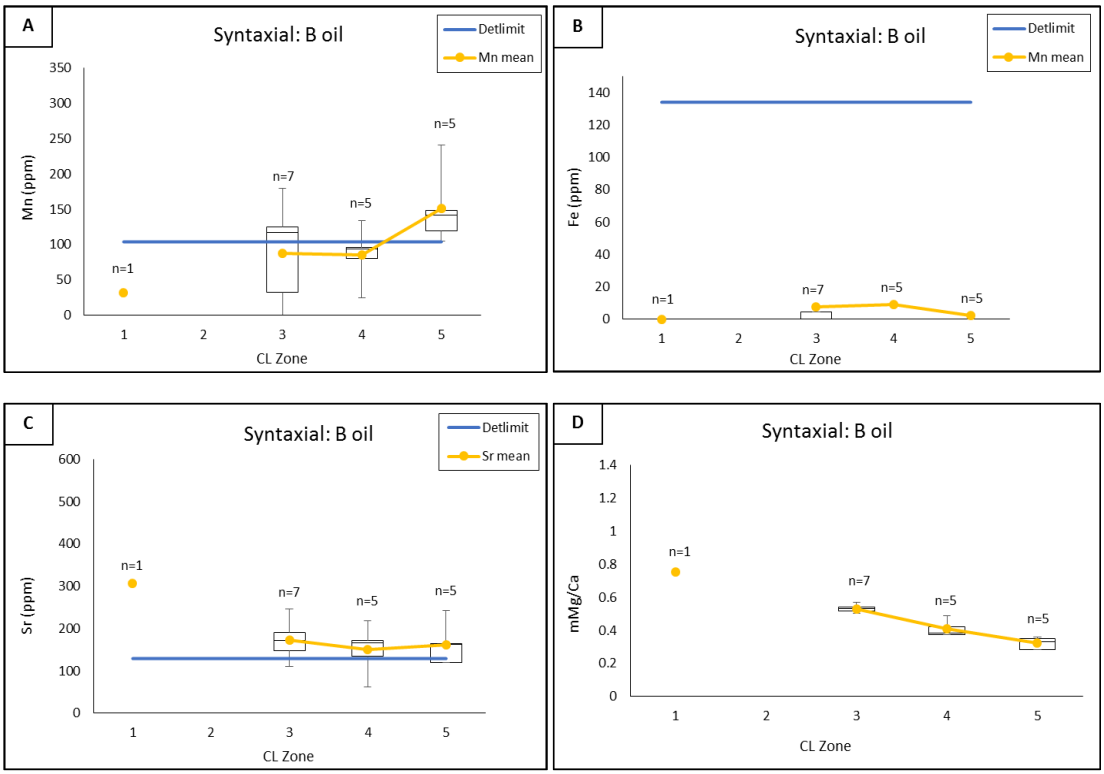


Figure 4.6: Element concentrations of syntaxial calcite cement in Reservoir B in oil leg: A) Mn content in general is low and increases towards younger cement Zones. B) Fe content across CL zones. Fe values in all zones are below the detection limit. C) Sr content across CL zones. Higher Sr content can be found in Zones 1 and 5. D) mMg/Ca ratio with general decline towards younger cement zones. Note that the lowest mMg/Ca ratio recorded in Zone 3.

The Mn trend in Reservoir A starts with low concentration at Zone 1 (mean=62 ppm) then increases towards Zone 4 (mean=192 ppm; Figure 4.7A). Following that, Mn content decreases gradually towards Zones 5 and 6 (mean= 156 ppm) to finish up with slight increase at Zone 7 (193 ppm). Similar to Reservoir B, all Fe values in all CL zones are below the detection limit (non-ferroan) (Figure 4.7B). Sr concentration trend is the reverse of Mn trend (Figure 4.7C). Just like the previous reservoir,

mMg/Ca decreases through younger cement zones to reach the lowest mean value of 0.5 at youngest Zone 7 (Figure 4.7D).

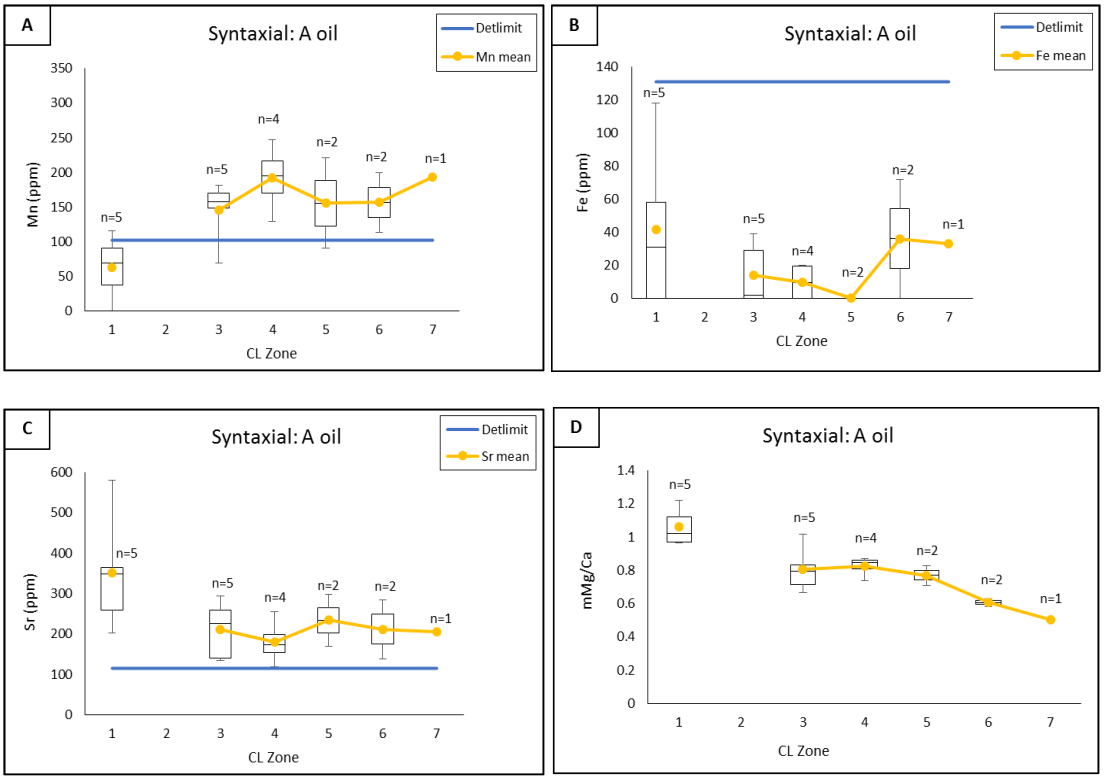


Figure 4.7: Element concentrations of syntaxial calcite cement in Reservoir A in oil leg: A) Mn content showing general increase towards younger cement zones. Note low Mn values in Zone 1 compared with other zones. B) Fe content across CL zones. Fe values in all zones are below the detection limit. C) Sr content across CL zones. Sr content in all cement zones is laying almost within the same range. Note also that Sr trend is reflecting the reverse trend of Mn. D) mMg/Ca ratio with general decline towards younger cement zones.

Overall, Mn concentration in the lower Reservoirs G and F is high and becomes low (almost vanished) in Reservoirs C and B then starts to rise again to become abundant in Reservoir A. Fe concentration is below the detection limit in all reservoirs except for Reservoir F and one CL zone in Reservoir G and C. Overall, Fe concentration decreases stratigraphically through upper reservoirs (B and A contain zero Fe). Sr content decreases towards younger reservoirs. mMg/Ca molar ration

varies through different stratigraphic units with lowest values recorded in Reservoir B. Generally, mMg/Ca molar ratio shows a general decreasing away from grain centre; towards pore wall (younger cement zones) in all calcite cements.

#### 4.3.1.2 Equant Calcite

All Mn values recorded in Reservoir G are above the detection limit (Figure 4.8A). The Mn concentration is fluctuating through CL zones. It starts with high value at Zone 1 (mean= 248 ppm) which decreases towards younger cement zones to reach minimum mean value of 177 ppm at youngest Zone 5. Fe trend in this cement is like the trend found in syntaxial cement; an extreme value at oldest cement Zone 1 (mean= 1553; ferroan) an almost zero concentration in younger cement zones (Figure 4.8B). All Sr values are above the detection limit with highest mean values recorded at cement Zone 4 (342 ppm; Figure 4.8C). In the last two Zones 4 and 5, Mn and Sr follow the same trend. The mMg/Ca is lower in oldest cement Zone 1 (mean= 0.8) compare with younger cement Zone 4 (mean= 0.9). Similar observation have been noted in syntaxial calcite; mMg/Ca is lower in oldest cement zone compared with a younger cement zone. The mMg/Ca decreases again from Zone 4 (mean= 0.9) to Zone 5 (mean= 0.7) (Figure 4.8D).

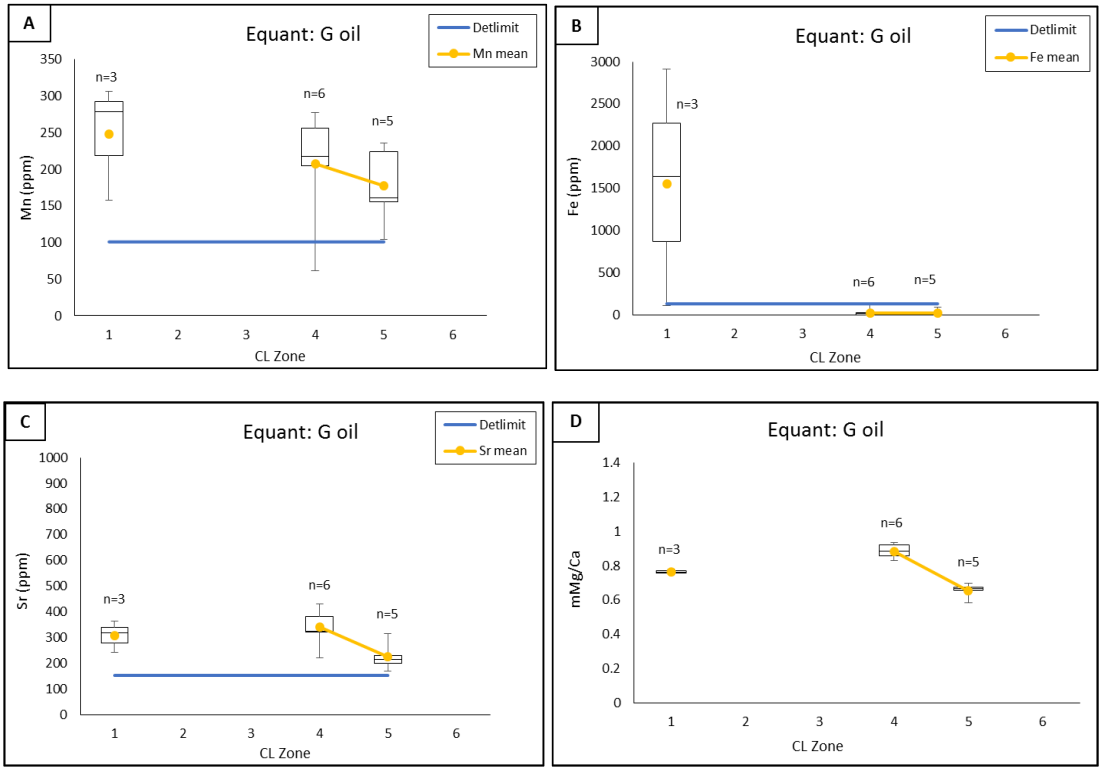


Figure 4.8: Element concentrations of equant calcite cement in Reservoir G in oil leg: A) Mn content fluctuating through CL zones. B) Fe content across CL zones. Note the high concentration in Zones 1 and 3. C) Sr content across CL zones. Note the higher Sr content in the older CL Zones compared with younger Zones. D) mMg/Ca ratio with slightly increasing trend towards younger cement zones.

The Mn concentration trend in Reservoir F shows an increase from Zone 1 (mean= 97 ppm) to Zone 2 (mean= 139 ppm) and continues to at youngest Zone 3 (mean= 158 ppm; Figure 4.9A). Fe content decreases from Zone 1 (mean= 314 ppm) to Zone 2 (mean= 109 ppm) then rises again (ferroan) towards Zone 3 (mean= 726 ppm; Figure 4.9B). Sr trend is opposite to Mn trend; highest mean value at oldest Zone 1 (mean= 520 ppm) and decreases dramatically towards younger zones to reach minimum mean value of 209 ppm at youngest Zone 3 (Figure 4.9C). A clear sharp decline in mMg/Ca ratio can be indicated with a maximum mean value of 1.2 at Zone 1 and a minimum mean value of 0.4 at Zone 3 (Figure 4.9D).

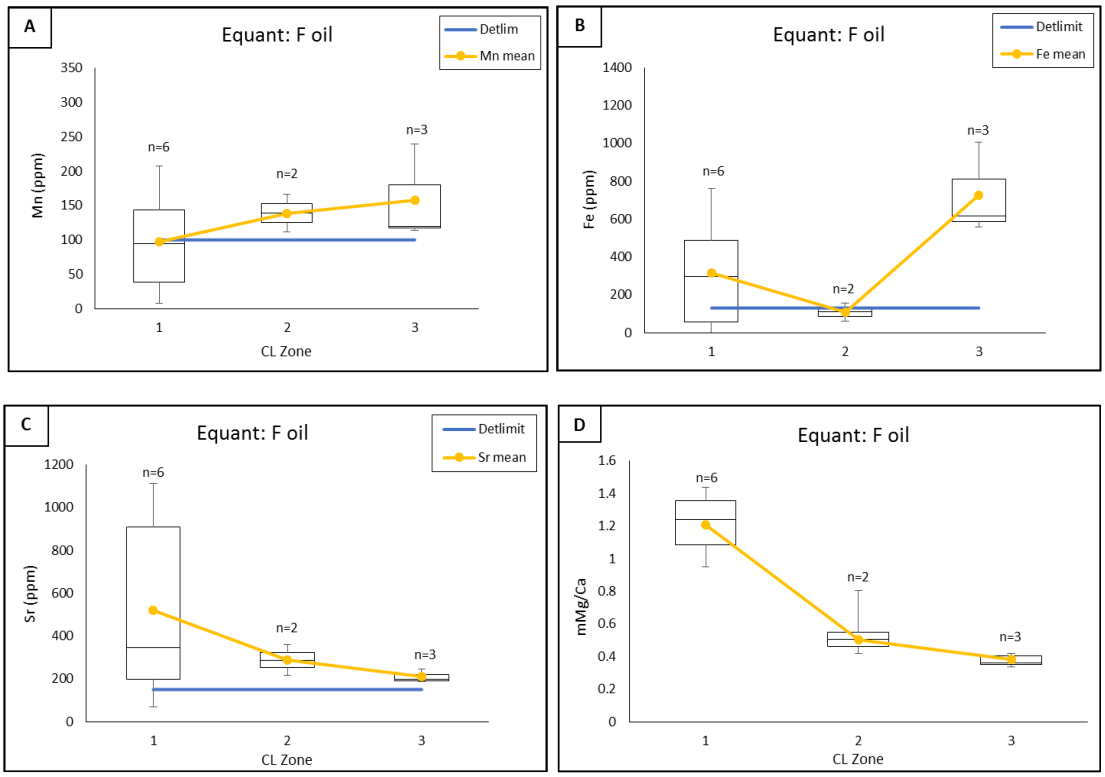


Figure 4.9: Element concentrations of equant calcite cement in Reservoir F in oil leg: A) Mn content across two CL zones showing increase from Zone 1 to Zone 3. B) Fe content across three CL zones illustrating an increase in Fe content from Zone 1 to Zone 2 and then decrease to Zone 3. C) Sr content across CL zones with decreasing trend toward younger zones. D) mMg/Ca ratio across CL zones. Note that both Sr content and mMg/Ca ratio decline from Zone 1 to Zone 3.

The Mn trend of equant calcite in Reservoir C records slight fluctuation in Mn concentration through CL zones (Figure 4.10A). It starts with higher value at oldest Zone 1 (mean= 155 ppm), decreases to mean= 111 ppm at Zone 4, and then rises again to mean value of 138 ppm at youngest Zone 5. Most Fe values are below the detection limit in Zone 1, decreases from Zone 3 (mean= 284 ppm) to Zone 4 (mean= 113 ppm) and increases again to Zone 5 (mean= 243 ppm) just like Mn trend for the younger cement zones (Figure 4.10B). Similarly, Sr follows similar Mn and Fe trends for the last 3 zones. (Figure 4.10C). Cement Zone 1 has the highest Sr concertation (mean= 289 ppm) compared with younger cement zones. The initial and maximum mean value

of mMg/Ca is 0.9 at Zone 1 which then decreases towards youngest Zone 5 to a minimum mean value of 0.4 (Figure 4.10D). Both mMg/Ca ration and Sr follow identical trend.

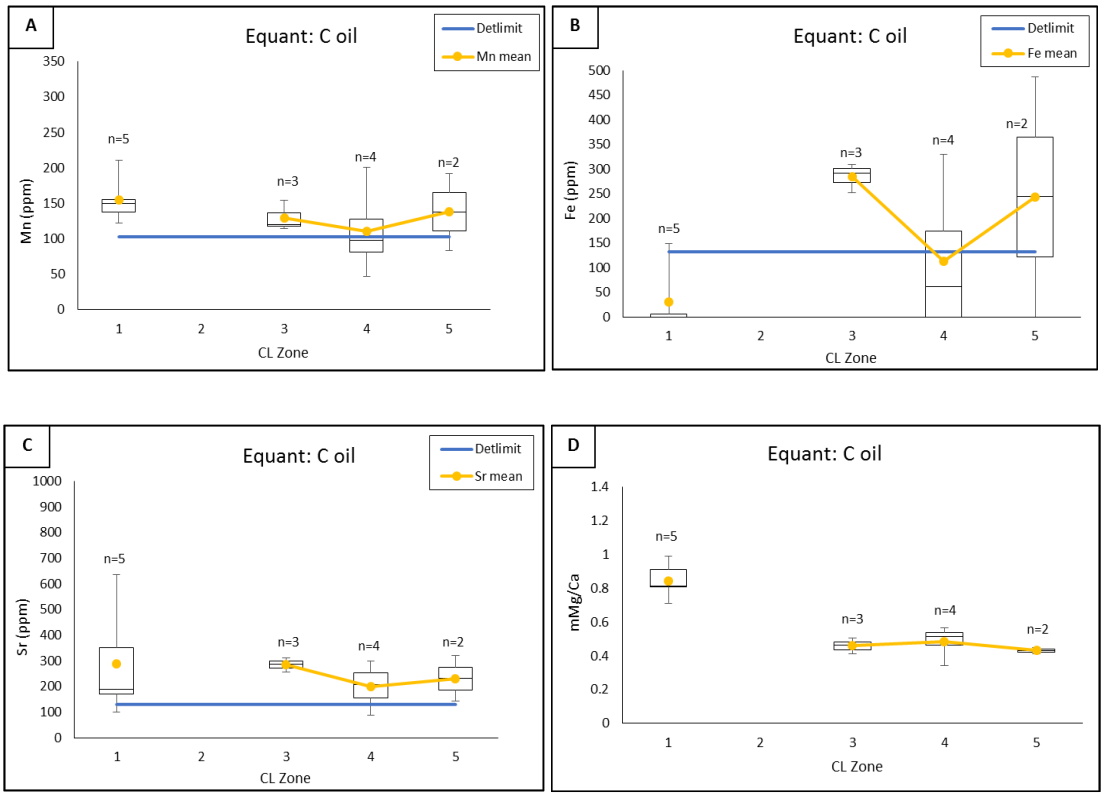


Figure 4.10: Element concentrations of equant calcite cement in Reservoir C in oil leg: A) Mn content is fluctuating through CL cement zones. Major Mn content can be found in Zones 1 and 4. B) Fe content across CL zones with detectable values in Zone 3. C) Sr content showing general decrease towards younger CL cement Zones. Zone 1 has the highest Sr values. D) mMg/Ca ratio illustrating a general decline towards younger cement zones.

In Reservoir B, the most Mn values are below the detection limit and the highest Mn concentration can be found in youngest Zone 5 (mean= 113 ppm; Figure 4.11A). Figure 4.11B indicates that all Fe values are below the detection limit (non-ferroan) and maximum mean value also in youngest Zone 5 (mean= 33 ppm). Overall, the Sr

concentration generally decreases from oldest cement Zone 1 (mean= 211 ppm) to youngest cement Zone 5 (mean= 62 ppm; Figure 4.11C). Similar to Sr, mMg/Ca declines from oldest cement Zone 1 (mean= 0.4) towards youngest Zone 5 (mean= 0.1; Figure 4.11D).

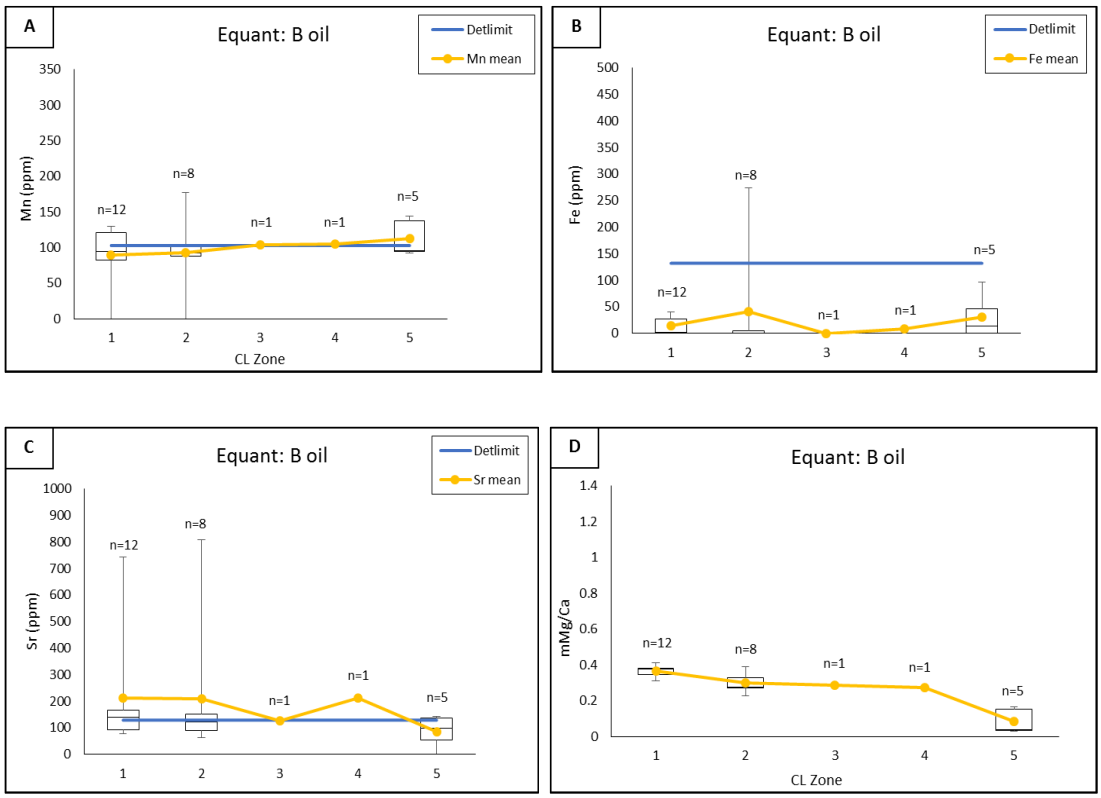


Figure 4.11: Element concentrations of equant calcite cement in Reservoir B in oil leg: A) Mn content with low values generally in all cement zones. B) Fe content across CL zones with detectable values only in CL Zone 5. C) Sr content with fluctuating trend across the zones. Higher Sr content can be found in Zones 1, 3 and 5. D) mMg/Ca ratio with general decline towards younger cement zones. Note that the lowest mMg/Ca ratio was recorded in Zone 2.

Overall, Mn concentration in equant calcite decreases towards upper Reservoirs C and B. No data for equant calcite were recorded in Reservoir A. The Fe content in this cement is similar to syntaxial calcite. Fe concentration is low in all reservoirs

except for Reservoir F and few cement zones in Reservoirs G and C. Like syntaxial cement, Sr content and mMg/Ca molar ratio decrease upwards through younger reservoirs and towards younger cement zones.

#### 4.3.1.3 Blocky Calcite

The Mn concentration in Reservoir G is low in the first three zones which then increases towards the younger zones (Figure 4.12A). The highest Mn mean value can be found at Zone 4 (181 ppm). Most Fe values are close to the detection limit except for Zone 1 where the highest Fe concentration (ferroan) was reported similar to equant and syntaxial calcite (1260 ppm; Figure 4.12B). The Sr is the highest at Zone 1 (869 ppm), close to the detection limit at Zones 2 and 3 (~150 ppm), reaches 280 ppm (mean) by Zone 4 and drops to 188 ppm (mean) by Zone 5 (Figure 4.12C). Both Mn and Sr are identical for the last three zones. A general increase in mMg/Ca ratio is noted; starting from initial mean value of 0.5 at oldest Zone 1 to final mean value of 0.8 at younger Zone 5 (Figure 4.12D). mMg/Ca reaches its highest at Zone 4 with a mean value of ~1.0.

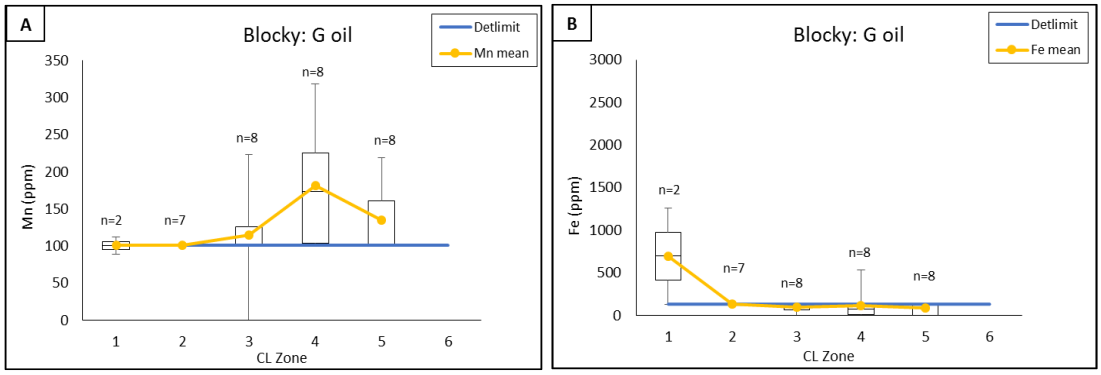

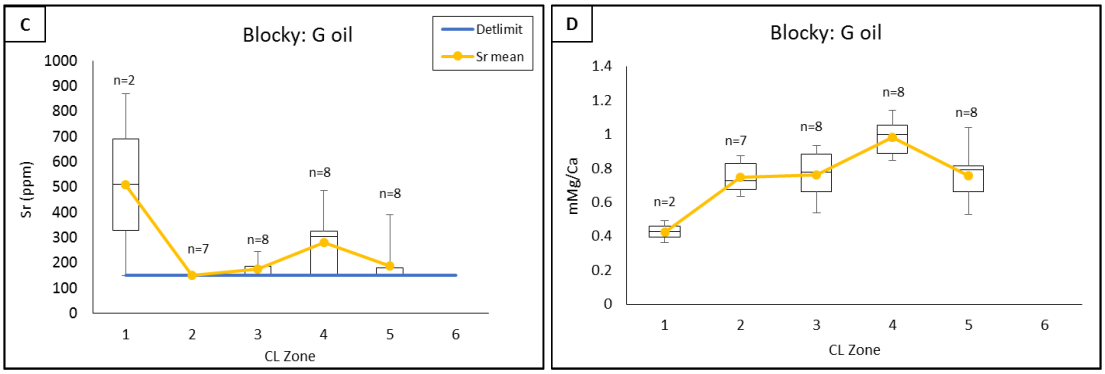


Figure 4.12: Element concentrations of blocky calcite cement in Reservoir G in oil leg: A) Mn content increases toward youngest CL zone. B) Fe content across CL zones. Note the higher concentration is only in Zones 1. C) Sr content across CL zones. Note the highest Sr value in Zone 1 and the increasing Sr content toward younger Zone 4. D) mMg/Ca ratio with general increasing trend towards younger cement zones.

Almost all Mn, Fe and Sr values are above detection limit in Reservoir F. Mn concentration trend illustrates gradual increase from Zone 1 (mean=210 ppm) to Zone 2 (mean=290 ppm) followed by a decrease from Zone 3 to youngest Zones (4 mean=192 ppm & 5 mean=182 ppm; Figure 4.13A). The Fe content trend is reverse to Mn and Sr trends (Figure 4.13B). Fe concentration decreases from Zone 1 (mean=2995 ppm; ferroan) to Zone 2 (mean=1658 ppm; ferroan) then increases sharply towards Zone 5 (mean=4690 ppm; ferroan) and drops dramatically by Zone 6 (mean=598 ppm). The general trend of Sr concentration is parallel to Mn and opposite of Fe (Figure 4.13C). mMg/Ca ration is higher and relatively constant in the older zones (mean=~1.1) and decreases towards younger zones (Zone 6 mean= 0.6; Figure 4.13D).

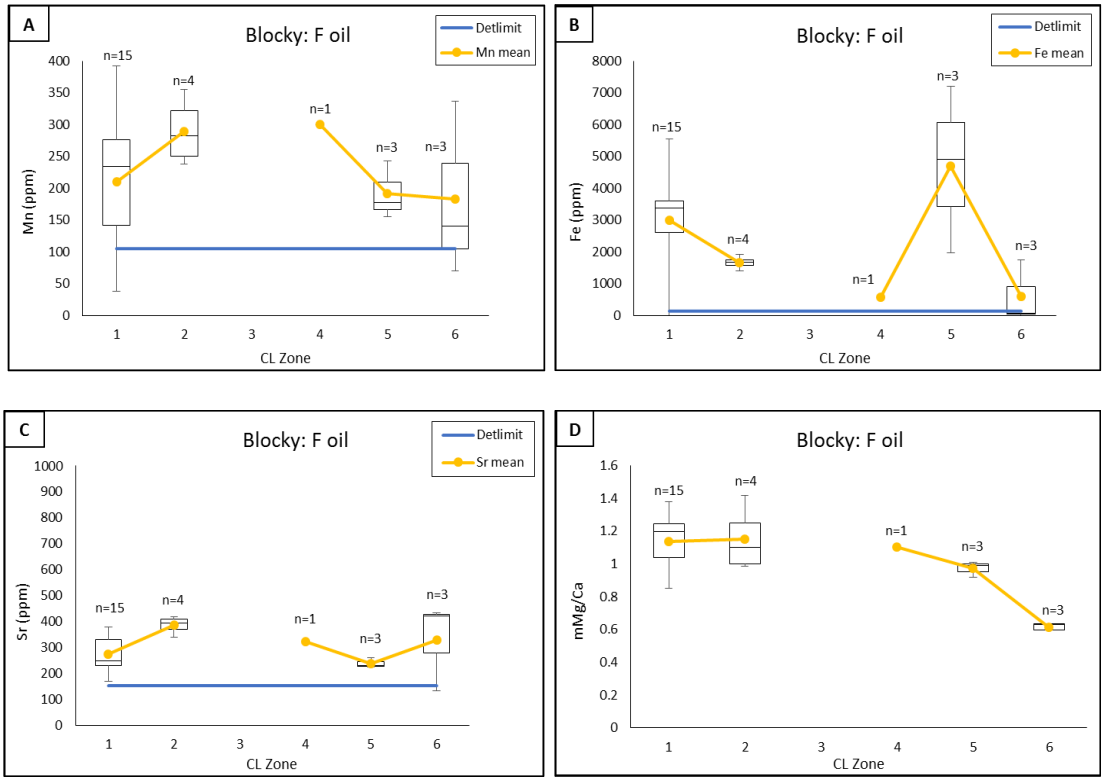


Figure 4.13: Element concentrations of blocky calcite cement in Reservoir F in oil leg: A) Mn content across two CL zones showing increase from Zone 1 to Zone 3 then decrease to Zones 4 and 5. B) Fe content across five CL Zones illustrating a decrease in Fe content from Zone 1 to Zone 3 and then increase to Zones 4 and 5. C) Sr content across CL zones with decreasing trend towards younger zones. D) mMg/Ca ratio across CL zones with slightly increasing value towards younger zones.

Most Mn and Sr values are above detection limit in Reservoir C (Figure 4.14A & C). The Mn content is relatively constant across the cement zones (mean range: 139-166 ppm) with a general decreasing trend towards younger zones. For Fe content, some values are below the detection limit however, a general trend can still be captured. Fe concentration is declining sharply from Zone 1 (mean=588 ppm; ferroan) to youngest Zone 4 (mean=42 ppm; Figure 4.14B). Just like Fe, Sr concentration decreases towards younger zones (Zone 1 mean=714 ppm, Zone 4 mean=179 ppm; Figure 4.14C). Like blocky calcite in Reservoir G, a clear increasing trend of mMg/Ca is shown in Figure

4.14D; starting form mean value of 0.4 at oldest Zone 1 which increases to 0.9 at Zone 3 and decline to 0.6 by Zone 4.

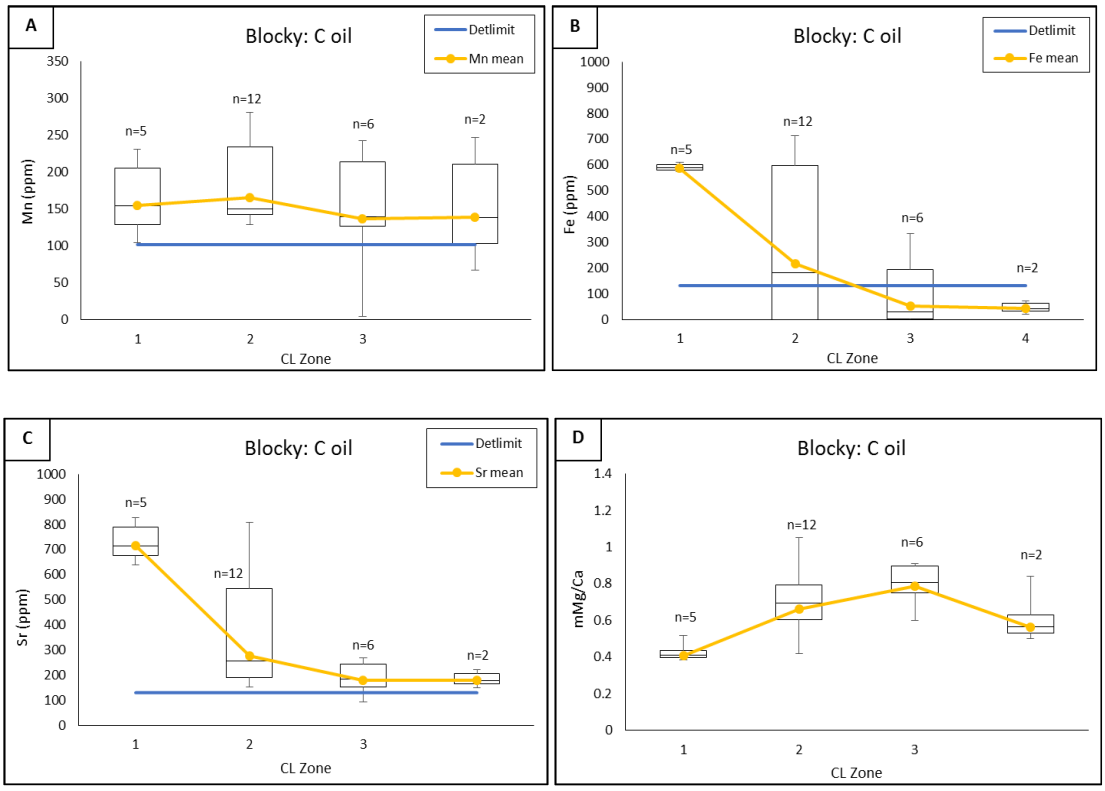


Figure 4.14: Element concentrations of blocky calcite cement in Reservoir C in oil leg: A) Mn content with increasing concentration towards younger cement zones. B) Fe content across CL zones with decreasing content towards younger cement zones. C) Sr content showing general decreases towards younger CL cement zones. Zone 1 has the highest Sr values. D) mMg/Ca ratio illustrating a general increase towards younger cement zones.

Most Mn values are below the detection limit in Reservoir B, but a clear increasing Mn content can be observed towards younger zones (Figure 4.15A). No Fe content (non-ferroan) was recorded above the detection limit in this cement (Figure 4.15B). Similarly, Sr shows an enrichment in its content towards younger zones (Figure 4.15C). The mMg/Ca ratio declines from oldest Zone 1 (mean=0.8) to youngest Zone 3. (mean=0.3; Figure 4.15D).

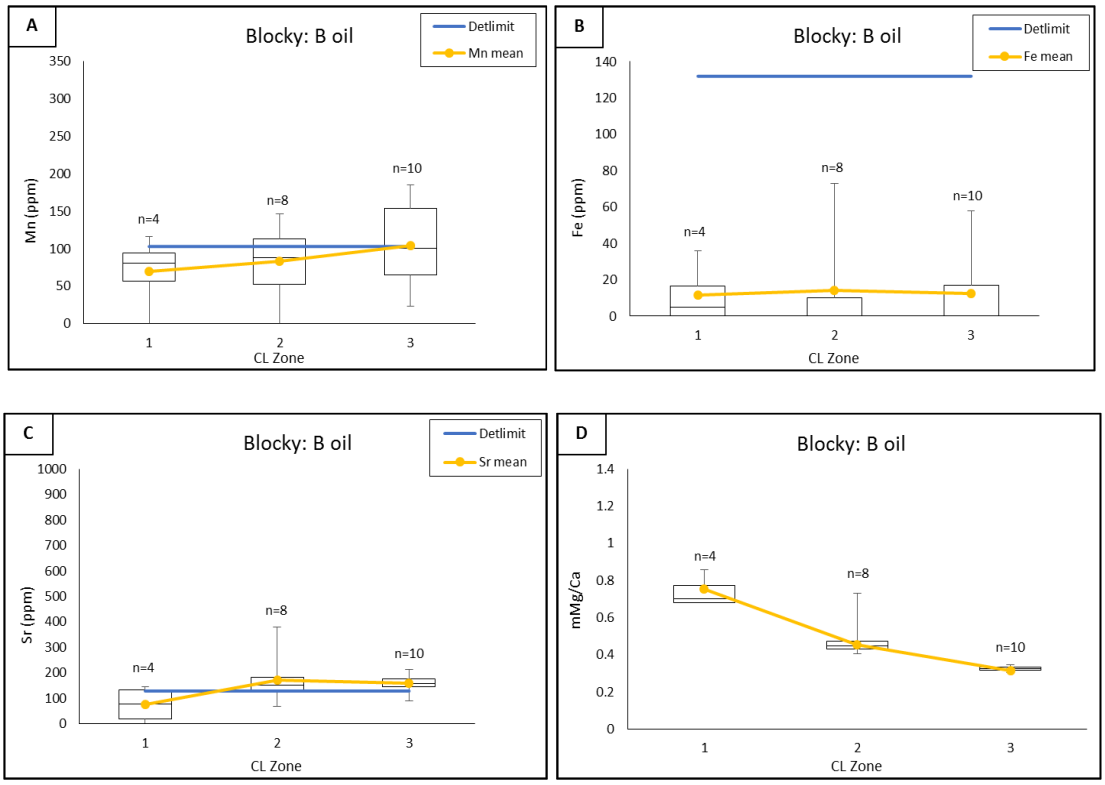


Figure 4.15: Element concentrations of blocky calcite cement in Reservoir B in oil leg: A) Mn content with increasing trend but generally low values in all cement zones. B) Fe content across CL zones with no detectable values in a single zone. C) Sr content with higher content in younger CL zones. D) mMg/Ca ratio with general decline towards younger cement zones. Note that the lowest mMg/Ca ratio was recorded in Zone 3.

In Reservoir A, most Mn values are above the detection limit (Figure 4.16A). The general Mn trend shows an overall increase in Mn concentration towards younger zones to record the highest Mn concentration in Zone 3 (mean=174 ppm). Most Fe values are below the detection limit increasing towards younger cement zones to reach its maximum by Zone 3 (mean=294 ppm; Figure 4.16B). Sr in this reservoir is higher than older Reservoir B. The Sr content starts with mean=281 ppm at Zone 1, declines slightly to mean=159 ppm by Zone 2 and rises again to mean=287 ppm by youngest Zone 3 (Figure 4.16C). Figure 4.16D illustrates a clear increasing mMg/Ca trend

towards younger zone. The mMg/Ca trend starts with mean value of 0.5 at Zone 1 and end up with mean value of ~1.0 at Zone 3.

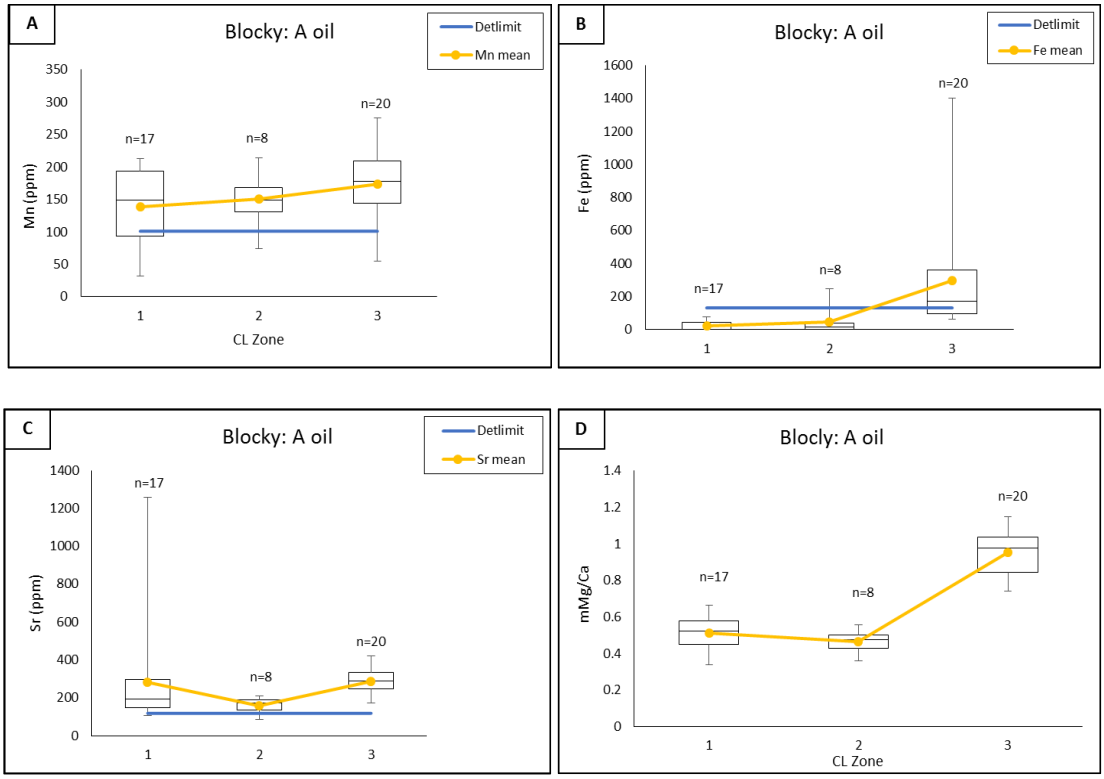


Figure 4.16: Element concentrations of blocky calcite cement in Reservoir A in oil leg: A) Mn content showing general increase towards younger cement zones. B) Fe content across CL zones. Fe values in all zones are below the detection limit except Zone 4. C) Sr content across CL zones. Sr content is decreasing towards younger zones. D) mMg/Ca ratio with general increase towards younger cement zones.

In summary, comparing Mn content in blocky calcite in Reservoir G with syntaxial and equant cements, it can be noted that Mn concentration is lower in blocky calcite especially for the first three CL cement zones. In contrast, the Mn concentration increases in the blocky calcite of Reservoir F to be higher than syntaxial and equant cements of the same reservoir. Overall, similar to syntaxial cement, Mn content decreases towards Reservoirs C and B and increases again in Reservoir A. Iron becomes more significant in blocky cement of Reservoirs F, C and A. The highest Fe

concentration was recorded in Reservoir F. With various concentrations, iron can be found above the detection limit in blocky calcite in all reservoirs except B. The Sr concentration has relatively similar range through reservoirs except for B which has lower Sr concentration. Unlike the syntaxial and equant cements, mMg/Ca molar ration of blocky cement in all reservoirs except F and B, shows increase towards younger cement zones.

### 4.3.2 Water Leg

#### 4.3.2.1 Syntaxial Calcite

Looking closely at Reservoir F, the Mn concentration is above the detection limit in all cement zones. The Mn content is lower in oldest Zone 1 (mean=141 ppm) and then gets higher by Zone 3 (mean=199 ppm) which followed by gentle increase towards younger cement zones (Figure 4.17A). Almost all Fe values are above the detection limit (Figure 4.17B). Fe content increases from Zone 1 (mean=671 ppm) to Zone 5 (mean=2765 ppm), then decreases sharply at youngest Zone 6 (mean=616 ppm). Cement Zone 5 records high and dramatic change in Fe content; from mean=1173 ppm at Zone 4 to mean=2765 ppm at Zone 5 (ferroan). Sr trend is quite similar to Fe trend especially for Zone 5 where both elements show higher values (Figure 4.17C). The mMg/Ca is decreasing from Zone 1 (mean=~1.0) to Zone 5 (mean=0.5) and then increasing by last Zone 6 (mean=0.7; Figure 4.17D).

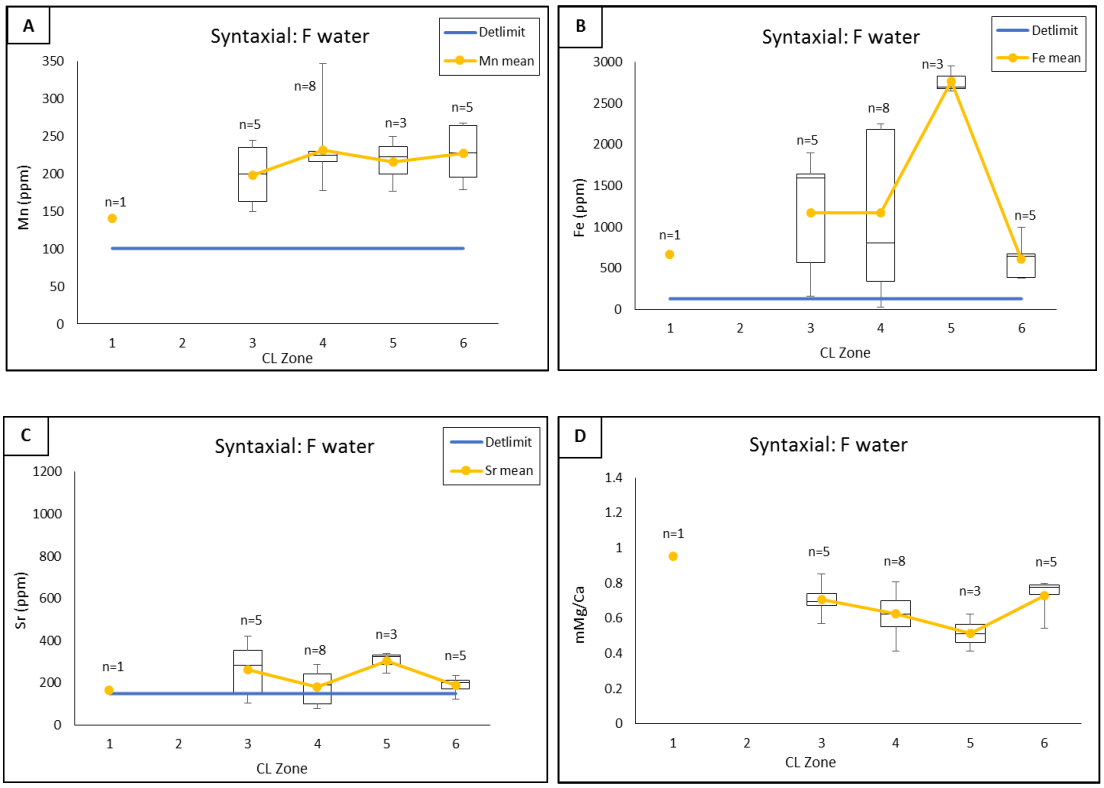


Figure 4.17: Element concentrations of syntaxial calcite cement in Reservoir F in water leg: A) Mn content across six CL zones indicating higher concentration in Zones 4 & 5. B) Fe content across CL zones illustrating an increase in Fe content at Zones 2, 3 & 5. C) Sr content across CL zones with highest concentration in Zone 5. D) mMg/Ca ratio across CL zones. Note all values are within the same range.

In Reservoir C, Mn starts with values under the detection limit at Zone 1 (mean=15 ppm; Figure 4.18A). A higher Mn content is recorded in Zone 3 (mean=168 ppm) declines gradually towards younger zones (Zone 6 mean=110 ppm). Fe mean values are all under detection limit except for Zone 5 (mean=723 ppm (ferroan); Figure 4.18B). The highest Sr concentration was recorded in Zone 1 (mean=551 ppm) which then declines towards younger zones to reach the lowest concentration by Zone 6 (mean=123 ppm; Figure 4.18C). Like oil leg, mMg/Ca ration decreases across younger zones (Figure 4.18D). mMg/Ca ratio starts with high mean value of 1.2 at Zone 1 and decreases to reach a lower mean value of 0.6 at youngest Zone 6.

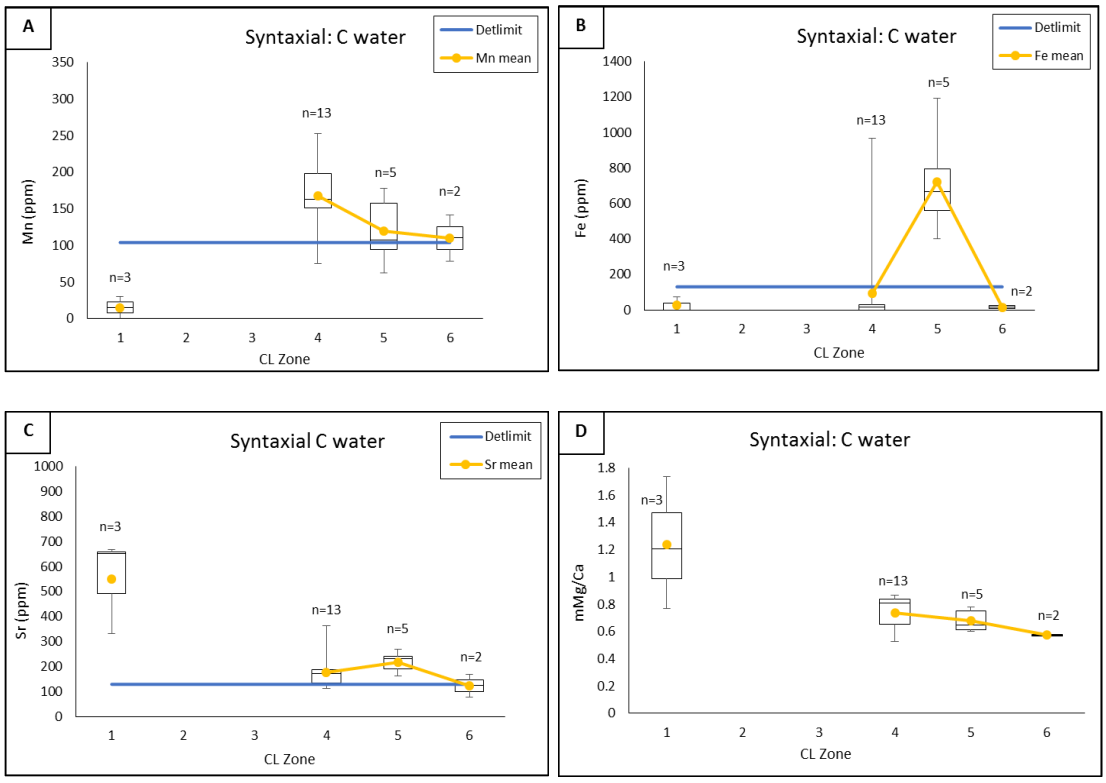


Figure 4.18: Element concentrations of syntaxial calcite cement in Reservoir C in water leg: A) Mn content is fluctuating through CL cement zones. Major Mn content can be found in Zones 4 and 5. B) Fe content across CL zones with highest concentration in Zone 5. C) Sr content showing general decline towards younger CL cement zones. Zone 1 has the highest Sr values. D) mMg/Ca ratio illustrating a general decline towards younger cement zones. Note that Sr, Mn, Fe and mMg/Ca ratio have low values in Zone 6.

Reservoir B has some Mn values above the detection limit (Figure 4.19A). Mn has higher concentration in Zones 1 (mean=137 ppm) and 4 (mean=136 ppm) compared with Zones 2 (mean=81 ppm) and 3 (mean=102 ppm). All values of Fe are under detection limit (non-ferroan) except for one value in Zone 3 (Figure 4.19B). Sr concentration increases slightly from Zone 1 (mean=178 ppm) to Zone 3 (mean=207 ppm) and then decreases by Zone 4 (mean=123 ppm; Figure 4.19C). A smooth decrease in mMg/Ca ratio through CL zones is illustrated in Figure 4.19D. The mean value of mMg/Ca goes from 0.9 at oldest Zone 1 to 0.4 at youngest Zone 4. The

youngest Zone 4 in this reservoir shows lower mMg/Ca, Fe and Sr but higher Mn content relative to the adjacent zones.

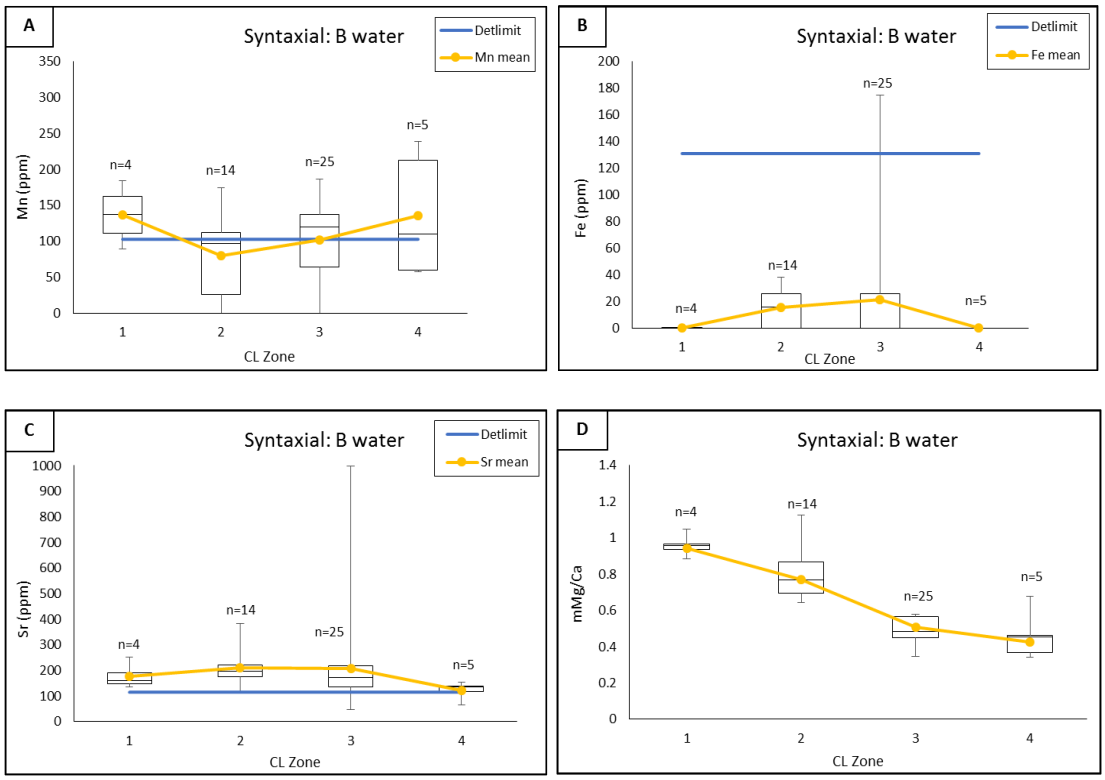


Figure 4.19: Element concentrations of syntaxial calcite cement in Reservoir B in water leg: A) Mn content in general is low and increases towards younger cement zones. B) Fe content across CL zones. Almost all Fe values in all zones are below the detection limit. C) Sr content across CL zones with decreasing trend towards younger zones. D) mMg/Ca ratio with general decline towards younger cement zones. Note that the lowest mMg/Ca ratio was recorded in last youngest zone.

Overall, Mn concentration in the deeper Reservoir F is higher and decreases towards the shallower Reservoirs C and B. Fe concentration decreases stratigraphically through upper reservoirs with the highest concentration in Reservoir F which decreases to Reservoir C and becomes very low at Reservoir B. Sr content is almost the same in all reservoirs. mMg/Ca molar ration varies through different stratigraphic units with lowest values recorded in Reservoir B. The mMg/Ca molar ratio shows a general

decreasing towards younger cement zones except for a slight increase in the last cement zone in Reservoir F.

### 4.3.2.2 Equant Calcite

Generally, the Mn content in Reservoir F shows gradual increase from Zone 1 to Zone 4 with a final drop at Zone 6 (Figure 4.20A). Most Fe values are at and above the detection limit (Figure 4.20B). Fe content is low in zones 1 (mean=259 ppm) and 6 (102 ppm) and higher in Zones 3 (mean=1867 ppm; ferroan) and 4 (mean=2026 ppm; ferroan). Generally, Sr content decreases towards younger zones; starts with mean=281 ppm at Zone 1 and ends up with 169 ppm at Zone 6 (Figure 4.20C). According to Figure 4.20D, the mMg/Ca ratio starts with very high mean value of 1.4 at Zone 1 which decreases through younger zones to reach minimum value of 0.4 by the last Zone 6. Youngest cement Zone 6 has low mMg/Ca, Mn, Fe, and Sr.

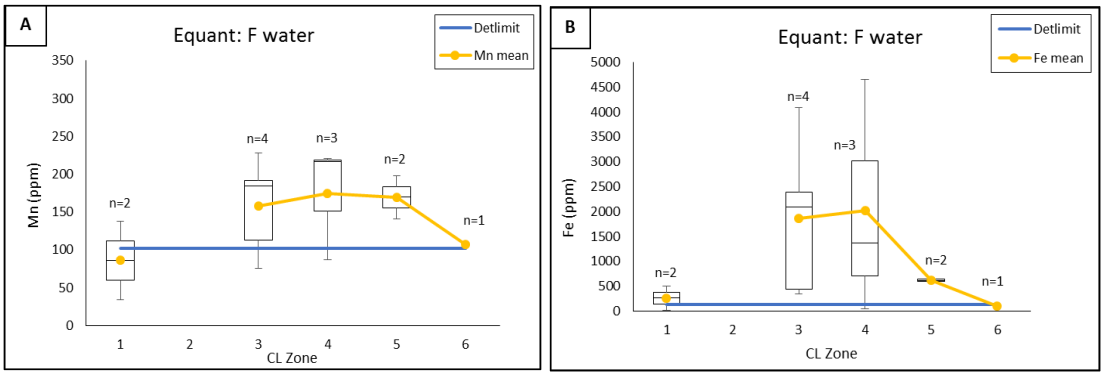

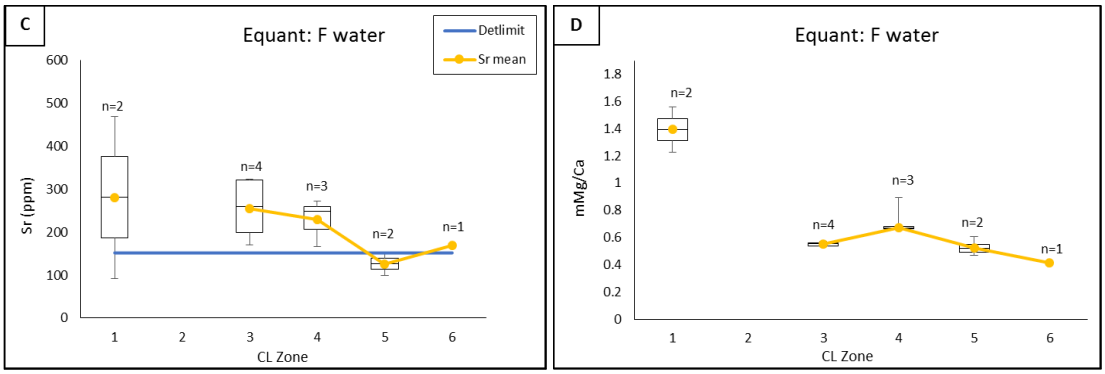


Figure 4.20: Element concentrations of equant calcite cement in Reservoir F in water leg: A) Mn content across CL zones showing increase from Zone 1 to Zone 4 and a drop at Zone 6. B) Fe content across three CL zones illustrating an increase in Fe content from Zone 1 to Zone 3 and then decrease to Zones 4 & 6. C) Sr content across CL zones. D) mMg/Ca ratio across CL zones. Note that both Sr content and mMg/Ca ratio decline as the cements get younger to reach their lowest values at youngest zone.

In Reservoir B, the Mn content decreases towards younger zones to reach minimum mean value of 78 ppm by youngest Zone 3 (Figure 4.21A). Similar to the Fe values found in equant calcite in the oil leg, Fe values are all below the detection (non-ferroan) limit except for one value in Zone 2 (Figure 4.21B). The Sr concentration is opposite to the Fe concentration; increases from Zone 1 (144 ppm) to Zone 2 (mean=416 ppm) and then decreases by Zone 3 (mean=151 ppm; Figure 4.21C). The mMg/Ca starts with 0.6 at Zone 1 and decreased to mean values of 0.4 at Zone 3 (Figure 4.21D).

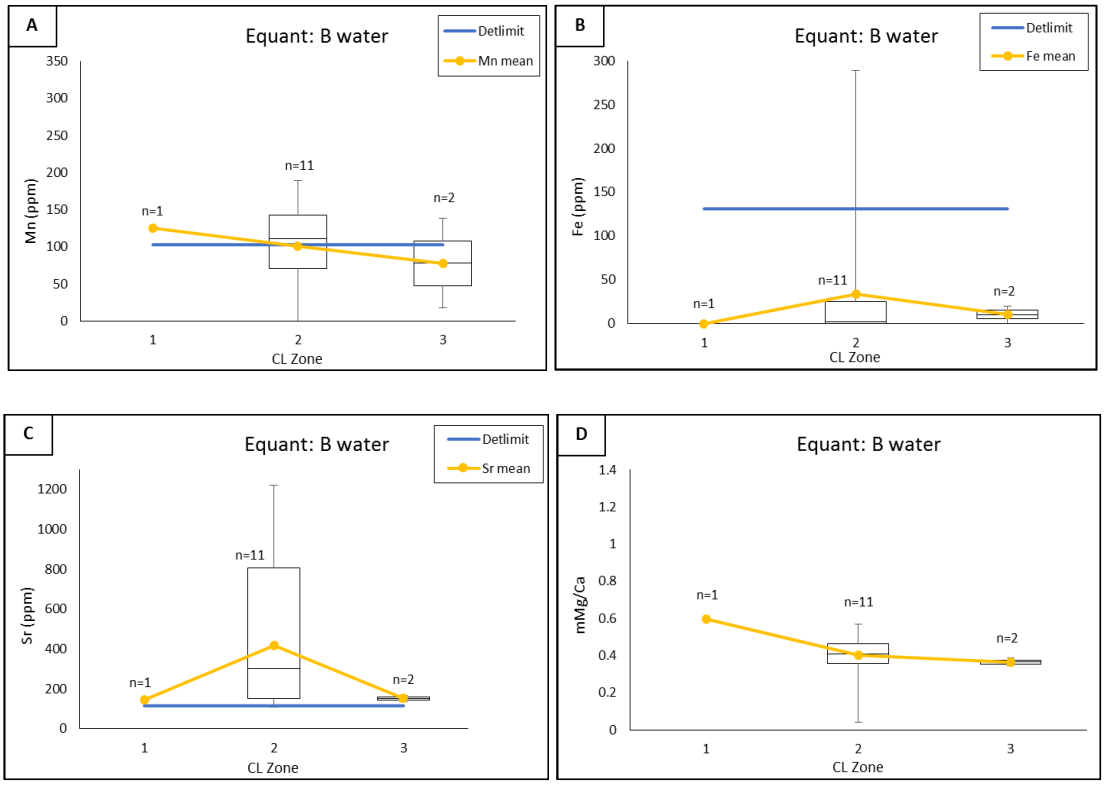


Figure 4.21: Element concentrations of equant calcite cement in Reservoir B in water leg: A) Mn content with low values generally in all cement zones. B) Fe content across CL zones with few detectable values only in CL Zone 3. C) Sr content with decreasing trend across younger oznes. D) mMg/Ca ratio with values below 1 and all are within same range. Note that the lowest mMg/Ca ratio and Fe content can be found in oldest zone whereas the highest Mn and Sr concentrations can be found in the same zone.

In summary, Mn concentration in equant calcite decreases towards upper reservoirs. Similar to syntaxial calcite, the Fe content is higher in lower reservoir Reservoir F than upper Reservoir B. The Sr content is higher in Reservoir B. mMg/Ca molar ratio is higher in Reservoir F than B. Sr content and mMg/Ca molar ratio decrease moving away from cement centre.

### 3.3.2.3 Blocky Calcite

Most Mn values are above the detection limit in Reservoir F (Figure 4.22A). The overall trend of Mn concentration is increasing towards youngest zone; lowest mean value at oldest cement Zone 1 (117 ppm) and highest at youngest Zone 5 (210 ppm). The Fe concentration shows very low mean value at Zone 1 (58 ppm) which increases significantly by Zone 2 (2313 ppm; ferroan) and then declines towards younger cement zones (Zone 5 mean=740 ppm; Figure 4.22B). Sr concentration decreases from Zone 1 (mean= 727 ppm) to Zone 3 (mean= 203 ppm) which is the lowest recorded Sr mean value. Then, it gradually increases to younger cement Zones 4 (mean= 415 ppm) and 5 (mean= 471 ppm; Figure 4.22C). The mMg/Ca ratio of blocky calcite in water leg is relatively similar to oil leg (Figure 4.22D). Blocky calcite in water leg displays decline in mMg/Ca toward younger cement zones; from mean value of 1.2 at Zone 1 to 0.6 at Zone 5.

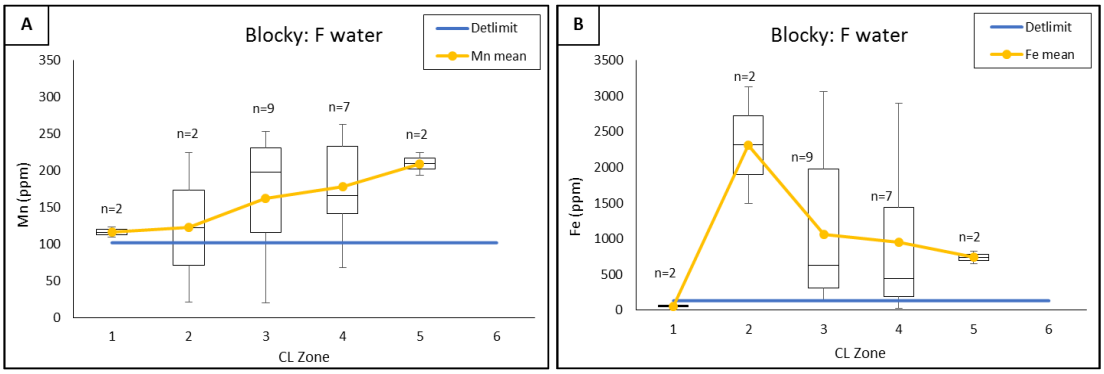

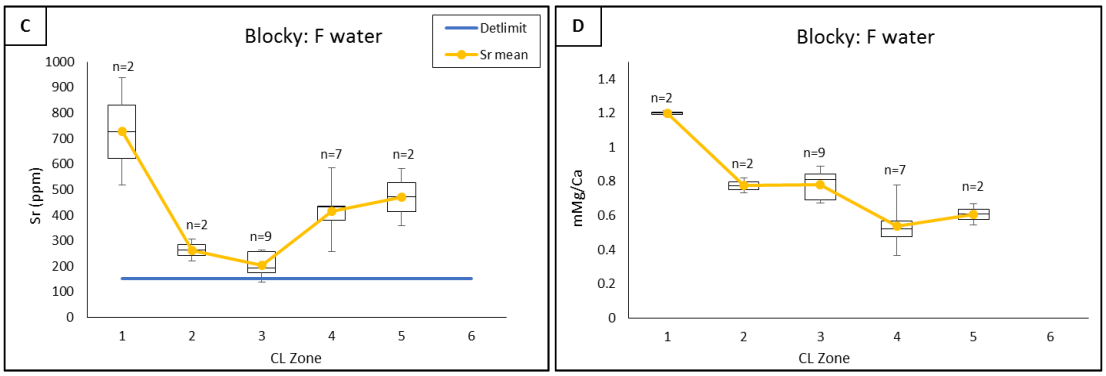


Figure 4.22: Element concentrations of blocky calcite cement in Reservoir F in water leg: A) Mn content across six CL zones showing general increase moving towards younger Zones. B) Fe content across five CL zones illustrating zero Fe content in the first two Zones which increases to be detectable values at younger Zones. C) Sr content across CL zones with decreasing trend towards younger Zones. D) mMg/Ca ratio across CL Zones with decreasing trend also towards younger Zones.

Based on the three analysed CL zones of blocky calcite in Reservoir C, Mn and Fe contents are as following. Mn content decreases first from Zone 2 (mean= 148 ppm) to Zone 3 (mean= 105 ppm) and then increases towards Zone 4 (mean= 146 ppm). Fe content starts with high mean value of 485 ppm which decreases towards younger Zone 4 (mean= 28 ppm; Figures 4.23A & B). The Sr is also declining from older cement Zone 2 (mean= 270 ppm) to younger cement Zone 4 (mean= 238 ppm; Figure 4.23C). The mMg/Ca molar ratio is decreasing from older Zone 2 (mean= 0.7) to younger Zone 4 (mean= 0.6; Figure 4.23D). The difference in both Sr and mMg/Ca ratio is very small between individual zone.

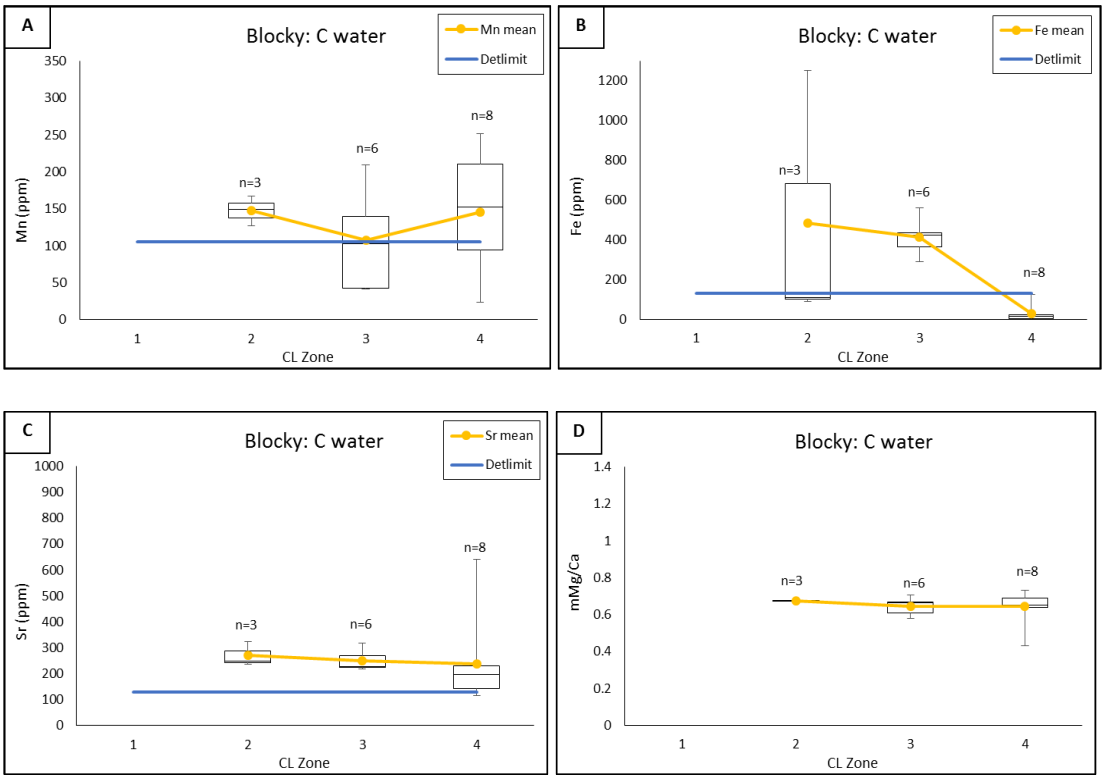


Figure 4.23: Element concentrations of blocky calcite cement in Reservoir C in water leg: A) Mn content with increasing concentration towards younger cement Zone. B) Fe content across CL zones with decreasing content towards younger cement zone. C) Sr content showing general decrease towards younger CL cement zone. Zone 1 has the highest Sr values. D) mMg/Ca ratio illustrating a slight increase towards younger cement zone.

Overall, Mn and Fe contents in blocky calcite in Reservoir F are higher than C. There is no big difference in Sr content in both reservoirs. mMg/Ca molar ratio of blocky calcite is higher in Reservoir F than C. In both reservoirs, mMg/Ca molar ratio decreases towards younger CL cement zones.

### 4.3.3 Results Summary

In summary, for syntaxial calcite a clear difference in Mn and Fe contents in water versus oil leg can be observed in Reservoir F (Figures 4.24 & 4.25). Both Fe and Mn contents in the water leg are higher than in the oil leg. Moving directly to the reservoir above F, which is C, there no significant difference in Mn and Fe content between syntaxial cements in the oil and water legs (Figure 4.24 & 4.25). In Reservoir B, a slight increase in Mn and Fe concentrations is noted in water leg (Figure 4.24 & 4.25). However, most Fe values are still below the detection limit in both legs. Comparing the Sr content in oil versus water leg in Reservoirs F, C and B, it can be noted that the water leg contains a higher Sr content (Figure 4.26). Generally, the general Sr trend is the same in both legs, with Sr decreaseing through the younger reservoirs.

Almost all mMg/Ca trends of all cement types show a general decline towards youngest CL cement zones (Figure 4.27). Comparing mMg/Ca ratio in the water and oil legs in Reservoirs F, C and B, the following is noted: the mMg/Ca ratio is lower in water leg of Reservoir F than oil leg, quite similar in both legs in Reservoir C, and the mMg/Ca ratio in oil leg of Reservoir B is lower than water leg.

In the equant calcite, no notable difference in Mn content in oil versus water is observed in syntaxial calcite in Reservoir F (Figures 4.24 & 4.25). However, the Fe content in the water leg is higher than in the oil leg. Similarly, no significant difference in Mn and Fe contents between oil and water leg in Reservoir B. The Sr content measured from both the oil and water legs is lower in the upper Reservoir B (Figure 4.26). Overall, a lower mMg/Ca ratio can be found in equant cement in Reservoirs F and B with clear decreasing trend towards younger cement zones (Figure 4.27).

The pattern of Mn and Fe changes in the water and oil leg in the blocky calcite is the reverse of that observed in syntaxial calcite. The blocky calcite oil in Reservoir F hosts higher Mn and Fe concentrations than the blocky water (Figures 4.24 & 4.25). Likewise in Reservoir C, Mn and Fe concentrations of blocky calcite in oil leg are

slightly higher than in water leg (Figures 4.24 & 4.25). In terms of Sr content, lower Reservoir F has slightly higher Sr than the upper Reservoir C. Generally, the Sr content in oil and water legs are quite similar (Figure 4.26). The general trend of mMg/Ca of blocky calcite in water leg is different than blocky in oil especially for Reservoir F (Figure 4.27).

The final mMg/Ca data (Figure 4.27) was combined with CL images to produce the cement stratigraphic scheme shown as “integrated” in Figure 4.28.

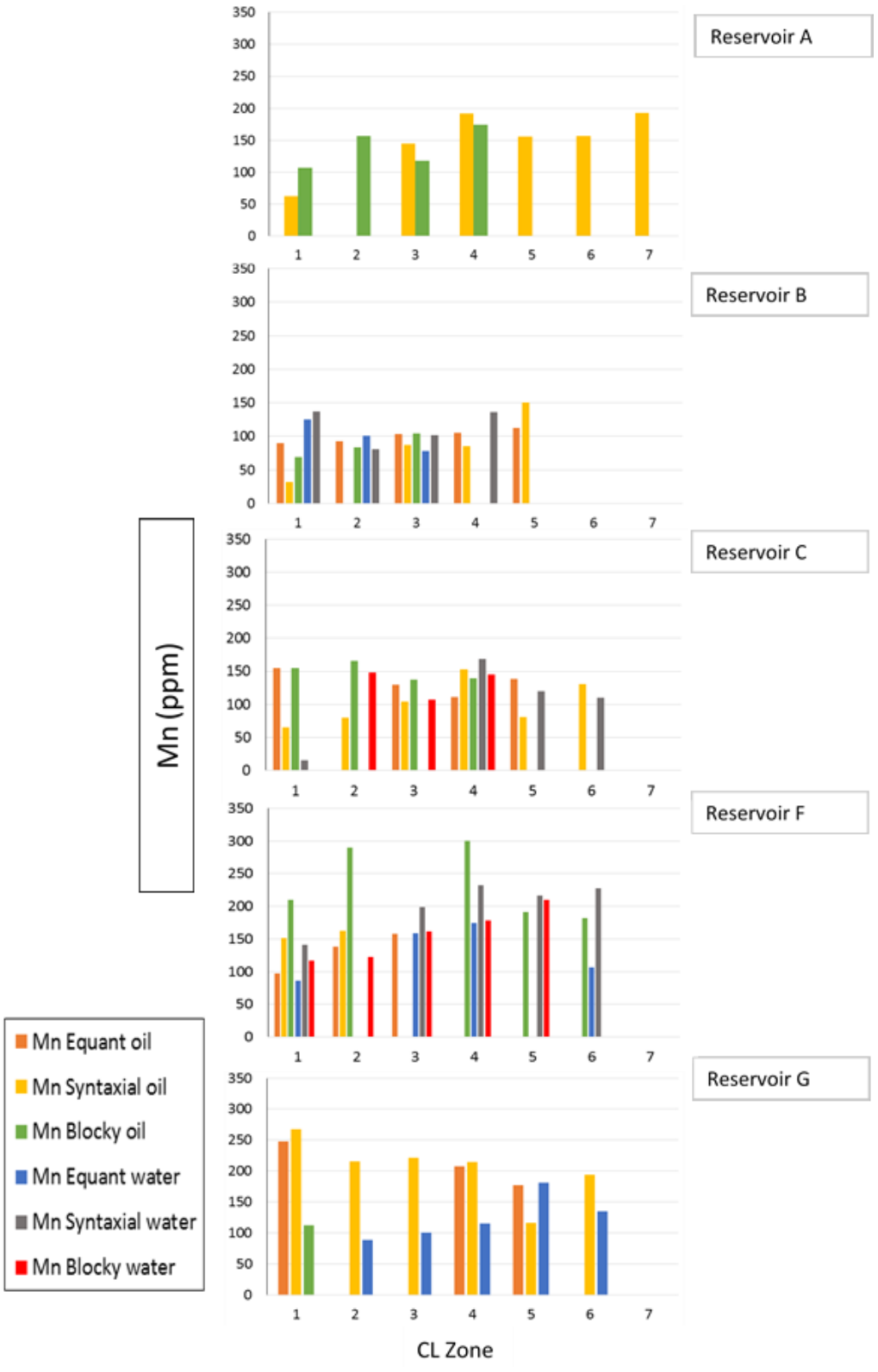


Figure 4.24: Summary of Mn means for syntaxial, equant and blocky calcite in all reservoirs: oil versus water. CL cement Zones are from 1 to 7. Note that each reservoir has been treated separately.

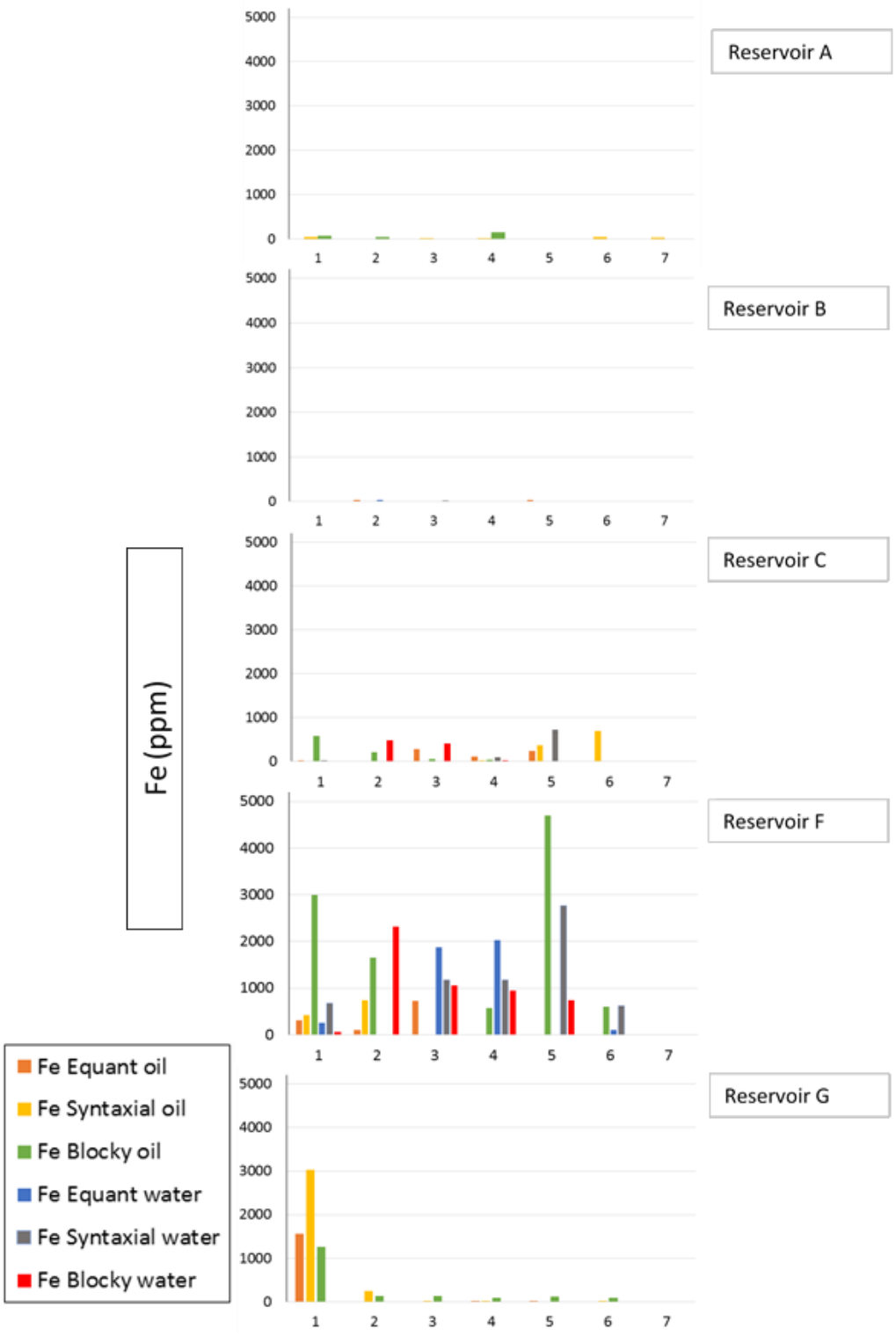


Figure 4.25: Summary of Fe means for syntaxial, equant and blocky calcite in all reservoirs: oil versus water. CL cement Zones are from 1 to 7. Note that each reservoir has been treated separately.

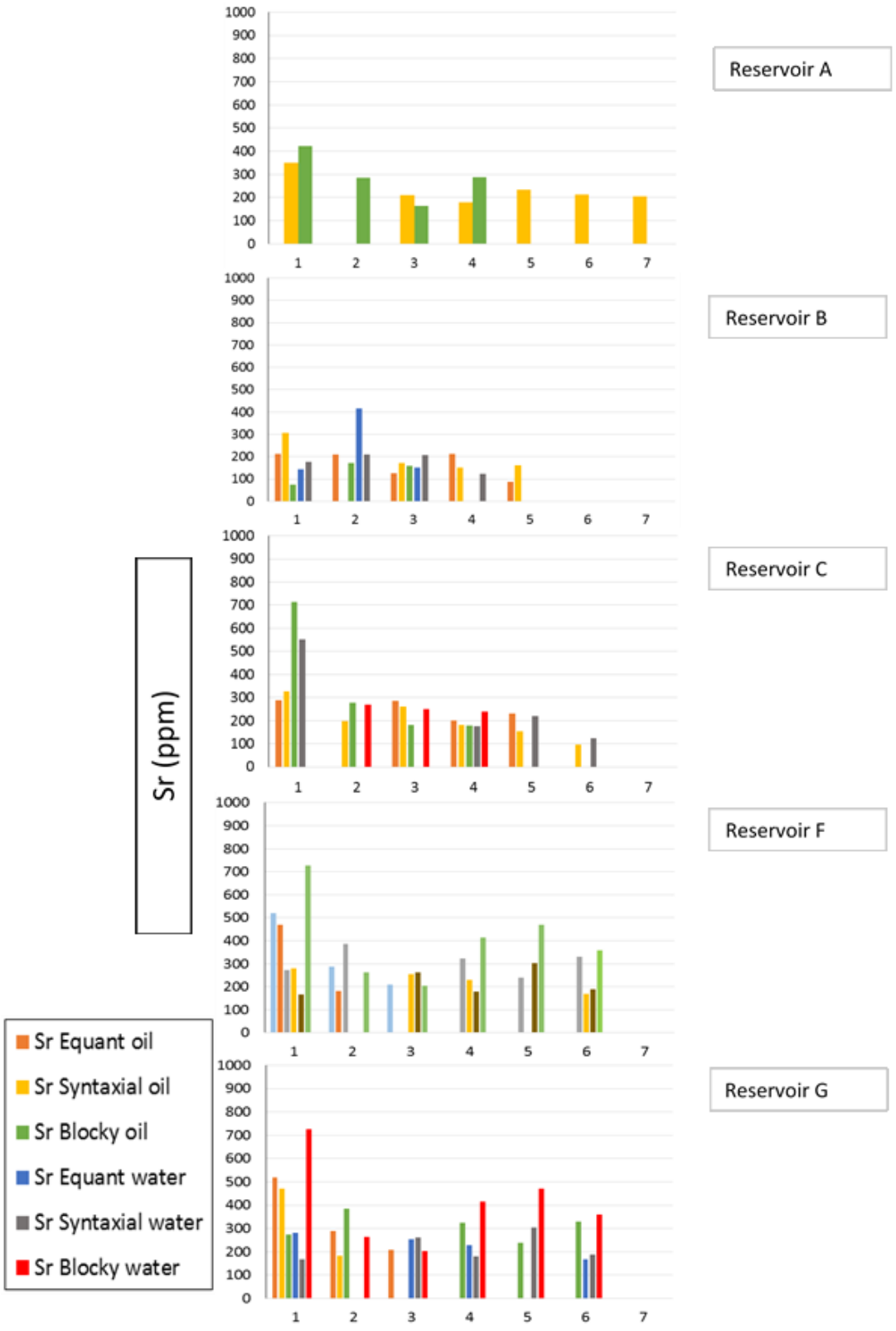


Figure 4.26: Summary of Sr means for syntaxial, equant and blocky calcite in all reservoirs: oil versus water. CL cement Zones are from 1 to 7. Note that each reservoir has been treated separately.

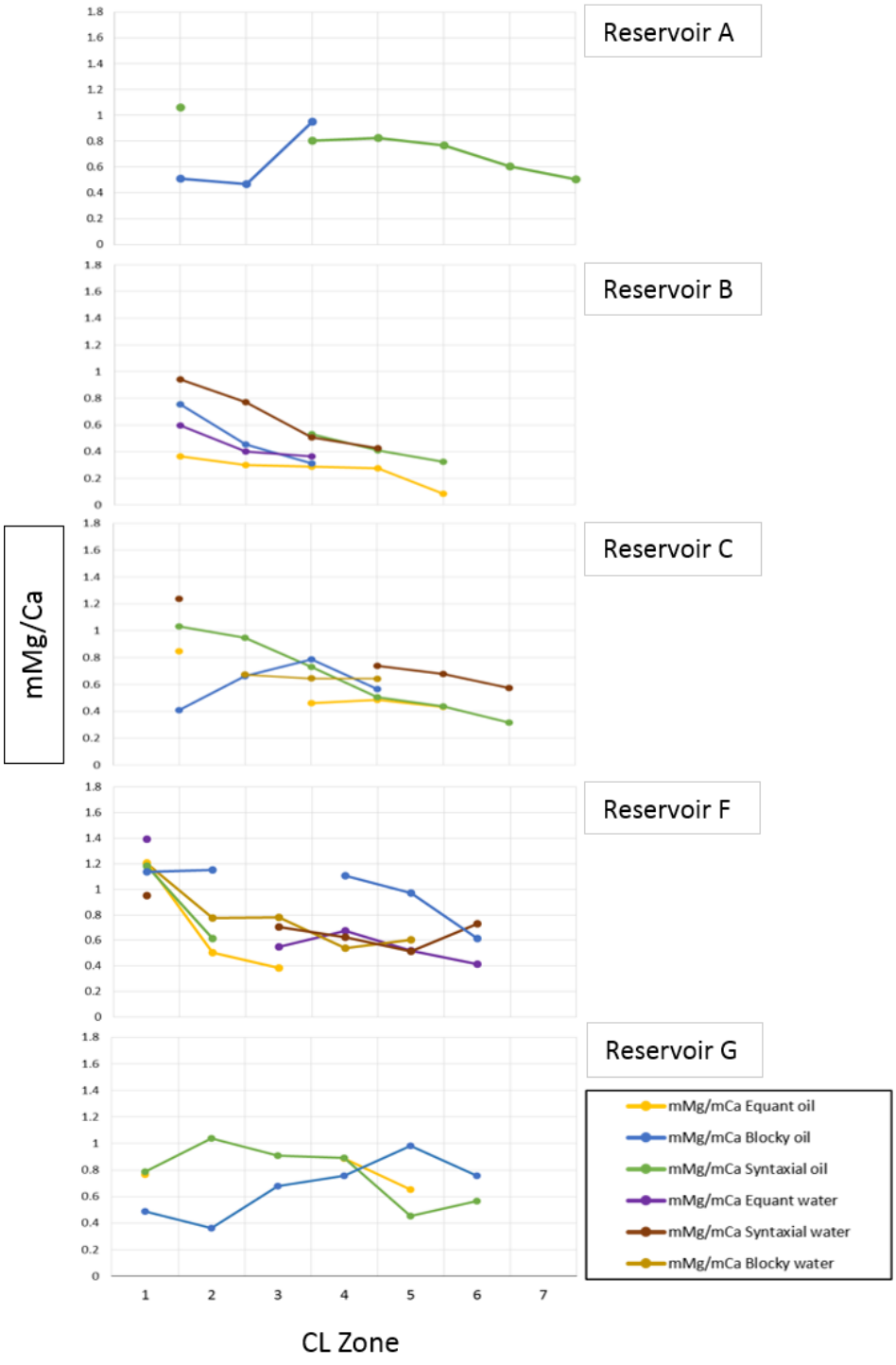


Figure 4.27: Summary of mMg/Ca molar ratio means for syntaxial, equant and blocky calcite in all reservoirs: oil versus water. CL cement Zones are from 1 to 7. Note that each reservoir has been treated separately.

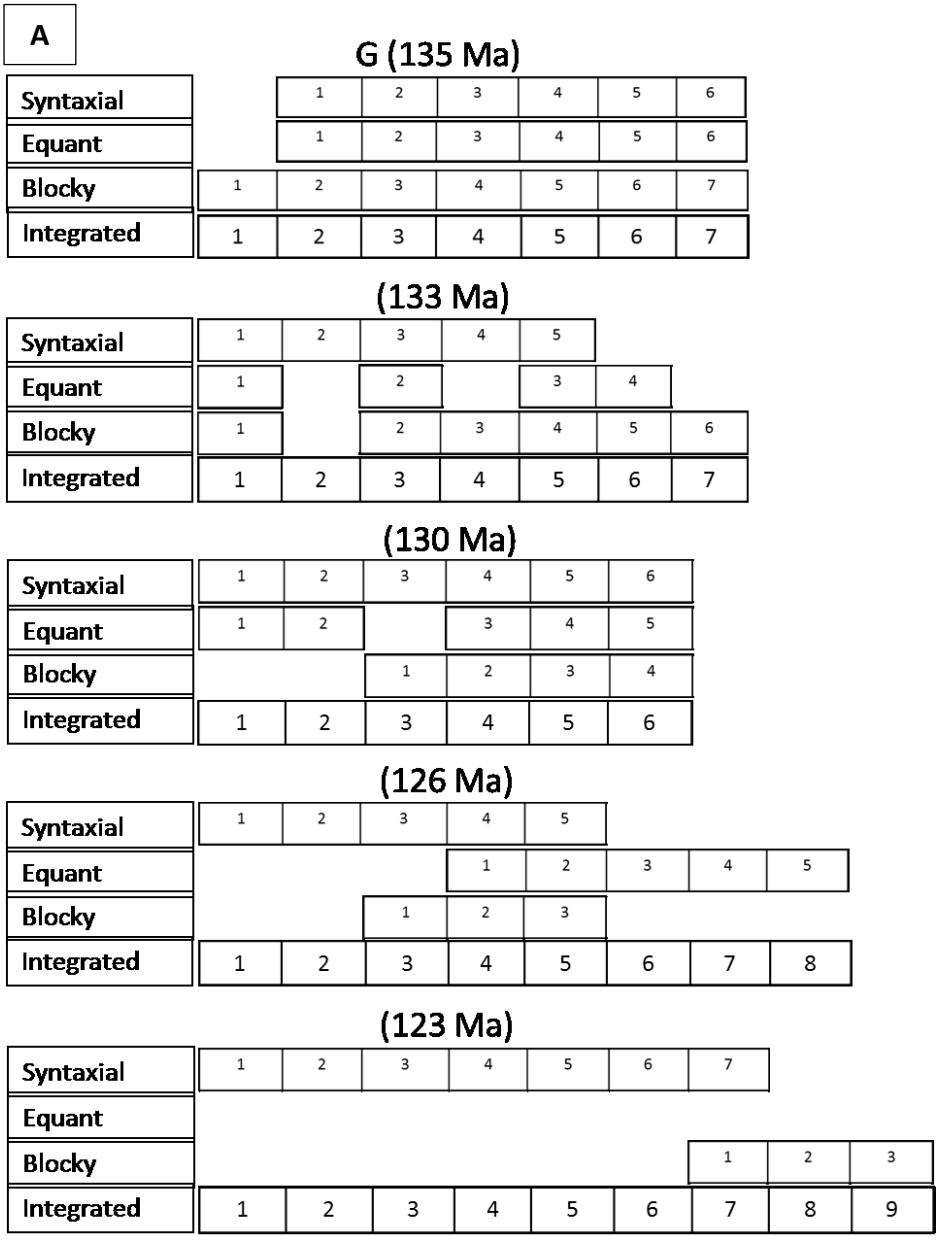
A
G (135 Ma)
Syntaxial
Equant
Blocky
Integrated
(133 Ma)
(130 Ma)
(126 Ma)
(123 Ma)

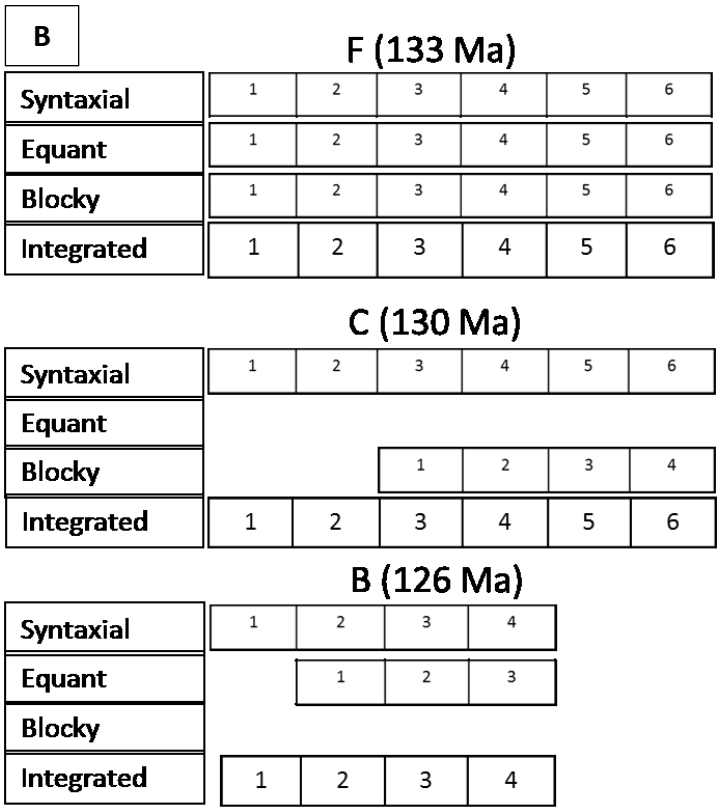


Figure 4.28: Summary of the relative cement stratigraphy integrating CL data and mMg/Ca ratio including syntaxial, equant, and blocky calcite in A) Oil leg for all Reservoirs. B) Water leg for Reservoirs F, B, and C. The final scheme is shown as "integrated".

## 4.4 Discussion

Overall, the highest and lowest mean Fe content was recorded in Reservoir F and B respectively. In parallel the highest and lowest mean Mn content was recorded in Reservoir F and B respectively. Mean Sr contents with the highest value can be found in Reservoirs G & F, while the lowest values are found in Reservoir B. For the mean mMg/Ca ratio, the highest and lowest ratios were reported in Reservoir F and B, respectively. The mean mMg/Ca ratio and all element concentrations increase moving down stratigraphically. The mMg/Ca ratio, Sr, Mn and Fe concentrations through different stratigraphic units in the oil versus water are discussed below.

### 4.4.1 Origin of Older Calcite Cement Zones in Oil and Water Legs: first zones of syntaxial and equant calcite

The older cement zones of equant and syntaxial calcite in oil and water legs of each reservoir host similar chemical composition revealing that they were precipitated more or less under the similar conditions (Figures 4.24-4.28). The higher Fe, and Mn content of syntaxial and equant cements in lower Reservoirs F & G compared with the upper Reservoirs (C, B & A) indicates that cements in the lower reservoirs were precipitated in anoxic environments rich in Fe and Mn. Elemental results of syntaxial and equant calcite of Reservoir G suggest that the type of fluid corresponding to such cements started with elevated Fe and Mn (Zone 1) which then evolved through time to become depleted in Fe in the youngest cement zones, with almost no Fe but still preserving Mn. The elevated Fe in the first ferroan zone reflects the dull zone that can be seen under CL (Figures 3.1-3.5). The early depletion of Fe in this reservoir (Figures 4.3B & 4.8B) indicates that pore fluids have been evolved earlier compared with Reservoir F. The higher Fe content in Reservoir F both in syntaxial and equant calcite makes them look more dull and distinguishable from Reservoir G calcite cements under CL. The higher Fe, Mn and Sr concentrations in the lower reservoirs may be due to the higher clay content. Clay is known to be rich in Mn, Fe and Sr. Clay content in this Field is typically distinguished by gamma ray log which can be found with higher content in Dense Zones (Figures 1.6 & 1.9). Most of the clay occurs as laminae that was deposited in deeper environment during high sea level episodes which is marked as MFS. Dense Zones are mud supported facies which are characterized by firmgrounds and interbedded organic and siliciclastic-rich limestone (Alsharhan and Kendall, 1991; Strohmenger et al., 2006). Thorpe (2014), suggested that the dewatering of the underlying Dense Zones in Thamama Reservoirs could be a possible source for iron.

The depleted Mn, Fe and Sr content in the upper reservoir cements (older cement zones of syntaxial and equant) implies that these cements were precipitated in a

shallower oxic non-luminance environment. This can be seen in upper reservoirs especially Reservoir B which contain lower Mg content compared with other reservoirs (Figure 4.11D). The rise in Mn content from Reservoir B to the most upper Reservoir A suggests that this reservoir has been supplied by Mn rich fluids, possibly silicate rich source. A possible source rock for Reservoir A is Bab Member source rocks, probably Lower Shuaiba shale which is located stratigraphically above this reservoir (Lijmbach et al. 1992). Moreover, there was a period of major exposure after Shuaiba deposit marked by second order SB which could be allowed for siliciclastic inputs (see Figure 1.5). Furthermore, Reservoir A is the upper most reservoir of Thamama formation which could be more exposed to silicate input than other reservoirs.

Water-rock interaction could be another cause for compositional variation of pore fluids in all reservoirs. Diagenetic alterations due to equilibrium of sea with freshwater could result on an enrichment of Mn and Fe and reduction of Sr and Mg (Uwe and Veizer, 1980). As a consequence of compositional variation of sea and meteoric water, continuous dissolution-reprecipitation series (water-rock interaction) will take place until equilibrium phase is reached. One of these series is the textural alteration from micrite to microspar and then to pseudospar which leads to depletion in Sr and Mg, and possibly Mn and Fe enrichment as stated above. This could be true especially for syntaxial and equant cements and to some extent blocky calcite. The depletion in Sr and mMg/Ca ratio moving away from grain centre towards younger cement zones can be seen almost in all reservoirs which more or less support the interpretation of water-rock interaction. Another piece of evidence can be added is the abundant moldic and vugy pores found in the rocks which are known to be formed as a result of aragonite leaching (Morad et al., 2010; 2012; Tucker, 2009). There is still some doubts whether this series of transformations (water-rock interaction) took place in meteoric or burial diagenesis (Al-Aasm et al., 2009; Al-Aasm and Azmy, 1996; Lambert et al.; 2006). Stable oxygen isotopes should provide more information regarding origin of pore fluid from which early equant and syntaxial calcite were precipitated (Section 6.4.1.1).

### 4.4.2 Origin of Younger Calcite Cement Zones (blocky and last cement zones in equant and syntaxial) - oil versus water leg

Unlike the older calcite cements (in syntaxial and equant), the last cement zones of the blocky calcite of Reservoir G were precipitated from fluid rich in Mn and low Fe. This implies that the overall fluids in Reservoir G evolved from anoxic to slightly oxic environment through time. Similarly, blocky calcite of Reservoir F precipitated from Mn and Fe fluid even richer than equant and syntaxial cements. Despite the fluctuation in Fe and Mn content in Reservoir F, the overall cement precipitation condition is anoxic which become more and more anoxic towards the younger cement zones. Fe content becomes slightly significant in younger cement zone of blocky calcite compared with older cements in the upper Reservoir A. This suggests that the latest cement zone had been through anoxic condition. Whereas calcite cements including both old and young zones in Reservoir B were precipitated generally under oxic condition.

Basinal hot fluids might be important source of Mn and Fe at the time of precipitation of younger calcite cement zones. This could explain the change in fluid composition of blocky calcite and the higher Mn and Fe contents found in blocky calcite in oil leg compared with water leg in Reservoir F. Fractures in Reservoir F are more abundant in oil leg than in water leg. Basinal hot fluids could be possibly migrated through fractures and stylolites found in the reservoir (Luczaj et al., 2006; Marfil et al., 2005). The frequent association of saddle dolomite, coarse blocky calcite and anhydrite along and in the vicinity of fractures and stylolites support that they have been conduits for the fluids. Furthermore, these type of minerals have been interpreted to be deposited from hot basinal fluids (Davies and Smith, 2006; López-Horgue et al., 2010; Neilson and Oxtoby, 2008; Paganoni et al., 2016). Aqueous fluid inclusions found in burial blocky calcite and saddle dolomite show temperature range of 86-131°C and 125–140°C, and salinity of 6.0–18.1wt.% NaCl eq. and 21.5–22.1 wt.% NaCl eq. respectively suggesting evolved hot basinal brine. This could also explain the slightly elevated Fe and Mn content in younger cement zones in Reservoir G. Abundant fractures can be found in Reservoir G which can act as a path for basinal

fluids. However, there is a significant depletion in Fe concentration in Reservoir G compared with Reservoir F. This depletion could be related to the reaction of Fe from migrated brine with $H_2S$ which is generated during organic maturation to form pyrite (Heydari and Moore, 1993). This can be evidenced by the greater amount of coarse euhedral pyrite that can be found in Reservoir G rather than Reservoir F (Figure 2.18G & H).

The very low concentrations of Fe, Mn and Sr suggest that either fluids with higher Fe, Mn and Sr content have not influenced calcite cementation in oil leg of Reservoir B or theses elements have been consumed in other processes such as dolomitization. Unlike Reservoirs G and F (oil), Reservoir B oil leg has no substantial fracturing and stylolitization in the selected wells. Thus, fractures and styolites might have insignificant effect and role in transporting fluids. However, we cannot exclude that the studied samples were collected away from significant fractures and thus have ineffective transporting fluid system through fractures. Fractures and stytolites in these wells are smaller, almost open and postdate most of the cements. On the other hand, Fe, Mn and Sr rich fluids could had been influenced cements of water leg to some extent which can be revealed by 1) abundant fractures and stylolites in water leg samples, 2) higher Fe, Mn and Sr concentration compare with oil leg although it is still classified as low, 3) abundant saddle dolomite and massive blocky calcite cementation found in fractures, along and in the vicinity of stylolite filling intergranular pores and big molds, 4) association of anhydrite with blocky calcite and saddle dolomite. Another minor source of Mn could be pressure dissolution which can help in releasing Mn into the system (Heydari and Moore, 1993; Paganoni et al., 2016). This could explain the higher Mn content in water samples where abundant stylolites can be found compared with oil samples.

The equivalent trends of calcite cements in Reservoir C in both water and oil legs imply that cements were precipitated under same conditions in both legs. Older cement zones in syntaxial, equant and blocky calcite were precipitated from fluids that are depleted in Fe and Mn compared with lower reservoirs. However, younger cement

zones (particularly blocky calcite and youngest zone in equant and syntaxial calcite) have slightly higher Fe and Mn than older cement zones. Similarly, blocky calcite (younger cement) in Reservoir A shows higher Mn and Fe concentrations than older syntaxial cement. These younger cement zones might be affected by fluids rich in Fe and Mn at the very last stage of cementation perhaps basinal fluids.

### 4.4.3 mMg/Ca Molar Ratio

mMg/Ca molar ratio is believed to be a good temperature proxy for pore fluids which decreases substantially with increasing temperature (Figure 4.1). The mMg/Ca of syntaxial and equant calcite in all reservoirs as well as blocky calcite in Reservoir B and F decreases away from cement centres towards cement edges. Hence, precipitation temperature increases through time moving towards younger cement zones in each type of calcite cement. This finding is in agreement with Thorpe (2014) study, which comprises cements of the same Thamama Group but from different Field.

The mMg/Ca ratio of cements in oil leg is lower than in water. This may suggest that most cements in the oil leg generally precipitated at higher temperature than in water. Cementation may also have ceased in water leg prior to oil leg. However, blocky cement of oil in all reservoirs (except B and F) shows higher mMg/Ca ratio moving towards youngest cement zone (Figures 4.12D, 4.14D & 4.16D). The progressive increase in the average mMg/Ca in blocky calcite might be due to influx of fluids that are rich in Mg. By comparing for example Mg of equant (0.007 - 0.02 mol) and blocky (0.006 – 0.02 mol) calcite of Reservoir C, it can be noted that Mg (mol) of both calcite types lays within the same range. Thus, there is no significant difference in the precipitating fluid for both calcite types in terms of Mg content which therefore discards the first interpretation. Another reason could be that this cement was precipitated at stratigraphically shallower depth after the uplifting of the reservoirs. The two major tectonic events affecting Thamama Group did not start until the Late Cretaceous. The first compressional event is the Semail Ophiolite obduction established in Late Cenomanian until Early Masstrichtian. The second compressional

event comprised of the collision of Arabian and Eurasian Plates which resulted in a major uplift and erosion event in the area (see Section 1.4.1). But, if the whole field went through tectonic compression why we don't see such trend in other reservoirs.

Stratigraphically, one should suspect that cements in deeper reservoirs preserve higher temperature than cements in shallower reservoirs if precipitation conditions remained unchanged (same seawater composition, weather, oceanic spreading, diagenesis, etc.). The average mMg/Ca ratio in shallower reservoirs (particularly B) is lower than in deeper reservoirs (particularly F). Accordingly, cements in shallower reservoirs may have been precipitated at higher temperature compared with cements in deeper reservoirs. The causes of mMg/Ca ratio variation may be due to: 1) preferential removal of Mg from shallower reservoirs by diagenesis especially in open system (e.g. influx of meteoric water) which resulted in a lower mMg/Ca ratio. 2) change in composition of sea water due to change in ocean production rate.

The mMg/Ca ratios of most marine carbonate precipitates are believed to be altered by diagenesis and so cannot be used to monitor the mMg/Ca variation of ancient seawater (Morse and Bender 1990; Zeebe and Sanyal 2002). This is particularly apparent during diagenesis in open systems where there is a high water to rock ratio (Al-Aasm and Azmy, 1996). Many studies, however, have indicated that abiotic marine cements can retain ancient seawater isotope and elemental compositions if they have not subjected to extensive diagenesis (Budd, 1984; Carpenter et al., 1991; Carpenter and Lohmann, 1992; Cicero and Lohmann, 2001; Gonzalez and Lohmann, 1985; Hasiuk and Lohmann, 2008). In a closed system, pore fluid could evolve as a result of water-rock interaction through burial influencing the mMg/Ca values of calcite cement, which generally become enriched in Mg during burial (Heydari and Moore, 1993). Cicero and Lohmann (2001) found that diagenetically altered abiotic marine calcite cements reflected similar Sr/Mg and mMg/Ca of ancient Late Silurian and Middle Triassic seawater suggesting by that such cements might be used to reconstruct ancient ocean chemistry.

The study of Dickson (2004) provides important clue as to how echinoderm stereom can be preserved before skeletal alteration by the infilling of the stereom pore system by stable ferroan calcite cement. Hasiuk and Lohmann (2008) suggested that such non-luminescent cement in "crinoid clothing" can survive diagenesis and hence retain ancient seawater chemistry. To investigate this, the mMg/Ca ratios of the first (earliest) zone of syntaxial non-luminescent calcite cement of echinoderms (First-Syn.) with later precipitated syntaxial, equant and blocky calcite cements from the five reservoirs were plotted separately and compared with the general mMg/Ca trend of global seawater (Figure 4.29).

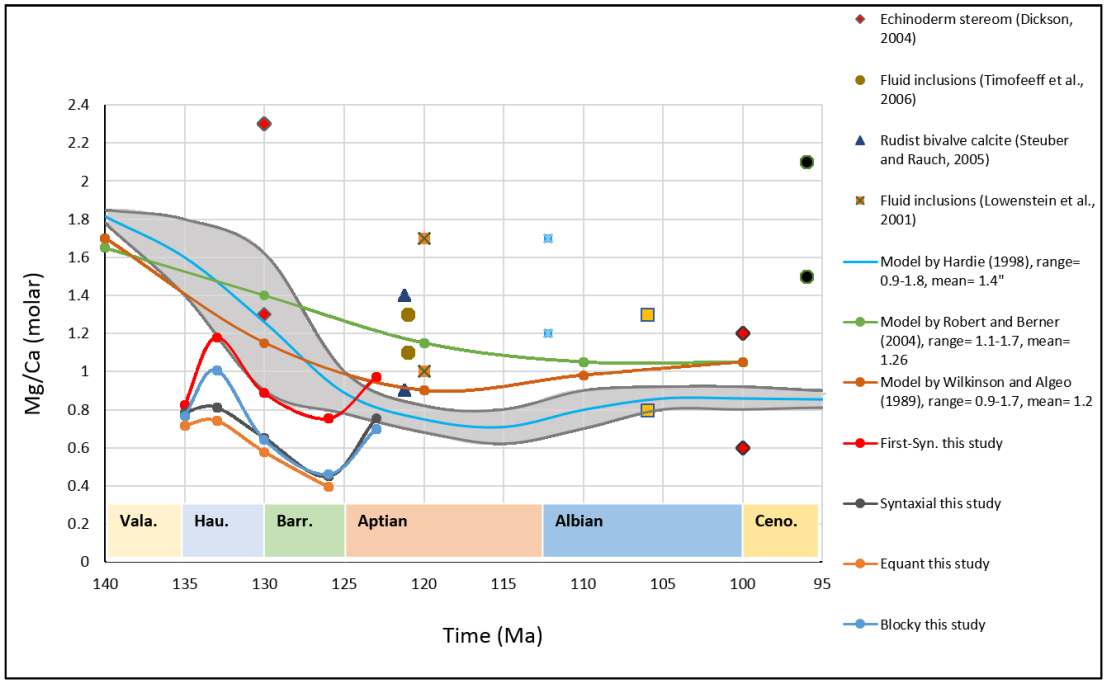


Figure 4.29: Modelled and measured mMg/Ca ratios from the Lower Cretaceous. mMg/Ca measured from this Filed shown as First-Syn, Syntaxial, Equant and Blocky.

All measured mMg/Ca ratios agree with other measured proxies and models that low Mg/Ca ratios dominate the Lower Cretaceous (Hauterivian-Albian), particularly during Late Barremian-Albian time (Figure 4.29). This study shows mean mMg/Ca ratios of echinoderm 'clothing' calcite (First-Syn.) from 0.8 to 1.2 between 135 to 123Ma, with the lowest value recorded at 126 Ma and the highest at 133 Ma. This general trend of mMg/Ca ratios noted broadly follows the Hardie (1998) model of

mMg/Ca ratios (Figure 4.29), and this suggest that this represents the closest values to contemporary seawater except for Reservoir G. Indeed, mean mMg/Ca ratios from all cement types (syntaxial, equant and blocky) parallel this trend but with variable offsets from the First-Syn. calcite, and record the lowest values at 126 Ma and the highest at 133 Ma. The identical mMg/Ca trend noted in all analyzed calcite cements suggests, however, that the cementation in these reservoirs occurred in a relatively closed system, where pore waters hosted the ancient seawater trend. The $^{\delta 13}C_{VPDB}$ of the 126 Ma reservoir of bulk micrite, equant and blocky calcite cements, blocky calcite macrocements and calcite cements in fractures shows values of +2.7 to +4.3‰, mean +3.8‰ (Cox et al., 2010; Morad et al., 2016) +2.3‰ to +3.7‰, mean +3.4‰, respectively (Paganoni et al., 2016), and ~ 0.7 ‰ to ~ 3.5 ‰ (Thorpe, 2014). These are similar to inferred Cretaceous seawater from ~+1 to ~+5‰ (Föllmi, 2012; Sprovieri et al., 2006; Vahrenkamp, 1996; Vahrenkamp, 2010; Veizer et al., 1999). This indicates that calcite cements that precipitated in pore spaces are sourced locally from host limestone that contains pores of seawater signature, supporting the suggestion that cementation occurred in compartmentalized reservoirs. The presence of low permeability TST intervals and hardgrounds at sequence boundaries interbedded with reservoir intervals is the likely cause of synsedimentary or early reservoir compartmentalization (Alsharhan, 1993).

The general variation in mMg/Ca of seawater has been attributed mainly to the changes in oceanic crust production rates. Over the past 150 m.y., the maximum ocean crust production can be found in Middle Cretaceous (Hays and Pitman, 1973; Larson, 1991; Larson and Olson, 1991; Richards and Engebretson, 1992) around 126-112 Ma (Larson and Erba, 1999) or 120-100 Ma (Gaffin, 1987). Hence, the lowest mMg/Ca during 150 m.y. should be found between 126 Ma and 100 Ma which is matching with measured mMg/Ca and models (Figure 4.29). The lowest mMg/Ca ratio recorded in this study can be found around 126 Ma (Late Barremian- Early Aptian) which lays within the same age ranges proposed by Larson and Erba (1999). This is the equivalent time of precipitation of Reservoir B of Thamama Group.

Additionally, Figure 4.30 illustrates mMg/Ca, Sr, Mn and Fe means of syntaxial, equant and blocky calcite in oil leg with time equivalent of each reservoir. The Sr, Mn and Fe trends of each calcite cement type are all following the same trend as mMg/Ca. This means that for every decrease in mMg/Ca there is a decrease in Sr, Mn and Fe and vice versa in each reservoir. For example, calcite cements in Reservoir B are precipitated from fluids of low mMg/Ca, Sr, Mn and Fe. While in Reservoir F, composition of calcite precipitation fluids are higher in mMg/Ca Sr, Mn and Fe.

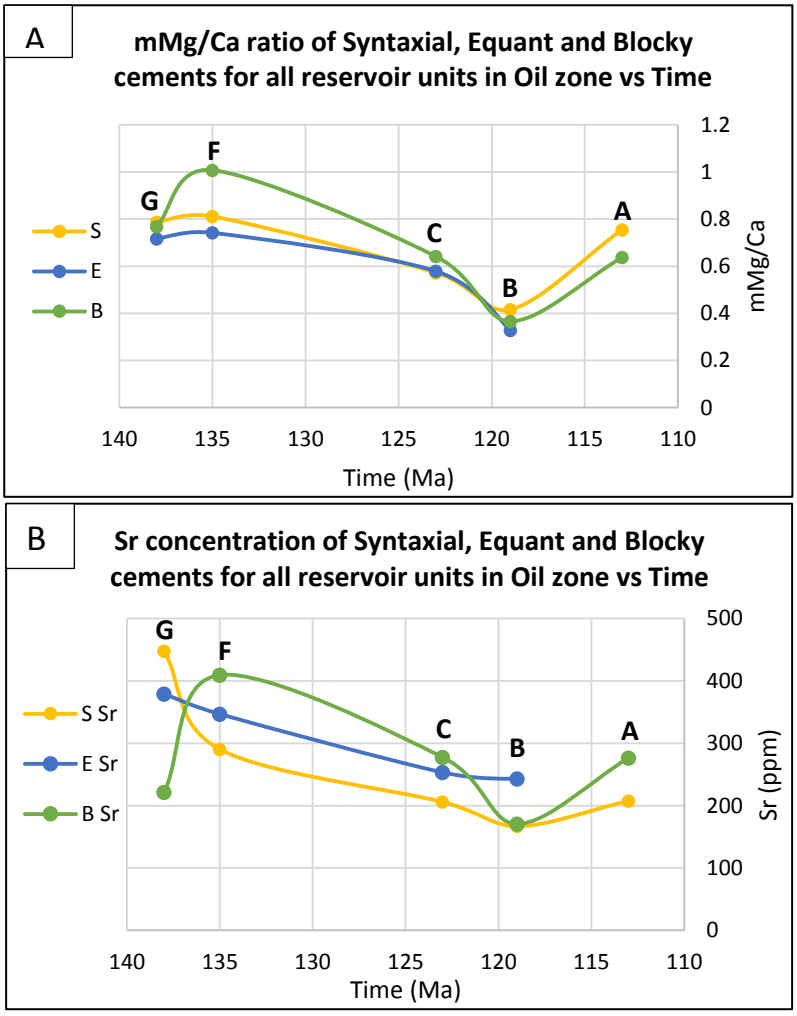

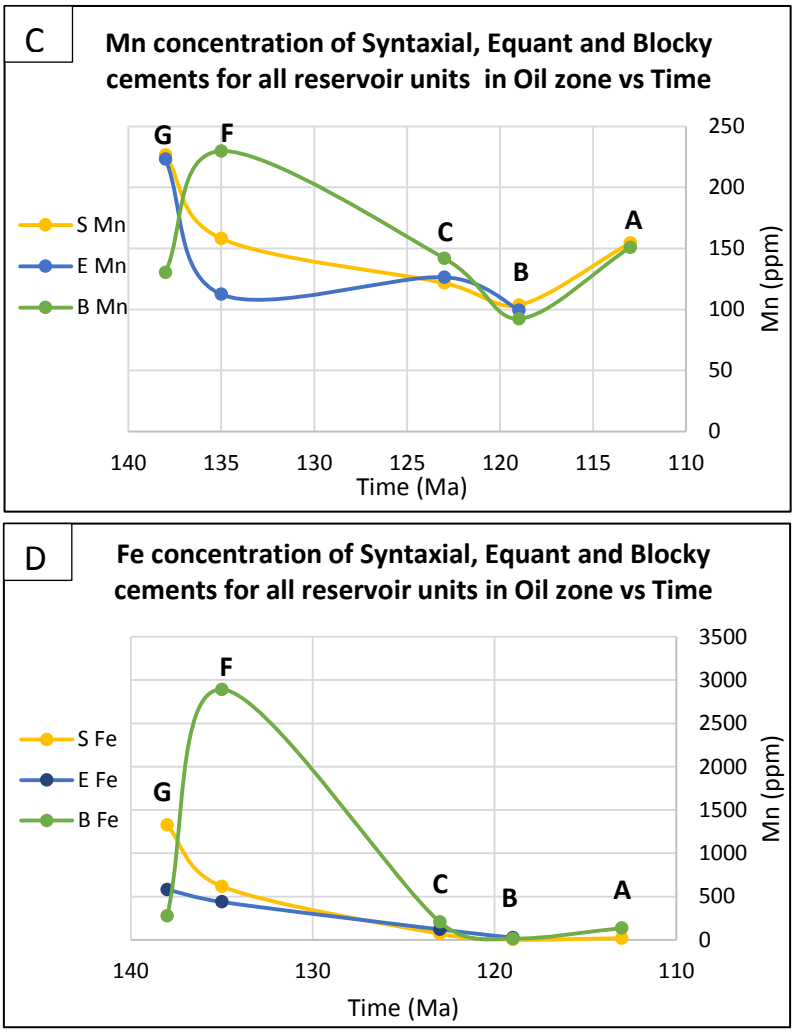


Figure 4.30: Means of trace element of syntaxial, equant and blocky calcite cements for all reservoirs in oil leg through time. A) mMg/Ca with lowest value at Reservoir B. Note how this trend matches with Stanley & Hardie (1998) trend in Figure 3.28. B) Sr concentration. Note also the lowest Sr concentration in Reservoir B. C) Mn concentration. Note the highest concentration in Reservoirs G & F. D) Fe concentration. Note the big difference in Fe concentration of blocky calcite in Reservoir F than other cement types and other reservoirs. Note also that all trace elements follow more or less the same trend.

Elaborating more on mMg/Ca ratio, high mMg/Ca ratio (high $Mg^{2+}$ concentration) typically results in aragonite precipitation while low mMg/Ca ratio

(high $Ca^{2+}$ concentration) favours precipitation of calcite (Berner, 1975; Steuber, 2002). Folk (1974) suggested a value of mMg/Ca Ca ratio as a Calcite-Aragonite boundary; mMg/Ca value below 2, is favoured by low-Mg calcite while high-Mg calcite and aragonite will be abundant above 2. According to this boundary, Sandberg (1983, 1985), Hardie (1996) and Spencer and Hardie (1990) divided the global mMg/Ca seawater curve of Phanerozoic into calcite and aragonite dominated seas (Figure 4.31). Thamama Reservoirs selected in this study were precipitated between Upper Valanginian and Upper Aptian. According to the Calcite-Aragonite seas curve (Figure 4.31) these Reservoirs should be deposited during Calcite Seas. The calculated mMg/Ca ratios of all Reservoirs in this study are all below 2 which further confirm a deposition period of Calcite Seas.

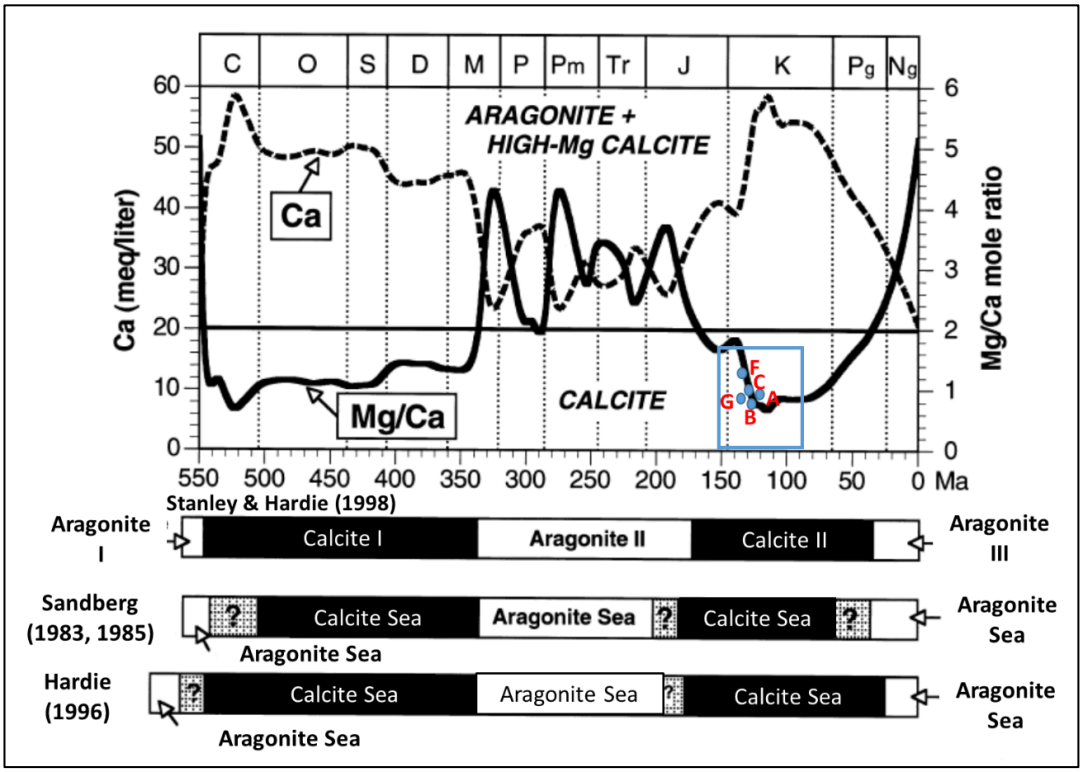


Figure 4.31: Classification of Calcite and Aragonite Seas time intervals based on mMg/Ca ratio modified from Stanley & Hardie (1998). Comparison of three studies including Sandberg (1983, 1985), Hardie (1996) and Stanley & Hardie (1998). Note the reservoirs shown in red fitted into mMg/Ca curve. mMg/Ca ratio is the mean of earliest (first) ferroan calcite in each reservoir.

## 4.5 Summary

Fluid compositions of all precipitated calcite cements in all Reservoirs evolved through time and stratigraphically. The older cements zones in all Reservoirs have trace elements possibly sourced from depositional input. The dewatering of the underlying Dense Zones in Thamama Reservoirs could be a possible fluid source for older cements in each reservoir. The higher Fe, Mn and Sr concentrations in the lower Reservoirs than in upper Reservoirs implies that cements in the lower Reservoirs were precipitated in an anoxic environment that is richer in Fe and Mn compared with shallower Reservoirs C and B. Mn and Sr increases in cements of Reservoir A and interpreted to be sourced by silica rich rock possibly Lower Shuaiba shale.

The mMg/Ca of syntaxial and equant calcite in all Reservoirs as well as blocky calcite in Reservoirs B and F indicates that the precipitation temperature increases through time towards younger cement zones. According to mMg/Ca, in shallower Reservoirs cements were precipitated at higher temperature (e.g. lower mMg/Ca) compared with cements in deeper Reservoirs. This could be due to diagenesis and/or change in composition of sea water due to change in ocean production rate. The maximum ocean crust production can be found around 126-100 Ma which corresponds to the lowest mMg/Ca during the same period. The lowest mMg/Ca ratio during the same period can be found in cements of Reservoir B in this study. This suggests that cements of Reservoir B were precipitated during high rate of ocean production. Related subject can be found in Sections 6.4.1.1 and 6.4.1.2.

Comparing mMg/Ca ratio in oil versus water leg, it can be concluded that most cements in the oil leg continued to precipitate at higher temperature than in the water leg. However, blocky cement of oil leg in all Reservoirs (except B and F) shows lower precipitation temperature (higher mMg/Ca) moving towards the youngest cement zone. These younger cement zones also contain higher Mn, Fe and Sr compared with older cement zones. The progressive increase in the average mMg/Ca and enrichment of Mn, Fe and Sr might be due to influx of fluids that are rich in Mg Mn, Fe and Sr by

exotic fluids and/or uplifting of the Reservoirs. Basinal fluids appear to be important source for precipitation of these younger cements in reservoir G, F and C. Fractures and stylolites are interpreted to be conduits for basinal fluids. The frequent association of saddle dolomite, coarse blocky calcite and anhydrite along and in the vicinity of fractures and stylolites support this interpretation. No evidence of similar minerals was found in Reservoir A. Sr. Alternative source could be silica rich deposit.

Despite the variations in mMg/Ca, Sr, Fe, and Mn between individual cement zone, the overall mean values of mMg/Ca, Sr, Fe, and Mn measured from First Syntaxial non-luminescent calcite zone of echinoderms (First-Syn.), syntaxial, equant and blocky calcite, evolve in a similar way in each reservoir (Figures 4.29 & 4.30). The mMg/Ca of First-Syn. calcite is matching the broadly modelled mMg/Ca of seawater. Also, mean mMg/Ca ratios from syntaxial, equant and blocky follow same trend but with variable offsets from the First-Syn. calcite. These offsets are most likely due to evolution of pore fluid through burial in relatively close system. This suggest that Reservoirs were compartmentalize early by TST intervals and hardgrounds at sequence boundaries interbedded with reservoir intervals.

Although we have evidence of late exotic fluids which might have affected very late calcite cementation, the early calcite cementations have not affected and still preserve early precipitation conditions.

# Chapter 5: Origin, Occurrence and Evolution of Dolomite in Thamama Reservoirs

## 5.1 Introduction

Dolomites have been widely reported as important hydrocarbon reservoir rocks (Collins & Lake, 1989; Davies & Smith, 2006; Morrow, 1982; Qing, 1998). Limestones can be completely dolomitized to form dolostone or partially dolomitized preserving the original textures. Dolostone has been found to be a barrier in some reservoirs and as a permeable productive rock in others (Meyer et al. 2000; Swart et al., 2005). Partial dolomitization, particularly microcrystalline rhombic dolomite, is believed to be a parameter of reservoir quality enhancement as it can support and preserve intergranular porosity from further compaction (Morad et al., 2012). Dolomitization can also result in formation of intercrystalline porosity and thus enhance permeability of the rock. Structurally controlled hydrothermal dolomite reservoirs are of particular significant economic value (Davies & Smith, 2006; Haeri-Ardakani et al., 2013; Smith, 2006). Hydrothermal dolomitization has been closely linked to fracturing and faulting (Davies and Smith, 2006; Haeri-Ardakani et al., 2013; Lonnee and Machel, 2006).

Dolomite, however, can also retard reservoir quality by infilling the pre-existing pores resulting in porosity and permeability reduction (Al-Aasm et al., 2009; Morad et al., 2012). Thus study of dolomite and understanding the processes formation mechanism and its evolution through time is crucial to better understand and predict reservoir quality as well as for hydrocarbon exploration and production.

Dolomite is a carbonate mineral with a chemical formula of $CaMg(CO_3)_2$. It can be formed (1) directly from seawater or primary dolomite and (2) diagenetically in diverse sedimentary environments extending from Earth's surface down to deep sedimentary basins (Burns and Baker, 1987; Gregg et al., 2015; Irwin, 1980; Rodriguez-Blanco, et al., 2015). The direct precipitation of dolomite is linked with periods of "aragonite-seas" which are characterized by high Mg seas. In contrast, indirect dolomite formation "diagenetically-induced dolomite" can be typically found in "calcite seas"; periods characterized by lower Mg seas (Hardie, 1996; Sandberg, 1983, 1985; Stanley & Hardie, 1998; Rodriguez-Blanco, et al., 2015). The samples in this study are from a Lower Cretaceous 'calcite sea' thus one should expect diagenetic dolomite in the studied rocks (Figure 4.30).

Dolomite is one of the most poorly understood carbonate minerals due to the difficulty in precipitating it in laboratory under temperature less than 100°C, which makes understanding of formation mechanisms difficult (Gregg et al., 2015; Morrow, 1982; Rodriguez-Blanco, et al., 2015). This is probably due to the kinetics related to crystal structure ordering which prevent nucleation and growth of dolomite crystal at ambient temperatures and pressures. Moreover, an appropriate source of Mg must be available to form dolomite because an adequate supply of Mg is needed. Various dolomitization models which reflect different dolomitization fluids have been published to understand formation mechanism of dolomite. Dolomitization models include 1) reflux model in sabkha environments forming by evaporitic marine brines (Adams and Rhodes 1960, Deffeyes et al. 1965; Warren, 2000); 2) mixed water model in the mixing zone sourced by freshwater and seawater (Morrow, 1982; Warren, 2000); 3) normal marine model by seawater in subsurface environment (Warren, 2000); 4) burial compaction model sourced by pore water (Morrow, 1982), and 5) tectonic or hydrothermal dolomite model sourced by various fluids in subsurface environment (Davies and Smith, 2006).

Recent studies have proposed microbial-organogenic dolomite model as one of the early phase dolomitization model based on experimental work (Krause et al. 2012; Vasconcelos et al. 1995; Vasconcelos et al. 2005; Warthmann et al. 2000, Wright and

Wacey 2004, Roberts et al. 2013). The studies claim that microbes and organic matter can produce dolomite experimentally under low temperature conditions similar to those in nature. Gregg et al. (2015) criticized this model reporting that none of these studies have shown evidence of cation ordering using X-ray diffraction (XRD). Microbes and organic matter can induce formation of Very High-Magnesium Calcite (VHMC) experimentally with no evidence of cation ordering (Kaczmarek, et al., 2017). Kaczmarek, et al. (2017) added that the experiments of microbial dolomite resulted in precipitation rather than replacement of non-rhombohedral crystals (spheroidal, globules and dumbbells) which contradict with both the natural replacement habit of dolomite and the rhombohedral crystal shape. Accordingly, the processes of microbial dolomitization remain poorly understood, and requires further investigation.

Dolomite can also occur as a replacive or non-replacive "cement" (Sibley and Gregg, 1987). It can be further classified based on the shape and size of the crystal ranging from planar euhedral micro-crystaline rhombic, less than 100 μm to greater than 250 μm non-planar saddle dolomite (Qing, 1998; Rifai et al., 2006; Sibley and Gregg, 1987; Swart et al., 2005). Rhombic matrix replacive dolomite can be initiated during early diagenesis from seawater and further recrystallized during burial or late hydrothermal flux (Haeri-Ardakani et al., 2013). Replacive dolomite can be also formed together with saddle dolomite as a result of late hydrothermal events (Haeri-Ardakani et al., 2013; Davies and Smith, 2006; Lonnee and Machel, 2006). The formation of saddle dolomite is commonly attributed to flux of hydrothermal fluids from deeper parts of the basin (Lavoie and Morin, 2004; Luczaj, 2006; Machel, 2005; Merino and Canals, 2011).

It is important to mention the idea of stoichiometric versus non-stoichiometric dolomite in addition to the order of cations that build the structure of dolomite. Stoichiometric dolomite has 50% $mMgCO_3$ whereas non-stoichiometric dolomite contains less than 50% $mMgCO_3$ (Rodriguez-Blancon et al., 2015). Dolomite stoichiometry has been of significant interest, as several studies argue whether a mineral with high mole $\%MgCO_3$ is a "Dolomite" or a "VHMC" (Gaines, 1977;

Gidman, 1978; Graf & Goldsmith, 1956; Gregg et al., 2015; Land, 1980; Sibley et al., 1994; Zhang et al., 2010,). Land (1980) and Gregg et al. (2015) agreed to refer "VHMC" to the non-stoichiometric mineral with no or poorly ordered peaks, and "dolomite" to the stoichiometric mineral with ordering peaks. In this chapter, for simplicity all dolomite minerals will be called as "dolomite".

This chapter presents trace elements of three dolomites: rhombic, coarse and saddle dolomite. Data are from different reservoirs, and in oil versus water legs. The trace elements Ca, Mg, Mn, Fe, and Sr were analysed in this study to unravel the chemical composition of pore fluids corresponding to precipitation of different dolomite types using Sr and redox elements sensitivity (Fe, Mn).

Sr variations can be used as a tool for palaeosalinity indicator of seawater (Vincent et al., 2006). During dolomitization processes in relatively open systems, significant amounts of Sr can be lost resulting in low Sr content in newly formed cement (Al-Hashimi, 1976).

Changes in $Mn^{2+}$ and $Fe^{2+}$ in pore fluid can be used to understand the environment of cementation including the redox conditions of pore fluids. Ferroan dolomite with high Fe concentration must be formed under reducing conditions (Taylor and Sibley, 1986), whereas, dolomite with low Fe and Mn concentrations represent an oxidizing environment. Several studies suggested that ferroan dolomite formation can be initiated at or near surface and continue to grow with depth (Burns and Baker, 1987; Choquette, 1971; Curtis, 1978; Dickson and Coleman, 1980; Irwin, 1980; M'rabet, 1981, Wong and Oldershaw, 1981). Ferroan dolomite can be formed 1) at shallow burial and low temperature; 2) in organic rich sediments; 3) at high temperature near 100˚C during burial processes. Moreover, Mg:Ca ratio can be used in dolomite classification as well as fluid indicator when correlated with salinity (Folk and Land, 1975; Warren, 2015).

Stable isotope analysis has been widely used in studies of various minerals (Al-Aasm et al., 2009; Paganoni et al., 2016; Puce´at et al., 2003). These provide average

$\delta^{18}O_{VPDB}$ and $\delta^{13}C_{VPDB}$ values which can infer conditions of pore fluid chemistry and temperature at which particular cement was precipitated. No stable isotopes have been reported in this study, but published isotopic data will be incorporated to infer the origin of dolomite in the Thamama Group.

## 5.2 Aims

This study aims to investigate the chemical composition of the different dolomite types in the Thamama in order to unravel the origin of pore fluids which involved in formation of dolomite. In particular, in order to:

- Understand and track dolomitization fluid evolution through time using Sr and redox elements sensitivity (Fe and Mn).
- Use mMg:Ca ratios and Sr to understand potential origin of pore fluid and its evolution through dolomitization.
- Propose possible dolomitization models that can better explain formation mechanism of different types of dolomite.

## 5.3 Methods and Sampling Procedure

Electron Probe Microanalysis (EPMA) was used to analyse 10 thin sections containing dolomite from different reservoirs from oil and water legs. For more information about EPMA methods see Section 1.5.2.3.

Samples were selected to capture trace element concentrations in each identified CL cement zone in different dolomite morphologies. This is to understand pore fluid evolution of different dolomites through time. Similar to the procedure followed for calcite; a transect was run through each cement stratigraphy that was established by CL work.

Sample selection was based on 1) availability of cements in each reservoir, oil versus water leg, 2) cement stratigraphy; number of cement zones that can be identified in each type of cement, 3) thickness of each CL zone. The first was decided by conventional petrography work. The second and the third were based on CL work. The maximum apparent length of each crystal and the number of CL zones of the same crystal were used to estimate the length of individual transect and spacing between data point in a single transect and therefore the number of data points to be analysed through a single transect. The closest spacing that has been tested in order to capture the very thin CL zones is around 9.5 μm.

From the petrography and paragenetic sequence (Figure 5.1) established in Chapter 2, three dolomite types have been identified. The first to form is Type 1: Rhombic micro-crystalline dolomite (=< 10 μm across). Dolomite type 2 is the second to form. It is a coarse dolomite (>50 μm) with subhedral-anhedral crystals. This type of dolomite is placed after dissolution seams and first stylolitization event in paragenetic sequence. Saddle dolomite is classified as Type 3 which is characterized by non-planar (anhedral), very coarse crystal (>250 μm). This dolomite type predates the second stylolitization event and postdates the second fracture generation.

The most abundant dolomite type in all reservoirs is saddle dolomite cement. All reservoirs commonly-rarelly contain saddle dolomite except Reservoir A. Coarse and rhombic dolomites can be found rarely to commonly in some reservoirs (see Table 5.1). Moreover, Reservoirs B, C and F have been sampled from oil and water legs which allowed for comparison between different fluid zones.

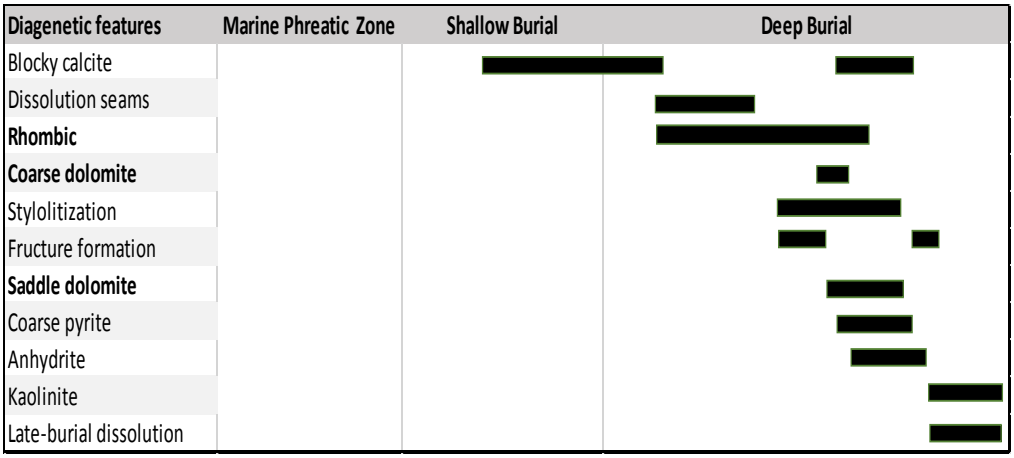


Figure 5.1: Summary of paragenetic sequence including three types of dolomite and other relevant events. For complete paragenetic sequence story see Section 2.5.1.

Table 5.1: Abundance of rhombic, coarse and saddle dolomite in each reservoir, and in oil and water legs. R: Rare, C: Common, A: Abundant, NF: Not Found.

| Reservoir | Cement Type | Oil Leg | Water Leg |
|---|---|---|---|
| **A** | Rhombic dolomite | R | No samples |
| | Coarse dolomite | NF | |
| | Saddle dolomite | NF | |
| **B** | Rhombic dolomite | A | R |
| | Coarse dolomite | R | R |
| | Saddle dolomite | C-R | A |
| **C** | Rhombic dolomite | C | NF |
| | Coarse dolomite | R | NF |
| | Saddle dolomite | C | C |
| **F** | Rhombic dolomite | NF | R |
| | Coarse dolomite | R | NF |
| | Saddle dolomite | C | A |
| **G** | Rhombic dolomite | NF | No samples |
| | Coarse dolomite | NF | |
| | Saddle dolomite | A | |

Fe is more abundant in dolomite than in calcite especially in the lower reservoirs. Table 5.2 illustrates the detection limits of Fe, Mn and Sr for different dolomite across different reservoirs.

Table 5.2: Detection limit in the available dolomite in all reservoirs in oil and water legs.

| Leg | Dolomite Type | Reservoir | Mn | Fe | Sr |
|---|---|---|---|---|---|
| Oil | Rhombic | A | 93 ± 2 | 120 ± 4 | 124 ± 3 |
| | | B | 94 ±1 | 123 ±2 | 123 ± 3 |
| | Coarse | B | 92 ± 2 | 118 ± 4 | 121 ± 4 |
| | | C | 93 ±2 | 127 ±5 | 123 ± 3 |
| | Saddle | C | 93 ± 3 | 122± 2 | 124 ± 2 |
| | | F | 93 ± 1 | 123 ± 5 | 124 ±2 |
| | | G | 93 ±2 | 134 ±2 | 122 ±2 |
| Water | Rhombic | F | 94± 1 | 145 ±5 | 126± 3 |
| | Saddle | B | 92 ± 1 | 120 ± 2 | 125 ± 2 |
| | | C | 93±2 | 129±2 | 125±3 |
| | | F | 93 ± 1 | 135 ± 5 | 126 ± 2 |

## 5.4 Results

### 5.4.1 mMg:Ca Molar Ratio of Dolomite

The mMg:Ca ratio was calculated for each dolomite type in both water and oil legs. The ratio in all dolomite types ranges from 1.0 to 1.5 (Figure 5.2). The rhombic dolomites for oil (RO) and water leg (RW) show higher ratios compared with coarse dolomite (CO) in oil leg and saddle dolomites in oil (SO) and water leg (SW). Rhombic dolomite in water leg shows slightly higher mMg:Ca mean values compared with oil leg (Figure 5.3). While saddle dolomite both in oil and water show approximately similar mMg:Ca. Comparing the mMg:Ca ratio for rhombic and saddle dolomites

across different reservoirs, the highest mMg:Ca mean values for both rhombic (1.38; reported mostly in older rhombic dolomite) and saddle (1.14) dolomites are in Reservoir F water leg, while the lowest mMg:Ca mean value for rhombic dolomite (1.19, reported mostly in younger rhombic dolomite) occur in Reservoir A oil leg and saddle dolomite (1.09) in Reservoir B water leg (Figure 5.4).

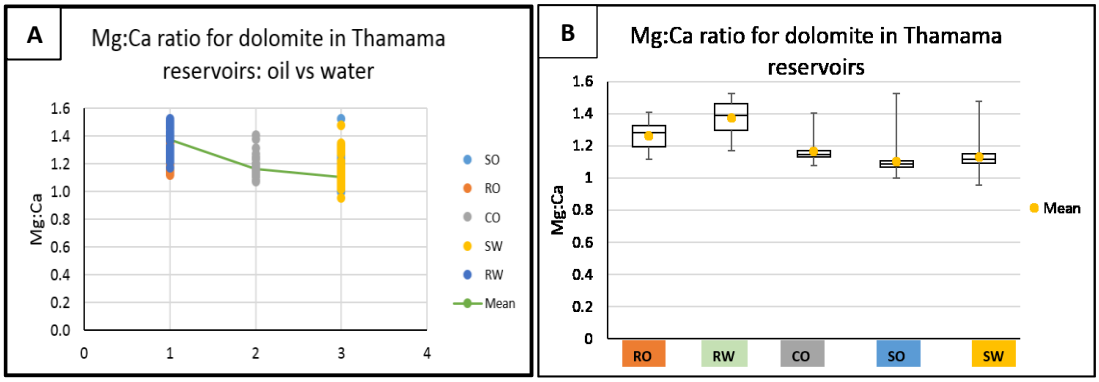


Figure 5.2: mMg:Ca ratio for dolomite in all reservoirs in oil and water legs: A) All data points plotted as; 1 for rhombic dolomite (oil and water), 2 for coarse dolomite (oil), 3 for saddle dolomite (oil and water). B) box-and-whisker with mean value and quartiles for each dolomite type.

RO: Rhombic Oil, RW: Rhombic Water, CO: Coarse Oil, SO: Saddle Oil, SW: Saddle Water.

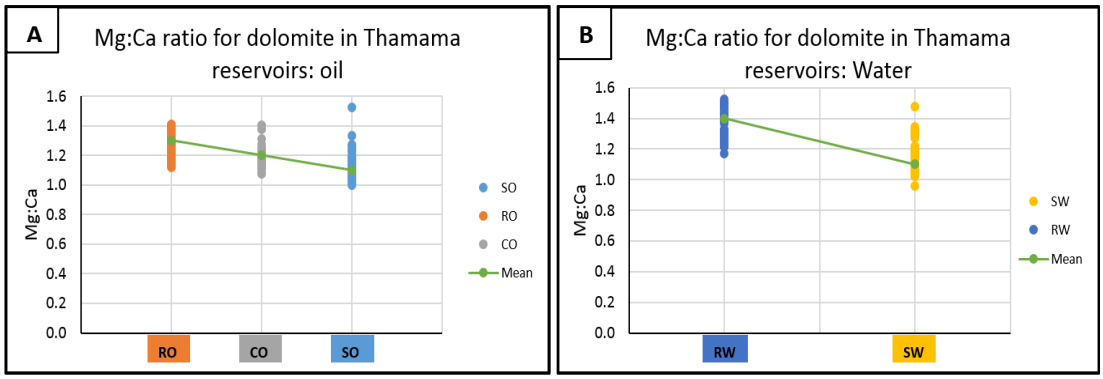


Figure 5.3: mMg:Ca ratio for dolomite in all reservoirs in oil and water legs: A) mMg:Ca ratio of dolomite in oil leg, data points plotted as; RO for Rhombic Oil, CO for Coarse Oil, SO for Saddl Oil. B) mMg:Ca ratio of dolomite in water leg, data points plotted as RW for Rhombic Water and SW for Saddle Water.

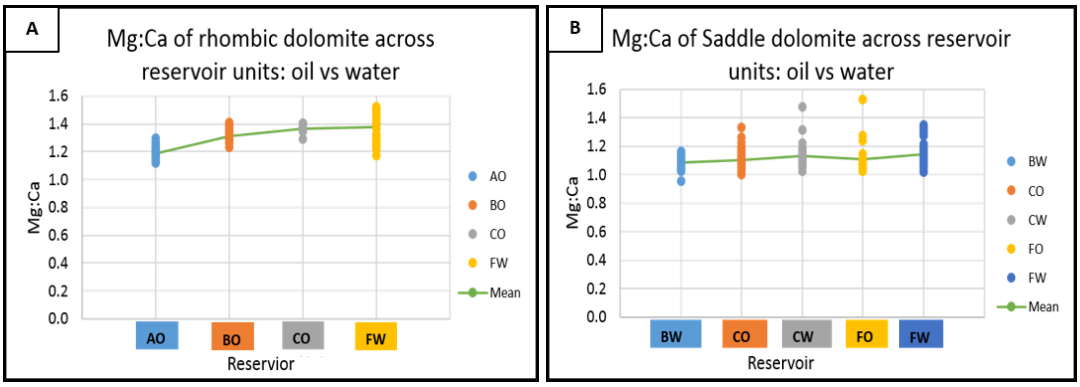


Figure 5.4: mMg:Ca ratio for rhombic and saddle dolomite in across different reservoirs in oil and water legs: A) mMg:Ca ratio of rhombic dolomite, data points plotted as; AO for Reservoir A Oil, BO for Reservoir B Oil, CO for reservoir C Oil and FW for Reservoir F Water. B) mMg:Ca ratio of saddle dolomite, data points plotted as BW for Reservoir B Water, CO for Reservoir C Oil, CW for Reservoir C Water, FO for Reservoir F Oil and FW for Reservoir F Water.

### 5.4.2 Type 1: Rhombic Replacive Dolomite

Rhombic dolomite is the first dolomite to precipitate in the Thamama (Figure 5.1). It is a micro-crystaline dolomite (=< 10 µm across) with planar; subhedral-euhedral crystals. This type of dolomite has zoned crystals under the CL in certain reservoirs reflecting ferroan and non-ferroan cements. The maximum number of CL cement zones found in this dolomite is five. In the oil leg, Type 1 can be only found in Reservoirs A, B and C. More volumetrically in Reservoirs B and C concentrated along dissolution seams and scattered in mud rich facies. Similarly, in the water leg rhombic dolomite can be found along dissolution seams and scattered in mud rich facies. It can be found in Reservoirs B and F. It could not be traced in other reservoirs from water leg since no samples were collected from A and G and few samples from C are available.

In general, the Sr content in rhombic dolomite is higher than coarse and saddle dolomites (Figures 5.5, 5.10 & 5.13). The rhombic dolomite of B "oil" contains the highest Sr content among the other measured rhombic dolomite in the other reservoirs oil versus water (Figure 5.5). The Sr means in Reservoir A "oil", "B" oil, C "oil" and F "water" in ppm are 336 (Max. 476), 579 (Max. 2095), 346 (Max. 800) and 516 (Max. 1445) respectively (Table 5.3). In general, Mn and Fe contents in the water leg are higher than oil leg. Rhombic dolomite of Reservoir F "water" hosts the highest Mn and Fe contents (Figure 5.5). The Mn and Fe mean values in ppm are as follows: Reservoir A "oil" (Mn: 120; Max. 238, Fe: 4331; Max. 27252), Reservoir B "oil" (Mn: 110 Max. 203, Fe: 4128; Max. 9479), C "oil" (Mn: 40.0; Max. 70, Fe: 2223; Max. 5762) and Reservoir F "water" (Mn: 221; Max. 646, Fe: 9460; Max. 55798).

Table 5.3: Sr, Mn and Fe content and number of data points (n) of rhombic dolomite for reservoirs in oil versus water leg.

| **Reservoir** | **Sr (ppm)** | **Mn (ppm)** | **Fe (ppm)** |
|---|---|---|---|
| **Oil leg** | | | |
| Reservoir A | Range: 138-476<br>Mean: 336<br>n= 31 | Range: 49-238<br>Mean: 120<br>n= 31 | Range: 32-27252<br>Mean: 4331<br>n= 31 |
| Reservoir B | Range: 223-2095<br>Mean: 579<br>n= 50 | Range: 0-203<br>Mean: 110<br>n= 50 | Range: 327-9479<br>Mean: 4128<br>n= 50 |
| Reservoir C | Range: 226-800<br>Mean: 346<br>n= 6 | Range: 0-70<br>Mean: 40<br>n= 6 | Range: 241-5762<br>Mean:2223<br>n= 6 |
| **Water leg** | | | |
| Reservoir F | Range: 46-1445<br>Mean: 516<br>n= 18 | Range: 65-646<br>Mean: 221<br>n= 18 | Range: 545-55798<br>Mean: 9460<br>n= 18 |

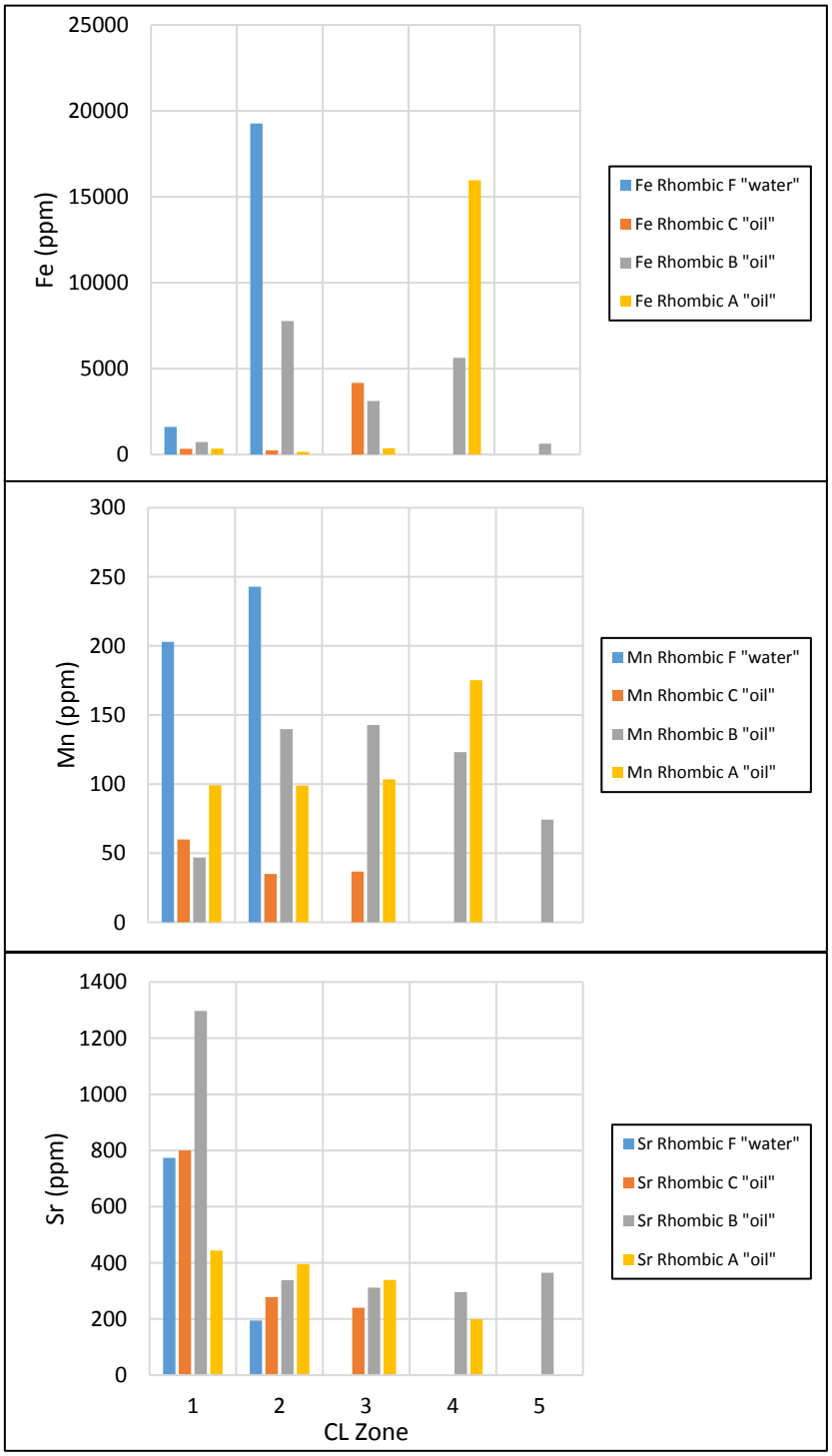


Figure 5.5: Summary of Fe, Mn and Sr means for rhombic dolomite in all reservoirs: oil versus water. CL cement zones are from 1 to 5. Note that each cement zone is identical for each reservoir.

Figure 5.6 illustrates the Fe, Mn and Sr concentrations through CL zones found in Reservoir F "water". The Fe and Mn contents increase towards the younger cement zones (Fe Zone 2 mean=19264 ppm; Mn Zone 2 mean=243 ppm; Figure 5.6A & B), whereas the Sr decreased towards the younger zones (Zone 2 mean= 195 ppm; Figure 5.6 C).

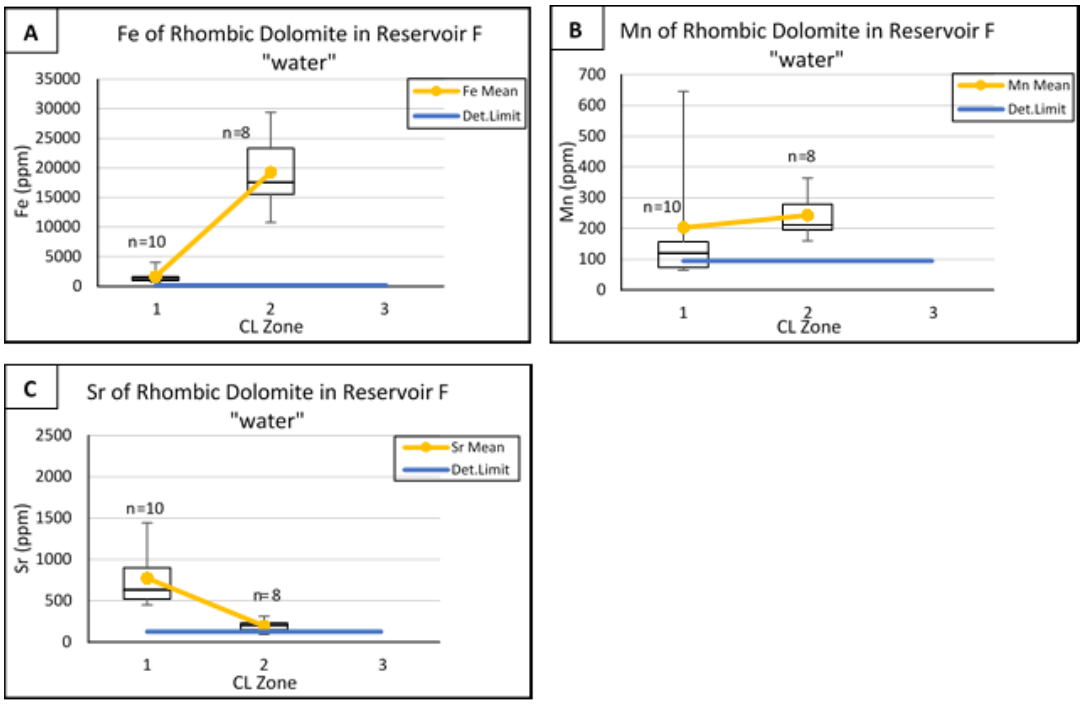


Figure 5.6: Element concentrations of rhombic dolomite in Reservoir F in water leg: A) Fe content across CL zones with highest content in Zone 2. B) Mn content across CL zones with highest content in Zone 1. C) Sr content across CL zones. Note the Sr trend is the reverse of the Fe trend.

Fe in Reservoir C "oil" rises (Zone 3 mean=4267 ppm; Figure 5.7A) while the Sr drops towards younger cement zones (Zone 3 mean=240 ppm; Figure 5.7C). The Mn content is very low in this reservoir; all measured values are below the detection limit (Figure 5.7B).

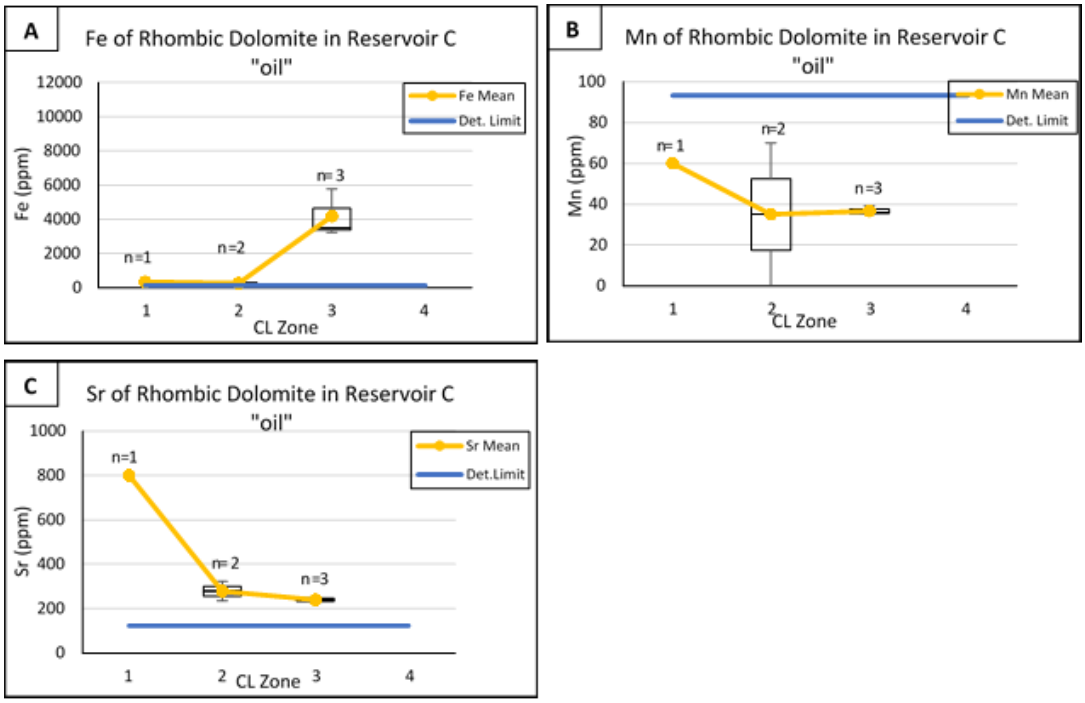


Figure 5.7: Element concentrations of rhombic dolomite in Reservoir C in oil leg: A) Fe content across CL zones with highest content in Zone 3. B) Mn content across CL zones. C) Sr content across CL zones having the highest concentration in Zone 1. Note the Sr trend is the reverse of the Fe trend similar to previous sample from Reservoir F "water".

In Reservoir B "oil", the Fe content varies substantially across the cement zones with two significant increases recorded in cement Zones 2 (mean=7771 ppm) and 4 (mean=5627 ppm; Figure 5.8A). The Mn is low at Zone 1 (mean=47 ppm) becomes higher at Zone 2 (mean=140 ppm) and then decreases towards younger cement zones (Zone 5 mean=74 ppm; Figure 5.8B). The Sr has its highest concentration in Zone 1 which then decreases towards the younger zones (Zone 5 mean= 364 ppm; Figure 5.8C).

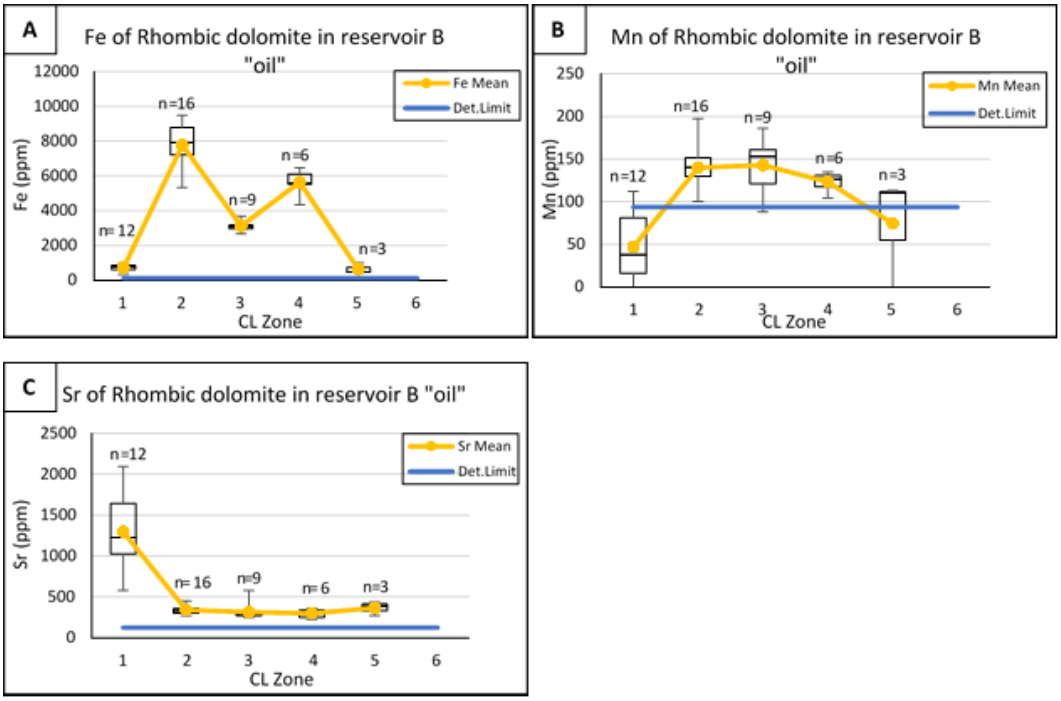


Figure 5.8: Element concentrations of rhombic dolomite in Reservoir B in oil leg: A) Fe content across CL zones with two peaks at Zones 2 & 4. B) Mn content across CL zones. Note the anticline trend with low values at the edges (Zones 1 & 5) and higher values at the crest (Zones 2, 3 & 4). C) Sr content across CL zones having the highest concentration in Zone 1.

Likewise, Reservoirs C and F, Fe level in Reservoir A "oil" show an increase towards younger cement zones with the highest Fe level reported in the youngest cement zone (mean=15966 ppm; Figure 5.9A). Also, the Mn content increases towards the younger cement zones (Zone 1 mean=99 ppm, Zone 4 mean=175 ppm; Figure 5.9B). Whereas, Sr content drops towards the younger cement zones; from mean=444 ppm at Zone 1 to mean=199 ppm at Zone 4 (Figure 5.9C).

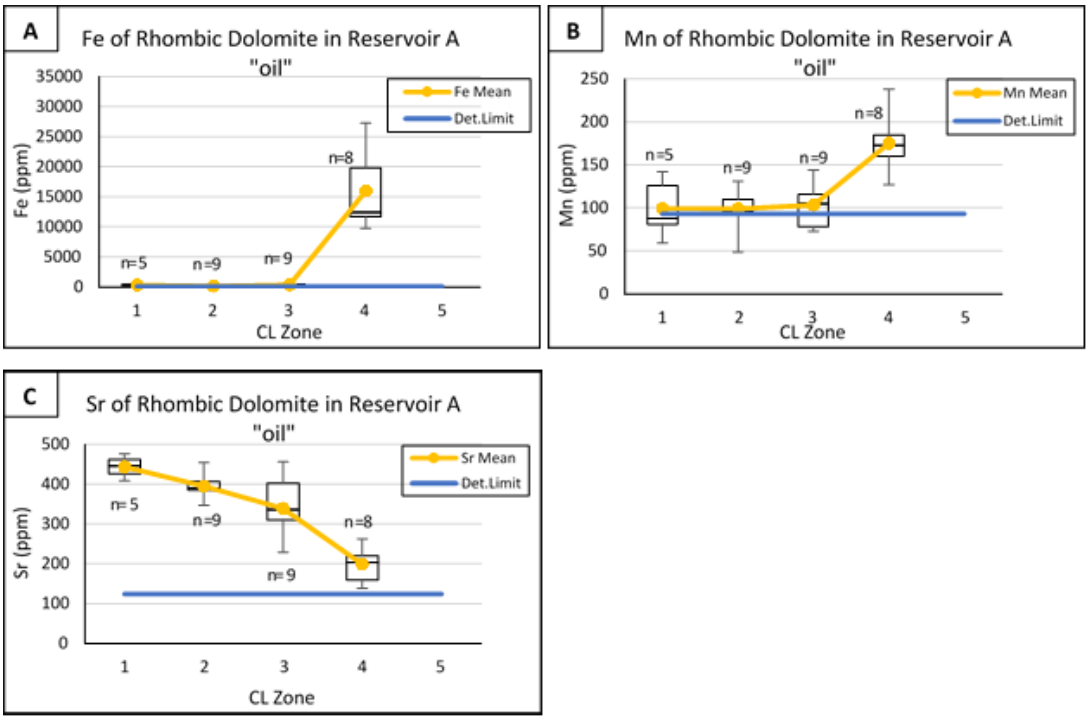


Figure 5.9: Element concentrations of rhombic dolomite in Reservoir A in oil leg: A) Fe content across CL zones with the highest value at youngest zone. B) Mn content across CL zones. Note also the highest value at youngest zone similar to Fe. C) Sr content across CL zones having the highest concentration in Zone 1.

### 5.4.3 Type 2: Coarse Dolomite

This type of dolomite is the second to precipitate (Figure 5.1). It consists of subhedral-anhedral coarse crystal (>50 μm) with sweeping extinction. Most of the crystals show cement zonation under the CL. It occurs only in Reservoirs B, C and F of oil leg; along stylolite, in molds and vugs. In water leg this type of cement can be only found in Reservoir B. Data were collected only from oil leg of Reservoirs C and B.

In general, this type of cement contains higher Sr, Mn and Fe contents in Reservoir C than B (Figure 5.10). Sr values in Reservoir B are mostly below the

detection limit with mean value of 85 ppm (Max. 324 ppm; Table 5.4). In Reservoir C, Sr has a mean of 210 ppm and maximum value of 800 ppm (Table 5.4). All Mn values in Reservoir B are below the detection limit (0-77 ppm; Avg. 19), while in Reservoir C few values are above the detection limit (0-170 ppm; Avg. 71). All Fe values in Reservoir B are above the detection limit and very few values in Reservoir C below the detection limit. The Fe means of Reservoir B and C in ppm are 1880 (Max. 4221) and 11046 (Max. 33308) respectively (Table 5.4).

Table 5.4: Sr, Mn and Fe content and number of data points "n" of coarse dolomite for Reservoirs B and C in oil leg.

| **Reservoir** | **Sr (ppm)** | **Mn (ppm)** | **Fe (ppm)** |
|---|---|---|---|
| **Oil leg** | | | |
| Reservoir B | Range: 0-324<br>Mean: 85<br>n= 50 | Range: 0-77<br>Mean: 19<br>n= 50 | Range: 377-4221<br>Mean: 1880<br>n= 50 |
| Reservoir C | Range: 6-800<br>Mean: 210<br>n= 34 | Range: 0-170<br>Mean: 71<br>n= 34 | Range: 35-33308<br>Mean: 11046<br>n= 34 |

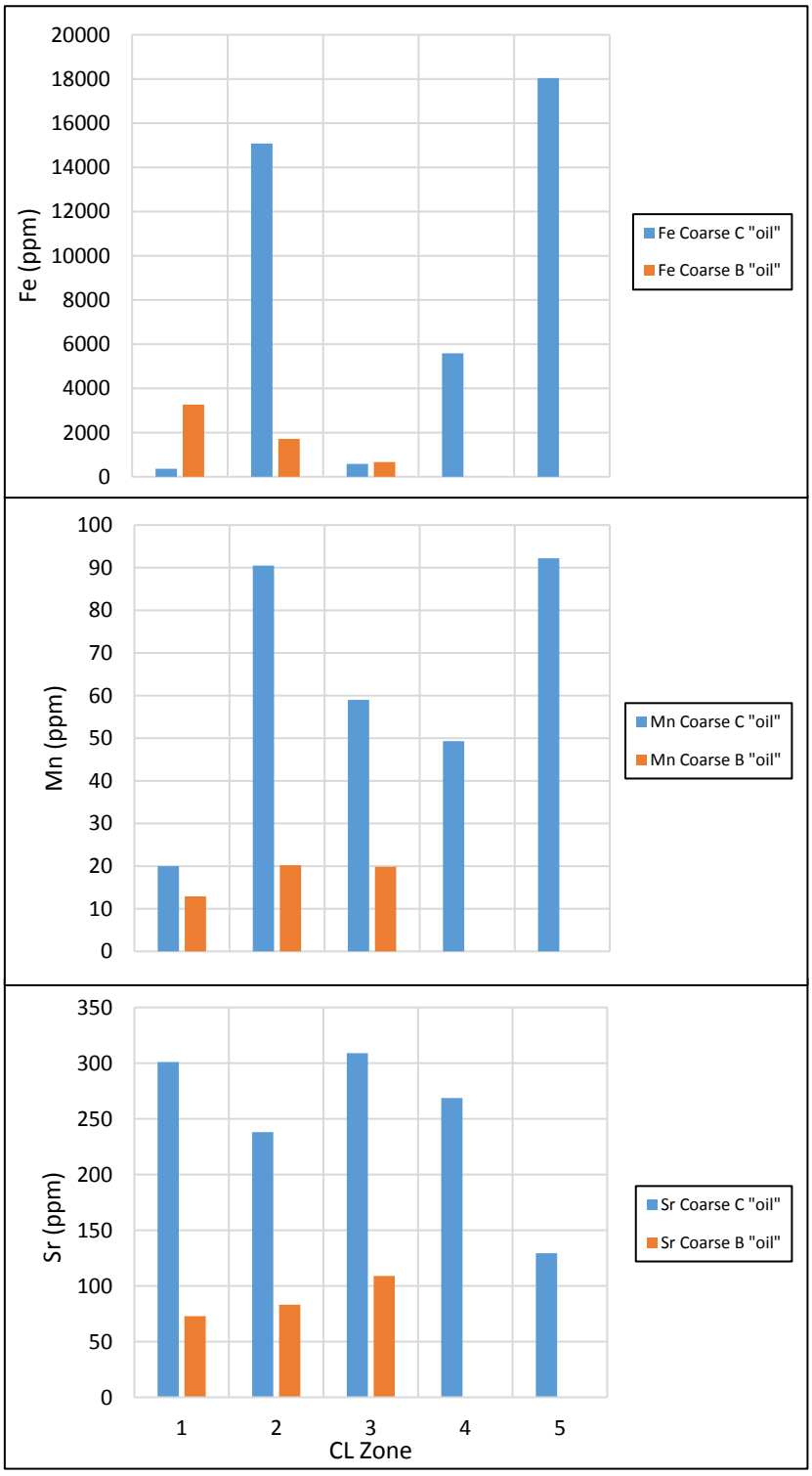


Figure 5.10: Summary of Fe, Mn and Sr means for coarse dolomite in Reservoirs B and C of oil leg. CL cement zones are from 1 to 5. Note that each cement zone identical for each reservoir.

The Fe trend in Reservoir B decreases towards the younger cement zones; having the highest (mean=3264 ppm) Fe content in the oldest cement zone and the lowest (mean=671 ppm) in the youngest cement zone (Figure 5.11A). Mn and Sr are with low values for this dolomite type in this reservoir (Figure 5.11B & C).

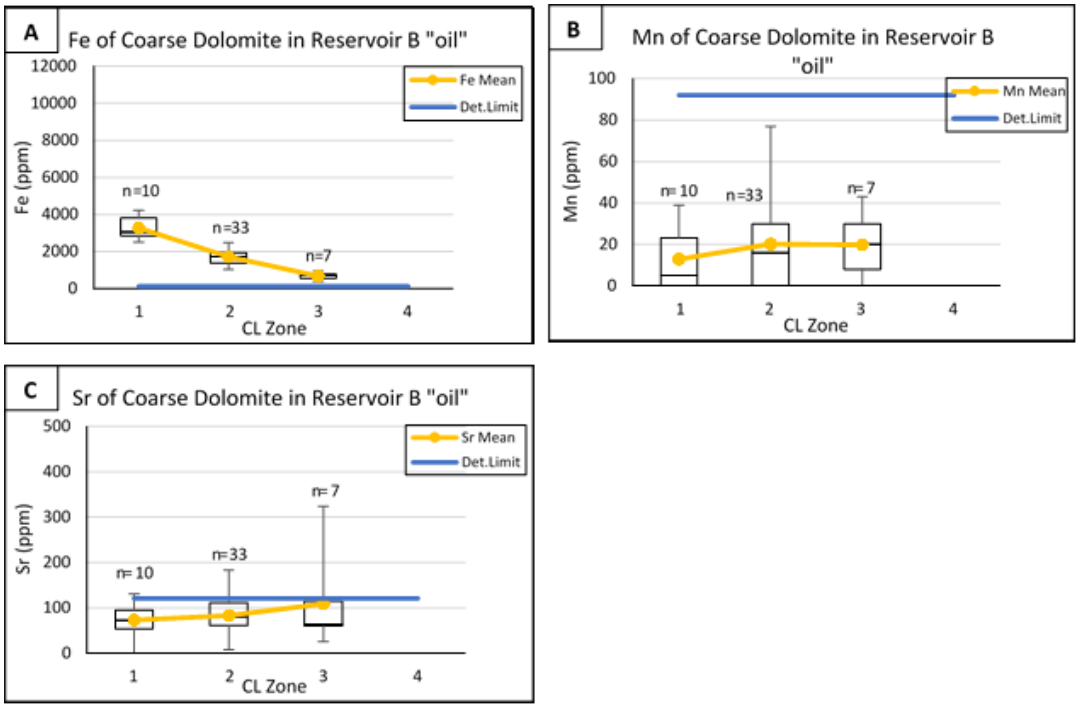


Figure 5.11: Element concentrations of coarse dolomite in Reservoir B in oil leg: A) Fe content across CL zones with decreasing trend from older to younger cement zones. B) Mn content across CL zones. Note that all values are below the detection. C) Sr content across CL zones having the highest concentration in Zone 3. Most values are below the detection limit. The Sr trend is reverse to Fe trend.

By contrast, Reservoir C shows a fluctuating Fe content starting from a very low value (366 ppm) in the first cement zone which increases dramatically in the second zone (mean=15085 ppm) followed by a significant drop in Zone 3 (mean=584 ppm) and finally an increase towards the last two cement zones (Zone 4 mean=5585 ppm, Zone 5 mean=18045 ppm; Figure 5.12A). The Mn content mostly low with slight increase in the youngest cement zone (Figure 5.12B). Unlike the Fe, the Sr values

decrease towards the youngest cement zones; starts with 301 ppm at Zone 1 and ends up with mean=129 ppm at Zone 5 (Figure 5.12C).

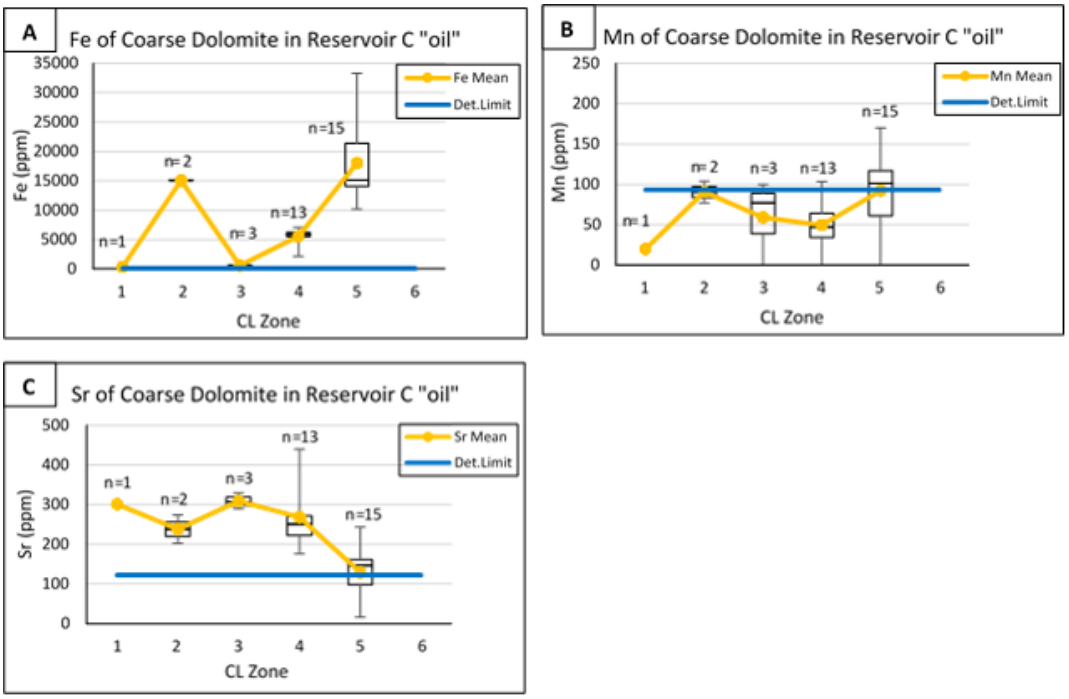


Figure 5.12: Element concentrations of coarse dolomite in Reservoir C in oil leg: A) Fe content across CL zones with two peaks at Zones 2 & 5. B) Mn content across CL zones. Note that most values are below the detection with highest values at Zone 5. C) Sr content across CL zones with reverse trend to Fe similar to previous dolomite samples.

### 5.4.4 Type 3: Saddle Dolomite

This type of dolomite is the latest to precipitate (Figure 5.1). Saddle dolomite is characterized by non-planar (anhedral), very coarse crystal (>250 µm) with distinguish undulose extinction feature. Saddle dolomite in all reservoirs has at least three distinguished CL zones like Reservoir F and C in oil leg and Reservoir B in water leg. Reservoirs F and C "water" contain up to four CL zones. The two common CL zones which contain similar Fe content across all reservoirs are the very dark thick older cement zone and the very bright luminance thick younger cement zone.

This dolomite was reported in all reservoirs in oil leg except Reservoir A. In water leg, only three reservoirs were studied including F, C and B. Saddle dolomite can be found in different pores, in fractures and along stylolites. Table 5.5 illustrates occurrence of saddle dolomite across the reservoirs in oil versus water leg.

Table 5.5: Occurrence of saddle dolomite across the reservoirs in oil versus water leg.

| **Reservoir** | **Oil leg** | **Water leg** |
|---|---|---|
| Reservoir A | NO saddle dolomite was reported | No samples |
| Reservoir B | Mostly along stylolites and rarely-commonly in molds | Along stylolites and filling the molds |
| Reservoir C | Mostly in molds and along fractures and rarely in intergranular pores | Mostly in molds and rarely in large intergranular pores |
| Reservoir F | Only in molds and maybe fractures | Along stylolites and filling molds and large intergranular pores |
| Reservoir G | In fractures and maybe along stylolites | No samples |

Most Sr values both in oil and water leg for all reservoirs are below the detection limit except for some high values in Reservoir C. Similarly, the Mn values are mostly below the detection limit except for higher Mn content in Reservoir F. Regarding the Fe values, some show low Fe content like Reservoir B, some with intermediate content like Reservoir C and some have very high content like Reservoir F. Table 5.6 shows the Sr, Mn and Fe content as well as number of data points (n) for all reservoirs in oil versus water leg. Sr mean values for oil leg Reservoirs C and F in ppm are 72 (Max. 854) and 84 (Max. 144) respectively. In water leg Reservoirs B, C and F have Sr mean values reported in ppm as 64 (Max. 128), 113 (Max. 261) and 65 (Max. 196) respectively. Mn mean values in ppm in oil and water legs are as following: C “oil”; 58 (Max. 150), F “oil”; 254 (Max. 406), B “water”; 72 (Max. 147), C “water”; 69

(Max. 167), F "water"; 160 (Max. 612). For Fe the following mean values have been reported in ppm (Table 4.6): C "oil"; 4149 (Max. 26232), F "oil"; 8753 (Max. 57759), B "water"; 2899 (Max. 10087), C "water"; 10030 (Max. 16131), F "water"; 17928 (Max. 57638).

Table 5.6: Sr, Mn and Fe content and "n" of saddle dolomite for all reservoirs in oil versus water leg.

| Reservoir | Sr (ppm) | Mn (ppm) | Fe (ppm) |
|---|---|---|---|
| **Oil leg** | | | |
| Reservoir C | Range: 0-854<br>Mean: 72<br>n= 59 | Range: 0-150<br>Mean: 58<br>n= 59 | Range: 0-26232<br>Mean: 4149<br>n= 59 |
| Reservoir F | Range: 7-144<br>Mean:84<br>n=23 | Range: 136-406<br>Mean:254<br>n=23 | Range: 0-57759<br>Mean:8753<br>n=23 |
| **Water leg** | | | |
| Reservoir B | Range: 0-128<br>Mean: 64<br>n= 23 | Range: 0-147<br>Mean: 72<br>n= 23 | Range: 0-10087<br>Mean: 2899<br>n= 23 |
| Reservoir C | Range: 0-261<br>Mean: 113<br>n=60 | Range: 0-167<br>Mean: 69<br>n=60 | Range: 0-16131<br>Mean: 10030<br>n=60 |
| Reservoir F | Range: 0-196<br>Mean: 65<br>n=67 | Range: 85-612<br>Mean: 160<br>n=67 | Range: 0-57638<br>Mean: 17928<br>n=67 |

There is a significant variation in the Fe content within each reservoir. However, the general trend for Fe content is decreasing towards the younger cement zones (Figures 5.13, .14A, 5.15A, 5.16A, 5.17A & 5.18A). Reservoir F in "water" records the same Fe decreasing trend towards the younger cement zones except for the youngest reservoir zone which shows a dramatic increase in Fe content (up to 50000 ppm; Figure 5.14A). Generally, the highest Fe content can be found in Reservoir F (mean=48465 ppm; Figure 5.13). Similarly, the highest Mn content was reported in Reservoir F (mean=329 ppm) whereas, the highest Sr content was recorded in C (mean=127 ppm) in particularly oil leg (Figure 5.13). In Reservoir F "water", the Mn content increases away from the older cement zones, whereas in oil leg the concentration decreases moving towards younger cement zones (Figures 5.14A & 5.15A). However, there is no much variation in Mn content between individual zones. The Sr is with low values in both oil and water leg of Reservoir F. Reservoir C both in water and oil leg contains cement with an increasing Mn trend and a decreasing Sr trend moving towards younger cement zones (Figures 5.16B, 5.16C, 5.17B & 5.17C). In Reservoir B "water", the highest Fe can be found in Zone 1 (mean=7602 ppm) which decreases towards younger (Zone 3 mean=2687 ppm). Most Mn values are below the detection limit and the higher content can be found in cement Zone 2 (mean= 92 ppm; Figure 5.18B). The Sr values are all below the detection limit (Figure 5.18C).

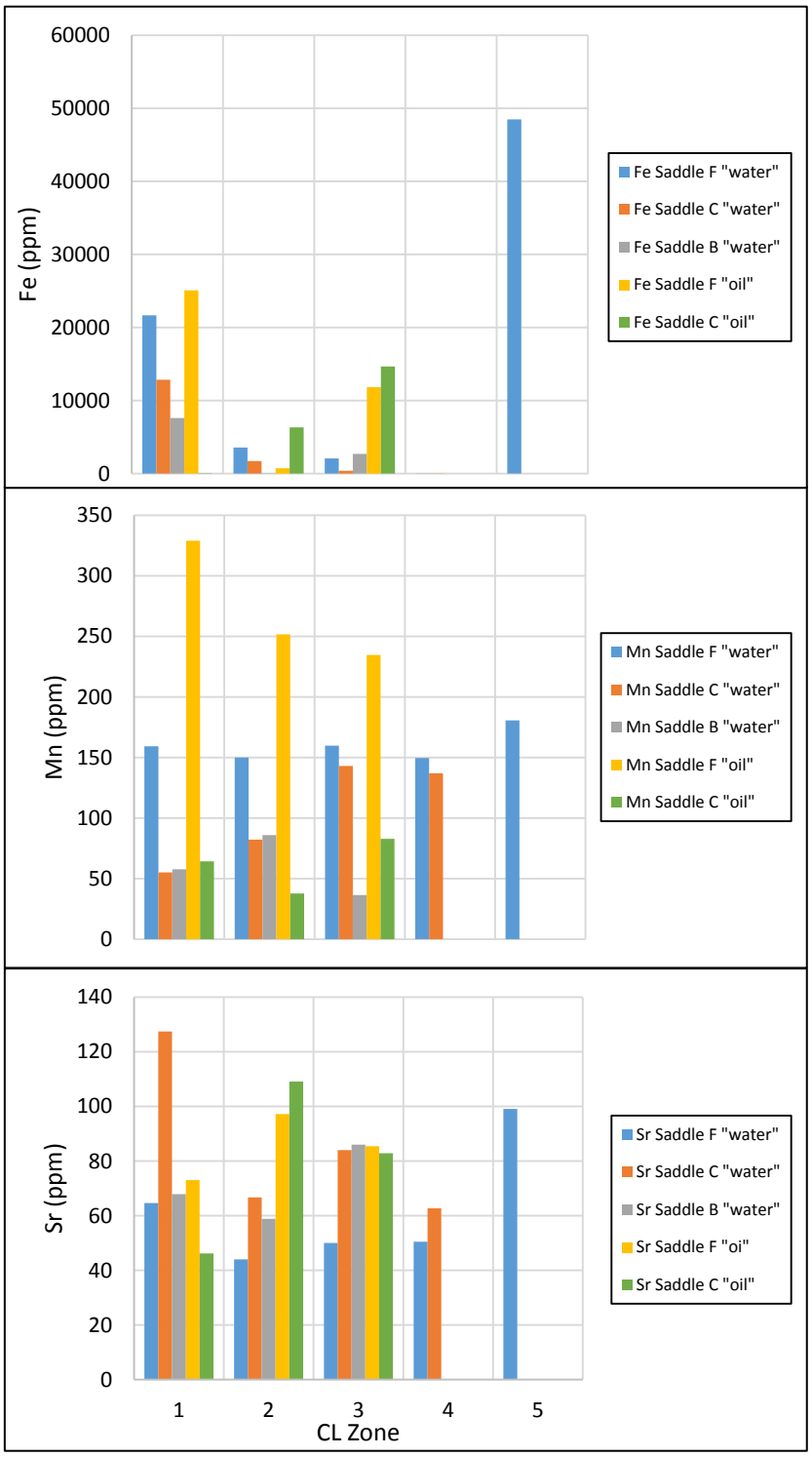


Figure 5.13: Summary of Fe, Mn and Sr concentrations (mean values) for saddle dolomite in all reservoirs: oil versus water. CL cement zones are from 1 to 5. Note that each cement zone is identical for each reservoir.

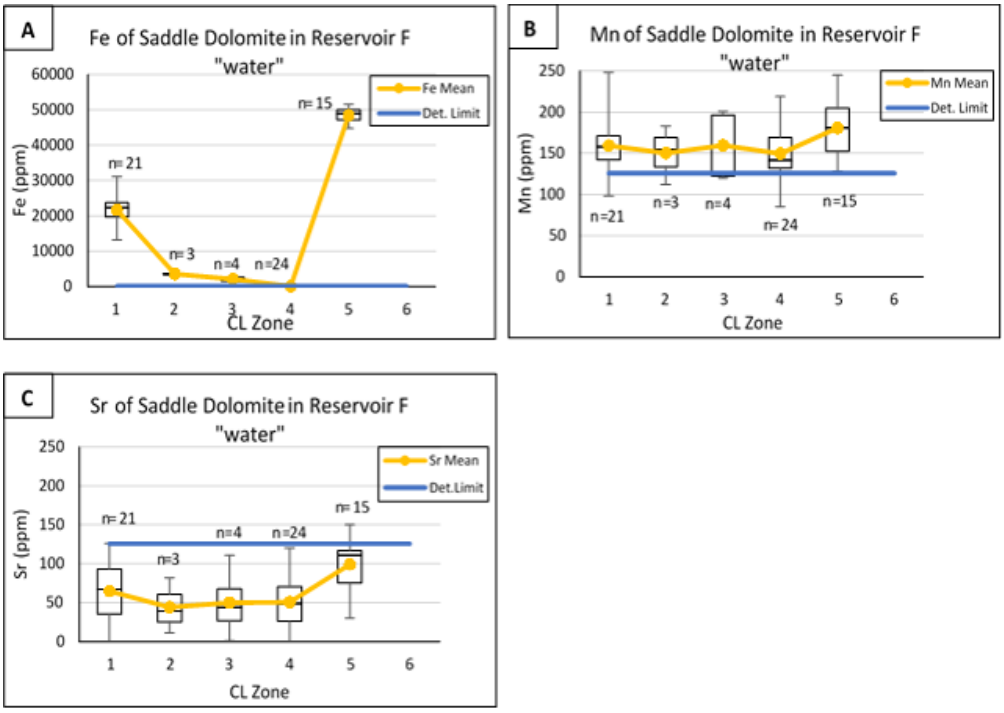


Figure 5.14: Element concentrations of saddle dolomite in Reservoir F in water leg: A) Fe content across CL zones. Note the syncline trend with two peaks at the edges (Zones 1 & 5). B) Mn content across CL zones. Note that there is no significant variation in Mn between cement zones. C) Sr content across CL zones is blow the detection limit, but there is similar trend to Mn. Note that all mean values are below the detection limit.

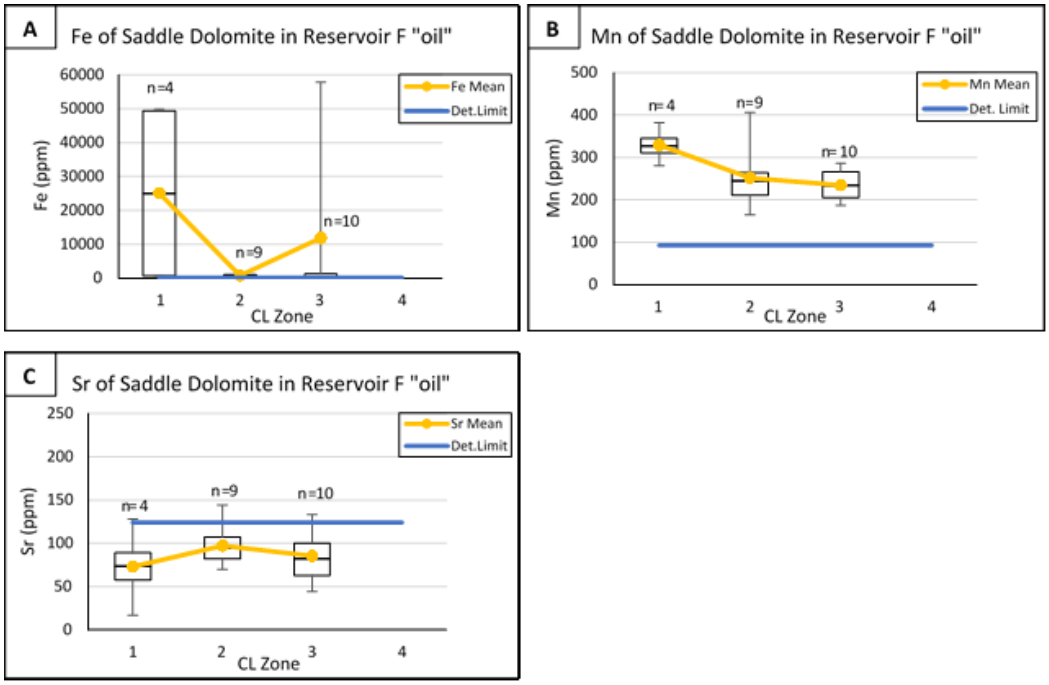


Figure 5.15: Element concentrations of saddle dolomite in Reservoir F in oil leg: A) Fe content across CL zones with highest values in cement Zone 1. B) Mn content across CL zones with highest values in Zone 1. Note the higher Mn content in this sample compared with previous ones. C) Sr content across CL zones with reverse trend to Fe. Note that all mean values are below the detection limit.

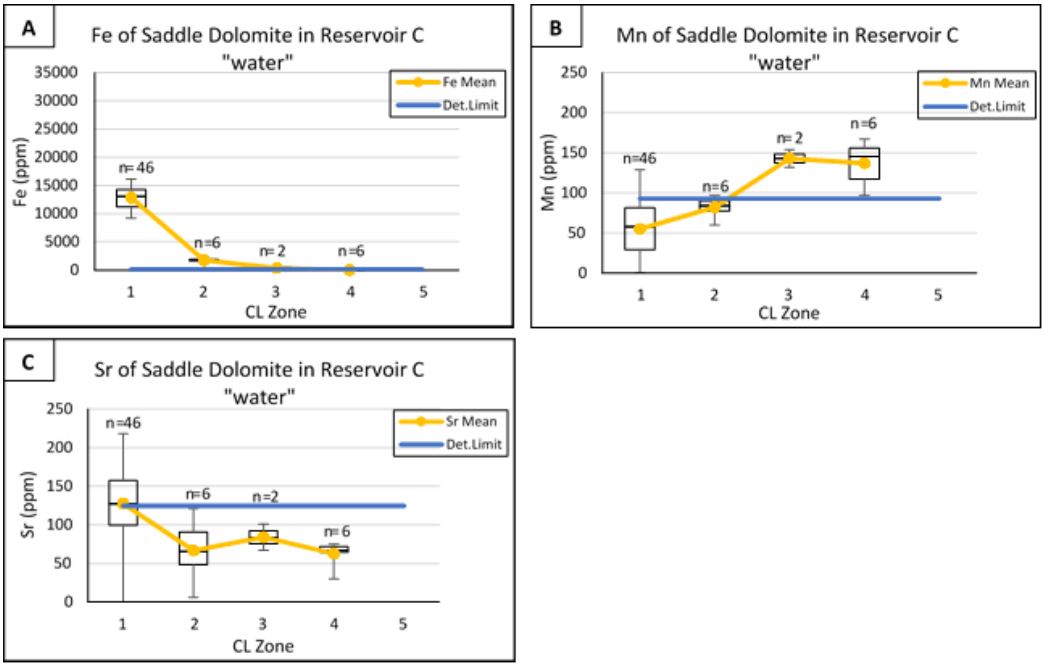


Figure 5.16: Element concentrations of saddle dolomite in Reservoir C in water leg: A) Fe content across CL zones showing decreasing trend towards younger cement zones. B) Mn content across CL zones with highest values in youngest zone. The Mn is increasing towards younger zones. C) Sr content across CL zones with highest values at cement Zone 1. Note that the Sr in this sample has similar trend to Fe and reverse to Mn.

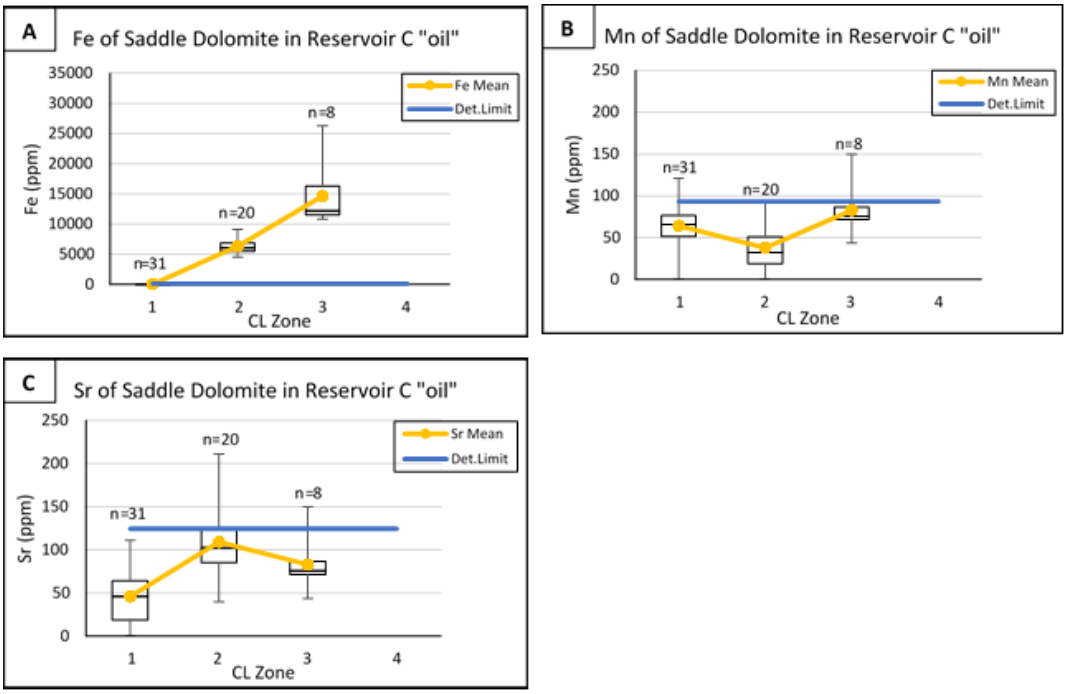


Figure 5.17: Element concentrations of saddle dolomite in Reservoir C in oil leg: A) Fe content across CL zones showing increasing trend towards younger cement zones opposite to the previous sample. B) Mn content across CL zones with all mean values below the detection limit. C) Sr content across CL zones having a reverse trend to Mn. Note that all mean values are below the detection limit having the highest in cement Zone 2.

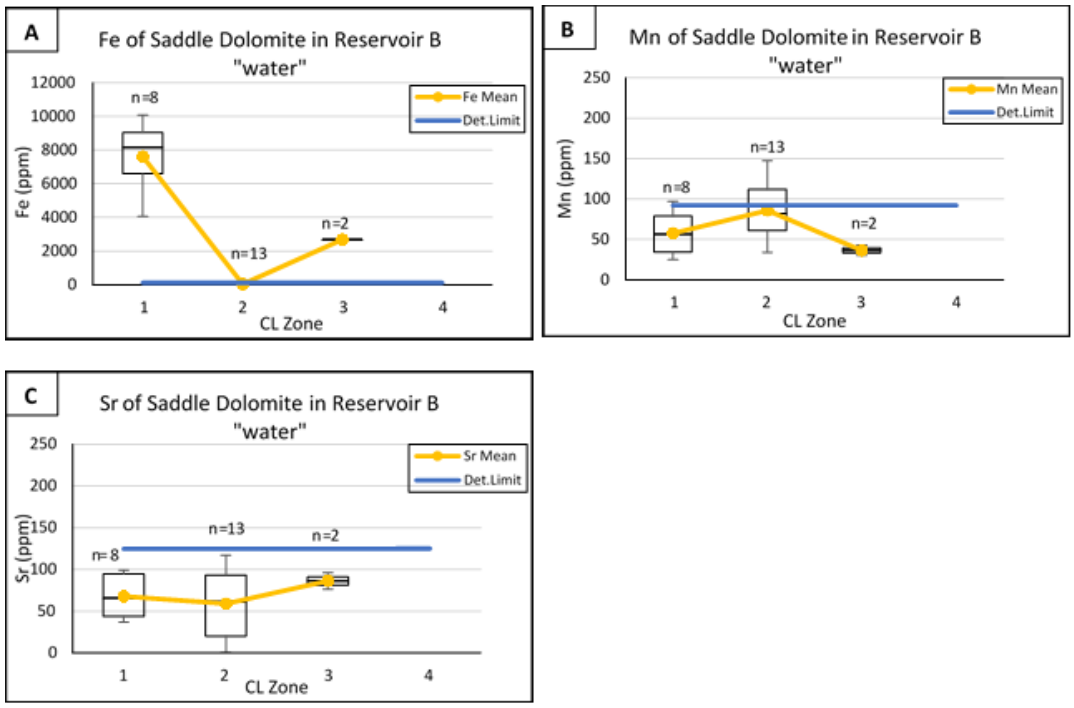


Figure 5.18: Element concentrations of saddle dolomite in Reservoir B in water leg: A) Fe content across CL zones with highest values in cement Zone 1. B) Mn content across CL zones with all mean values below the detection limit. C) Sr content across CL zones having a reverse trend to Mn. Note that all values are below the detection limit.

## 5.5 Discussion

Overall, the highest and lowest Fe content was recorded in saddle dolomite particularly in Reservoir F "water leg" (Figures 5.5, 5.10 & 5.13). In parallel, the highest Mn content was recorded in saddle dolomite in Reservoir F "oil" and rhombic dolomite in Reservoir F "water", while the lowest Mn content was reported in coarse dolomite of Reservoir B "oil". The Sr content with the highest value can be found in rhombic dolomite of Reservoir B "oil", while the lowest value can be found in saddle dolomite in all reservoirs both oil and water legs. The Fe, Mn and Sr concentrations through different stratigraphic unit in oil versus water leg are interpreted below.

### 5.5.1 Origin and Evolution of Rhombic and Coarse Dolomites

The thin zonation of ferroan and non-ferroan replacive rhombic dolomite reflects short sequences of oxic and anoxic episodes. The anoxic episode is represented by the high Fe and Mn content and the opposite for the oxic episode. The high Sr content in rhombic dolomite suggests precipitation from high Sr source. The highest Sr content in the oldest cement Zone 1 across all reservoirs water versus oil indicates that replacive rhombic dolomites in all reservoirs have been supplied with Sr from the same source (i.e. fluids higher in Sr content). The typical source for high Sr in this field is the clay and mud-rich facies found within all stratigraphic units as well as trapped seawater and other exotic silicate rich sources particularly for Reservoir A (see also Section 4.4.1 for clay interpretation). Rhombic dolomite of Arab Formation hosts $^{87}Sr/^{86}Sr$ ratio similar to Jurassic seawater which indicates precipitation from marine pore water (Morad et al., 2012). Moreover, Sr could also be liberated to solution and thus to cement from early aragonite dissolution (Perrin et al., 2014). Al-Hashimi (1976) reported that most of the Sr content removed from the limestone can be lost by progressive dolomitization and only a small amount can be found in newly formed cement. Dolomitization in the studied samples could explain the progressive decrease in the Sr content moving towards younger cement zones in rhombic dolomite (Figures 5.6, 5.7, 5.8 & 5.9).

Comparing the distribution of Mn, Fe and Sr of rhombic and coarse dolomite stratigraphically, it can be found that these elements become more enriched as we move down to deeper reservoirs. This suggest that dolomitization in the lower reservoirs occurred in a more reducing environment compared with upper reservoirs.

The formation of replacive rhombic dolomite may have been initiated in the host limestone prior to stylolitization. This can be supported by 1) the presence of this dolomite in various mud-supported facies with no evidence of stylolitization (Figure 2.17), 2) the clear cross cutting relationship between rhombic dolomite and the stylolites; stylolites cross cut rhombic dolomite (Figures 2.19D & 2.20C), and 3) the consistent carbon isotopic values of these dolomites (+2.8‰ to +4.2‰) similar to Cretaceous seawater reported by Paganoni et al., (2016) which suggest that the dissolved carbon has been most probably supplied by host limestone. However, in some cases rhombic dolomite is found along dissolution seams and stylolites. This rhombic dolomite has been concentrated as less soluble residues as a result of stylolite development and progressed further after stylolite to form younger rhombic dolomite (Paganoni et al., 2016). As a consequence of further burial and stylolite development, younger rhombic dolomite continued to further more extensive replacement of the limestone (Figure 2.20D; Wierzbicki et al., 2006). Thus, stylolites might have acted as conduits for flux of fluids with various compositions, which promoted the formation of further younger rhombic dolomite. This can be supported by the higher inferred temperatures (114–124 °C; average 119 °C) and salinities (9.6–15.0 wt.% NaCl eq.; average 11.2 wt.% NaCl eq.) of rhombic dolomite found along stylolites in both water and oil leg as derived from fluid inclusions (Paganoni et al., 2016). Further dolomitization may result in the formation of latter dolomite as coarser, sub- to anhedral crystals (Merino and Canals, 2011; Wierzbicki et al., 2006).

Generally, the high Fe content in coarse sub-anhedral dolomite in Reservoir B "oil" reveals formation under anoxic conditions. However, the notable decreasing Fe trend suggests that formation fluids become less anoxic towards the younger cement zones (Figure 5.11). The low Mn content supports the same interpretation.

Coarse dolomite in Reservoir C "oil" shows that two significant anoxic events have occurred (Figures 5.12A & B). The first during precipitation of cement Zone 2 and the second significant event during precipitation of the youngest cement zone (Zone 5). The same dolomite records another two intervening oxic events; the first one resulted in precipitation of cement Zone 1 and the second one resulted in cement Zone 3.

### 5.5.2 Origin and Evolution of Saddle Dolomite

The well documented ferroan and non-ferroan zones in saddle dolomite make the transition between anoxic and oxic environments very clear. The highest Fe content found in this type of dolomite indicates that the most anoxic event through dolomite precipitation history occurred during saddle dolomite precipitation. The similarities in some CL zones across the reservoirs suggest that this type of dolomite have been precipitated more or less at the same time in different reservoirs. The general decreasing Fe trend towards younger cement zones found in saddle dolomite in different reservoirs reports changing of precipitation environment from extremely anoxic to oxic environment. This also applies to Reservoir F "water" except for the youngest cement zone which indicates another extreme anoxic event.

Saddle dolomite formation has been attributed by a number of studies to the flux of deep basinal hydrothermal fluids (Breesch et al., 2010; Lavoie and Morin, 2004; Luczaj, 2006; Machel, 2005; Merino and Canals, 2011; Sirat et al, 2016). The main conduit for basinal fluids is believed to be major faults which transport fluids from deeper part of the basin to the overlying sediments which then travel laterally through the strata. Another possible conduit for fluid migration could be stylolites (Wierzbicki et al., 2006). Evidence of this is the ultimate association of volumetrically high dolomite along and around the vicinity of stylolites (Figures 2.19C & D).

Hydrothermal dolomitization has been closely linked to the tectonic faulting and fracturing (Haeri-Ardakani et al., 2013; Davies and Smith, 2006; Lonnee and Machel,

2006). In field A, hot basinal (hydrothermal) fluids were most likely transported originally via the NW-SE faults that cross the field and then migrated along fractures and stylolites into permeable rocks causing dolomitization. The high temperature (125–140 °C; average 136 °C), and high salinities (21.5–22.1 wt.% NaCl eq.; (average 21.7 wt.%) from fluid inclusions found in the saddle dolomite particularly along stylolites possibly indicates an origin from warm, saline hydrothermal fluid (Haeri-Ardakani et al., 2013; Paganoni et al., 2016). This fluid has probably undergone several phases of chemical evolution as reflected by the zonation found in saddle dolomite. The elevated Fe content in dark zones implies that the hot basinal brine was interacted with Fe rich source. The most likely known Fe rich source is the siliciclastic sediments (Ruppel and Cander, 1988; Woronick and Land, 1985). The interaction of the fluids with silicate rich sediments can be further supported by the existence of kaolinite which is Al and Si rich mineral. Possible silicate rich source rocks for Thamama Reservoirs is the Lower Shuaiba shale or Upper Jurassic Diyab Formation (Alsharhan and Scott, 2000; Al-Suwaidi et al., 2000; Gumati, 1993; Loutfi and El Beshlawy, 1986; Murris, 1980; Oswald et al., 1995).

### 5.5.3 mMg:Ca Ratio and Dolomitization Model

According to the calculated mMg:Ca ratios (Figure 5.2) all types of dolomite are Ca rich suggesting that this mineral is non-stoichiometric. Thus, dolomite in this field could be referred as calcic dolomite. Moreover, knowing that this is a Ca-rich dolomite one can infer from the modified Warren's (2000) dolomite classification (Figure 5.19) that all rocks with dolomite 0 to 50% should occupy either the Dolomitic Limestone (DL) or Impure Dolomitic Limestone (IDL) fields. Thus, all dolomite types in the studied rocks fall in the category of Dolomitic Limestone.

The higher mean mMg:Ca ratio (~1.4) in rhombic dolomite than coarse and saddle dolomite provides another clue as to differences in the origin of the precipitating. Higher mMg:Ca ratio in rhombic suggests that dolomite have been supplied with fluids characterized by lower Mg and higher Ca compared with saddle

dolomite. However, we still need to consider about a higher Mg source in order to produce rhombic dolomite; in general dolomitization requires higher Mg in order to occur. A possible source is the dewatering from the same and/or surrounding strata especially if the source rock is rich in silica. The dewatering of dense intervals which are rich in clay can possibly provide fluids with higher Mg, Sr and possibly Fe and Mn. The enrichment of Mg (lower mMg:Ca, mean= ~1.2) and Sr in rhombic dolomite of Reservoir A compared with other reservoirs (mean: B=1.3, C=1.4, F=1.4) is due to higher silica content in the source rock (see Section 5.5.1). Moreover, Reservoir A contains thick and abundant dissolution seams compared with other reservoirs (Figure 2.20A). This implies that Reservoir A has undergone considerable dewatering which resulted in realise of higher Sr and Mg content and the insoluble residues have accumulated as thick dissolution seams.

Hence the best dolomitization model that can explain the formation mechanism of earlier rhombic dolomite is the burial compaction model sourced by pore water. The original chemical composition of this earlier rhombic dolomite should be different from the later phase found along stylolites. The most likely fluid source for earlier rhombic dolomite is the trapped seawater (Morad et al., 2012; Paganoni et al., 2016). In general, carbonate cements of similar studied rocks have carbon isotopic signatures $\delta^{13}C_{VPDB}$ similar to Cretaceous seawater which indicate that carbonate cements were probably sourced by pore fluid that contain dissolved carbonate of host limestone (Paganoni et al., 2016).

The processes of microbial dolomitization remains poorly understood and experimental work failed to show both the natural replacement habit of dolomite and the rhombohedral crystal shape. However, a microbial-organogenic dolomite model might still explain the formation of some rhombic dolomite in this studied section. Evidence of microbial activity can be supported by the abundant micritization found in this study (Section 2.5.2) and the spheroidal particles reported in same reservoir of different study (Morad et al., 2016). The core of rhombic dolomite found in this field is mud-rich (Figure 2.17D-F). Hence, dolomitization may have been initiated by microbial-organogenic dolomitization indicated by the mud rich cores of older

(earlier) rhombic dolomite compared with poor mud core of the younger rhombic dolomite (Figure 2.17G). The further rhombohedral crystals may have been obtained as dolomitization progress further; dolomite continued to precipitate as an overgrowth mechanism (like the case of syntaxial calcite) to form rhombohedral crystal.

Dewatering is not a sufficient source to precipitate coarse dolomite and a volumetrically higher saddle dolomite cement. Thus, coarse and saddle dolomite have probably been sourced by an exotic fluid which is sufficient to precipitate a high volume of dolomite (see Section 5.5.2). This exotic fluid has higher Mg than the source fluid of rhombic dolomite which is indicated by the lower mMg:Ca ratio of coarse and saddle dolomite compared with rhombic dolomite.

As the mMg:Ca ratio is lower in saddle dolomite than the other dolomites and the Fe content is higher in saddle dolomite, we can infer that the Ca cations in saddle dolomite have been replaced mostly by Fe cations. Interestingly, the mMg:Ca ratios for all saddle dolomite in water versus oil have mean values close to 1.1 (Figure 5.4) which suggests that saddle dolomite in all reservoirs (oil versus water) have been precipitated at the same time and from the same dolomitizing fluids.

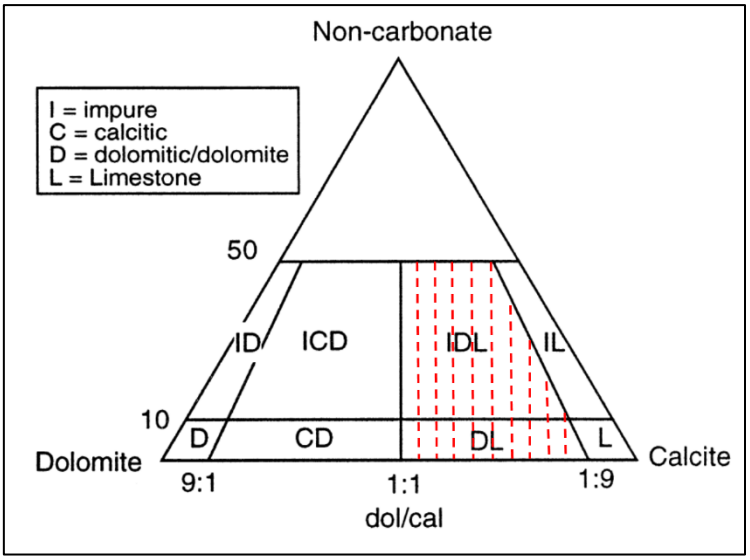


Figure 5.19: Dolomite classification based on dol/cal ratio and dolomite %, modified after Warren (2000) (after Leighton and Pendexter, 1962). The shaded interval is the mostly field where the dolomite of this study could lay.

The dolomitization model that can best describe the formation mechanism of this late (burial) saddle dolomite in this field is the tectonic-hydrothermal model. The model may also be the source for the formation mechanism of younger rhombic and coarse dolomite. The lines of evidences are 1) the similar elements properties between the younger cement zones of rhombic dolomite, coarse dolomite and early cement zones of saddle dolomite. 2) some $\delta^{18}O_{VPDB}$ values of rhombic dolomite overlap with $\delta^{18}O_{VPDB}$ values of saddle dolomite. 3) the mMg:Ca ratio for some rhombic dolomite and saddle dolomite lies within the same range. 4) the dolomitization fluid is suggested to be subsurface brine which is believed to be transported via major faults, fractures and stylolites. 5) the ultimate association of saddle dolomite and sometime rhombic and coarse dolomite in the vicinity, along stylolites and in fractures (only saddle dolomite in fractures).

## 4.5 Summary

Dolomites are an important hydrocarbon reservoir rocks which can be formed directly from seawater and/or diagenetically in several sedimentary environments. Despite several attempts to precipitate dolomite in the laboratory under ambient temperatures and pressures, dolomite remains poorly understood due to its low kinetics. The kinetic problem is related to crystal structure ordering which controls nucleation and growth of dolomite. This crystal structure ordering together with mineral stoichiometry is used to classify a high Mg mineral as stoichiometric or non-stoichiometric dolomite or HMC/VHMC. Our dolomite is mostly Ca rich calcic dolomite referring to non-stoichiometric dolomite.

Three dolomites are noted; type 1: rhombic dolomite (old and young), type 2: coarse dolomite, type 3: saddle dolomite. All dolomite types show zonation containing ferroan and non-ferroan zones. The ferroan zones reflect significant time of anoxic precipitation while the non-ferroan zones represent periods of oxic precipitation. The fluctuating episodes of oxic and anoxic suggest that dolomitization fluids have

undergone dynamic chemical evolutions. The highest Fe content was reported in saddle dolomite indicating that the most anoxic event through dolomite precipitation history occurred during saddle dolomite precipitation.

The Sr content in rhombic dolomite is higher than coarse and saddle dolomites which suggests precipitation from high Sr source. The highest Sr content was found in the oldest cement Zone 1 across all reservoirs water versus oil. This indicates that replacive rhombic dolomites in all reservoirs have been supplied with Sr from the similar source which is rich in Sr. Possible high Sr sources are the clay and mud rich facies, exotic silicate rich sources (especially for Reservoir A), and early aragonite cement dissolution.

The difference in mMg:Ca ratios between rhombic and saddle dolomite suggest different formation conditions at different times. Higher mMg:Ca ratio in older rhombic dolomite suggests fluids characterized by lower Mg and higher Ca compared with younger rhombic, coarse and saddle dolomite.

The burial compaction model is proposed for the formation of older rhombic dolomite. Here, rhombic dolomite in this model can be sourced by pore fluids which contain dissolved carbonate of the host limestone. This has been interpreted based on the carbon isotopic signatures found in rhombic dolomite which have δ13CVPDB similar to Cretaceous seawater.

Saddle dolomite is found more often associated with fractures and stylolites and in large moldic pores nearby. In order to precipitate dolomite an adequate supply of Mg is required. Mg may be supplied from exotic fluids which are likely to be hydrothermal fluids. The best dolomitization model that describes this formation mechanism is the tectonic-hydrothermal model. Younger rhombic and coarse dolomite are believed to be precipitated from same dolomitizing fluid. This interpretation is based on 1) the similar elemental properties for these three dolomites, 2) a similar mMg;Ca for younger rhombic dolomite and saddle dolomite, 3) the association of saddle dolomite and sometimes rhombic and coarse dolomite in the vicinity and along

stylolites, 4) similar $\delta^{18}O_{VPDB}$ values for rhombic dolomite and saddle dolomite (Paganoni et al., 2016). Subsurface brine is suggested to be the likely source for this dolomitization mechanism based on higher, Mg content (lower mMg:Ca ratios), temperature and salinity found in late dolomites.

# Chapter 6: Understanding the Temperatures of Calcite Cementation

## 6.1 Introduction

The existence and the origin of isotopes in nature was proven by Frederick Soddy in 1913 leading him to the 1921 Nobel Prize in chemistry. Since then, isotopes have been applied broadly for investigating different aspects including hydrology, ecology, meteorology, geochemistry, and climatology (Sharp, 2017). Stable isotope geochemistry can be applied for wide range of elements, however the most commonly used elements are H, C, N, O and S due to their higher abundance in living organism's tissues. The use of stable isotopes is built on the principle of isotope fractionation established first by Briscoe and Robinson (1925). Isotope fractionation is based on the differences in the masses and thermodynamic properties of two different isotopes (heavy versus light). The difference in the absolute isotope ratio between two isotopes can be expressed as "δ".

In Earth Sciences, stable isotopes have been used (1) as thermometry to infer to the formation temperatures of gas systems, minerals and rocks as well as in reconstructing the past climatic conditions, (2) as tracers for the origin of rocks, fluids, plants, etc., (3) in reaction mechanisms to investigate the state at which the reactions have occurred (e.g. open versus close system), and (4) for chemostratigraphy in which the stable isotope excursions are used as indicators for stratigraphy, ocean productivity and atmospheric chemistry.

The use of $\delta^{16}O$ and $\delta^{18}O$ oxygen isotopes as a thermometer was not effective until 1947 when Urey determined the significance of temperature coefficient of fractionation between $CaCO_3$ and $H_2O$ in shells as temperature proxy. Urey stated "I

suddenly found myself with a geological thermometer in my hand". Since then, oxygen isotope thermometer has been broadly applied in different research areas.

Factors affecting seawater isotopes are summarized by Sharp (2017). The main factors that can lower $\delta^{18}O$ include continental and seawater weathering and lower salinity caused by the introduction of fresh water. In contrast, higher $\delta^{18}O$ can be attained by hydrothermal alteration of ocean basalt, glaciation and higher salinity (higher than normal seawater).

Stable oxygen and carbon isotopes have been widely used to constrain the environment of deposition of sedimentary rocks because they thought to retain the compositions of the environmental water (Clayton and Degens, 1959; Keith and Weber, 1964; Keith et al., 1964; Pucéat, et al., 2003). The $\delta^{18}O/ \delta^{16}O$ ratios of carbonate rocks are known to often decrease with increasing geological age/depth (Kasting et al., 2006). The stable isotope proxies of carbonate skeletons have been used to reconstruct marine palaeotemperatures and global climatic changes (Barrera et al., 1987; Clarke and Jenkyns, 1999; Ditchfield et al., 1994; Huber et al., 2002; Kolodny and Raab, 1988; Puce´at, et al., 2003). Carbon isotopes have been used as redox indicator for the periods of anoxic ocean deposits, which are thought to be important for hydrocarbon accumulation (Gröcke et al, 1999; Herrle et al., 2015; Méhay et al., 2009; Stein et al., 2012; Westermann et al., 2013).

Many studies consider the use of oxygen isotopes to infer to the temperatures, compositions and evolution of fluids at which cements were precipitated in Thamama rocks (Alsharhan et al., 2000; Cox. et al., 2010; Morad et al., 2016; Neilson et al., 1998; Oswald et al., 1996; Paganoni et al., 2016; Thorpe, 2014; Vahrenkamp et al., 2014). These studies reported various compositions of $\delta^{18}O$ suggesting precipitation conditions of marine seawater that evolved to higher temperatures through water-rock interaction in a relatively closed system and/or from variety of water compositions.

Water-rock interaction is the process between the solid rock and the existing pore water that involves chemical and thermal exchanges. The $\delta^{18}O$ is thought to alter by

water-rock interaction with various amplitudes in closed versus open systems (Sharp, 2017). In a closed system, marine carbonate that precipitates at a temperature close to the original marine water will most likely return the original isotopic composition. The isotopic composition of very early cement should remain unaltered in this case. However, later precipitated cements may record a shift in $\delta^{18}O$ due to the increased water-rock interaction with progressive burial. Both oxygen isotopes and trace elements have been applied successfully to understand both ancient seawater isotope and elemental compositions as well as the evolution of pore fluids through time (Budd, 1984; Carpenter and Lohmann, 1992; Carpenter et al., 1991; Cicero and Lohmann, 2001; Cox. et al., 2010; Gonzalez and Lohmann, 1985; Hasiuk and Lohmann, 2008; Thorpe, 2014). On the other hand, a marine carbonate may lose the original marine isotopic composition due to the higher water-rock interaction in an open system (Al-Aasm and Azmy, 1996; Uwe and Veizer, 1980; Sharpe, 2017). However, marine carbonate may escape significant diagenetic alteration and preserve original isotopic compositions in such system (Al-Aasm and Azmy, 1996; Sharpe, 2017).

This chapter aims to study the $\delta^{18}O$ of Cretaceous carbonate rocks from five reservoirs to:

1) Investigate the temperature evolution of pore fluids from which equant, syntaxial and blocky (first generation: BI) calcite cements were precipitated using in-situ (SIMS) $\delta^{18}O$ data,

2) Compare mMg/Ca ratio with in-situ $\delta^{18}O$ data to understand the temperature evolution of pore fluid stratigraphically and across individual reservoirs, and

3) Reconstruct the timing and chemical conditions of individual calcite cements relative to each other and to the timing of oil emplacement.

## 6.2 Samples and Methodology

Different types of calcite cement were analyzed, including syntaxial, equant and blocky from the oil leg (see Table 6.1 for more details). Results are compared to another study that covered Reservoirs G, B and A (Thorpe, 2014). In situ (SIMS) oxygen isotope data were collected from the oldest to youngest zones through each cement. The spacing between data points was decided based on the apparent length of each crystal, number of CL zones in each crystal and beam size. Then, number of measurement in each CL zone was passed on apparent width and length of each CL zone that can fit ion beam size of 10-15 μm diameter. For example CL zone with apparent width of 35μm and length of 90μm will not allow for more than 3 measurements.

Five polished thin sections were used to obtain in-situ $\delta^{18}O_{VPDB}$ on a Cameca 1270 in-house ion microprobe. These thin sections were also used for prior EPMA and CL studies so that cementation conditions (temperature, fluid composition and relative timing) can be tested using different independent variables.

Samples are 24 - 24.5mm in diameter and less than 12 mm thick, and were coated with gold. Analysis can cover the area within ~9 mm of the center but for high precision the coverage was reduced to +/- 5 mm from the center. For all performed analysis the standard was mounted within the samples.

Two methods were used to prepare the samples. In the first method, the standard was embedded in a hole (~ 2.5 mm) drilled in the center of the thin section using an ultrasonic drill. In the second method, multiple specimens were mounted into an Indium block together with the standard. Each core is ~ 2.0 mm in diameter. All samples were then cleaned with Acetone and then Ethanol. The instrument can take up to two samples at a time and each sample needs four to five hours to be analyzed. A Cs ion beam of 10-15 μm diameter spot was used in this analysis. The internal precision of each spot is ranging between 0.009 and 0.015 (% standard

Error). The external precision is estimated according to the consecutive analysis of a UWC (University of Wisconsin Calcite) standard (~0.3‰-0.4‰) and it is assessed to be homogenous.

Since the navigation under the ion probe is difficult samples were mapped using SEM and reflected light microscope before final cleaning and coating. The Reflected light photo-micrograph provided much closer view to the ion microprobe than SEM and hence they were used to navigate to the areas of interest under ion probe. For more details see Section 1.5.2.5.

Table 6.1: Distribution of measurements run in different calcite cement types and reservoirs.

| Reservoir | Run (R) Number | Calcite Type | Number of Measurements |
|---|---|---|---|
| G | R 1 | Blocky | 6 |
| | R 2 | Blocky | 4 (1 cancelled) |
| | R 3 | Syntaxial | 5 |
| | R 4 | Equant | 2 |
| | R 5 | Syntaxial | 2 |
| | R 6 | Syntaxial | 2 |
| | R 7 | Blocky | 4 (1 cancelled) |
| | R 8 | Blocky | 2 |
| | R 9 | Blocky | 3 |
| F | R 1 | Blocky | 7 (2 cancelled) |
| | R 2 | Equant | 3 |
| | R 3 | Syntaxial | 3 |
| | R 4 | Equant | 2 |
| C | R 1 | Syntaxial | 5 |
| | R 2 | Syntaxial | 5 |
| | R 3 | Syntaxial | 5 |
| | R 4 | Syntaxial | 2 (all cancelled) |
| | R 5 | Syntaxial | 3 (2 cancelled) |
| | R 6 | Syntaxial | 10 |
| | R 7 | Blocky | 10 |
| B | R 1 | Equant | 2 |
| | R 2 | Syntaxial | 5 |
| | R 3 | Equant | 4 |
| | R 4 | Equant | 5 |

## 6.3 Results

### 6.3.1 Cement Stratigraphy

Figure 6.1 gives a summary of cement stratigraphy in the oil and water legs constructed from the CL zonation established in Chapter 3. Overall, the shallower Reservoirs including B and A record longer cementation history compared with deeper Reservoirs (F and C). Furthermore, Reservoir B oil shows that cementation continued for a longer time compared to the water leg. Reservoirs F and C show more or less similar cementation times in both oil and water.

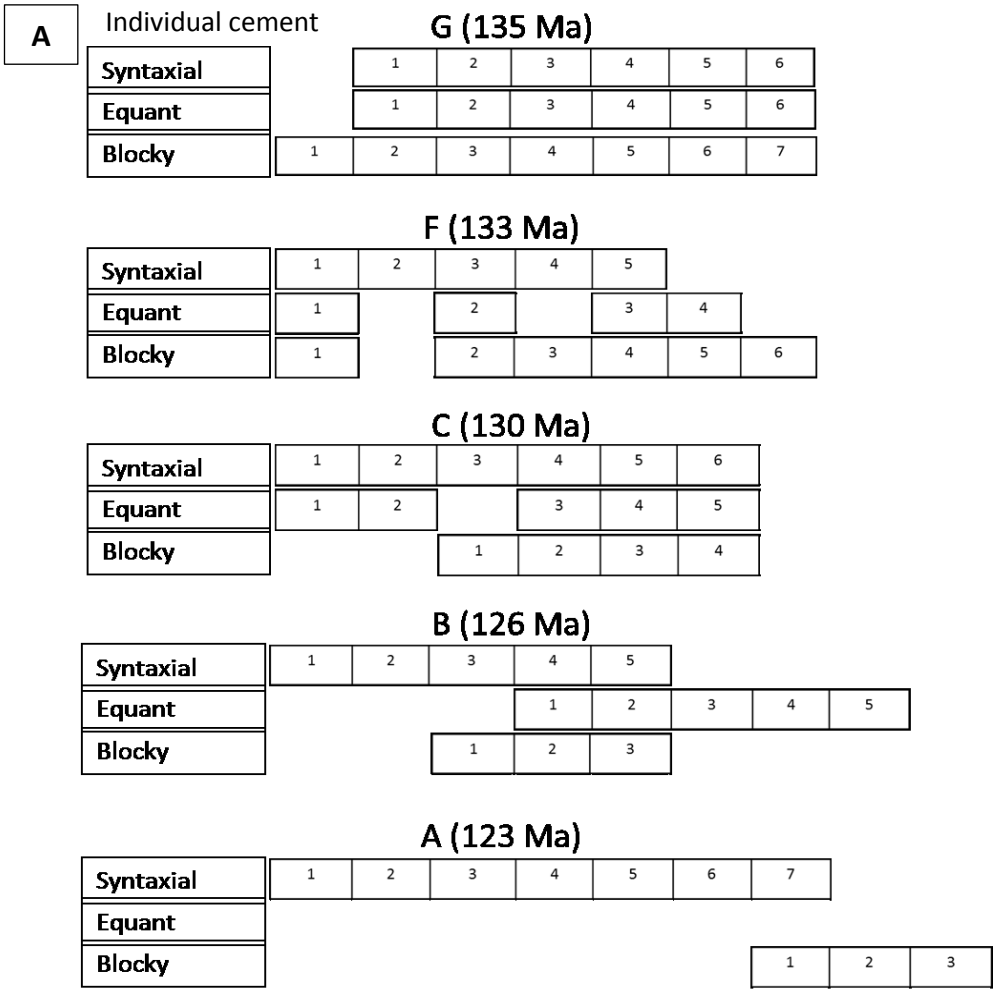

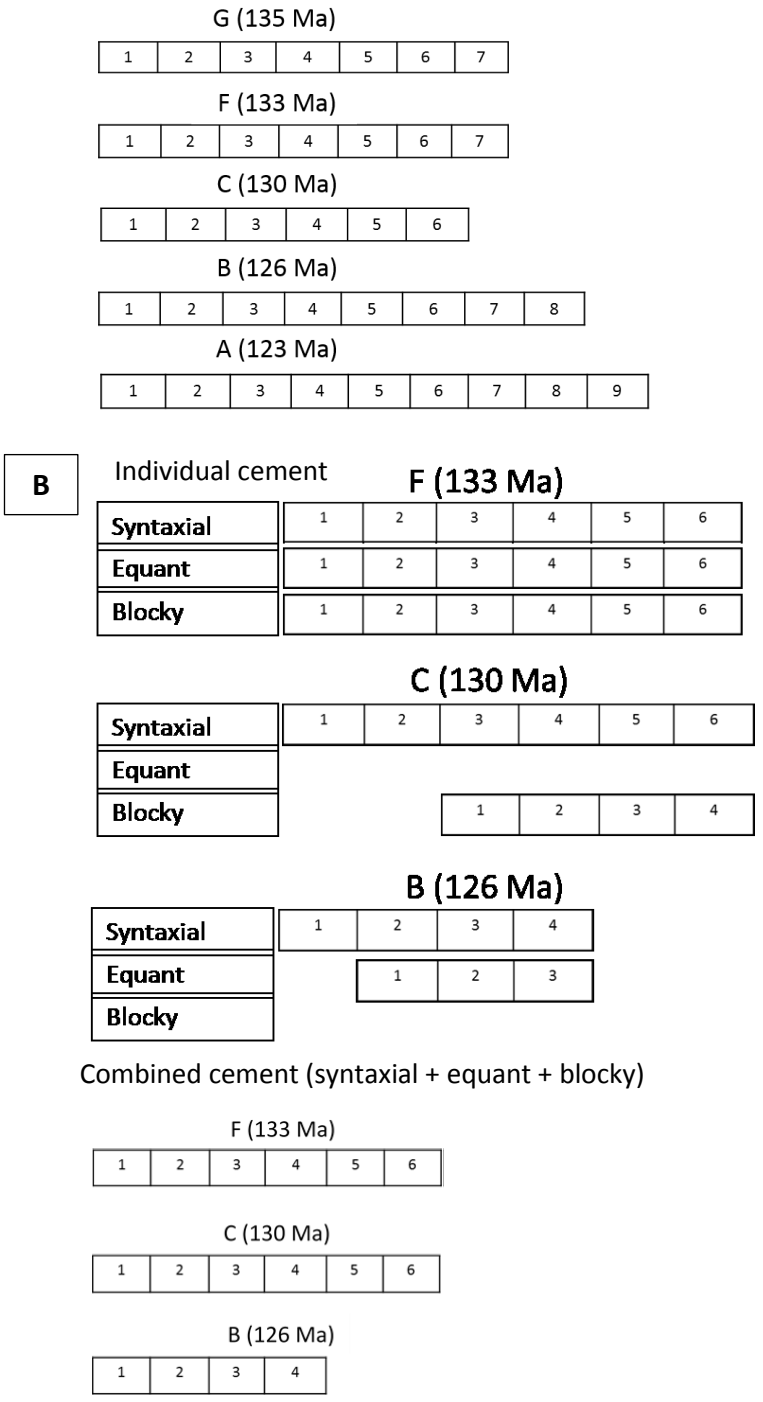


Figure 6.1: Summary of the relative cement stratigraphy including individual syntaxial, equant, and blocky calcite and combined cement in A) Oil leg for all Reservoirs. B) Water leg for Reservoirs F, B, and C.

### 6.3.2 SIMs Oxygen Isotope Data

This section contains results from this study (Field A) and another study which contains two nearby fields (Fields B & C) of the same age (Thorpe, 2014). All data are given in Appendix D.

The measured $\delta^{18}O_{VPDB}$ of this study differs across the different reservoirs (Figure 6.2A). Figure 6.2 summarizes the mean and range of $\delta^{18}O_{VPDB}$ shown by boxplots of all analyzed calcite cements, syntaxial (Figure 6.2B), equant (Figure 6.2C) and blocky (Figure 6.2D) in all reservoirs. $\delta^{18}O_{VPDB}$ is more depleted in Reservoir G (135 Ma, mean= -8.98‰), B (126 Ma, mean= -9.65‰) and A (123 Ma, mean= -9.66‰) compared with F (133 Ma, mean= -2.42‰) and C (130 Ma, mean= -5.39‰) for all calcite types. Overall, Reservoir B hosts the most depleted $\delta^{18}O_{VPDB}$ of the studied successions.

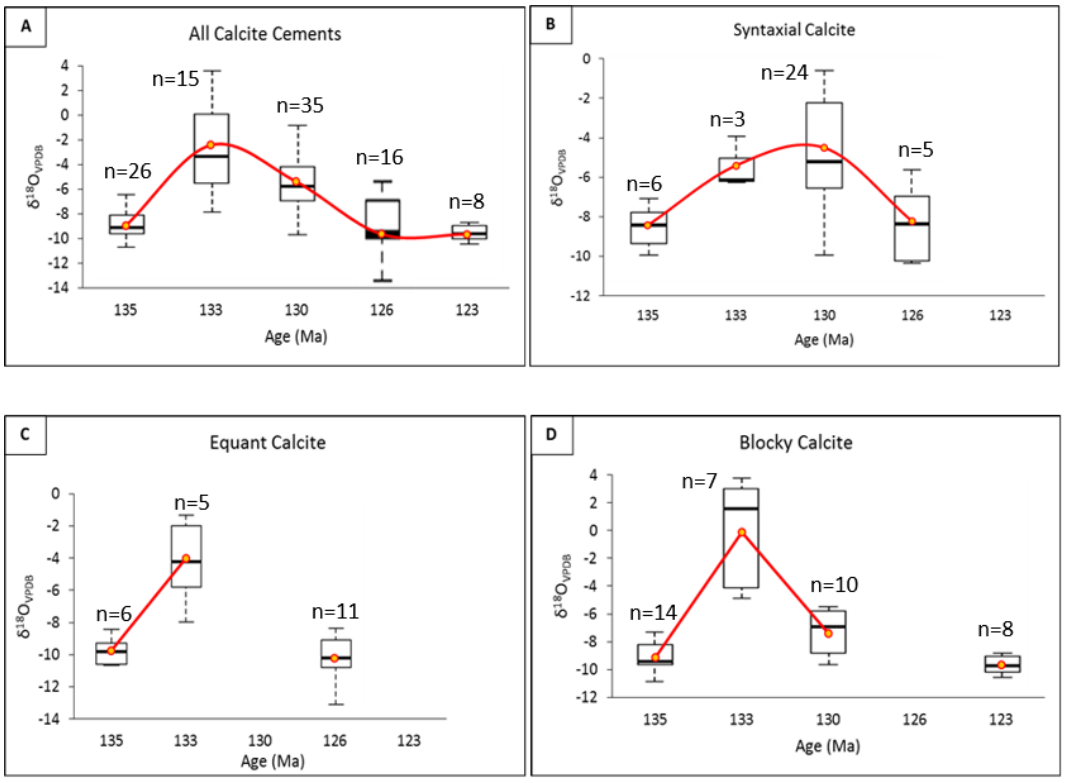


Figure 6.2: $\delta^{18}O_{VPDB}$ of syntaxial, equant and blocky calcite across the five reservoirs. A) $\delta^{18}O_{VPDB}$ for all calcite in individual reservoir. B) $\delta^{18}O_{VPDB}$ for syntaxial calcite only. C) $\delta^{18}O_{VPDB}$ for equant calcite only. D) $\delta^{18}O_{VPDB}$ for blocky calcite only.

Figure 6.3 shows all measured $\delta^{18}O_{VPDB}$ including early and late cements in Field A with the published $\delta^{18}O_{VPDB}$ of Cretaceous seawater including major glaciation and Oceanic Anoxic Events (OAE) for period from 140-70 Ma (Pucéat et al., 2003). The data show wide spread range within each reservoir and across different stratigraphic units. Reservoirs F and C record $\delta^{18}O_{VPDB}$ values mostly close to Cretaceous seawater. While Reservoirs G and B mostly contain higher negative $\delta^{18}O_{VPDB}$ values compared with Cretaceous seawater.

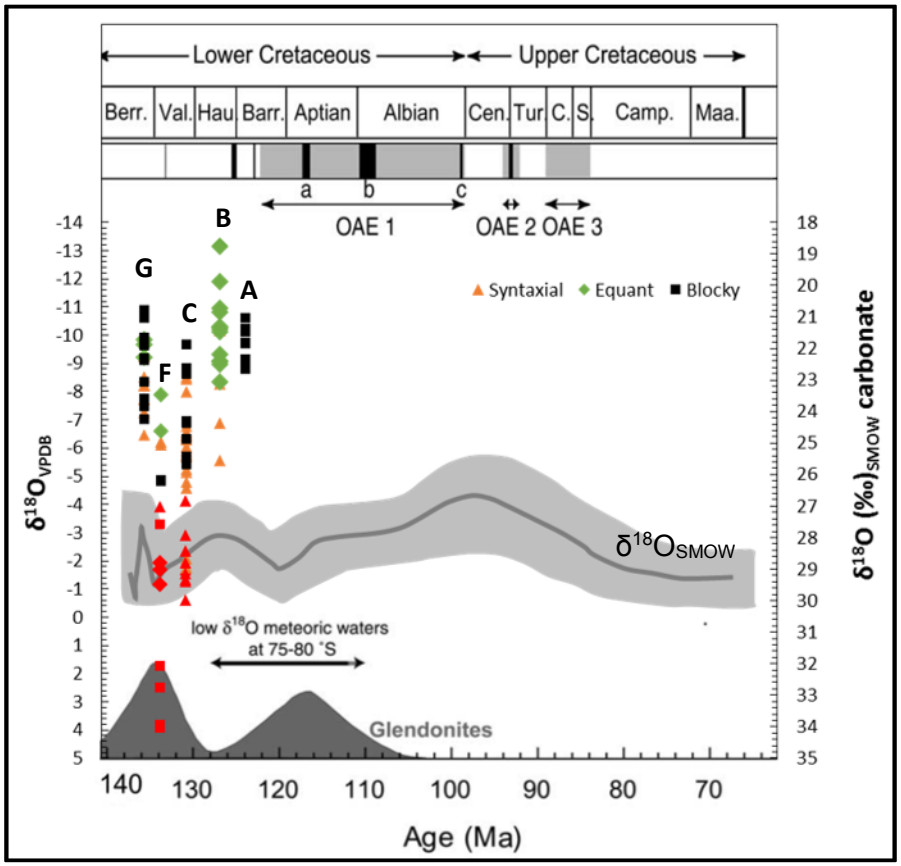


Figure 6.3: Measured $\delta^{18}O_{VPDB}$ of equant, syntaxial and blocky calcite for all reservoirs with published $\delta^{18}O_{SMOW}$ of Cretaceous seawater (Modified after Pucéat et al., 2003). Red symbols indicate early (oldest) cement zones.

Considering the $\delta^{18}O_{VPDB}$ run along individual CL zones in different calcite types (Figure 6.4), $\delta^{18}O_{VPDB}$ generally becomes more negative from older cement zones towards younger cement zones. The $\delta^{18}O_{VPDB}$ of Reservoir A starts with -1.20‰

(individual measurement) at Zone 1 (equant, Field B) and ends up with -10.32‰ at Zone 9 (blocky, Field A; Figure 6.4A). In Reservoir B (Figure 6.4B), $\delta^{18}O_{VPDB}$ varies from -5.56‰ at cement Zone 3 (syntaxial, Field A) to -13.16‰ at cement Zone 8 (equant, Field A). In Fields B and C, $\delta^{18}O_{VPDB}$ ranges from mean= -11.20‰ at Zone 8 to mean= -11.90‰ at Zone 9 and from -4.80‰ at Zone 2 to mean= -10.70‰ at Zone 9 respectively (Thorpe, 2014).

Reservoir C starts with $\delta^{18}O_{VPDB}$ mean of -1.39‰ at cement Zone 1 (syntaxial, Field A) and ends up with mean= -8.5‰ (syntaxial, Field A) and mean= -9.2‰ (blocky, Field A) at cement Zone 6 (Figure 6.4C). The oldest cement zone in Reservoir F has $\delta^{18}O_{VPDB}$ mean value of -1.57‰ (equant, Field A) and 3.00‰ (blocky, Field A) while the younger cement Zone 5 has $\delta^{18}O_{VPDB}$ mean values of -7.24‰ measured from equant calcite (Figure 6.4D). The measured $\delta^{18}O_{VPDB}$ at older cement Zone 2 (blocky, Field A) from Reservoir G is -8.23‰ which is depleted to -10.89‰ and -10.40‰ (mean) at younger cement Zone 7, blocky and equant respectively. Field C shows lower negative $\delta^{18}O_{VPDB}$ in the older cement zones compared with measured ones. Cement Zone 2 has $\delta^{18}O_{VPDB}$ mean of -5.9‰ which depletes to -7.00‰ at cement Zone 5 (Thorpe, 2014).

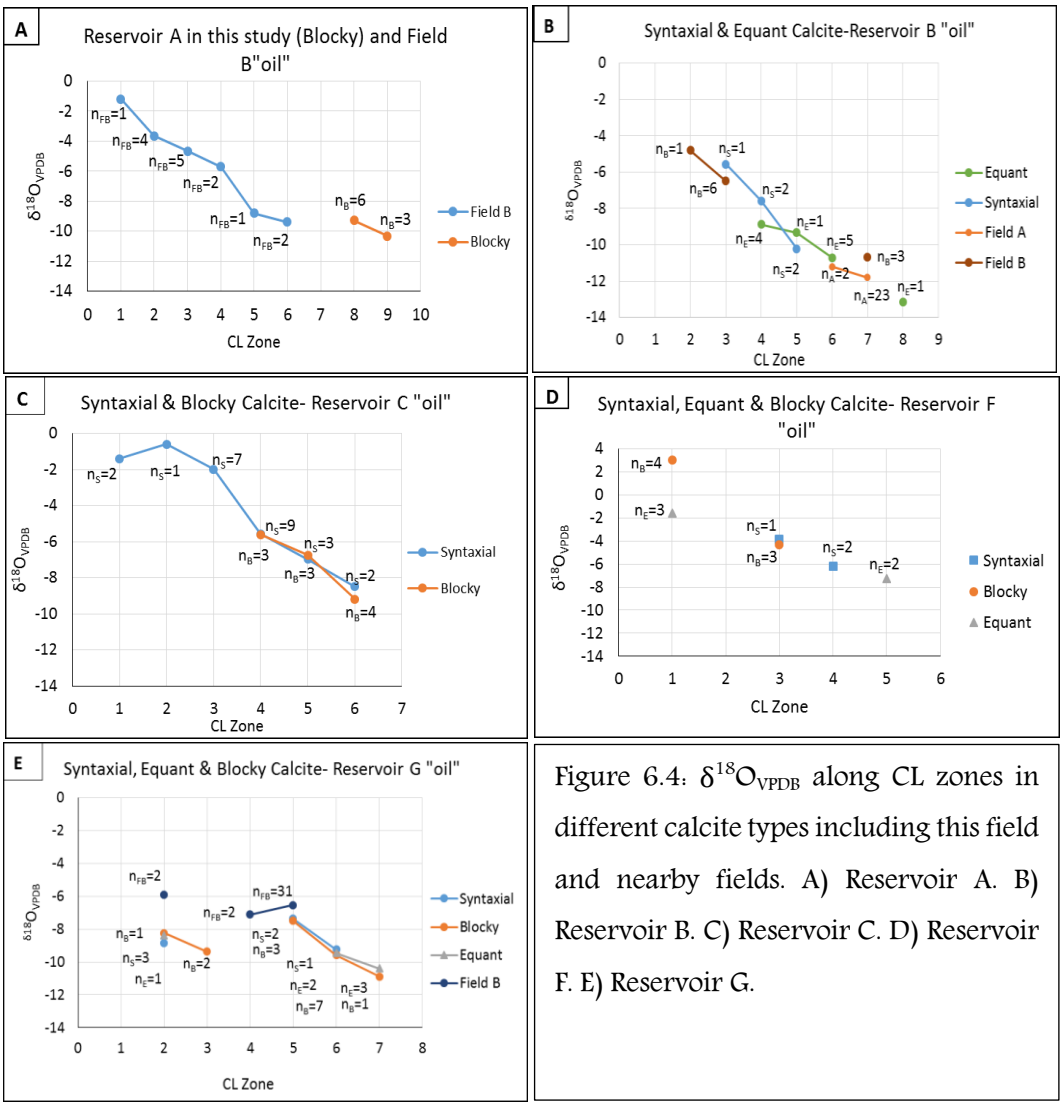


Figure 6.4: $\delta^{18}O_{VPDB}$ along CL zones in different calcite types including this field and nearby fields. A) Reservoir A. B) Reservoir B. C) Reservoir C. D) Reservoir F. E) Reservoir G.

## 6.4 Discussion

### 6.4.1 Origin and Evolution of Calcite Cement Pore Fluids

#### 6.4.1.1 Early Cementation: Evidence of Precipitation from Early Cretaceous Seawater

The oldest cement zones record lower negative $\delta^{18}O_{VPDB}$ values compared with younger cement zones. The first (oldest) dull cement Zone 1 which is found in

syntaxial and sometimes equant and blocky calcite in all reservoir intervals (except G) shows a $\delta^{18}O_{VPDB}$ close to Cretaceous seawater (Figures 6.3 & 6.4). This infers that cementation was formed in equilibrium with Cretaceous seawater. There is no record of $\delta^{18}O_{VPDB}$ of cement Zone 1 in Reservoir B oil leg, however, Zone 1 of the water sample has $\delta^{18}O_{VPDB}$ value of -2.70‰ (individual measurement) suggesting precipitation from close to Cretaceous seawater (Thorpe, 2014). The fringing calcite has a similar $\delta^{18}O_{VPDB}$ (-1.20‰ to -4.00‰, Thorpe, 2014) to cement Zone 1 inferring similar precipitation conditions and time. The oldest cement zone in Reservoir G contains higher negative $\delta^{18}O_{VPDB}$ (mean = -5.90‰) compared with Cretaceous seawater indicating precipitation from other fluids having depleted $\delta^{18}O_{VPDB}$.

Comparing cement Zone 1 stratigraphically, the $\delta^{18}O_{VPDB}$ mean value is higher -1.57‰ at Reservoir F and -1.39‰ at Reservoir C which decreases to -2.70‰ at Reservoir B and then increases again to -1.20‰ at Reservoir A. This suggests that the Cretaceous seawater has evolved during 133-123 Ma (Hauterivian-Aptian). The average $\delta^{18}O_{VPDB}$ of this cement zone is close to the $\delta^{18}O_{VPDB}$ of Early Cretaceous seawater (Pucéat et al., 2003). The higher $\delta^{18}O_{VPDB}$ values found in the lower reservoirs and upper reservoir would be probably affected by the two possible glaciation events of Hauterivian and Aptian which broadly coincide with depositional time of these reservoirs (Price, 1999; Pucéat et al., 2003). This can be supported by the positive $\delta^{18}O_{VPDB}$ found in lower Reservoir F (mean= +3.0‰, Figure 6.3). In contrast, the higher negative $\delta^{18}O_{VPDB}$ reported in Reservoir B might be due to the ice melting and the first major oceanic anoxic event (OAE) of Lower Cretaceous. The first OAE most likely occurred during Early Aptian where a positive pulse in $\delta^{13}C$ and carbon-rich oceanic sediments are found (AlHusseini, 2017; Immenhauser et al., 2005; Menegatti et al., 1998; Ogg et al., 2004; Westermann et al., 2013;). The OAEs of the Middle Cretaceous have been linked to the increase in the oceanic crust production (Kerr, 1998; Steuber, 2002). The highest oceanic production period of the past 160 m.y. was reported to be between 126 and 112 Ma (Barremian-Aptian) (Section 4.4.3; Larson and Erba, 1999).

### 6.4.1.2 Pore Fluid Evolution

**Pore Fluid Evolution Stratigraphically using mMg/Ca and $\delta^{18}O_{VPDB}$**

The means of $\delta^{18}O_{VPDB}$ and mMg/Ca of all calcite cements in all stratigraphic units (G-A) are shown in Figure 6.5. mMg/Ca is thought to decrease with increasing temperature (Heydari and Moore, 1993). Here the two independent proxies follow same trend, both suggesting lower precipitation temperature at lower Reservoir F which increases towards Reservoir B where the highest precipitation temperature can be found through the whole stratigraphic units and then decreases again towards Reservoir A.

Having two independent proxies that give similar precipitation conditions which follow the global marine, tectonic and climatic conditions imply that Thamama Reservoirs are compartmentalized. Additionally, both Sr and Mn give a similar signature which further emphasizes the compartmentalization in these reservoirs (Figure 6.5). Thus, these reservoirs were deposited at different conditions and calcite cementation in each reservoir have evolved from their original fluid composition. Stratigraphically, calcite cementation began with mMg/Ca mean= 0.76 and $\delta^{18}O_{VPDB}$ mean=-8.98‰ by time of Reservoir G (135 Ma), increased to mMg/Ca mean= 0.91 and $\delta^{18}O_{VPDB}$ mean= -2.42‰ by Reservoir F (133 Ma), declined again to mMg/Ca mean= 0.63 and $\delta^{18}O_{VPDB}$ mean= -5.39‰ by 130 Ma which is the equivalent time of Reservoir C precipitation, reached mMg/Ca mean= 0.42 and $\delta^{18}O_{VPDB}$ mean= -9.65‰ by Reservoir B (126 Ma), and finally increased again to mMg/Ca mean= 0.71 and $\delta^{18}O_{VPDB}$ mean= -8.95‰ by Reservoir A (123Ma). The higher $\delta^{18}O_{VPDB}$ in Reservoirs F and C might be due to Hauterivian global cooling as discussed previously. Whereas the lower $\delta^{18}O_{VPDB}$ in the shallower reservoir intervals is suggested to be due to OAE and related mid oceanic ridge production events which involve warming of seawater (Section 6.4.1.1).

The Late Barremian–Albian period is well known for OAE1, which is documented globally (AlHusseini, 2017; Granier et al., 2008; Immenhauser et al., 2005; Menegatti et al., 1998; Ogg et al., 2004; Westermann et al., 2013). The OAE is thought to be an environment of reducing conditions characterized by depleted oxygen and higher Fe, Mn and probably Sr concentrations. This event has been traced widely using a positive $\delta^{13}C$ excursion as an indicator for such event. The shift in $\delta^{13}C$ is thought to be due to the changes in continental weathering inputs and rates of global volcanic and mid oceanic ridge (MOR) activities. Moreover, these changes are believed to have major effect on seawater chemistry variation including mMg/Ca ratio and $\delta^{18}O_{VPDB}$ during Lower Cretaceous. However, during the Late Barremian-Early Aptian an anomaly of negative $\delta^{13}C$ shift has been documented in some places that preceded the positive excursion of the OAE1 (Li et al., 2008; Menegatti et al., 1998; Stein et al., 2012; Westermann, et al., 2013). The negative shift in $\delta^{13}C$ reflects a period of oxidizing conditions which is inferred to lower seawater Fe, Mn and probably Sr. Rocks of Reservoir B and A which were deposited during late Barremian-Early Aptian should more or less contain records of similar conditions (oxic vs anoxic).

Considering the mMg/Ca and $\delta^{18}O_{VPDB}$ fluctuation during 135-123 Ma (Figure 6.5) it can be found that both the lowest mMg/Ca and $\delta^{18}O_{VPDB}$ is around ~126 Ma which is the equivalent time of precipitation of Reservoir B. The first interpretation that can be drawn is that this time may reflect the OAE1 incidence, which is characterized by an increase in reducing environments with depleted $\delta^{18}O_{VPDB}$. However, this time also coincided with lower Mn and Sr which reflect oxic conditions. Therefore, this time would be better interpreted as a time of oxic conditions which possibly presents the abrupt negative $\delta^{13}C$ excursion just before the major OAE1. The depletion in $\delta^{18}O_{VPDB}$ is interpreted as a result of the initial $CO_2$ degassing from volcanoes which resulted in warmer climate with the onset to OAE1 (Mehay et al., 2009; Suzuki et al., 2007). The same abrupt event has been observed also onset to the OAE2 (Turgeon and Creaser, 2008). Moreover, a warmer episode have been documented preceding to the OAE1 and has been attributed to the massive release of $CH_4$ or $CO_2$ (Ando et al., 2008).

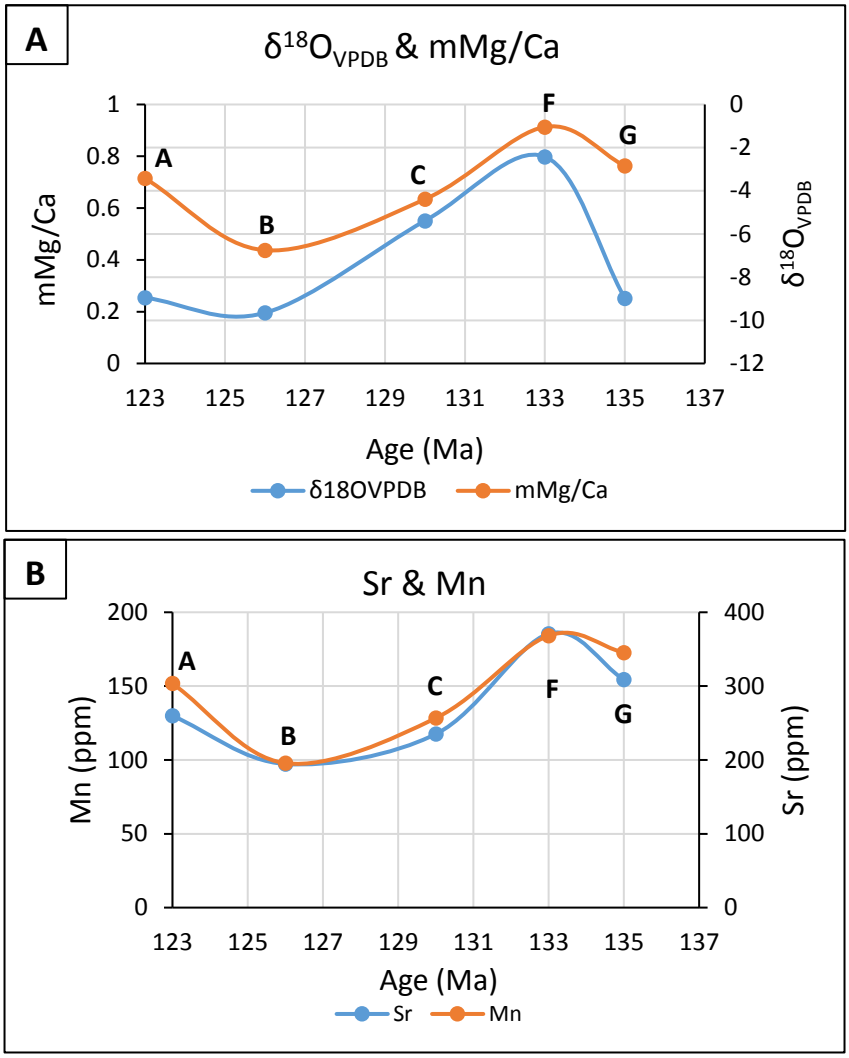


Figure 6.5: Pore fluid evolution through time. A) $\delta^{18}O_{VPDB}$ and mMg/Ca means of all calcite cements. B) Sr and Mn means for all calcite cements.

**Fluid Evolution in Individual Reservoirs**

The progressive depletion of $\delta^{18}O_{VPDB}$ from older cement zones to younger cement zones indicates the evolution of pore fluids through time in all reservoirs. This has been explained as due to increasing temperature and water-rock interaction during burial which yield mineralogical stabilization resulting in depleted $\delta^{18}O$ (Alsharhan et al., 2000; Cox. et al., 2010; Paganoni et al., 2016; Vohrenkamp et al., 2014). Therefore,

the $\delta^{18}O_{VPDB}$ of calcite is linked to temperature and $\delta^{18}O_{SMOW}$ composition of water which is expressed by Kim and O'Neil, (1997) as:

$$1000\ln\alpha_{(calcite\_water)} = 18.03\ (10^3T^{-1}) - 32.42$$

Using seawater temperatures of 15-20˚C, 50-70˚C for shallow burial water and 100-120˚C for deeper burial temperature (Neilson et al., 1998; Vohrenkamp et al., 2014; Paganoni et al., 2016) in addition to $\delta^{18}O_{VPDB}$ of all calcite cements, the $\delta^{18}O_{SMOW}$ compositions were obtained (Figure 6.6). The $\delta^{18}O_{SMOW}$ evolved from -2 ‰ to +8‰ across the reservoirs which agrees with previously proposed $\delta^{18}O_{SMOW}$ range (Cox. et al., 2010; Paganoni et al., 2016; Thorpe, 2014; Vohrenkamp et al., 2014).The $\delta^{18}O_{SMOW}$ increases successively with burial moving towards higher temperatures. This gives an indication that cementation in Thamama Group went through different conditions starting from Cretaceous seawater at a shallow temperature and then evolved to more depleted fluids at higher temperatures. This can be explained as calcite cements precipitated from in-situ trapped pore seawater that evolved in a relatively close system to higher precipitation temperatures. Such progressive evolution could be caused by synsedimentary or early reservoir compartmentalization which is probably related to the hardgrounds and low porosity transgressive sequences which acted as seals for reservoir intervals. These hardgrounds are represented as sequence boundaries interbedded with reservoir interval and can be traced for tens to hundreds of kilometers across the platform (Strohmenger et al., 2006).

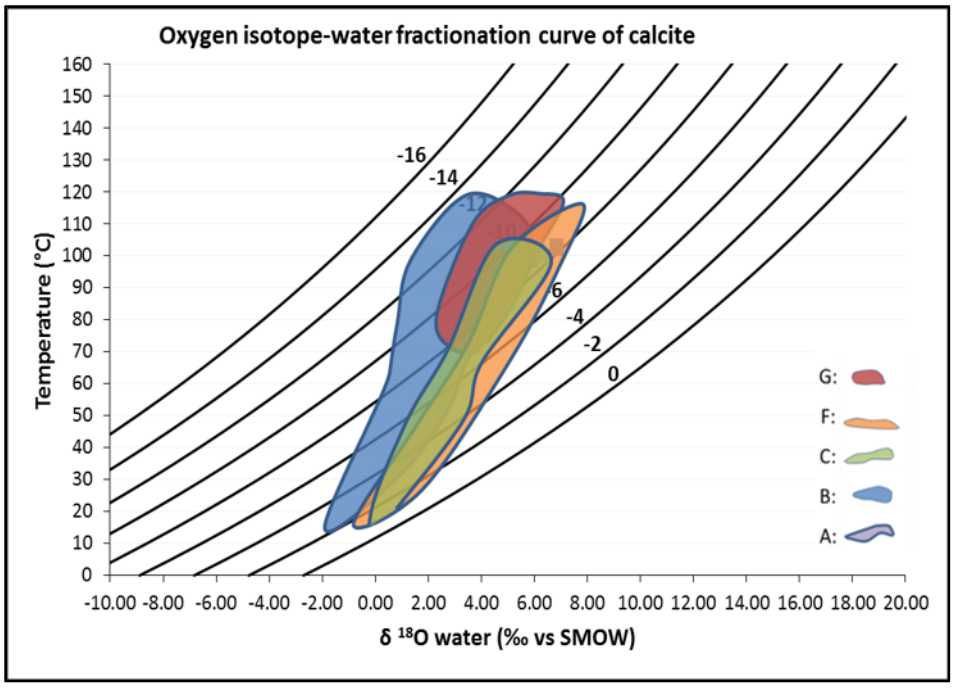


Figure 6.6: Mean Oxygen fractionation curve of water and calcite for Reservoirs G, F, C, B and A including ranges obtained from $\delta^{18}O_{VPDB}$ of syntaxial, equant and blocky calcite. Trend lines were obtained using Equation 1.

Precipitation time of equant, syntaxial and blocky calcite varies in the five reservoirs. The timing of equant calcite has been interpreted to be synchronous with syntaxial based on the paragenetic sequence and CL zones (Figure 6.1; Table 3.3). This was also probably either 1) during the younger CL cement zones as in Reservoirs G, F and C, or 2) at late stage of syntaxial calcite precipitation like the case in Reservoir B. Blocky calcite precipitated earlier than equant like Reservoirs B and G, at the same time of equant like Reservoir F, or shortly after equant like Reservoir C.

**Reservoir G**

Calcite cementation in Reservoir G started with higher $\delta^{18}O_{VPDB}$ compared with the other reservoirs both in this Field and Field C (-5.90‰- -8.2‰; Figure 6.4E). This is quite distinct from Cretaceous seawater which suggests precipitation from a

different fluid composition. Depleted values of $\delta^{18}O_{VPDB}$ may reflect meteoric or hot basinal water (Davies and Smith, 2006; Jenkin et al., 1994; López-Horgue et al., 2010). This reservoir is noteworthy as it contains highly fractured rocks. Indeed the petrography shows several fracture generations some filled with granular calcite (fracture generation I) and some with high volumes of blocky calcite and saddle dolomite (fracture II and III) close to the sampled area from which the $\delta^{18}O_{VPDB}$ measurements were obtained. The same fluid would probably cause cementation in nearby pores in matrix. Moreover, the granular calcite in fracture I has similar CL properties to calcite cement in the pores. This may suggest a similar fluid origin for calcite in both pores and fracture I.

The $\delta^{18}O_{VPDB}$ of modern meteoric water is thought to be -4.00‰ at ~20˚C (Rosales and Perez-Garcia, 2010). Moreover, meteoric water calcite cement has typically a higher Mn relative to Fe and Mg (Boles, 1998; Morad, 1998). The obtained mean $\delta^{18}O_{VPDB}$ from this field and Field C of the oldest cement zones is <-5.90‰ (Thorpe, 2014). Furthermore, this reservoir records higher Mn content relative to Fe and Mg and the Mn content is the highest across the other reservoirs (e.g. Figures 4.3 & 4.8). Hence both $\delta^{18}O_{VPDB}$ and trace elements may suggest precipitation from meteoric water, although there is no evidence of subaerial exposure. This can be explained by the sequence has been subjected to short period of meteoric flux or meteoric lens. Alternatively, cements with depleted $\delta^{18}O_{VPDB}$ can be precipitated from hot basinal fluids (Davies and Smith, 2006; López-Horgue et al., 2010; Neilson and Oxtoby, 2008; Paganoni et al., 2016). Having burial cements such as blocky calcite and saddle dolomite in nearby fractures may suggest influence of basinal fluids in calcite cementation in matrix.

Based on CL cement stratigraphy (Figure 6.1; Table 3.3), blocky calcite is the first to precipitate in Reservoir G followed by equant and syntaxial calcite. The $\delta^{18}O_{VPDB}$ also agrees with the established cement stratigraphy. The mean $\delta^{18}O_{VPDB}$ of first cement zone (Zone 2 in Figure 6.4E) of syntaxial calcite is -8.86‰ (mMg/Ca mean= 0.79) is equivalent to cement Zone 2 in blocky ($\delta^{18}O_{VPDB}$ mean = -8.23‰; mMg/Ca mean= 0.75) and first cement zone equant ($\delta^{18}O_{VPDB}$ one measurement= -

8.36‰; mMg/Ca mean= 0.77). This suggests that calcite cementation started at higher temperatures compared with other reservoirs. Calcite precipitation started at ~90˚C from fluid of $\delta^{18}O_{SMOW}$=~+6.0‰ which is probably similar to the calcite cement in fracture I. A decrease in the temperature was reported at cement Zone 5 both by syntaxial ($\delta^{18}O_{VPDB}$ mean= -7.37‰) and blocky ($\delta^{18}O_{VPDB}$ mean= -7.50‰) calcite. The change in $\delta^{18}O_{VPDB}$ and mMg/Ca indicates that the composition and temperature of fluid have changed at that time. This change might be due to the late fracturing episodes (fracture generations II and III), which may have transported fluid to the rock. Fluid then continued to evolve in relatively closed system from Zone 5 to Zone 7 having equant syntaxial and blocky calcite with equivalent $\delta^{18}O_{VPDB}$. At cement Zone 7, the temperature reached ~ 120˚C reported from equant and blocky calcite ($\delta^{18}O_{VPDB}$ mean= -10.52‰). The general change in temperature is similar to the change reported by mMg/Ca of syntaxial, equant and blocky calcite. The average mMg/Ca in Reservoir G goes approximately from ~0.75 at the older cement zone to ~1.0 at younger cement zone and to ~0.6 at youngest cement zone.

**Reservoir F**

There is no record of $\delta^{18}O_{VPDB}$ of cement Zone 1 syntaxial calcite for Reservoir F, however cement Zone 1 equant calcite hosts a mean $\delta^{18}O_{VPDB}$ of -1.57‰ indicating shallow marine precipitation conditions (Figures 6.1 & 6.4D). Cement Zone 1 of blocky calcite shows a positive $\delta^{18}O_{VPDB}$ (3.00‰) which is elevated compared with equivalent Zone 1 equant (-1.57‰). The positive value is interpreted to be due to global cooling during Hauterivian (Section 6.4.1.1). In addition, the second proxy, mMg/Ca, of cement Zone 1 shows 1.21, 1.18 and 1.14 for equant, syntaxial and blocky calcite respectively. At cement Zone 3, the $\delta^{18}O_{VPDB}$ is equal to -3.88‰ and -4.31‰ (mean) for syntaxial and blocky respectively. This suggests that at the time of Zone 3, syntaxial and blocky calcite were growing synchronously at similar conditions. Accordingly, syntaxial, equant and blocky calcite started to precipitate from marine waters in a phreatic environment and continued to precipitate with syntaxial calcite ceasing first at cement Zone 5 and equant ceasing shortly after syntaxial calcite (Table

3.3). The maximum recorded $\delta^{18}O_{VPDB}$ mean in syntaxial and equant are -6.16‰ and -7.24‰, which give temperatures of ~75˚C and ~90˚C, respectively. This confirms the initial interpretation from CL analysis.

**Reservoir C**

In Reservoir C, syntaxial calcite started to precipitate from near marine seawater values of $\delta^{18}O_{VPDB}$ mean= -1.39‰ which modified to -0.60‰ at Zone 2 and then return back to mean= -2.00‰ at Zone 3 (Figures 6.1 & 6.4C). This is also in good agreement with mMg/Ca ratio which changed from 0.83 at Zone 1 to 0.95 at Zone 2 and then returned to 0.73 at Zone 3. This suggests that at Zone 2, the temperature dropped and fluid composition changed. Cementation continued with syntaxial, equant and blocky calcite from Zone 4 on word to more evolved fluids and higher temperature. At Zone 4 both syntaxial and blocky calcite show similar fluid composition $\delta^{18}O_{VPDB}$ -5.56‰ (mean mMg/Ca=0.51) and -5.61‰ (mean mMg/Ca=0.66) which is equivalent to 55˚C. At Zone 6 where all calcite cements are believed to terminate, the temperature reached ~102˚C and ~106˚C measured from $\delta^{18}O_{VPDB}$ mean of -8.48‰ and -9.19‰ from syntaxial and blocky calcite, respectively.

**Reservoir B**

Precipitation of equant calcite in Reservoir B is believed to have started coincident with the late stage of syntaxial calcite and ceased after it (Figure 6.1; Table 3.3). The mean $\delta^{18}O_{VPDB}$ of first cement zone in equant calcite is -8.87‰ suggesting a much later precipitation time compared with earlier cement zone in syntaxial calcite (Zone 3 $\delta^{18}O_{VPDB}$ mean= -5.56‰). There is no record for first two zones from this study, but a previous study shows a mean $\delta^{18}O_{VPDB}$ -2.7‰ (Figure 6.4B). The first cement in equant calcite ($\delta^{18}O_{VPDB}$ mean = -8.87‰; mMg/Ca mean = 0.37) is interpreted to be formed at time equivalent to cement Zone 4 of syntaxial calcite ($\delta^{18}O_{VPDB}$ mean = -7.58‰; mMg/Ca mean = 0.41) or later. However, the equant calcite

precipitated at the same time has a mean $\delta^{18}O_{VPDB}$ of -8.87‰ which is lower compared with coeval syntaxial calcite. This suggests that equant calcite might be precipitated later compared to syntaxial cement Zone 4 at higher temperature. Moreover, the last equant calcite cement zone has $\delta^{18}O_{VPDB}$ value of -13.16‰ in contrast to a maximum mean value of -10.22‰ (~120˚C) in last cement zone of syntaxial calcite which confirms further precipitation of equant calcite at a temperature of ~144˚C.

There is no record of $\delta^{18}O_{VPDB}$ of blocky calcite however CL suggests that the starting precipitation time of blocky calcite is equivalent to cement Zone 2 of the syntaxial calcite. The mMg/Ca ratio of cement Zone 2 synaxial calcite has no record, however Zone 4 (syntaxial) which is equivalent to Zone 2 in blocky calcite shows a mMg/Ca of 0.41 and 0.46, respectively, suggesting contemporary precipitation of both calcites.

Generally, calcite cement in Reservoir B precipitated close to Cretaceous seawater (older syntaxial cement mMg/Ca= 0.75) and continued to evolved through burial as a result of increasing temperature and water-rock interaction in relatively closed system. Equant calcite is thought to be precipitated from a higher temperature most likely during oil charge. The syntaxial and blocky calcite terminated in pores at approximately similar conditions (syntaxial: $\delta^{18}O_{VPDB}$ mean= -10.22‰, mMg/Ca mean= 0.32; blocky: mMg/Ca mean= 0.31) whereas equant calcite continued further ($\delta^{18}O_{VPDB}$ = -13.16‰) reporting higher precipitation temperature.

**Reservoir A**

Calcite cementation in Reservoir A started from a fluid composition ($\delta^{18}O_{VPDB}$ = -1.20‰, mMg/Ca mean= 1.10) similar to Cretaceous seawater, as measured from syntaxial cement. Fluids evolved progressively with burial to reach maximum recorded mean $\delta^{18}O_{VPDB}$= -9.40‰ (mean mMg/Ca = 0.61) at Zone 6 of the syntaxial cement (Figure 6.4A). This suggests a change in temperature from ~20˚C to 106˚C

through the full syntaxial calcite precipitation history. Blocky calcite precipitation began at the last cement zone of syntaxial (Zone 7) with a mean mMg/Ca of 0.50 and 0.51 for syntaxial and blocky, respectively. Blocky calcite continued to precipitate from evolved fluid in a closed system until Zone 9 with a $\delta^{18}O_{VPDB}$ mean of -10.32‰ and mMg/Ca mean of 0.47 (~120˚C). The mMg/Ca ratio (mean = 0.95) records a shift in fluid composition in last blocky calcite cement Zone 10 which might be due to the uplift of the strata to form an antiform during Late Cretaceous (Section 4.4.3).

### 6.4.2 Calcite Cementation in Relation to Oil Charge

The volume of precipitated cement in the water leg is higher than in the oil leg resulting in lower porosity in water leg (Figure 3.8). Pores including micro, intergranular, moldic, vuggy and intragranular are partially occluded in the oil leg whereas in the water leg they are partially to completely filled. Having higher primary intergranular and micropores remaining in the oil than water leg highlights the role of the present medium (oil versus water) in preventing or retarding further cementation from destroying pores at an earlier stage. The difference in porosity in oil (22-23%) versus water (12-13%) leg has been documented in several studies, which has been closely linked to early oil emplacement in crest versus flank (Feazel and Schatzinger, 1985; Neilson et al., 1998; Oswald et al, 1995; Paganoni et al., 2016; Thorpe, 2014). Cementation in the presence of oil decreases or stops because minerals have near zero solubility in hydrocarbon fluids (Feazel and Schatzinger, 1985). Further cementation after oil charge can be due to wettability and higher irreducible water saturations because oil reservoirs remain oil wet (Heasley et al., 2000; Marzouk et al., 1995).

Comparing $\delta^{18}O_{VPDB}$ in water versus oil leg of Reservoir B, a value of -8.95‰ (mean) was found in last precipitated syntaxial cement Zone 4 in water and a value of -9.92‰ (mean) in the equivalent cement Zone 5 in oil leg. This indicates that the cementation in water has ceased under slightly different conditions than oil. This is also in agreement with the mMg/Ca ratio (cement Zone 4 water= 0.43, cement Zone 5 oil= 0.32). Cementation in the water leg ceases at cement Zone 4 and total precipitated

cement occludes most of the pores (Figure 3.7A). Whereas in the oil leg, cementation continued further to higher negative $\delta^{18}O_{VPDB}$ (-13.16‰) at cement Zone 8 but with a lower cementation leaving most of the pores open (Figure 3.6B). The first presence of oil inclusions was recorded around Zone 5 (Thorpe, 2014) where here a significant drop in the total precipitated cement volume was noted (Figure 3.6B). However, this cannot be concluded as the onset time of oil charge, which might be prior to cement Zone 5. This time is also considered to be the start of precipitation of equant calcite. The change in calcite morphology to lower volume equant calcite could be due to less available solute for cementation or to slower growth rate inhibited by oil emplacement (Section 3.2). Primary petroleum inclusions were also found in equant sparry calcite and dolomite in Thamama Reservoir B (Neilson et al, 1998). This may suggest that equant calcite was precipitated concurrently with oil emplacement at higher temperature. Similarly, in Reservoir A oil inclusions were reported in cement zones equivalent to cement Zones 5 and 6 (Cox. et al., 2010; Thorpe, 2014) where also a drop in cementation rate has been reported (Figure 3.6A). This may suggest that cement precipitation rate has been affected by oil emplacement.

The calcite cementation history curve of Reservoir C is similar in the water and oil legs except for the total precipitated cement (Figures 3.6C & 3.7B); calcite cement in the water leg is much higher than the oil leg. The last precipitated cement Zone 6 which is equivalent in both legs has mMg/Ca (mean) of 0.31 and 0.57 in oil and water leg, respectively. This cement zone and others as well return similar CL properties but different mMg/Ca ratios. The difference in mMg/Ca ratio could be due to the effect of increasing temperature with burial as well as oil migration. The first difference in mMg/Ca (syntaxial) between oil and water can be found at cement Zone 4 (mMg/Ca mean= 0.51) in oil and its equivalent Zone 4 in water (mMg/Ca mean= 0.74). This could be the time when oil was emplaced into the system and resulted in continuous cementation in oil leg to higher temperature which probably affected the mMg/Ca.

Calcite cementation history and conditions in Reservoir F were almost the same in oil versus water leg (Figure 3.8). Syntaxial calcite cementation in both oil and water leg continued under similar conditions to cement Zone 3 (oil) and its equivalent Zone

4 in water. These two Zones have similar mMg/Ca ratio (mean) of 0.62 and 0.63 for oil and water, respectively. The depletion in $\delta^{18}O_{VPDB}$ from -3.88‰ at cement Zone 3 to -6.12‰ at Zone 4 may be due to the progress of cementation with burial. Equant calcite, which is thought to continue after cessation of syntaxial calcite in oil leg (Figure 6.1; Table 3.3), shows a lower mMg/Ca (mean = 0.38) in the youngest cement zone. In contrast, equant calcite in water leg shows a mean mMg/Ca value of 0.52 in the younger cement zone. The difference in mMg/Ca may suggest cementation in oil leg has continued to higher precipitation temperatures. The increase in temperature could be due to the progressive burial and/or due to interact with high temperature fluid passing through the system (e.g. basinal fluids). Little difference found in mMg/Ca ration of earlier-intermediate cement zones between oil and water leg, which implies that oil charge was probably at a very late cementation stage. Thus, cementation in oil leg has continued into higher temperature after oil while in the water leg cementation has ceased earlier.

According to Alsharhan (1989), Burruss et al. (1985) and Oswald et al. (1995), oil charging of Thamama Group began during the early Cretaceous prior to stylolitization and continued to the early Tertiary. The wide range of charging times indicates that some reservoirs will be filled prior to others. The difference in precipitation conditions between oil and water leg in shallower reservoirs was indicated at an earlier cementation stage compared with deeper reservoirs (see interpretation above). Moreover, the final cementation $\delta^{18}O_{VPDB}$ values are lower in the upper reservoirs compared with lower reservoirs. For example, Reservoirs B and A record negative value of -13.12‰ and -10.61‰, respectively, whereas Reservoirs F and C have lower negative values (-7.90‰ and -9.68‰ respectively). The higher negative values in the upper reservoirs indicate higher precipitation temperatures (~ 120-144˚C) than in lower reservoirs (~100-110˚C). This is more likely due to the earlier oil charge in the shallower reservoirs which encounter gradual filling of the structure from top of the crest downwards. The higher temperature (144˚C) recorded in the shallower reservoir could be also due to hot basinal brine. Similar temperature was reported by Thorpe (2014) and Paganoni et al. (2016) in burial calcite. Paganoni et al. (2016) provides aqueous fluid inclusion data (. homogenization temperatures ($T_h$)

between 86°C and 131°C and a salinity of 6.0–18.1wt.% NaCl eq.) revealing source of hot basinal (hydrothermal) brine.

## 6.5 Summary

Stable oxygen isotopes are a vital tool to reconstruct the origin of pore fluid composition and to trace its evolution through time. More interestingly, using this proxy in parallel with another independent proxy (mMg/Ca) we can infer similar precipitation temperatures at specific times. These data also coincide with trace element observations including Mn and Sr. All these indicators show fluctuations in Cretaceous seawater during 135-123Ma caused by global changes in climate and oceanic crust production rates. Lower Reservoirs including F (133Ma) and C (130Ma) were more probably affected by the Hauterivian global cooling which resulted in higher $\delta^{18}O_{VPDB}$ in the early precipitated cements. Precipitation in upper Reservoir B (126Ma) was most likely affected by the abrupt warm episode just before the OAE1. Reservoir A (123Ma) precipitation may be affected by the Early Aptian cooling episode and the OAE1.

In summary, cements in the matrix including equant, sytaxial and blocky calcite (BI) have precipitated from marine pore fluid which then evolved in relatively closed system through burial. A closed system could be due to the early sealing of the reservoirs by low permeability hardground intervals. Early emplacement of the oil in the shallower reservoirs increased the cementation temperature of rocks in the oil leg to reach maximum precipitation temperatures of ~144˚C. In the water leg, cementation continued to a temperature of ~110˚C. Furthermore, oil charge in the lower reservoirs occurred later compared with upper reservoirs which allowed the cementation in the lower reservoirs to ceases at lower temperatures (~100-110˚C). Cementation conditions in the matrix remained closed and most equant, syntaxial and early blocky (BI) cementation was completed before stylolitization and fracture formation.

Cementation in Reservoir G was affected by depleted $\delta^{18}O_{VPDB}$ fluids from early stage, perhaps hot, basinal waters.

# Chapter 7: Conclusions

## 7.1 Introduction

Diagenesis play important role in reservoir quality of Thamama Group. Thus, understanding these processes is crucial to better predict reservoir quality. Calcite cementation is considered as one of significant diagenetic overprints in Thamama Reservoirs. Indeed, calcite cementation can be used to investigate the origin and pore fluid evolution by conducting detailed analysis such as EPMA and in-situ $\delta^{18}O_{VPDB}$ (Cox. et al., 2010; Thorpe, 2014). Furthermore, the rate of calcite cementation can be affected by the setting under which the precipitation occurs for example water versus oil leg. In water leg, calcite could go to more extensive cementation whereas in oil leg cementation may cease or retard and hence preserves higher porosity and permeability.

The thesis expands work done by Neilson et al. (1998), Cox et al. (2010) and Thorpe (2014) and has added important new understanding of the effect of climate on initial seawater for cementation in five carbonate reservoirs. The thesis also provides better understanding of the controls on calcite cementation, evolution of cements, and the role of calcite cementation with relation to oil charge in reservoir quality within individual Thamama Reservoirs which became compartmentalized early by hardground surfaces. The five Reservoirs are part of Lower Cretaceous Thamama Group and were sampled from Field A located in onshore Abu Dhabi, UAE. This work can be used to understand origin and evolution of calcite cementation in local nearby and global fields which hosts rocks deposited in Cretaceous or similar climate. Formation of hardground seems to be unique phenomenon of calcite seas such as Cretaceous, Ordovician and Cambrian that were formed rapidly at sea floor due to early cementation (Dickson et al., 2005; Wilson and Palmer, 1992). The early lithification of hardgrounds can provide compartmentalized rocks which can host seawater signature, cause cement to evolve in a close system and hence make cement

evolution and reservoir quality more predictable. Therefore, investigating and predicting occurrence of hardgrounds should be of valuable application for climate and hydrocarbon studies.

Conventional petrography was conducted to provide comprehensive record on overall diagenesis processes, timing of each diagenetic process relative to the other and impact of these processes on reservoir quality. Ion Microprobe along with cathodoluminescence (CL), electron probe microanalysis (EPMA) and oil inclusions analysis were undertaken to understand origin of pore fluid and calcite cement evolution in response to oil charge. CL was used as a first step to construct cement stratigraphy to be used to trace cement evolution through time as well as how the pore space is occluded and how much cement was precipitated in oil versus water leg. Then, along with cement stratigraphy, trace elements and $\delta^{18}O_{VPDB}$ were used to understand the temperature and pore fluid chemistry from which a calcite cement zone precipitated at certain cement zone time. Oil inclusions have been placed in the content to understand the timing relationship between calcite growth and oil charge.

## 7.2 Overview of Diagenesis and Reservoir Quality

At the beginning an overview about diagenesis in Thamama Reservoirs were given to assess the impact of general diagenesis in reservoir quality. This was done by comparing diagenesis in oil versus water leg. Paragenetic sequence was also constructed to understand timing of diagenetic events relative to each other and to oil emplacement. Figure 7.1 illustrates evolution of rock from deposition to late burial and highlights the main diagenetic events through time in Thamama Reservoirs. The main diagenetic events and their relative timing in Thamama Reservoirs are as following: 1) micritization and initial microporosity creation, (2) aragonite dissolution and precipitation of circumgranular calcite followed by equant, syntaxial overgrowth and first blocky calcite generation ( BI ), (3) formation of dissolution seams followed by rhombic dolomite, (4) stylolitization and fracture formation (perpendicular to stylolite), (5) later stage of fracturing, (6) flux of exotic fluids through fractures and

stylolites, (7) development of coarser dolomite and pyrite, (8) precipitation of second generation of blocky calcite (BII), saddle dolomite and rare anhydrite followed by kaolinite, bitumen and coarse euhedral pyrite precipitation, (9) late burial dissolution and porosity enhancement (micro and macro). Oil charge was placed prior to stylolitization and burial cementation in the paragenetic sequence (Oswald et al., 1995; Neilson et al., 1998).

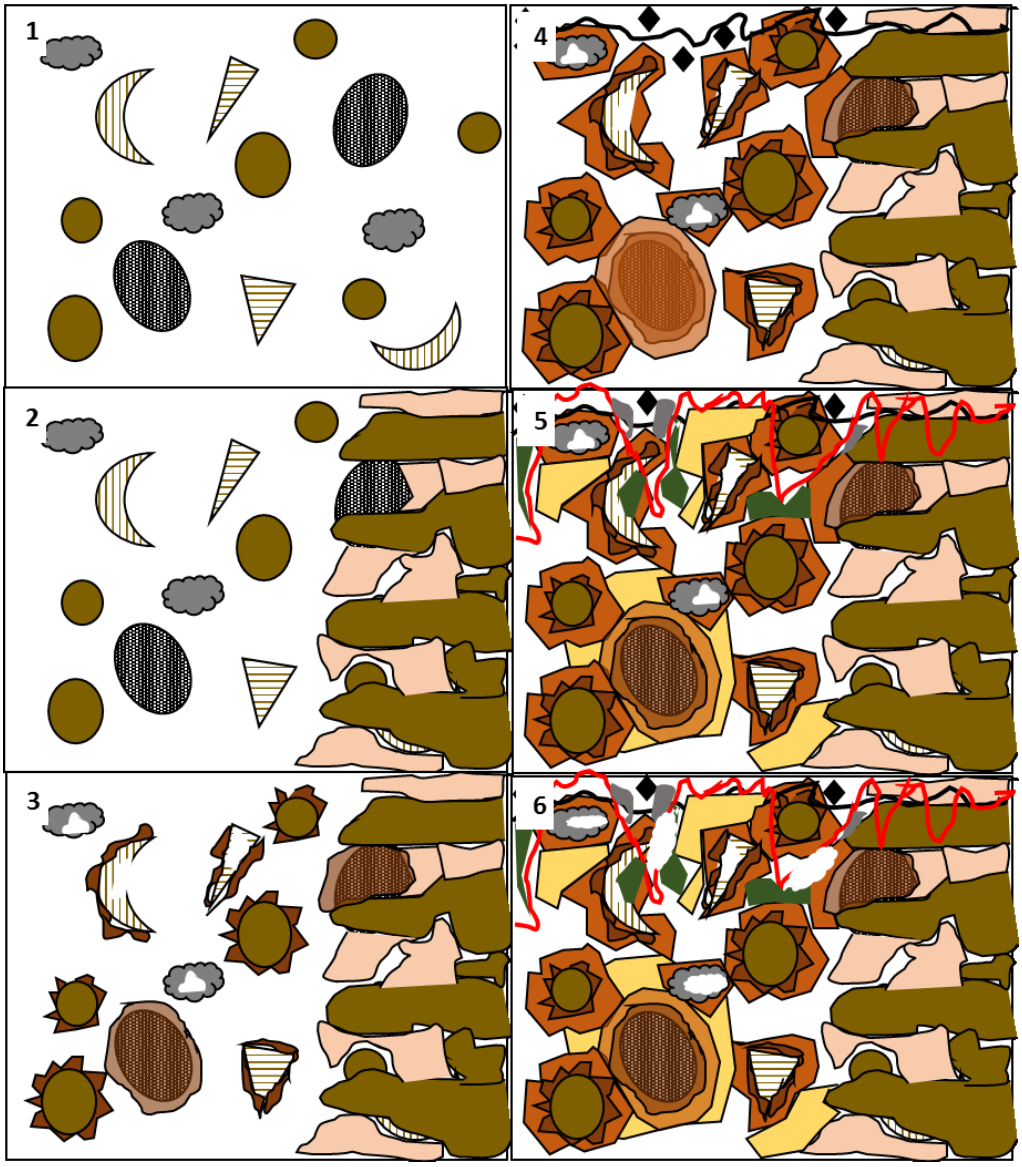

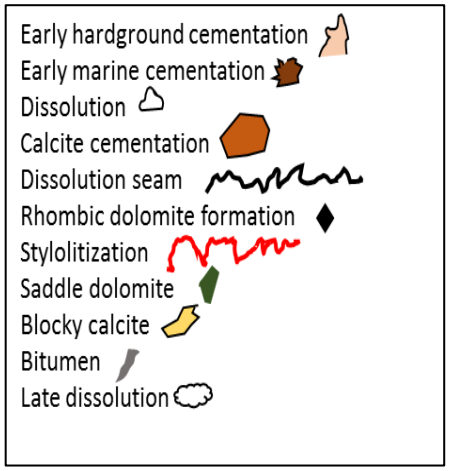


Figure 7.1: Thamama rock evolution through time. 1) rock at time of deposition. 2) Syndepositional: early hardground cementation. 3) early marine diagenesis: formation of circumgraular calcite and first phases of syntaxial and equant calcite. 4) early burial diagenesis: formation of dissolution seams, rhombic dolomite, early blocky calcite and later phases of syntaxial and equant calcite. 5) late burial: formation of stylolites, saddle dolomite, blocky calcite and bitumen. 6) late dissolution phase at late burial.

Major porosity in Thamama Reservoirs include micropores, intergranular, vugs and moldic pores. Micritization has significant impact on reservoir properties by creating tiny micrite particles (spherical to sub-spherical) introducing microporosity which further dissolved during late dissolution. Moreover, some of the tiny micrite particles have been dolomitized and replaced by microcrystalline rhombic dolomite which generated new microporosity in the rocks. In addition the precipitation of circumgranular calcite rim around the grains in grainstones and packstones has helped to some extent in preserving some of the depositional intergranular porosity. Open and partially filled fractures also have positive effect on porosity and permeability. Generally, calcite cementation in matrix has negative effect on reservoir properties. Calcite cement including syntaxial, equant and blocky has affected reservoir quality by different magnitude at different geological time in different Reservoirs.

The amount of precipitated cement in the water leg is higher than oil leg. This indicates that calcite cementation has greater impact on reservoir quality in water leg than oil leg. This is probably due to the influence of oil charge. The absence of hydrocarbons in the flank of the structure resulted in extensive diagenesis including cementation and chemical compaction which therefore destroyed the reservoir quality. This conclusion also agrees with broadly noted findings on Thamama (Neilson et al., 1998; Oswald et al., 1995; Paganoni et al., 2016; Strohmenger et al., 2006). In some cases, lots of late burial cement, such as blocky calcite, saddle dolomite, kaolinite and

pyrite, can be seen accumulated along stylolites inferring that stylolites have deteriorated reservoir quality. However, in other cases dissolution around and along stylolites can be seen suggesting that stylolites have enhanced reservoir quality to some extent. This type of dissolution is probably due to the flux of corrosive fluid along stylolite. The same fluid flux may have caused the formation of type II secondary pores (including micropores, vuggy and moldic pores).Thorpe (2014) and Paganoni et al. (2016) propose organic acid which is generated during hydrocarbon migration as source of such dissolution and use the existence of kaolinite in the reservoir as proof of this. The $Al^{3+}$ in kaolinite can't be transported for long distance unless it is formed complex compound with acid (De Bona et al. 2008; Maliva et al., 1999). Therefore, we also conclude flux of organic acid which contributed to significant dissolution and enhancement of reservoir quality at late stage.

Taking calcite cementation further, a simple qualitative assessment of total precipitated cement in the oil versus water leg was under taken. This used the total thickness of the calcite simply by measuring the apparent maximum widths of cement zones. This assessment confirms that the amount of precipitated calcite in the water leg in higher than oil leg. Thus, the rate of flux of saturated fluid with respect to the mineral is higher in the water than oil leg. The apparent width could be also used to infer to the precipitation time of certain cement zone; for example higher apparent width can refer to longer precipitation time and vice versa. Cycles of higher and lower cementation episodes may reflect change in fluid saturation where higher cementation episodes representing higher fluid saturation and lower cementation episodes showing lower fluid saturation. This could be due to the change in water-rock interaction as rocks get buried through time.

## 7.3 Fluid Composition and Evolution of Calcite Cements: mMg/Ca and trace elements

The mMg/Ca, Mn, Sr and Fe of calcite were measured through cement stratigraphy from oldest to youngest cement Zone. Data show that pore fluid

composition evolved through time. The oldest (early) cement Zones in all Reservoirs are rich in Sr compared with younger cement Zones, in oil and water legs (oldest non-luminance from syntaxial). This indicates an initial precipitation source rich in Sr, possibly from a depositional input as clay is known to be rich in Sr. An increase in clay content was noted towards Dense Zones (Figure 1.6) inferred from Gamma ray log suggesting clay as a likely source for initial cementation (Strohmenger et al., 2006). Higher Fe, Mn and Sr concentrations were found in the lower Reservoirs compared to the upper Reservoirs implying that cements in the lower Reservoirs were precipitated in an anoxic and relatively deeper environment. Mn and Sr in cements of shallowest Reservoir A is higher compared with underlying Reservoir B. Lower Shuaiba shale is the most likely source for the higher Sr and Mn content in Reservoir A (Section 4.4.1). The higher Sr in the oldest cement zone could be also originated from marine pore water. The $^{87}Sr/^{86}Sr$ ratio and $\delta^{13}C_{VPDB}$ obtained from bulk packstone and grainstone of similar Thamama rocks show average values of 0.707469 and +3.7‰ respectively (Morad et al., 2016) which are similar to ambient Cretaceous seawater (Scholle & Arthur 1980; Veizer et al. 1999). Indeed, the Sr found in the same rocks range between 259 ppm and 596 ppm (Average 245 ppm) which is similar to the Sr range found in oldest cement zones in our rocks (Figure 4.26). Thus, the higher Sr amounts in these cement zones were probably precipitated from marine pore water of Cretaceous origin.

The mMg/Ca of syntaxial and equant calcite in all Reservoirs as well as blocky calcite in Reservoirs B and F indicates a decreases toward younger cement Zones inferring progressively higher precipitation temperatures through time. Comparing mMg/Ca stratigraphically, mMg/Ca in the shallower Reservoirs are lower compared with deeper Reservoirs. Thus, it can be concluded that cements in shallower Reservoirs were precipitated at higher temperatures compared with cements in deeper Reservoirs. Stratigraphically, deeper Reservoirs should have higher precipitation temperatures than shallower Reservoirs if all have precipitated from same pore fluid (same seawater composition). However, diagenesis and/or changes in composition of seawater can alter mMg/Ca. Variation in seawater composition has been closely linked to changes in oceanic crust production rates (Balthasar and Cusack, 2015; Bots et al., 2011; Hardie, 1996; Morse et al., 1997; Steuber, 2002; Timofeeff et al., 2006). The maximum

rate ocean crust production is proposed to be around 126-100 Ma which coincides with the lowest mMg/Ca during Lower Cretaceous (Larson and Erba, 1999). In our study, the lowest mMg/Ca ratio is found around 126 Ma which is equivalent to time of precipitation of Reservoir B. Thus, we conclude that our older cement precipitation was controlled by the change seawater chemistry during Lower Cretaceous time.

mMg/Ca ratios of younger cements in oil versus water leg suggest higher precipitation temperature for cements in the oil than water leg. Most of the pore spaces in water leg are occluded due to progressive higher cementation rate leaving few or no free pore spaces for further cementation. Whereas in the oil leg, the rate of cementation was retarded due earlier oil charge which preserved higher porosity. Therefore, cementation in water leg ceased at lower temperature compared with oil leg. However, blocky cement of oil in some Reservoirs (A, C and G) indicates lower precipitation temperature (higher mMg/Ca) moving towards the youngest cement Zone. This could be due be due to influx of fluids that are rich in Mg and/or uplifting of the units.

## 7.4 Origin and Evolution of Dolomite

Fluid composition of dolomite was also assessed using mMg:Ca ratio, Sr, Mn and Fe for three types of dolomites; type 1: rhombic dolomite (older & younger), type 2: coarse dolomite, type 3: saddle dolomite. A common pattern of alternating oxic and anoxic conditions were noted in all dolomite types; zonation containing ferroan and non-ferroan zones. This infers a dynamic chemical evolution of dolomitization fluids through time. Saddle dolomites hosts the highest Fe content suggesting that saddle dolomite was precipitated at extremely high reducing conditions.

Generally, coarse and saddle dolomites contain lower Sr than rhombic dolomite. Similar to calcite cement, the oldest cement Zone 1 in rhombic dolomite hosts the highest Sr content across all Reservoirs in the water and oil legs. This indicates that both oldest cement zones in replacive rhombic dolomites and calcite have been

precipitated from Sr rich fluids. Similar to the interpretation for calcite, the Sr could be derived from clay and mud rich facies.

The difference in mMg:Ca ratio between older rhombic dolomite and other dolomite types indicates different formation conditions. Older rhombic dolomite show a higher mMg/Ca compared with younger rhombic, coarse and saddle dolomite. Dolomitizing fluids for older rhombic dolomite are more likely characterized by lower Mg and higher Ca compared with others. Saddle dolomite in all Reservoirs in both oil and water legs shows same mMg:Ca. Thus, it can be concluded that saddle dolomite in all Reservoirs have precipitated from the same dolomitizing fluids and probably at an equivalent time. The timing of saddle dolomite formation in all Reservoirs is placed after stylolitization and fracturing in the paragenetic sequence more probably during or after the major tectonic compressional events in Late Cretaceous-Tertialy time.

Saddle dolomite is found more often associated with fractures and stylolites and in large moldic pores nearby. In order to precipitate dolomite an adequate supply of Mg is required. Mg may be supplied from exotic fluids which are likely to be hydrothermal fluids. The best dolomitization model that describes this formation mechanism is the tectonic-hydrothermal model. Younger rhombic and coarse dolomite are believed to be precipitated from same dolomitizing fluid. This interpretation is based on 1) the similar elemental properties for these three dolomites, 2) a similar mMg;Ca for younger rhombic dolomite and saddle dolomite, 3) the association of saddle dolomite and sometimes rhombic and coarse dolomite in the vicinity and along stylolites, 4) similar $\delta^{18}O_{VPDB}$ values for rhombic dolomite and saddle dolomite (Paganoni et al., 2016).

The burial compaction model is proposed for the formation of older rhombic dolomite. Here, rhombic dolomite in this model can be sourced by pore seawater fluids which contain dissolved carbonate of the host limestone. The carbon isotopic signatures found in rhombic dolomite are similar to Cretaceous seawater (Paganoni et al., 2016).

## 7.5 Calcite Cements as Temperature and Cretaceous Seawater Proxies

To understand the dynamics of cementation the origin of calcite cement was first investigated. The oldest cement Zone is non-luminance calcite cement found in syntaxial and sometimes in equant calcite. This non-luminance calcite was referred to as "crinoid clothing", and can survive diagenesis and hence retain ancient seawater chemistry (Dickson, 2004; Hasiuk and Lohmann, 2008). Based on this, mMg/Ca and $\delta^{18}O_{VPDB}$ were measured for this oldest cement and compared with the Lower Cretaceous seawater to investigate the origin.

The mMg/Ca of echinoderm 'clothing' non-luminance calcite shows a change in mean values from 0.8 to 1.2 between 135 to 123 Ma. This general range of mMg/Ca broadly matches measured (from skeletal material and fluid inclusions) and modelled of mMg/Ca (Dickson, 2004; Hardie, 1998; Lowenstein et al., 2001; Robert and Berner, 2004; Steuber and Rauch, 2005; Timofeeff et al., 2006; Wilkinson and Algeo, 1989). Hence, our findings may represent values close to contemporary seawater. Moreover, the $\delta^{18}O_{VPDB}$ shows mean from -0.13‰ to -2.95‰ between 135 to 123Ma which also matches with the general Lower Cretaceous trend (Pucéat et al., 2003). This provide further evidence for the origin of early precipitated cement, which is close to Lower Cretaceous seawater. The variation in chemical composition of oldest cement Zone across the Reservoirs is a result of variation in seawater chemistry governed by global changes in climate and oceanic crust production rates. Our four Reservoirs were precipitated between Hauterivian and Early Aptian time and during that period several changes have occurred including episodes of global cooling and OAE1. The $\delta^{18}O_{VPDB}$ data from the early cement of the four Reservoirs track these global changes. Lower Reservoirs including F (133Ma) and C (130Ma) were more probably affected by the Hauterivian global cooling which resulted in higher $\delta^{18}O_{VPDB}$ (+3.94‰ - -3.27‰ and -0.60‰ - -4.11‰ respectively) in the early precipitated cements (Föllmi, 2012; Price, 1999; Pucéat et al., 2003). Precipitation in upper Reservoir B (126 Ma) was most likely affected by the abrupt warm episode just before the OAE1 (-2.7‰ - -4.8‰; Li et al.,

2008; Menegatti et al., 1998; Stein et al., 2012; Westermann, et al., 2013). Reservoir A (123Ma) $\delta^{18}O_{VPDB}$ (-1.2‰ - -4.6‰) may record the Early Aptian cooling episode and the OAE1 (Pucéat et al., 2003). Reservoir G does not record a $\delta^{18}O_{VPDB}$ similar to Cretaceous seawater. Older cements in Reservoir G show depleted $\delta^{18}O_{VPDB}$ (-5.8‰ - -7.01‰) suggesting a different fluid origin, perhaps hot, basinal waters. The mMg/Ca of this Reservoir is also deviates from the general trend of Lower Cretaceous seawater.

Using the independent proxies $\delta^{18}O_{VPDB}$ and mMg/Ca, precipitation temperature through cement stratigraphy was inferred from older to younger cement Zones. Both proxies show progressive increase in cementation temperature towards younger cement Zones. The increase in temperature is typically attributed to the increase in water-rock interaction with burial. Thus, we conclude that in our Reservoirs, calcite cement was precipitated in-situ from initial seawater trapped in pores and continued to evolve to higher temperature during burial. Looking closely to mMg/Ca of echinoderm 'clothing' non-luminance calcite, syntaxial, equant and blocky calcite, we can see that all cements follow identical trend but with variable offsets from the oldest non-luminance calcite (Figure 7.2A). Having identical trend of different calcite cements adds another piece of evidence that the cementation in these Reservoirs occurred in a relatively closed system, where waters pore hosted the ancient seawater trend. Thus, diagenesis have not totally destroyed the original trend of ancient seawater and hence can be used to reconstruct ancient ocean chemistry. This also has been suggested by Cicero and Lohmann (2001) where they found Sr/Mg and Mg/Ca of diagenetically altered abiotic marine calcite cements similar to ancient Late Silurian and Middle Triassic seawater. Indeed, many studies indicate that ancient seawater chemistry can be retained from abiotic marine cements if have not undergone through extensive diagenesis (Budd, 1984; Carpenter et al., 1991; Carpenter and Lohmann, 1992; Cicero and Lohmann, 2001; Gonzalez and Lohmann, 1985; Hasiuk and Lohmann, 2008).

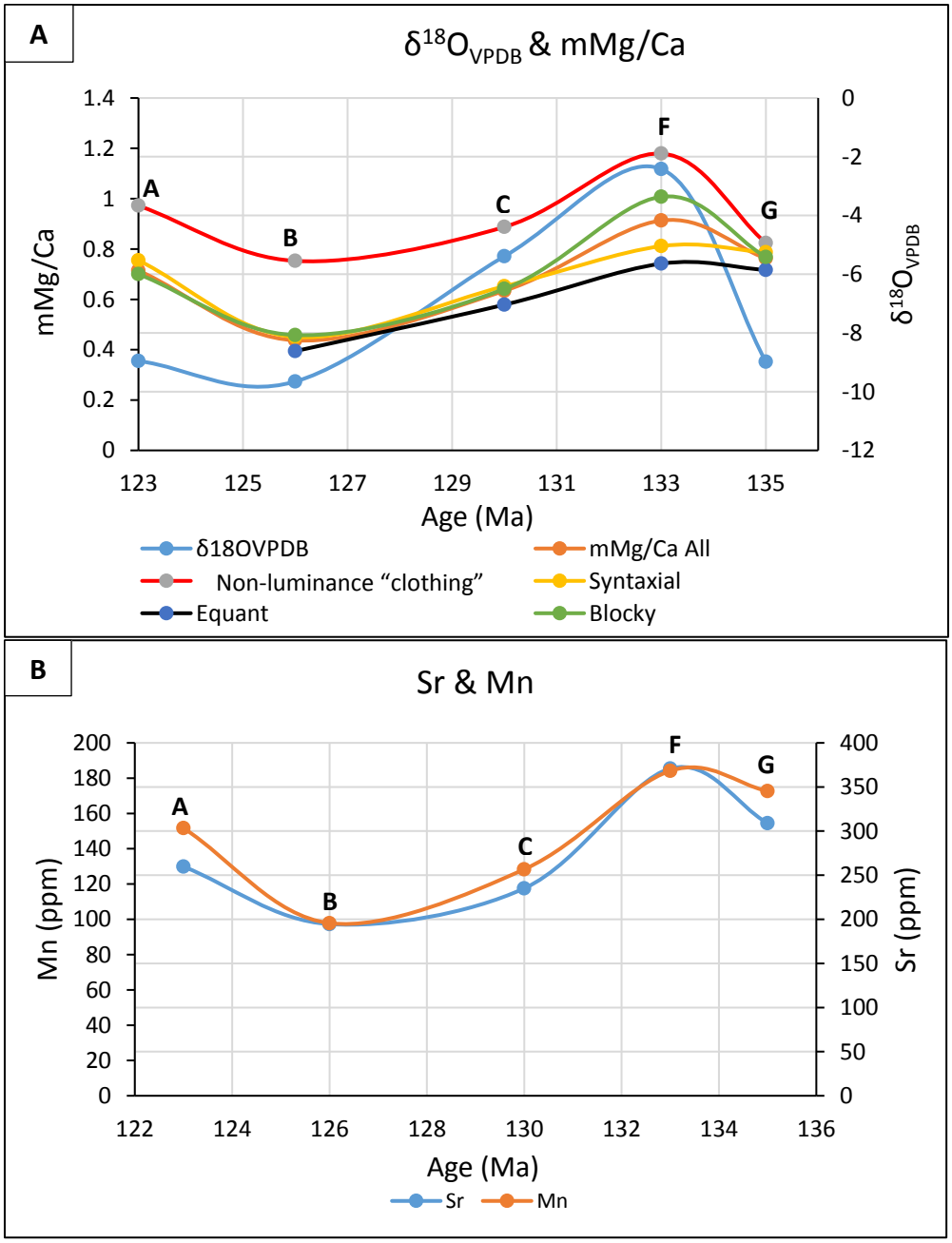


Figure 7.2: Pore fluid evolution through time for different Reservoirs. A) means of echinoderm 'clothing' non-luminance calcite, syntaxial, equant, blocky, all calcite cements, and $\delta^{18}O_{VPDB}$ of all calcite cements. B) Sr and Mn means for all calcite cements.

Elaborating more on this subject, after combining all data (syntaxial, equant and blocky) including $\delta^{18}O_{VPDB}$, mMg/Ca, Sr and Mn, it was found that the means of all these parameters follow same trend at each individual Reservoir (Figure 7.2A & B).

The lowest means for $\delta^{18}O_{VPDB}$, mMg/Ca, Sr and Mn (-9.65‰, 0.44, 195 and 152 respectively) are found in Reservoir B whereas the highest (-2.42‰, 0.91, 371 and 184 respectively) in Reservoir F. All these indicators are sensitive to major global change in seawater composition and they preserve and mimic this global trend. This further supports the model of the evolution of calcite cement with burial in a relatively close system. The presence of hardgrounds and Dense Zones interbedded with Reservoirs form effective seals compartmentalized Reservoirs from an early stage. In fact, these Dense Zones form local seals across the entire platform and can be traced into other nearby fields (Strohmenger et al., 2006).

By correlating in-situ $\delta^{18}O_{VPDB}$ with oil inclusions, an earlier oil charge can be proposed in the shallower Reservoirs relative to the deeper Reservoirs and coeval water leg. The early emplacement of oil caused cementation in shallower Reservoirs to continue with lower rates and preserved porosity from earlier time. Conversely, larger volumes of cement precipitated in the water leg to occlude most of the pore spaces. We can show that calcite cementation in the shallower Reservoirs of the oil leg continued to a maximum precipitation temperatures of ~144˚C. Whereas, in the water leg and deeper Reservoirs, cementation ceased between ~100 ˚C and 110˚C. These range of temperatures also agree with previous findings on Thamama Reservoirs (Cox. et al., 2010; Neilson et al., 1998; Paganoni et al., 2016; Vohrenkamp et al., 2014; Thorpe, 2014).

## 7.6 Future Work

Micritization is thought to be important process for developing microporosity in Thamama Group, particularly in Reservoir B. Further investigation will yield a better understanding of the origin and mechanize of micritization. This can be done for example by 1) conducting EPMA to investigate chemical composition, 3) examination of the 3D geometry of micrite particles and their relationship with surrounding pores and cements using SEM, 3) comparing micrite particles in different settings (different depositional environments, and in oil vs water leg).

Considerable attention should be given to the late dissolution event which partially dissolved some dolomite and kaolinite. This process also washed away some bitumen, enhanced microporosity formation, and created vugs that cross cut the small fractures. Dissolution also occurred along stylolites and dissolution seams. Reservoir quality seems to be significantly affected by this event. Thus, it will worth understanding the origin of the corrosive fluid which involved in this process. Also, investigating the direction of migration of this fluid will help to better trace and predict the pathway of dissolution and hence trace higher poroperm areas.

In Chapter 3, for total precipitated cement calculation the following have not considered: As a cement gets bigger, the volume increases for the same apparent width of CL zone. This should be considered for future work to get better and closer estimate to precipitated calcite in individual Reservoir.

EPMA data show depletion in Mn, Fe and Sr contents in the upper Reservoir cements (older cement Zones of syntaxial and equant) indicating that these cements were precipitated in a shallower, oxic environment (Section 4.4.1). In terms of stratigraphic location, upper Reservoir cements were precipitated at shallower depth compared with lower Reservoirs at the time where accommodation space was filled by sediments of the lower Reservoirs. This means that sediments of upper Reservoirs did not reach the deepest depositional point of the accommodation space that was reached by lower Reservoirs. Hence there will be variation in some factors including clay deposit and pore water redox conditions. The variation in clay content can be indicated from Figure 1.5 (Chapter 1) where clay concentration in Dense Zones decreases towards the upper Reservoirs. The decline in clay content is in parallel with the decline in Mn, Fe and Sr content for Reservoirs C and B but not A. Hence, looking at this trend in terms of stratigraphy, changes in relative sea level, and local subsidence history in the region might help to clarify this.

The higher mMg/Ca found in younger cements of blocky calcite in some Reservoirs A and G needs more detailed study. The higher mMg/Ca might be due to influx of fluids that are rich in Mg. These younger cement Zones might have been

precipitated at stratigraphically shallower depth after the uplifting of t units probably as a result of the second major tectonic event in the Late Eocene-Miocene. The second compressional event resulted in a major uplift and erosion in the area. This can be tested by analysing cements precipitated at the same time, perhaps cements precipitated in fractures after this event, and comparing them with the results of this study. Analysis might include EPMA and stable oxygen isotopes.

Both mMg/Ca and $\delta^{18}O_{VPDB}$ of older cement Zones in Reservoir G show very different values compared with global Lower Cretaceous trend. Limited areas were samples from Reservoir G older cements because syntaxial calcite is rare in this Reservoir. Also, the analysed cements were sampled from an area close to fractures. Thus, it is possible that these cements have been influenced by fluids transported via the fracture. Accordingly, sampling more areas away from fractures and from non-fractured well cores, will reveal a better understanding of the origin of these younger cement zones.

As seen from elemental and oxygen isotope data that $\delta^{18}O_{VPDB}$, mMg/Ca, Sr and Mn behave generally in a predictable and same way and follow global seawater change caused probably by hardground seals. This is of interest for both climatic change predictions and for investigating potential Reservoirs. Reservoir B is consider as the most profitable Reservoir interval in Field A and in many nearby Fields. This Reservoir was deposited at a time of lower $\delta^{18}O_{VPDB}$, mMg/Ca as well as Sr and Mn. Further investigation and correlation of these data with seawater change might enable the behaviour of other potential Reservoirs to be predicted.

Formation of hardground seems to be unique phenomenon of the upwelling and organic-rich micrite periods which comprise subsurface bacterial induced cementation during higher sea level episodes (Dickson et al., 2005; Mutti and Bernoulli, 2003). The Early Cretaceous is well known as extreme greenhouse climate characterized by high $CO_2$ level (Larson, 1991), which resulted in higher sea level compared with today's sea level (Föllmi, 2012; Miller et al., 2005). The flooding at that time produced broadly distinguish shallow marine depositional facies and also probably caused hardgrounds

formation due to early lithification by diagenesis at seafloors (Dickson et al., 2005; Wilson and Palmer, 1992). The formation of hardgrounds are also interpreted to be due to subaerial exposure (e.g. Strohmenger et al., 2006), however no evidence of subaerial exposure was found in this study. Negative shift in $\delta^{13}C$ was reported in Miocene hardground (Mutti and Bernoulli, 2003) as well as Lower Cretaceous hardground (Dickson et al., 2005) interpreted to be due to microbial activity supplied probably by nutrients from upwelling. The negative $\delta^{13}C$ shift was also reported at the onset of OAE 1a coincides with high nutrient level during Early Aptian (Westermann, et al., 2013). The negative shift was also reported preceded the OAE1 during the Late Barremian-Early Aptian in some places (Li et al., 2008; Menegatti et al., 1998; Stein et al., 2012). It appears to be correlation between hardground formation, negative $\delta^{13}C$ excursion, and upwelling during higher sea level episodes. Therefore, an investigation on this subject should provide better explanation about the origin of hardgrounds which consider important seals for significant Reservoirs particularly for Thamama Group.

# Bibliography

Adams, J. E., and M. L. Rhodes, 1960, Dolomitization by seepage refluxion: AAPG Bulletin, v. 44, p. 1912-1920.

Al-Aasm, I. S., and K. K. Azmy, 1996, Diagenesis and evolution of microporosity of middle-upper Devonian Kee Scarp Reefs, Norman wells, northwest territories, Canada: petrographic and chemical evidence: AAPG bulletin, v. 80, p. 82-99.

Al-Aasm, I., S. Morad, S. Durocher, and I. Muir, 1996, Sedimentology, C, S, Fe relationships and stable isotopic compositions in Devonian black mudrocks, Mackenzie Mountains, Northwest Territories, Canada: Sedimentary Geology, v. 106, p. 279-298.

Al-Hashimi, W. S., 1976, Significance of strontium distribution in some carbonate rocks in the Carboniferous of Northumberland, England: Journal of Sedimentary Research, v. 46.

Ali, M. Y., 1995, Carbonate cement stratigraphy and timing of diagenesis in a Miocene mixed carbonate-clastic sequence, offshore Sabah, Malaysia: constraints from cathodoluminescence, geochemistry, and isotope studies: Sedimentary Geology, v. 99, p. 191-214.

Al-Hosani, I., 2006, High Resolution Sequence Stratigraphy and Reservoir Characterization of a Lekhwair Reservoir Unit (Lower Cretaceous, United Arab Emirates).

Al-Suwaidi, A. S., A. K. Taher, A. S. Alsharhan, and M. G. Salah, 2000, Stratigraphy and geochemistry of Upper Jurassic Diyab Formation, Abu Dhabi, UAE.

Al-Zaabi, N., C. Strohmenger, W. Soroka, J. Dervieux, M. Abdelsattar, R. Rosell, and S. Ali, 2005, Seismic Sequence Stratigraphy and Reservoir Distribution of the Early Cretaceous Habshan Formation in the UAE: International Petroleum Technology Conference.

Ali, M. Y., and A. Watts, 2009, Subsidence history, gravity anomalies and flexure of the United Arab Emirates (UAE) foreland basin: GeoArabia, v. 14, p. 17-44.

Alsharhan, A., 1989, Petroleum geology of the United Arab Emirates: Journal of Petroleum Geology, v. 12, p. 253-288.

Alsharhan, A. S. 2014. Petroleum systems in the Middle East. Geological Society, London, Special Publications 2014, v.392; p361-408.
Alsharhan, A., 1990, Geology and reservoir characteristics of Lower Cretaceous Kharaib Formation in Zakum Field, Abu Dhabi, United Arab Emirates: Geological Society, London, Special Publications, v. 50, p. 299-316.

Alsharhan, A., 1993, Asab Field--United Arab Emirates, Rub Al Khali Basin, Abu Dhabi.

Alsharhan, A., and C. S. C. Kendall, 1991, Cretaceous chronostratigraphy, unconformities and eustatic sealevel changes in the sediments of Abu Dhabi, United Arab Emirates: Cretaceous research, v. 12, p. 379-401.

Alsharhan, A., and A. Nairn, 1986, A review of the Cretaceous formations in the Arabian Peninsula and Gulf: Part I. Lower Cretaceous (Thamama Group) stratigraphy and paleogeography: Journal of Petroleum Geology, v. 9, p. 365-391.

Alsharhan, A. S., I. S. Al-Aasm, and M. G. Salah, 2000, Stratigraphy, stable isotopes, and hydrocarbon potential of the Aptian Shuaiba Formation, UAE.

Alsharhan, A. S., and J. L. Sadd, 2000, Stylolites in Lower Cretaceous carbonate reservoirs, UAE.

Alsharhan, A. S., and Salah, M. G., 1997, Tectonic implications of diapirism on hydrocarbon accumulation in the United Arab Emirates: Bulletin of canadian petroleum geology, v. 45, no. 3, p. 279-296.

Alsharhan, A. S., Rizk, Z. A., Nairn, A. E. M., Bakhit, D. W., and Alhajari, S. A., 2001, Geology of the Arabian Peninsula and Gulf, Hydrogeology of an Arid Region: The Arabian Gulf and Adjoining Areas: The Netherlands, Elsevier Science, p. 55-77.

Alsharhan, A. S., and R. W. Scott, 2000, Hydrocarbon potential of Mesozoic carbonate platform-basin systems, UAE.

Al-Aasm, I., F. Ghazban, and M. Ranjbaran, 2009, Dolomitization and related fluid evolution in the Oligocene–Miocene Asmari Formation, Gachsaran area, SW Iran: petrographic and isotopic evidence: Journal of Petroleum Geology, v. 32, p. 287-304.

Ando, A., K. Kaiho, H. Kawahata, and T. Kakegawa, 2008, Timing and magnitude of early Aptian extreme warming: unraveling primary δ 18 O variation in indurated pelagic carbonates at Deep Sea Drilling Project Site 463, central Pacific Ocean: Palaeogeography, Palaeoclimatology, Palaeoecology, v. 260, p. 463-476.

Azer, S., and C. Toland, 1993, Sea level changes in the Aptian and Barremian (Upper Thamama) of offshore Abu Dhabi, UAE: Middle East Oil Show.

Balthasar, U., and M. Cusack, 2015, Aragonite-calcite seas—Quantifying the gray area: Geology, v. 43, p. 99-102.

Bagrintseva, K. I., 2015, Carbonate Reservoir Rock Properties and Previous Studies: Carbonate Reservoir Rocks, p. 1-11.

Barnaby, R. J., and J. D. Rimstidt, 1989, Redox conditions of calcite cementation interpreted from Mn and Fe contents of authigenic calcites: Geological Society of America Bulletin, v. 101, p. 795-804.

Barrera, E., B. T. Huber, S. M. Savin, and P. N. Webb, 1987, Antarctic marine temperatures: Late Campanian through early Paleocene: Paleoceanography, v. 2, p. 21-47.

Bathurst, R., 1966, Boring algae, micrite envelopes and lithification of molluscan biosparites: Geological Journal, v. 5, p. 15-32.

Berner, R., 1975, The role of magnesium in the crystal growth of calcite and aragonite from sea water: Geochimica et Cosmochimica Acta, v. 39, p. 489-504.

Berner, R. A., 2004, A model for calcium, magnesium and sulfate in seawater over Phanerozoic time: American Journal of Science, v. 304, p. 438-453.

Boggs, S., and D. Krinsley, 2006, Application of cathodoluminescence imaging to the study of sedimentary rocks, Cambridge University Press.

Boles, J., 1998, Carbonate cementation in Tertiary sandstones, San Joaquin basin, California: Carbonate Cementation in Sandstones: Distribution Patterns and Geochemical Evolution (Special Publication 26 of the IAS), v. 64, p. 261.

Boles, J. R., P. Eichhubl, G. Garven, and J. Chen, 2004, Evolution of a hydrocarbon migration pathway along basin-bounding faults: Evidence from fault cement: AAPG bulletin, v. 88, p. 947-970.

Bots, P., L. Benning, R. Rickaby, and S. Shaw, 2011, The role of SO4 in the switch from calcite to aragonite seas: Geology, v. 39, p. 331-334.

Braithwaite, C., 1993, Cement Sequence Stratigraphy in Carbonates: PERSPECTIVE: Journal of Sedimentary Research, v. 63.

Brand, U., and J. Veizer, 1980, Chemical diagenesis of a multicomponent carbonate system--1: Trace elements: Journal of Sedimentary Research, v. 50.

Breesch, L., R. Swennen, B. Vincent, R. Ellison, and B. Dewever, 2010, Dolomite cementation and recrystallisation of sedimentary breccias along the Musandam Platform margin (United Arab Emirates): Journal of Geochemical Exploration, v. 106, p. 34-43.

Briscoe, H. V. A., and P. L. Robinson, 1925, XCIX.—A redetermination of the atomic weight of boron: Journal of the Chemical Society, Transactions, v. 127, p. 696-720.

Budd, D. A., 1984, Freshwater diagenesis of Holocene ooid sands, Schooner Cays, Bahamas, University of Texas at Austin.

Budd, D. A., 1989, Micro-rhombic calcite and microporosity in limestones: a geochemical study of the Lower Cretaceous Thamama Group, UAE: Sedimentary Geology, v. 63, p. 293-311.

Burchette, T. P., 2012, Carbonate rocks and petroleum reservoirs: a geological perspective from the industry: Geological Society, London, Special Publications, v. 370, p. 17-37.

Burns, S. J., and P. A. Baker, 1987, A geochemical study of dolomite in the Monterey Formation, California: Journal of Sedimentary Research, v. 57.

Burruss, R. C., 1991, Practical aspects of fluorescence microscopy of petroleum fluid inclusions.

Burruss, R. C., K. R. Cercone, and P. M. Harris, 1985, Timing of hydrocarbon migration: evidenced from fluid inclusions in calcite cements, tectonics and burial history.

Callot, J.-P., L. Breesch, N. Guilhaumou, F. Roure, R. Swennen, and N. Vilasi, 2010, Paleo-fluids characterisation and fluid flow modelling along a regional transect in Northern United Arab Emirates (UAE): Arabian Journal of Geosciences, v. 3, p. 413-437.

Carpenter, A. B., 1980, The Chemistry of Dolomite Formanon I: The Stability of Dolomite.

Carpenter, S. J., and K. C. J. G. e. C. A. Lohmann, 1992, SrMg ratios of modern marine calcite: Empirical indicators of ocean chemistry and precipitation rate, v. 56, p. 1837-1849.

Carpenter, S. J., K. C. Lohmann, P. Holden, L. M. Walter, T. J. Huston, and A. N. Halliday, 1991, δ18O values, 87Sr86Sr and Sr/Mg ratios of Late Devonian abiotic marine calcite: implications for the composition of ancient seawater: Geochimica et Cosmochimica Acta, v. 55.

Chafetz, H., and A. Reid, 2000, Syndepositional shallow-water precipitation of glauconitic minerals: Sedimentary Geology, v. 136, p. 29-42.

Bibliography

Choquette, P. W., 1971, Late ferroan dolomite cement, Mississippian carbonates, Illinois Basin, USA, Carbonate cements, v. 19, Johns Hopkins University Press Baltimore, p. 339-346.

Cicero, A. D., and K. C. Lohmann, 2001, Sr/Mg variation during rock-water interaction: Implications for secular changes in the elemental chemistry of ancient seawater: Geochimica et Cosmochimica Acta, v. 65, p. 741-761.

Clarke, L. J., and H. C. Jenkyns, 1999, New oxygen isotope evidence for long-term Cretaceous climatic change in the Southern Hemisphere: Geology, v. 27, p. 699-702.

Clayton, R. N., and E. T. Degens, 1959, Use of carbon isotope analyses of carbonates for differentiating fresh-water and marine sediments: AAPG Bulletin, v. 43, p. 890-897.

Collins, J., and J. Lake, 1988, Sierra reef complex, Middle Devonian, northeastern British Columbia. In: Reefs, Canada and Adjacent Areas (eds H. H. J. Geldsetzer, N. P. James and G. E. Tebbutt), Canadian Soc. Petroleum Geology Memoir, v. 13, p. 414-421.

Cox, P., R. Wood, J. Dickson, H. Al Rougha, H. Shebl, and P. Corbett, 2010, Dynamics of cementation in response to oil charge: Evidence from a Cretaceous carbonate field, UAE: Sedimentary Geology, v. 228, p. 246-254.

Davies, G. R., and L. B. Smith Jr, 2006, Structurally controlled hydrothermal dolomite reservoir facies: An overview: AAPG bulletin, v. 90, p. 1641-1690.

De Bona, J., N. Dani, J. Ketzer, and L. De Ros, 2008, Dickite in shallow oil reservoirs from Recôncavo Basin, Brazil: diagenetic implications for basin evolution: Clay Minerals, v. 43, p. 213-233.

de Periere, M. D., C. Durlet, E. Vennin, L. Lambert, R. Bourillot, B. Caline, and E. Poli, 2011, Morphometry of micrite particles in cretaceous microporous limestones of the Middle East: Influence on reservoir properties: Marine and Petroleum Geology, v. 28, p. 1727-1750.

Deffeyes, K., 1965, Dolomitization of recent and Plio-Pleistocene sediments by marine evaporite waters on Bonaire, Netherlands Antills: Dolomitization and Limestone Diagenesis, p. 71-88.

Dickson, J., 1965, A modified staining technique for carbonates in thin section.

Dickson, J., 2004, Echinoderm skeletal preservation: calcite-aragonite seas and the Mg/Ca ratio of Phanerozoic oceans: Journal of Sedimentary Research, v. 74, p. 355-365.

Dickson, J., and M. Coleman, 1980, Changes in carbon and oxygen isotope composition during limestone diagenesis: Sedimentology, v. 27, p. 107-118.

Dickson, J., R. Wood, H. B. Al Rougha, and H. Shebl, 2008, Sulphate reduction associated with hardgrounds: Lithification afterburn!: Sedimentary Geology, v. 205, p. 34-39.

Ditchfield, P., J. Marshall, and D. Pirrie, 1994, High latitude palaeotemperature variation: new data from the Thithonian to Eocene of James Ross Island, Antarctica: Palaeogeography, Palaeoclimatology, Palaeoecology, v. 107, p. 79-101.

Dromgoole, E. L., and L. M. Walter, 1990, Iron and manganese incorporation into calcite: Effects of growth kinetics, temperature and solution chemistry: Chemical Geology, v. 81, p. 311-336.

Bibliography

Egeberg, P. K., and P. Aagaard, 1989, Origin and evolution of formation waters from oil fields on the Norwegian shelf: Applied Geochemistry, v. 4, p. 131-142.

Ehrenberg, S. N., A. A. Aqrawi, and P. H. Nadeau, 2008, An overview of reservoir quality in producing Cretaceous strata of the Middle East: Petroleum Geoscience, v. 14, p. 307-318.

Ehrenberg, S. N., S. Morad, L. Yaxin, and R. Chen, 2016, Stylolites and Porosity In A Lower Cretaceous Limestone Reservoir, Onshore Abu Dhabi, UAE: Journal of Sedimentary Research, v. 86, p. 1228-1247.

Ehrenberg, S., and P. Nadeau, 2005, Sandstone vs. carbonate petroleum reservoirs: A global perspective on porosity-depth and porosity-permeability relationships: AAPG bulletin, v. 89, p. 435-445.

Feazel, C. T., 1985, Prevention of carbonate cementation in petroleum reservoirs.

Feazel, C. T., and R. A. Schatzinger, 1985, Prevention of carbonate cementation in petroleum reservoirs.

Flügel, E., 2004, Carbonate Depositional Environments, Microfacies of Carbonate Rocks, Springer, p. 7-52.

Folk, R. L., 1974, The natural history of crystalline calcium carbonate: effect of magnesium content and salinity: Journal of Sedimentary Research, v. 44.

Folk, R. L., and L. S. Land, 1975, Mg/Ca ratio and salinity: two controls over crystallization of dolomite: AAPG bulletin, v. 59, p. 60-68.

Friedman, I., and J. R. O'Neil, 1977, Compilation of stable isotope fractionation factors of geochemical interest, v. 440, USGPO.

Froelich, P. N., G. Klinkhammer, M. L. Bender, N. Luedtke, G. R. Heath, D. Cullen, P. Dauphin, D. Hammond, B. Hartman, and V. Maynard, 1979, Early oxidation of organic matter in pelagic sediments of the eastern equatorial Atlantic: suboxic diagenesis: Geochimica et cosmochimica acta, v. 43, p. 1075-1090.

Föllmi, K. B., 2012, Early Cretaceous life, climate and anoxia: Cretaceous Research, v. 35, p. 230-257.

Gaffin, S., 1987, Ridge volume dependence on seafloor generation rate and inversion using long term sealevel change: American Journal of Science, v. 287, p. 596-611.

Gaines, A. M., 1977, Protodolomite redefined: Journal of Sedimentary Research, v. 47.

Garland, J., J. Neilson, S. E. Laubach, and K. J. Whidden, 2012, Advances in carbonate exploration and reservoir analysis: Geological Society, London, Special Publications, v. 370, p. 1-15.

Glennie, K. W., 2000, Cretaceous tectonic evolution of Arabia's eastern plate margin: a tale of two oceans.

Goldstein, R., and T. Reynolds, 1994, Systematics of fluid inclusions in diagenetic minerals: SEPM Short Course Notes, 31.

Bibliography

Gonzalez, L. A., and K. C. Lohmann, 1985, Carbon and oxygen isotopic composition of Holocene reefal carbonates: Geology, v. 13, p. 811-814.

Graf, D. L., and J. R. Goldsmith, 1956, Some hydrothermal syntheses of dolomite and protodolomite: The Journal of Geology, v. 64, p. 173-186.

Granier, B., A. S. Al Suwaidi, R. Busnardo, S. K. Aziz, and R. Schroeder, 2003, New insight on the stratigraphy of the" Upper Thamama" in offshore Abu Dhabi (UAE): Carnets de géologie/Notebooks on geology, Maintenon, Article, v. 5.

Granier, B., M. Moullade, P. Ropolo, G. Tronchetti, and W. Kuhnt, 2008, The Aptian stage: Input from the historical stratotype: Symposium “Stratigraphic subdivisions of the Cretaceous System: State of the art”, 33rd IGC Congress, Oslo.

Gregg, J. M., D. L. Bish, S. E. Kaczmarek, and H. G. Machel, 2015, Mineralogy, nucleation and growth of dolomite in the laboratory and sedimentary environment: a review: Sedimentology, v. 62, p. 1749-1769.

Gröcke, D. R., S. P. Hesselbo, and H. C. Jenkyns, 1999, Carbon-isotope composition of Lower Cretaceous fossil wood: Ocean-atmosphere chemistry and relation to sea-level change: Geology, v. 27, p. 155-158.

Gumati, Y., 1993, Kinetic modelling, thermal maturation and hydrocarbon generation in the United Arab Emirates: Marine and Petroleum Geology, v. 10, p. 153-161.

Haeri-Ardakani, O., I. Al-Aasm, and M. Coniglio, 2013, Petrologic and geochemical attributes of fracture-related dolomitization in Ordovician carbonates and their spatial distribution in southwestern Ontario, Canada: Marine and Petroleum Geology, v. 43, p. 409-422.

Haq, B. U., J. Hardenbol, and P. R. Vail, 1988, Mesozoic and Cenozoic chronostratigraphy and cycles of sea-level change.

Hardie, L. A., 1996, Secular variation in seawater chemistry: An explanation for the coupled secular variation in the mineralogies of marine limestones and potash evaporites over the past 600 my: Geology, v. 24, p. 279-283.

Harris, P., S. Frost, G. Seiglie, and N. Schneidermann, 1984, Regional unconformities and depositional cycles, Cretaceous of the Arabian Peninsula.

Hasiuk, F. J., and K. C. Lohmann, 2008, Mississippian paleocean chemistry from biotic and abiotic carbonate, Muleshoe Mound, Lake Valley formation, New Mexico, USA: Journal of Sedimentary Research, v. 78, p. 147-164.

Hays, J. D., and W. C. PITMAN III, 1973, Lithospheric plate motion, sea level changes and climatic and ecological consequences: Nature, v. 246, p. 18.

Heasley, E. C., R. H. Worden, and J. P. Hendry, 2000, Cement distribution in a carbonate reservoir: recognition of a palaeo oil–water contact and its relationship to reservoir quality in the Humbly Grove field, onshore, UK: Marine and Petroleum Geology, v. 17, p. 639-654.

Herrle, J. O., C. J. Schröder-Adams, W. Davis, A. T. Pugh, J. M. Galloway, and J. Fath, 2015, Mid-Cretaceous High Arctic stratigraphy, climate, and oceanic anoxic events: Geology, v. 43, p. 403-406.

Bibliography

Heydari, E., and C. H. Moore, 1993, Zonation and geochemical patterns of burial calcite cements: Upper Smackover Formation, Clarke County, Mississippi: Journal of Sedimentary Research, v. 63.

Heydari, E., and W. J. Wade, 2002, Massive recrystallization of low-Mg calcite at high temperatures in hydrocarbon source rocks: Implications for organic acids as factors in diagenesis: AAPG bulletin, v. 86, p. 1285-1303.

Hillgärtner, H., F. S. van Buchem, F. Gaumet, P. Razin, B. Pittet, J. Grötsch, and H. Droste, 2003, The Barremian-Aptian evolution of the eastern Arabian carbonate platform margin (northern Oman): Journal of Sedimentary Research, v. 73, p. 756-773.

Holail, H., and K. C. Lohmann, 1994, The role of early lithification in development of chalky porosity in calcitic micrites: Upper Cretaceous chalks, Egypt: Sedimentary geology, v. 88, p. 193-200.

Hutchins, G. A., 1979, Electron probe microanalysis, Surface and Colloid Science, Springer, p. 217-304.

Immenhauser, A., H. Hillgärtner, and E. Van Bentum, 2005, Microbial-foraminiferal episodes in the Early Aptian of the southern Tethyan margin: ecological significance and possible relation to oceanic anoxic event 1a: Sedimentology, v. 52, p. 77-99.

Irwin, H., 1980, Early diagenetic carbonate precipitation and pore fluid migration in the Kimmeridge Clay of Dorset, England: Sedimentology, v. 27, p. 577-591.

Jenkin, G., D. Craw, and A. Fallick, 1994, Stable isotopic and fluid inclusion evidence for meteoric fluid penetration into an active mountain belt; Alpine Schist, New Zealand: Journal of metamorphic geology, v. 12, p. 429-444.

Jones, C. E., and H. C. Jenkyns, 2001, Seawater strontium isotopes, oceanic anoxic events, and seafloor hydrothermal activity in the Jurassic and Cretaceous: American Journal of Science, v. 301, p. 112-149.

Kaczmarek, S., J. Gregg, D. Bish, H. Machel, and B. Fouke, 2017, Dolomite, very high-magnesium calcite, and microbes—implications for the microbial model of dolomitization: SEPM Special Publication.

Kaufmann, B., and J. Wendt, 2000, Calcite cement successions in Middle Devonian (Givetian) carbonate mud buildups of the southern Ahnet Basin (Algerian Sahara): Carbonates and Evaporites, v. 15, p. 149.

Keith, M., G. Anderson, and R. Eichler, 1964, Carbon and oxygen isotopic composition of mollusk shells from marine and fresh-water environments: Geochimica et cosmochimica acta, v. 28, p. 1757-1786.

Keith, M., and J. N. Weber, 1964, Carbon and oxygen isotopic composition of selected limestones and fossils: Geochimica et Cosmochimica Acta, v. 28, p. 1787-1816.

Kerr, A. C., 1998, Oceanic plateau formation: a cause of mass extinction and black shale deposition around the Cenomanian–Turonian boundary?: Journal of the Geological Society, v. 155, p. 619-626.

Kim, S.-T., and J. R. O'Neil, 1997, Equilibrium and nonequilibrium oxygen isotope effects in synthetic carbonates: Geochimica et Cosmochimica Acta, v. 61, p. 3461-3475.

Bibliography

Koepnick, R., 1987, Distribution and permeability of stylolite-bearing horizons within a Lower Cretaceous carbonate reservoir in the Middle East: SPE Formation Evaluation, v. 2, p. 137-142.

Kolodny, Y., and M. Raab, 1988, Oxygen isotopes in phosphatic fish remains from Israel: paleothermometry of tropical Cretaceous and Tertiary shelf waters: Palaeogeography, Palaeoclimatology, Palaeoecology, v. 64, p. 59-67.

Krause, S., V. Liebetrau, S. Gorb, M. Sánchez-Román, J. A. McKenzie, and T. Treude, 2012, Microbial nucleation of Mg-rich dolomite in exopolymeric substances under anoxic modern seawater salinity: New insight into an old enigma: Geology, v. 40, p. 587-590.

Lambert, L., C. Durlet, J.-P. Loreau, and G. Marnier, 2006, Burial dissolution of micrite in Middle East carbonate reservoirs (Jurassic–Cretaceous): keys for recognition and timing: Marine and Petroleum Geology, v. 23, p. 79-92.

Land, L. S., 1980, The isotopic and trace element geochemistry of dolomite: the state of the art.

Larson, R. L., 1991, Geological consequences of superplumes: Geology, v. 19, p. 963-966.

Larson, R. L., and E. Erba, 1999, Onset of the Mid-Cretaceous greenhouse in the Barremian-Aptian: Igneous events and the biological, sedimentary, and geochemical responses: Paleoceanography, v. 14, p. 663-678.

Larson, R. L., and P. Olson, 1991, Mantle plumes control magnetic reversal frequency: Earth and Planetary Science Letters, v. 107, p. 437-447.

Lavoie, D., and C. Morin, 2004, Hydrothermal dolomitization in the Lower Silurian Sayabec Formation in northern Gaspé–Matapédia (Québec): constraint on timing of porosity and regional significance for hydrocarbon reservoirs: Bulletin of Canadian Petroleum Geology, v. 52, p. 256-269.

Leythaeuser, D., O. Borromeo, F. Mosca, R. di Primio, M. Radke, and R. G. Schaefer, 1995, Pressure solution in carbonate source rocks and its control on petroleum generation and migration: Marine and Petroleum Geology, v. 12, p. 717-733.

Li, Y.-X., T. J. Bralower, I. P. Montañez, D. A. Osleger, M. A. Arthur, D. M. Bice, T. D. Herbert, E. Erba, and I. P. Silva, 2008, Toward an orbital chronology for the early Aptian oceanic anoxic event (OAE1a,~ 120 Ma): Earth and Planetary Science Letters, v. 271, p. 88-100.

Lijmbach, G., J. Toxopeus, T. Rodenburg, and L. Hermans, 1992, Geochemical study of crude oils and source rocks in onshore Abu Dhabi: Abu Dhabi Petroleum Conference.

Lonnee, J., and H. G. Machel, 2006, Pervasive dolomitization with subsequent hydrothermal alteration in the Clarke Lake gas field, Middle Devonian Slave Point Formation, British Columbia, Canada: AAPG bulletin, v. 90, p. 1739-1761.

Lowenstein, T. K., M. N. Timofeeff, S. T. Brennan, L. A. Hardie, and R. V. Demicco, 2001, Oscillations in Phanerozoic seawater chemistry: Evidence from fluid inclusions: Science, v. 294, p. 1086-1088.

Loutfi, G., and S. El Bishlawy, 1986, Habitat of hydrocarbon in Abu Dhabi, UAE: Symposium on Hydrocarbon Potential of Intense Thrust Zones, Abu Dhabi, December 1986, p. 63-124.

Lucia, F. J., 2007, Carbonate reservoir characterization: An integrated approach, Springer Science & Business Media.

Luczaj, J. A., W. B. Harrison III, and N. S. Williams, 2006, Fractured hydrothermal dolomite reservoirs in the Devonian Dundee Formation of the central Michigan Basin: AAPG bulletin, v. 90, p. 1787-1801.

Lyon, I., S. Burley, P. McKeever, J. Saxton, and C. Macaulay, 2000, Oxygen isotope analysis of authigenic quartz in sandstones: a comparison of ion microprobe and conventional analytical techniques: Quartz cementation in sandstones, p. 299-316.

López-Horgue, M., E. Iriarte, S. Schröder, P. Fernández-Mendiola, B. Caline, H. Corneyllie, J. Frémont, M. Sudrie, and S. Zerti, 2010, Structurally controlled hydrothermal dolomites in Albian carbonates of the Asón valley, Basque Cantabrian Basin, Northern Spain: Marine and Petroleum Geology, v. 27, p. 1069-1092.

M'rabet, A., 1981, Differentiation of environments of dolomite formation, Lower Cretaceous of Central Tunisia: Sedimentology, v. 28, p. 331-352.

Machel, H-G., 1985, Cathodoluminescence in calcite and dolomite and its chemical interpretation: Geoscience Canada, v. 12, p. 139-147.

Machel, H. G., 2005, Investigations of burial diagenesis in carbonate hydrocarbon reservoir rocks: Geoscience Canada, v. 32.

Mackenzie, F. T., and J. W. Morse, 1992, Sedimentary carbonates through Phanerozoic time: Geochimica et Cosmochimica Acta, v. 56, p. 3281-3295.

Maliva, R., J. Dickson, and A. Fallick, 1999, Kaolin cements in limestones: potential indicators of organic-rich pore waters during diagenesis: Journal of Sedimentary Research, v. 69.

Marfil, R., M. Caja, M. Tsige, I. Al-Aasm, T. Martin-Crespo, and R. Salas, 2005, Carbonate-cemented stylolites and fractures in the Upper Jurassic limestones of the Eastern Iberian Range, Spain: a record of palaeofluids composition and thermal history: Sedimentary Geology, v. 178, p. 237-257.

Marzouk, I., H. Takezaki, and M. Miwa, 1995, Geologic controls on wettability of carbonate reservoirs, Abu Dhabi, UAE: Middle East Oil Show.

Mason, R., 1987, Ion microprobe analysis of trace elements in calcite with an application to the cathodoluminescence zonation of limestone cements from the Lower Carboniferous of South Wales, UK: Chemical Geology, v. 64, p. 209-224.

Melville, P., O. Al Jeelani, S. Al Menhali, and J. Grötsch, 2004, Three-dimensional seismic analysis in the characterization of a giant carbonate field, onshore Abu Dhabi, United Arab Emirates.

Menegatti, A. P., H. Weissert, R. S. Brown, R. V. Tyson, P. Farrimond, A. Strasser, and M. Caron, 1998, High-resolution δ13C stratigraphy through the Early Aptian "Livello selli" of the Alpine Tethys: Paleoceanography, v. 13, p. 530-545.

Meyer, F. O., R. C. Price, and S. M. Al-Raimi, 2000, Stratigraphic and petrophysical characteristics of cored Arab-D super-k intervals, Hawiyah area, Ghawar field, Saudi Arabia: GeoArabia, v. 5, p. 355-384.

Bibliography

Miller, K. G., M. A. Kominz, J. V. Browning, J. D. Wright, G. S. Mountain, M. E. Katz, P. J. Sugarman, B. S. Cramer, N. Christie-Blick, and S. F. Pekar, 2005, The Phanerozoic record of global sea-level change: science, v. 310, p. 1293-1298.

Moore, C. H., and W. J. Wade, 1989, Carbonate reservoirs: Porosity and diagenesis in a sequence stratigraphic framework, v. 67, Newnes.

Morad, S., 1998, Carbonate cementation in sandstones: distribution patterns and geochemical evolution, in Morad, S., ed., Carbonate Cementation in Sandstones: International Association of Sedimentologists, Special Publication 26, p. 1–26.

Morad, D., M. Paganoni, A. Al Harthi, S. Morad, A. Ceriani, H. Mansurbeg, A. Al Suwaidi, I. S. Al-Aasm, and S. N. Ehrenberg, 2016, Origin and evolution of microporosity in packstones and grainstones in a Lower Cretaceous carbonate reservoir, United Arab Emirates: Geological Society, London, Special Publications, v. 435, p. SP435. 20.

Morad, S., 2009, Carbonate Cementation in Sandstones: Distribution Patterns and Geochemical Evolution (Special Publication 26 of the IAS), v. 72, John Wiley & Sons.

Morad, S., I. S. Al-Aasm, F. H. Nader, A. Ceriani, M. Gasparrini, and H. Mansurbeg, 2012, Impact of diagenesis on the spatial and temporal distribution of reservoir quality in the Jurassic Arab D and C members, offshore Abu Dhabi oilfield, United Arab Emirates: GeoArabia, v. 17, p. 17-56.

Morad, S., I. Al-Aasm, M. Sirat, and M. Sattar, 2010, Vein calcite in cretaceous carbonate reservoirs of Abu Dhabi: Record of origin of fluids and diagenetic conditions: Journal of Geochemical Exploration, v. 106, p. 156-170.

Morad, S., K. Al-Ramadan, J. M. Ketzer, and L. De Ros, 2010, The impact of diagenesis on the heterogeneity of sandstone reservoirs: A review of the role of depositional facies and sequence stratigraphy: AAPG bulletin, v. 94, p. 1267-1309.

Morrow, D., 1982, Diagenesis 2. Dolomite-part 2 dolomitization models and Ancient dolostones: Geoscience Canada, v. 9.

Morse, J. W., and M. L. Bender, 1990, Partition coefficients in calcite: Examination of factors influencing the validity of experimental results and their application to natural systems: Chemical Geology, v. 82, p. 265-277.

Morse, J. W., Q. Wang, and M. Y. Tsio, 1997, Influences of temperature and Mg: Ca ratio on CaCO3 precipitates from seawater: Geology, v. 25, p. 85-87.

Moshier, S. O., 1989, Development of microporosity in a micritic limestone reservoir, Lower Cretaceous, Middle East: Sedimentary geology, v. 63, p. 217-240.

Murris, R. J., 1980, Middle East: stratigraphic evolution and oil habitat: American Association of Petroleum Geologists Bulletin, v. 64, no. 5, p. 597-618.

Mutti, M., and D. Bernoulli, 2003, Early marine lithification and hardground development on a Miocene ramp (Maiella, Italy): key surfaces to track changes in trophic resources in nontropical carbonate settings: Journal of Sedimentary Research, v. 73, p. 296-308.

Méhay, S., C. E. Keller, S. M. Bernasconi, H. Weissert, E. Erba, C. Bottini, and P. A. Hochuli, 2009, A volcanic CO2 pulse triggered the Cretaceous Oceanic Anoxic Event 1a and a biocalcification crisis: Geology, v. 37, p. 819-822.

Neilson, J., and N. Oxtoby, 2008, The relationship between petroleum, exotic cements and reservoir quality in carbonates–A review: Marine and Petroleum Geology, v. 25, p. 778-790.

Neilson, J. E., N. H. Oxtoby, M. D. Simmons, I. R. Simpson, and N. K. Fortunatova, 1998, The relationship between petroleum emplacement and carbonate reservoir quality: examples from Abu Dhabi and the Amu Darya Basin: MARINE AND PETROLEUM GEOLOGY, v. 15, p. 57-72.

Neilson, J. E., N. H. Oxtoby, and M. D. Simmons, 1996, Effect of petroleum emplacement on reservoir quality in the Thamama reservoirs of Abu Dhabi: Abu Dhabi International Petroleum Exhibition and Conference.

Ogg, J. G., 2004, The cretaceous period: A geologic time scale, p. 344-383.

Oswald, E., H. Mueller, D. Goff, H. Al-Habshi, and S. Al-Matroushi, 1995, Controls on porosity evolution in Thamama Group carbonate reservoirs in Abu Dhabi, UAE: Middle East oil show & conference.

Paganoni, M., A. Al Harthi, D. Morad, S. Morad, A. Ceriani, H. Mansurbeg, A. Al Suwaidi, I. S. Al-Aasm, S. N. Ehrenberg, and M. Sirat, 2016, Impact of stylolitization on diagenesis of a Lower Cretaceous carbonate reservoir from a giant oilfield, Abu Dhabi, United Arab Emirates: Sedimentary Geology, v. 335, p. 70-92.

Paytan, A., M. Kastner, D. Campbell, and M. H. Thiemens, 2004, Seawater sulfur isotope fluctuations in the Cretaceous: science, v. 304, p. 1663-1665.

Perrin, C., L. Prestimonaco, G. Servelle, R. Tilhac, M. Maury, and P. Cabrol, 2014, Aragonite–calcite speleothems: identifying original and diagenetic features: Journal of Sedimentary Research, v. 84, p. 245-269.

Pinnington, D. J., 1981, Schlumberger Well Evaluation Conference. United Arab Emirates/Qatar, Schlumberger, Middle East., 271 p.
Price, G. D., 1999, The evidence and implications of polar ice during the Mesozoic: Earth-Science Reviews, v. 48, p. 183-210.

Price, G., and J. Mutterlose, 2004, Isotopic signals from late Jurassic–early Cretaceous (Volgian–Valanginian) sub-Arctic belemnites, Yatria River, Western Siberia: Journal of the Geological Society, v. 161, p. 959-968.

Price, G. D., and E. V. Nunn, 2010, Valanginian isotope variation in glendonites and belemnites from Arctic Svalbard: Transient glacial temperatures during the Cretaceous greenhouse: Geology, v. 38, p. 251-254.

Prokopovich, N., 1952, The origin of stylolites: Journal of Sedimentary Research, v. 22.

Pucéat, E., C. Lécuyer, S. M. Sheppard, G. Dromart, S. Reboulet, and P. Grandjean, 2003, Thermal evolution of Cretaceous Tethyan marine waters inferred from oxygen isotope composition of fish tooth enamels: Paleoceanography, v. 18.

Qing, H., 1998, Petrography and geochemistry of early-stage, fine-and medium-crystalline dolomites in the Middle Devonian Presqu'ile Barrier at Pine Point, Canada: Sedimentology, v. 45, p. 433-446.

Bibliography

Reid, R. P., and I. G. Macintyre, 1998, Carbonate recrystallization in shallow marine environments: a widespread diagenetic process forming micritized grains: Journal of Sedimentary Research, v. 68.

Richards, M. A., and D. C. Engebretson, 1992, Large-scale mantle convection and the history of subduction: Nature, v. 355, p. 437.

Rifai, R. I., M. M. Kolkas, H. M. Holail, and K. A. Khaled, 2006, Diagenesis and geochemistry of the Aptian dolomite (cretaceous) in the Razzak Oil Field, western Desert, Egypt: Carbonates and evaporites, v. 21, p. 176.

Roberts, J. A., P. A. Kenward, D. A. Fowle, R. H. Goldstein, L. A. González, and D. S. Moore, 2013, Surface chemistry allows for abiotic precipitation of dolomite at low temperature: Proceedings of the National Academy of Sciences, v. 110, p. 14540-14545.

Rodriguez-Blanco, J. D., S. Shaw, and L. G. Benning, 2015, A route for the direct crystallization of dolomite: American Mineralogist, v. 100, p. 1172-1181.

Ruppel, S. C., and H. S. Cander, 1988, Dolomitization of Shallow-Water Platform Carbonates by Sea Water and Seawater Derived Brines San Andres Formation (Guadalupian), West Texas.

Sandberg, P. A., 1983, An oscillating trend in Phanerozoic non-skeletal carbonate mineralogy: Nature, v. 305, p. 19.

Sandberg, P. A., 1985, Nonskeletal aragonite and pCO2 in the Phanerozoic and Proterozoic: The Carbon Cycle and Atmospheric CO: Natural Variations Archean to Present, p. 585-594.

Sharland, P. R., R. Archer, D. Casey, R. Davies, S. Hall, A. Heward, A. Horbury, and M. Simmons, 2013, Arabian plate sequence stratigraphy: GeoArabia, Journal of the Middle East Petroleum Geosciences, v. 18.

Sharp, Z., 2017, Principles of stable isotope geochemistry.

Sibley, D. F., and J. M. Gregg, 1987, Classification of dolomite rock textures: Journal of Sedimentary Research, v. 57.

Sibley, D. F., S. H. Nordeng, and M. L. Borkowski, 1994, Dolomitization kinetics in hydrothermal bombs and natural settings: Journal of Sedimentary Research, v. 64.

Sirat, M., I. Al-Aasm, S. Morad, A. Aldahan, O. Al-Jallad, A. Ceriani, D. Morad, H. Mansurbeg, and A. Al-Suwaidi, 2016, Saddle dolomite and calcite cements as records of fluid flow during basin evolution: Paleogene carbonates, United Arab Emirates: Marine and Petroleum Geology, v. 74, p. 71-91.

Sirat, M., S. de Jong, E. Werner, D. Sokoutis, E. Willingshofer, and M. Ali, 2007a, The tectonic evolution of Jebel Hafit and Al-Jaww Plain: structural style and fracture analysis.

Sirat, M., S. Salman, and S. Bellah, 2007b, Fracturing Mechanism and Fracture Systems Analysis of Carbonate Reservoir from Abu Dhabi-UAE: SPE/EAGE Reservoir Characterization and Simulation Conference.

Smith Jr, L. B., 2006, Origin and reservoir characteristics of Upper Ordovician Trenton–Black River hydrothermal dolomite reservoirs in New York: AAPG bulletin, v. 90, p. 1691-1718.

Soddy, F., 1913, Intra-atomic charge: Nature, v. 92, p. 399.

Spencer, R.J., Hardie, L.A., 1990, Control of seawater composition by mixing of river waters and mid-ocean ridge hydrothermal brines, In: Spencer, R.J., Chou, I.-M. (Eds.), Fluid– Mineral Interactions: A Tribute to H.P. Eugster, Geochemistry. Geological Society, London, Special Publications, v. 19, p. 409–419.

Sprovieri, M., R. Coccioni, F. Lirer, N. Pelosi, and F. Lozar, 2006, Orbital tuning of a lower Cretaceous composite record (Maiolica Formation, central Italy): Paleoceanography, v. 21.

Stanley, S. M., and L. A. Hardie, 1998, Secular oscillations in the carbonate mineralogy of reef-building and sediment-producing organisms driven by tectonically forced shifts in seawater chemistry: Palaeogeography, Palaeoclimatology, Palaeoecology, v. 144, p. 3-19.

Stein, M., S. Westermann, T. Adatte, V. Matera, D. Fleitmann, J. E. Spangenberg, and K. B. Föllmi, 2012, Late Barremian–Early Aptian palaeoenvironmental change: The Cassis-La Bédoule section, southeast France: Cretaceous Research, v. 37, p. 209-222.

Stentoft, N., P. Lapinskas, and P. Musteikis, 2003, Diagenesis of Silurian reefal carbonates, Kudirka oilfield, Lithuania: Journal of Petroleum Geology, v. 26, p. 381-402.

Steuber, T., 2002, Plate tectonic control on the evolution of Cretaceous platform-carbonate production: Geology, v. 30, p. 259-262.
Steuber, T., and M. Rauch, 2005, Evolution of the Mg/Ca ratio of Cretaceous seawater: implications from the composition of biological low-Mg calcite: Marine Geology, v. 217, p. 199-213.

Steuber, T., M. Rauch, J.-P. Masse, J. Graaf, and M. Malkoč, 2005, Low-latitude seasonality of Cretaceous temperatures in warm and cold episodes: Nature, v. 437, p. 1341.

Steuber, T., and J. Veizer, 2002, Phanerozoic record of plate tectonic control of seawater chemistry and carbonate sedimentation: Geology, v. 30, p. 1123-1126.

Strohmenger, C. J., T. Steuber, A. Ghani, D. G. Barwick, S. H. Al-Mazrooei, and N. O. J. B.-A. s. a. h. h. o. t. e. A. P. G. S. P. Al-Zaabi, 2010, Sedimentology and chemostratigraphy of the Hawar and Shu'aiba depositional sequences, Abu Dhabi, United Arab Emirates, v. 4, p. 341-365.

Strohmenger, C. J., L. J. Weber, K. A.-M. Ahmed Ghani, O. Al-Jeelani, A. Al-Mansoori, T. Al-Dayyani, L. Vaughan, S. A. Khan, and J. C. Mitchell, 2006, High-resolution sequence stratigraphy and reservoir characterization of Upper Thamama (Lower Cretaceous) reservoirs of a giant Abu Dhabi oil field, United Arab Emirates.

Suzuki, K., M. L. Tejada, J. Kuroda, R. Coccioni, N. Ohkouchi, T. Sakamoto, Y. Tatsumi, and J. Mahoney, 2007, Secular change of Early Cretaceous seawater Os isotope composition: an indicator of a LIP-OAE link: Japan Geoscience Union Meeting, 19–24 May 2007.

Swart, P. K., D. L. Cantrell, H. Westphal, C. R. Handford, and C. G. Kendall, 2005, Origin of dolomite in the Arab-D reservoir from the Ghawar Field, Saudi Arabia: evidence from petrographic and geochemical constraints: Journal of Sedimentary Research, v. 75, p. 476-491.

Ziegler, T. R., and D. F. Sibley, 1986, Petrographic and geochemical characteristics of dolomite types and the origin of ferroan dolomite in the Trenton Formation, Ordovician, Michigan Basin, USA: Sedimentology, v. 33, p. 61-86.

Taylor, K., and J. J. S. G. Macquaker, 2000, Early diagenetic pyrite morphology in a mudstone-dominated succession: the Lower Jurassic Cleveland Ironstone Formation, eastern England, v. 131, p. 77-86.

Thorpe, D. T., 2014, Controls on reservoir quality in Early Cretaceous carbonate oil fields and implications for basin modelling, Doctor of Philosophy, The University of Edinburgh, Edinburgh.

Timofeeff, M. N., T. K. Lowenstein, M. A. M. Da Silva, and N. B. Harris, 2006, Secular variation in the major-ion chemistry of seawater: Evidence from fluid inclusions in Cretaceous halites: Geochimica et Cosmochimica Acta, v. 70, p. 1977-1994.

Tucker, M., and R. Bathurst, 1990, C. Carbonate diagenesis. Reprint series volume 1 of the International Association of Sedimentologists, Oxford: Blackwell Scientific Publication.

Tucker, M. E., 2009, Sedimentary petrology: an introduction to the origin of sedimentary rocks, John Wiley & Sons.

Turgeon, S. C., and R. A. Creaser, 2008, Cretaceous oceanic anoxic event 2 triggered by a massive magmatic episode: Nature, v. 454, p. 323.

Urey, H. C., 1947, The thermodynamic properties of isotopic substances: Journal of the Chemical Society (Resumed), p. 562-581.

Vahrenkamp, V., 2010, Chemostratigraphy of the Early Cretaceous Shu'aiba Formation: A d13C reference profile for the Aptian Stage from the southern Neo-Tethys Ocean: Aptian Stratigraphy and Petroleum Habitat of the Eastern (Eds FSP Van Buchem, MI Al-Husseini, F. Maurer and HJ Droste), GeoArabia Spec. Publ, v. 4.

Vahrenkamp, V., J. Barata, P. J. Van Laer, P. Swart, and S. Murray, 2014, Micro Rhombic Calcite of a Giant Barremian (Thamama B) Reservoir Onshore Abu Dhabi-Clumped Isotope Analyses fix Temperature, Water Composition and Timing of Burial Diagenesis: Abu Dhabi International Petroleum Exhibition and Conference.

Vahrenkamp, V. C., 1996, Carbon isotope stratigraphy of the Upper Kharaib and Shuaiba Formations: implications for the Early Cretaceous evolution of the Arabian Gulf region: AAPG bulletin, v. 80, p. 647-661.

Valley, J. W., and N. T. Kita, 2009, In situ oxygen isotope geochemistry by ion microprobe: MAC short course: secondary ion mass spectrometry in the earth sciences, v. 41, p. 19-63.

Van Buchem, F., Al-Husseini, M., Maurer, F., Droste, H., and Yose, L., 2010, Sequence-stratigraphic synthesis of the Barremian–Aptian of the eastern Arabian Plate and implications for the petroleum habitat: GeoArabia, Journal of the Middle East Petroleum Geosciences, v. 1, no. 8, p. 9-48.

van Buchem, F., Pittet, B., Hillgärtner, H., Al Mansouri, A., Billing, I., Droste, H., Grötsch, J., and Oterdoom, H., 2002b, Regional sequence stratigraphic model for the Kharaib and Shuaiba formations (Barremian, Aptian) in northern Oman and UAE—depositional geometries and ecological change: GeoArabia, v. 7.

van Smeerdijk Hood, A., and M. W. Wallace, 2015, Extreme ocean anoxia during the Late Cryogenian recorded in reefal carbonates of Southern Australia: Precambrian Research, v. 261, p. 96-111.

Bibliography

Vasconcelos, C., J. A. McKenzie, S. Bernasconi, D. Grujic, and A. J. Tiens, 1995, Microbial mediation as a possible mechanism for natural dolomite formation at low temperatures: Nature, v. 377, p. 220.

Vasconcelos, C., J. A. McKenzie, R. Warthmann, and S. M. Bernasconi, 2005, Calibration of the δ18O paleothermometer for dolomite precipitated in microbial cultures and natural environments: Geology, v. 33, p. 317-320.

Veizer, J., D. Ala, K. Azmy, P. Bruckschen, D. Buhl, F. Bruhn, G. A. Carden, A. Diener, S. Ebneth, and Y. Godderis, 1999, 87Sr/86Sr, δ13C and δ18O evolution of Phanerozoic seawater: Chemical geology, v. 161, p. 59-88.

Vieira, M. M., L. F. De Ros, and F. H. R. Bezerra, 2007, Lithofaciology and palaeoenvironmental analysis of Holocene beachrocks in northeastern Brazil: Journal of coastal Research, v. 23, p. 1535-1548.

Vincent, B., C. Rambeau, L. Emmanuel, and J.-P. Loreau, 2006, Sedimentology and trace element geochemistry of shallow-marine carbonates: an approach to paleoenvironmental analysis along the Pagny-sur-Meuse Section (Upper Jurassic, France): Facies, v. 52, p. 69-84.

Vieira, M. M., and L. F. J. S. G. De Ros, 2006, Cementation patterns and genetic implications of Holocene beachrocks from northeastern Brazil, v. 192, p. 207-230.

Volery, C., E. Davaud, A. Foubert, and B. Caline, 2009, SHALLOW-MARINE MICROPOROUS CARBONATE RESERVOIR ROCKS IN THE MIDDLE EAST: RELATIONSHIP WITH SEAWATER Mg/Ca RATIO AND EUSTATIC SEA LEVEL: Journal of Petroleum Geology, v. 32, p. 313-325.

Volery, C., E. Davaud, A. Foubert, and B. Caline, 2010, Lacustrine microporous micrites of the Madrid Basin (Late Miocene, Spain) as analogues for shallow-marine carbonates of the Mishrif reservoir Formation (Cenomanian to Early Turonian, Middle East): Facies, v. 56, p. 385-397.

Walderhaug, O., 1994, Precipitation rates for quartz cement in sandstones determined by fluid-inclusion microthermometry and temperature-history modeling: Journal of Sedimentary Research, v. 64.

Warren, J., 2000, Dolomite: occurrence, evolution and economically important associations: Earth-Science Reviews, v. 52, p. 1-81.

Warthmann, R., Y. Van Lith, C. Vasconcelos, J. A. McKenzie, and A. M. Karpoff, 2000, Bacterially induced dolomite precipitation in anoxic culture experiments: Geology, v. 28, p. 1091-1094.

Westermann, S., M. Stein, V. Matera, N. Fiet, D. Fleitmann, T. Adatte, and K. B. Föllmi, 2013, Rapid changes in the redox conditions of the western Tethys Ocean during the early Aptian oceanic anoxic event: Geochimica et Cosmochimica Acta, v. 121, p. 467-486.

Wierzbicki, R., J. J. Dravis, I. Al-Aasm, and N. Harland, 2006, Burial dolomitization and dissolution of upper Jurassic Abenaki platform carbonates, Deep Panuke reservoir, Nova Scotia, Canada: AAPG bulletin, v. 90, p. 1843-1861.

Wilkinson, B. H., and T. J. Algeo, 1989, Sedimentary carbonate record of calcium-magnesium cycling: American Journal of Science, v. 289, p. 1158-1194.

Wong, P., and A. Oldershaw, 1981, Burial cementation in the Devonian, Kaybob reef complex, Alberta, Canada: Journal of Sedimentary Research, v. 51.

Worden, R. H., and E. C. Heasley, 2000, Effects of petroleum emplacement on cementation in carbonate reservoirs: Bulletin de la Societe geologique de France, v. 171, p. 607-620.

Worden, R., P. Smalley, and N. Oxtoby, 1996, The effects of thermochemical sulfate reduction upon formation water salinity and oxygen isotopes in carbonate gas reservoirs: Geochimica et Cosmochimica Acta, v. 60, p. 3925-3931.

Woronick, R., and L. Land, 1985, Late burial diagenesis, lower Cretaceous Pearsall and lower Glen Rose formations, south Texas.

Wright, D. T., and D. Wacey, 2004, Sedimentary dolomite: a reality check: Geological Society, London, Special Publications, v. 235, p. 65-74.

Wygrala, B., 1989, Integrated study of an oil field in the southern Po basin, northern Italy, Publikationen vor 2000.

Zeebe, R. E., and A. Sanyal, 2002, Comparison of two potential strategies of planktonic foraminifera for house building: Mg2+ or H+ removal?: Geochimica et Cosmochimica Acta, v. 66, p. 1159-1169.

Xie, X., W. W. Weiss, Z. J. Tong, and N. R. Morrow, 2005, Improved oil recovery from carbonate reservoirs by chemical stimulation: SPE Journal, v. 10, p. 276-285.

Zhang, F., H. Xu, H. Konishi, and E. E. Roden, 2010, A relationship between d 104 value and composition in the calcite-disordered dolomite solid-solution series: American Mineralogist, v. 95, p. 1650-1656.

Ziegler, M. A., 2001, Late Permian to Holocene paleofacies evolution of the Arabian Plate and its hydrocarbon occurrences: Geoarabia Manama, v. 6, p. 445-504.

# Appendices

## Appendix A

**Table 1:** Core slabs collected from 8 wells, ADCO core store, Abu Dhabi, UAE.

| Sample # | Well Name | Depth (ft) | Reservoir/Dense | Oil/Water |
|---|---|---|---|---|
| 1 | well 6 | 9549 | Reservoir B (rubble) | W |
| 2 | well 6 | 9630.8 | Reservoir B | W |
| 3 | well 6 | 9620.1 | Reservoir B | W |
| 4 | well 6 | 6902.8-7 | Reservoir B | W |
| 5 | well 6 | 9597.4-5 | Reservoir B | W |
| 6 | well 6 | 9561.8 | Reservoir B | W |
| 7 | well 6 | 9532.1 | Reservoir B | W |
| 8 | well 6 | 9527.5 | Reservoir B | W |
| 9 | well 6 | 9525.7 | Reservoir B | W |
| 10 | well 6 | 9505.8 | Reservoir B | W |
| 11 | well 6 | 9502.8-9 | Reservoir B | W |
| 12 | well 6 | 9498.5 | Reservoir B | W |
| 13 | well 6 | 9489'11" | Reservoir B (rubble) | W |
| 14 | well 7 | 9504.5 | Reservoir C | W |
| 15 | well 7 | 9501.6 | Reservoir C | W |
| 16 | well 7 | 9496.6 | Reservoir C | W |
| 17 | well 8 | 10428.8 | Dense F | W |
| 18 | well 8 | 10403.2 | Dense F | W |
| 19 | well 8 | 10395.5 | Reservoir F | W |
| 20 | well 8 | 10395.1 | Reservoir F | W |
| 21 | well 8 | 10373.4 | Reservoir F | W |
| 22 | well 8 | 10367 | Reservoir F | W |
| 23 | well 8 | 10362.8 | Reservoir F | W |
| 24 | well 8 | 10352.3 | Dense E | W |
| 25 | well 1 | 10376.1 | Dense G | O |
| 26 | well 1 | 10365 | Dense G | O |
| 27 | well 1 | 10362.5 | Dense G | O |
| 28 | well 1 | 10356.9 | Reservoir G | O |
| 29 | well 1 | 10355.4 | Reservoir G | O |
| 30 | well 1 | 10349.3 | Reservoir G | O |
| 31 | well 1 | 10347.9 | Reservoir G | O |
| 32 | well 1 | 10347.1 | Reservoir G | O |
| 33 | well 1 | 10345.5 | Reservoir G | O |
| 34 | well 1 | 10341.5 | Reservoir G | O |
| 35 | well 1 | 10341 | Reservoir G | O |
| 36 | well 1 | 10340.5 | Reservoir G | O |
| 37 | well 1 | 10336.4 | Reservoir G | O |
| 38 | well 1 | 10264.5 | Dense F | O |
| 39 | well 1 | 10335.9 | Reservoir G | O |

| | | | | |
|---|---|---|---|---|
| 40 | well 1 | 10329.8 | Dense F | O |
| 41 | well 1 | 10327.5 | Dense F | O |
| 42 | well 1 | 10322.8 | Dense F | O |
| 43 | well 1 | 10316.3 | Dense F | O |
| 44 | well 1 | 10250.3 | Reservoir F | O |
| 45 | well 1 | 10234.1 | Reservoir F | O |
| 46 | well 2 | 9379.5 | Reservoir C | O |
| 47 | well 2 | 9374.3 | Reservoir C | O |
| 48 | well 2 | 9363.2 | Dense C | O |
| 49 | well 2 | 9330.8 | Reservoir C | O |
| 50 | well 2 | 9312.9 | Reservoir C | O |
| 51 | well 2 | 9253.9 | Reservoir C | O |
| 52 | well 2 | 9253.3 | Dense B (hardground) | O |
| 53 | well 2 | 9307.4-3 | Reservoir C | O |
| 54 | well 2 | 9296.5-4 | Reservoir C | O |
| 55 | well 2 | 9288.7-6 | Reservoir C | O |
| 56 | well 2 | 9281.9-82 | Reservoir C | O |
| 57 | well 2 | 9264.9-65 | Reservoir C | O |
| 58 | well 3 | 9199.4 | Reservoir B | O |
| 59 | well 3 | 9198.7 | Reservoir B | O |
| 60 | well 3 | 9197.7 | Reservoir B | O |
| 61 | well 3 | 9195.8 | Reservoir B | O |
| 62 | well 3 | 9188.9 | Reservoir B | O |
| 63 | well 3 | 9181.2 | Reservoir B | O |
| 64 | well 3 | 9176.4 | Reservoir B | O |
| 65 | well 3 | 9174.3 | Reservoir B | O |
| 66 | well 3 | 9200.8 | Reservoir B | O |
| 67 | well 4 | 9186.5 | Bab Member | O |
| 68 | well 4 | 9281.1 | Reservoir A | O |
| 69 | well 4 | 9274.3 | Reservoir A | O |
| 70 | well 4 | 9270.4 | Reservoir A | O |
| 71 | well 4 | 9266.7 | Reservoir A | O |
| 72 | well 4 | 9263.2 | Reservoir A | O |
| 73 | well 4 | 9258.5 | Reservoir A | O |
| 74 | well 4 | 9250.3 | Bab Member | O |
| 75 | well 4 | 9236.8 | Dense A | O |
| 76 | well 5 | 8970.6 | Dense A | O |
| 77 | well 5 | 8996.1 | Dense A | O |
| 78 | well 5 | 8997.5 | Dense A | O |
| 79 | well 5 | 8998.5 | Dense A | O |
| 80 | well 5 | 8998.8 | Dense A | O |
| 81 | well 5 | 9119.1 | Reservoir B | O |
| 82 | well 5 | 9121.7 | Reservoir B | O |
| 83 | well 5 | 9126.6 | Reservoir B | O |
| 84 | well 5 | 9140.2 | Reservoir B | O |
| 85 | well 5 | 9147.3 | Reservoir B | O |
| 86 | well 5 | 8985.7 | Dense A | O |
| 87 | well 5 | 8986.5 | Dense A | O |
| 88 | well 5 | 8988.5 | Dense A | O |
| 89 | well 5 | 9013.1 | Reservoir B | O |
| 90 | well 5 | 9026.8 | Reservoir B | O |

| | | | | |
|---|---|---|---|---|
| 91 | well 5 | 9073.9 | Reservoir B | O |
| 92 | well 5 | 9087.8 | Reservoir B | O |
| 93 | well 5 | 9095.8 | Reservoir B | O |
| 94 | well 5 | 9151.8 | Reservoir B | O |
| 95 | well 5 | 9156.8 | Reservoir B | O |
| 96 | well 5 | 9163.2-63 | Dense B | O |
| 97 | well 5 | 9166.3 | Dense B | O |

## Appendix B

Elemental (EPMA) data of calcite cement discussed in Chapter 4 on a memory stick at the back of the thesis.

## Appendix C

Elemental (EPMA) data of dolomite cement discussed in Chapter 5 on a memory stick at the back of the thesis.

## Appendix D

In-situ (SIMS) $\delta^{18}O$ data of calcite cement discussed in Chapter 6 on a memory stick at the back of the thesis.